

Università degli Studi di Padova

DIPARTIMENTO DI INGEGNERIA INDUSTRIALE

SCUOLA DI DOTTORATO DI RICERCA IN INGEGNERIA INDUSTRIALE

CURRICULUM: MATERIALI

CICLO XXXI

Development of low cost waste-derived sintered glass-ceramics for energy saving and recovery

Supervisor: Prof. Enrico Bernardo

Ph.D. student: Acacio Rincón Romero

Acknowledgments

The author is grateful to the financial support of the European Community's Horizon 2020 Programme through Marie Skłodowska-Curie Innovative Training Network ("CoACH-ETN", g.a. no. 642557).

I would like to express my sincere gratitude to my supervisor Prof. Enrico Bernardo for his guidance and for giving me the opportunity to grow as a researcher thanks to his ongoing professional and personal support.

I would also like to thank all my colleagues from the Department of Industrial Engineering at the University of Padova, not only for their help and cooperation at the laboratory, but also for those everyday moments that made the PhD an invaluable personal experience. Special thanks to all the students who worked with me and helped me with the experiments over these years.

I would like to thank the whole team of the CoACH-ETN project, in particular Milena Salvo, Cristiana Contardi and Monica Ferraris for providing administrative support; all the junior researchers of the group; and the people who helped me during the time spent at Erlangen, Hitchin, Torino and Sasil S.r.l.

Special thanks go to all my friends and family, for their continuous support during these years.

Abstract

A new technique for the production of cellular glass and glass-ceramics foams is the main goal of the hereby presented research activities. It is based on a combination of alkali-activation of silica-rich materials, with subsequent inorganic gel casting foaming by means of a surfactant and final heat treatment through sinter-crystallisation process. This new process is less expensive and more environmentally sustainable than the current procedures based on mixtures of glass powders and foaming agents, which decompose and release gases at a temperature significantly above the softening glass point, and is conceived as an alternative route to valorise silica-rich waste materials

The alkali activation of glass waste allows to obtain well-dispersed concentrated suspensions, undergoing gelation by treatment at low temperature (40-80 °C), due to the formation of silicate hydrates. An extensive direct foaming was achieved by mechanical stirring of partially gelified suspensions, also comprising a surfactant. The final microstructure (total amount of porosity, cell size) can be directly correlated with the degree of gelation. A sintering treatment, at only 700 °C, was finally applied to stabilise the structures and limit the leaching of alkaline ions.

The approach proved to be extended to different glasses and industrial waste mixtures leading to different gels after alkali activation. Alkali activation of soda-lime waste glass was exploited through mixing with iron-rich inorganic waste from a copper slag and fly ash from coal combustion. The approach was also extended to different glass-based material coming from waste, such as an alumino-boro-silicate glass from the recycling of pharmaceutical vials, and vitrified bottom ashes from municipal solid waste incinerators. A considerable number of processing parameters combinations (such as surfactants, activating solution, curing times, conditions for heating treatments etc.) were explored and understood.

Apart from waste-derived materials and applications in the building industry, the technique was also applied to create highly porous bioactive glass-ceramics scaffolds; the successful production of highly homogeneous foams proves the versatility in the approach.

The progressive hardening associated with inorganic polymerisation configuring an 'inorganic gel casting' has also been used to produce advanced ceramics, such as mullite and cordierite foams and scaffolds. These materials were obtained through the thermal treatment of engineered alkali activated suspensions consisting of a Na-geopolymer enriched with reactive γ -Al₂O₃ powders in the case of mullite, and reactive γ -Al₂O₃ and talc in the synthesis of cordierite. The gelation was studied in order to have a proper viscosity for trapping air during vigorous mechanical stirring or maintaining the shape of the scaffold struts obtained by direct ink writing. After the hardened samples were obtained, sodium ions were extracted through ion exchange in ammonium nitrate solution. Finally, the ion-exchanged foams were successfully converted into pure mullite or cordierite foams and scaffolds with the application of a firing treatment.

Alkali activation was the basis for the manufacturing of lightweight granules according to a 'spheroidisation technique' consisting in the casting of fine glass powders on a rotary drum, before firing. The hardened suspensions of soda-lime glass obtained from alkaline activation, were reduced into fragments and cast on a rotary drum with dry glass. The firing of green granules was accompanied by a significant foaming, owing to the decomposition of hydrated compounds.

Table of contents

CHAPTER I - Overall introduction

I. 1 - Recycle of inorganic waste in glass-based materials	1
I. 2 - Inorganic waste as raw materials for glass-based products	2
I.2.1 - Wastes rich in glass-forming oxides	3
I.2.2 - Iron-rich wastes.....	6
I. 3 - Overview of glass-based products	8
I.3.1 - Glasses from the vitrification of inorganic waste	8
I.3.2 - Conventional glass-ceramic monoliths	10
I.3.3 - Glass-ceramic monoliths from alternative routes	11
I.3.4 - Cellular glass-based materials.....	14
I.3.5 - Hybrid glass-based materials	17
I. 4 - Main properties of waste-derived glass-based materials	18
I.4.1 - Structural and functional properties.....	18
I.4.2 - Magnetic properties	21
I.4.2 - Electric properties	22
I.4.4 - Other properties	23
I. 5 - Methodology	24
I. 6 - Characterization techniques	28

CHAPTER II - Glass foams from cullet produced by inorganic gel casting

II. 1 - Aim of the study	41
II. 2 - Production of glass foams through inorganic gel casting	42
II.2.1 - Introduction	42
II.2.2 - Experimental process.....	44
II.2.3 - Results and discussion	46
II. 3 - Semi-industrial production of glass foam lightweight panels by inorganic gel casting	59
II.3.1 - Experimental process.....	59

II.3.2 - Results and discussion.....	60
II. 4 - Conclusions	64
 CHAPTER III - Glass-ceramic foams trough inorganic gel casting from industrial waste and glass cullet	
III. 1 - Aim of the study.....	69
III. 2 - Functional Glass-ceramic foams from copper slag and glass cullet	71
III.2.1 - Introduction.....	71
III.2.2 - Experimental process	73
III.2.3 - Results and discussion.....	74
III.2.4 - Conclusions	85
III. 3 - Soda-lime waste glass and fly ash-based glass ceramic foams	86
III.3.1 - Introduction	86
III.3.2 - Experimental process	87
III.3.3 - Results and discussion.....	90
III.3.4 - Conclusions	101
 CHAPTER IV - Extension of the ‘inorganic gel casting’ process to up-cycling of glass waste into glass and glass-ceramic foams	
IV. 1 - Aim of the study.....	109
IV. 2 - Up-cycling MSWI vitrified bottom ash into glass-ceramic foams.....	111
IV.2.1 - Introduction.....	111
IV.2.2 - Experimental process	112
IV.2.3 - Results and discussion	114
IV.2.4 - Conclusions.....	122
IV. 3 - Borosilicate glass foams from discarded pharmaceutical vials	122
IV.3.1 - Introduction	122
IV.3.2 - Experimental process	124
IV.3.3 - Results and discussion	126
IV.3.4 - Conclusions	133

CHAPTER V - Bioactive Glass-Ceramic Foam Scaffolds from ‘Inorganic Gel Casting’ and Sinter-Crystallization

V. 1 - Aim of the study	141
V. 2 - Wollastonite-diopside bioactive glass-ceramics foams	142
V.2.1 - Introduction	142
V.2.2 - Experimental process	144
V.2.3 - Results and discussion.....	145
V.2.4 - Conclusions	151
V. 2 – CEL2 bioactive glass-ceramics foams	152
V.2.1 - Introduction	152
V.2.2 - Experimental process	154
V.2.3 - Results and discussion.....	155
V.2.4 - Conclusions	162

CHAPTER VI - Advance ceramics from engineered alkali activated suspensions

VI. 1 - Aim of the study	169
VI. 2 - Mullite ceramics produced from engineered alkali activated suspensions	170
VI.2.1 - Introduction.....	170
VI.2.2 - Experimental process	172
VI.2.3 - Results and discussion	173
VI. 3 - Cordierite ceramics produced from engineered alkali activated suspensions	181
VI.3.1 - Introduction.....	181
VI.3.2 - Experimental process	182
VI.3.3 - Results and discussion	183
VI. 4 - Conclusions	188

CHAPTER VII - Alternative conformation techniques of porous materials through inorganic gel casting

VII. 1 - Aim of the study	195
--	-----

VII. 2 - Production of Lightweight aggregates from glass cullet by inorganic gel casting	196
VII.2.1 - Introduction	196
VII.2.2 - Experimental process.....	198
VII.2.3 - Results and discussion	200
VII. 3 - Conclusions	204
 CHAPTER VIII	
Final Remarks.....	209

CHAPTER I

Overall introduction

I.1 - Recycle of inorganic waste in glass-based materials*

In general, we refer to organic or inorganic waste, with each category including both hazardous and non-hazardous waste. Organic wastes are currently destroyed with very high efficiency, even in the case of hazardous substances such as pesticides, polychlorinated biphenyls (PCBs) and persistent organic pollutants (POPs), by incineration.¹ The handling of inorganic waste (especially if hazardous), on the contrary, is still subject to some controversy, given the heterogeneity of waste streams and the availability of different technologies.

Hazardous inorganic waste derives mostly from metallurgical industrial processes, but can also come from the demolition of buildings and civil infrastructures (realised, for example, with asbestos-containing cement), or from combustion processes, particularly

* *The following text, and images are an adaptation of the results that were published in the review article: “A. Rincón, M. Marangoni, S. Cetin, E. Bernardo, Recycling of inorganic waste in monolithic and cellular glass-based materials for structural and functional applications, Journal of Chemical Technology & Biotechnology. 91 (2016) 1946–1961”. It is reproduced in this section with the incorporation of slight modifications.*

from municipal solid waste (MSW) incineration. Any form of management, from landfill disposal to recovery, implies a stabilisation step applied through several chemical and physical processes, among which vitrification may be treated as the most effective, considering its application even to radioactive waste (the ‘ultimate’ form of hazardous inorganic waste).²

High-value products can be roughly divided into ‘not glass-based’ and ‘glass-based’. ‘Not glass-based’ products are generally traditional ceramics, such as clay bricks and porcelain stoneware tiles, in which waste glass is used to ‘dilute’ the conventional raw materials;³ secondary options are represented by systems in which waste glasses are used as ‘inert’ components, such as concretes⁴ and bituminous mixtures.⁵ The use of waste-derived glass in a mass market application is highly attractive since it enables safe disposal of a large quantity of waste, but the waste glass contributes only to a limited extent to the final composition of the material, and the economic benefit is simply due to the saving of natural raw materials. ‘Glass-based’ products, in contrast, refer to waste glasses as the dominant component; they are not included in a mass market, but their value may be significantly higher than that of traditional ceramics, owing to particular functionalities, in turn, connected to the nature of the waste glass adopted. Common ‘glass-based’ products are (mostly) monolithic glass-ceramics, to be used in structural applications, as an alternative to natural stones or ceramic tiles, or glass foams (e.g. cellular glasses), to be used for thermal and acoustic insulation, as reported in a vast literature, including some review papers.^{3, 6, 7}

The manufacturing of both main classes of glass-based products actually depends on the application of a secondary thermal treatment, implying extra costs. Again, the cost/benefits balance may be adjusted favourably, typically by: (i) engineering the thermal treatment (e.g. reducing the costs of conversion of glass into glass-ceramics); (ii) obtaining glass-based products even avoiding preliminary vitrification, starting from engineered mixtures of inorganic wastes, comprising recycled glasses. Inorganic wastes, in this case, are (at least) partially dissolved in the liquid phase offered by the softening of the glass component, undergoing viscous flow sintering. The products evidently lack homogeneity, compared with those from melting, but they may be convenient for the stabilisation of wastes with limited hazardousness.^{3, 6}

I.2 - Inorganic waste as raw materials for glass-based products

Generally speaking, the inorganic waste, in view of conversion into glass-based products, can be divided on the basis of their content of glass formers, notably silica. In fact, silica-rich waste can be vitrified by themselves or by addition of limited quantities of additives, or lead to glass-based articles, directly by viscous flow sintering, as in the case of recycled glasses. Silica-poor waste, on the contrary, cannot lead to a glass-ceramics or glass-foams by themselves, either by vitrification and secondary processing

or by direct sintering; their use may compromise the overall economic sustainability (the stabilization is due to the use of significant amounts of additives), but we should consider the impact on functionalities of oxides present in these wastes, particularly in the case of iron oxides. The following paragraphs are intended to provide a short overview of the main categories of wastes.

I.2.1 - Wastes rich in glass-forming oxides

The most interesting silica-rich waste is actually represented by recycled glasses, as summarised in Table 1. The term ‘recycled’ is often misleading. Any glass is nominally 100% recyclable, e.g. scrap glass of any composition could be re-melted and used for the manufacturing of the original articles, in a condition of ‘closed-loop recycling’. Although recommended for limiting the consumption of energy and natural raw materials, the use of scrap glass in manufacturing new glass articles is only possible after an expensive sorting step, aimed at the separation of glass from other materials, like metallic or ceramic contaminants;⁸ the imbalance between the supply of and demand for coloured cullet is also an issue sending to landfill green glass cullet due to the lack of markets. (Butler and Hooper, as an example, specified in their study on glass recycling in the UK that glass manufacturers focus their production on clear glass, while the main cullet supply is heavily influenced by the presence of coloured imported wine and beer containers).⁹

Only a fraction of carefully ‘purified’ glass can actually be used for closed-loop recycling, with negative effects on the overall sustainability of the same starting glass articles. According to the LCA model by Vellini and Salvioli,¹⁰ glass containers can be more environmentally benign than PET containers only if the reuse and recycle factors are higher than a certain threshold (e.g. the glass container production scenario with an 80% reuse factor yields better performances than PET container production, whereas a scenario with a 25% reuse factor fails to do so). It is not surprising, as a consequence, that glass cullet should be considered also is in a condition of ‘open loop recycling’, i.e. reuse in articles different from the original ones, also termed ‘downcycling’,¹¹ starting from the production of traditional ceramics.⁸

For common soda-lime glass, a significant fraction enriched in contaminants remains practically unemployed and is mostly landfilled.^{8, 12} The ‘useless’ fraction is obviously more significant for glasses deriving from articles that are no longer produced or from articles employing by themselves a limited quantity of recycled materials,¹³ such as glasses from the dismantling of cathode ray tubes (CRTs),^{14, 15} lamps (bulbs, fluorescent lamps),¹⁶ liquid crystal and plasma displays,¹⁷⁻¹⁹ pharmaceutical containers.²⁰ ‘Unemployed recycled glass’ can be effectively referred to as ‘waste glass’ (whereas ‘waste-derived glass’ is the product of vitrification of wastes that may include unemployed recycled glass).

Oxide (wt%)	Soda lime glass	Borosilicate glass	Cathode ray tubes		LCD glass	Fluorescence lamps
			Panel	Funnel		
SiO ₂	70.8	72	57.87-60.7	51.5-54.1	61.20	67.9
Al ₂ O ₃	2.4	7	1.7-3.76	1.80-3.21	16.3	2.26
Na ₂ O	13	6	7.5-12.89	6.20-10.21	-	17.5
K ₂ O	1.1	2	6.9-7.29	8.2-9.47	-	1.6
CaO	9.4	1	0.10	3.5-3.77	1.5	5.09
MgO	2.1	-	-	1.43	1.16	2.96
BaO	0.2	<0.1	7.95-9.90	0.8-1.28	-	0.94
Fe ₂ O ₃	0.3	-	0.22	0.13	B.D.	0.08
MnO	-	-	-	-	-	-
B ₂ O ₃	0.12	12	-	-	10.72	-
PbO	0.07	-	0.01-0.02	18.40-22.00	-	0.79
ZnO	0.12	-	0.63	0.41	-	-
SrO	-	-	8.06	0.7-0.89	-	-
As ₂ O ₃	0.02	-	-	-	-	-
Sb ₂ O ₃	0.01	-	-	-	-	0.08

Table 1. Typical chemical compositions of selected waste glasses (wt%).

The manufacturing of new glass-based materials may be seen as the ultimate opportunity for open-loop recycling and has an undoubted environmental benefit compared with landfilling, as confirmed by recent LCA studies. Meylan et al.¹¹ assessed several scenarios of Swiss waste glass-packaging disposal and found that the local production of glass foams, for thermal and acoustic insulation, is not only an environmentally sound disposal option (compared even with the production of extruded polystyrene, widely used for the same applications), but it also buffers gross value added losses, in case domestic recycling (and thus glass-packaging production in Switzerland) ceases in the future. Rocchetti and Beolchini, as a second example, recently showed the sustainability of several open-loop recycling technologies for CRT glasses.²¹

Ashes from different combustion processes represent the second fundamental example of silica-rich waste.^{22, 23} Coal fly ashes from thermal power plants vary in their composition as a function of the type of coal used, the combustion conditions or the provenance, as shown in Table 2. Molten coal fly ashes may form glass directly^{24, 25} but

more commonly some additional oxides are added to lower the viscosity, from minerals,²⁶⁻²⁸ or from glass cullet.^{29, 30} The introduction of nucleating agents such as TiO₂ or Cr₂O₃ to achieve the easy transformation to glass-ceramics has also been reported.^{31, 32}

Oxide (wt%)	Coal fly ashes	MSWI fly ash	MSWI bottom ash	MBM ash	Sewage ash	Oil shale ash	Rice husk ash
SiO ₂	18.1-75.6	7.3-27.5	30.3-47.4	2.3	39.5	31.9-34.7	90.7
Al ₂ O ₃	7.6-55.5	3.2-11.0	9.9-13.0	0.2	17.2	9.1-9.4	0.06
CaO	0.8-37.8	16.6-19.5	18.8-23.1	46.4	7.2	27.6-27.7	1.2
MgO	3.5-9.0	2.6-3.1	2.8-2.9	1.3	2.1	3.4-5.9	0.8
Fe ₂ O ₃	3.1-9.9	1.4-5.0	4.3-10.2	8.7	11.1	3.8-4.4	0.3
Na ₂ O	0.2-2.6	13.1	1.9-4.5	8.7	1.2	0.2-0.3	-
K ₂ O	0.6-2.4	11.2	0.9-1.0	3.5	2.7	4.2-7.4	1.6
SO ₃	2.5-18.2	9.8	-	3.6	1.9	-	1.6
P ₂ O ₅	-	1.7	1.2-1.9	34	7.6	-	3.6
Cl ⁻	-	10.3-22.0	-	-	-	-	-

Table 2. Typical chemical compositions of selected ashes

Ashes from incineration of municipal solid waste (MSW) should be considered as belonging to two distinct categories: (a) MSW incinerator bottom ashes; (b) MSW incinerator fly ashes. Bottom ashes (consisting of glass, magnetic metals, minerals, synthetic ceramics, paramagnetic metals and unburned organic matter) are known to be poorly hazardous, especially in the form of coarse particles.³³⁻³⁵ On the contrary, MSWI fly ashes constitute a significant form of hazardous waste, since they contain dioxins or furans, to be destroyed, as well as leachable heavy metals (Cd, Cr, Cu, Pb), to be immobilised.³⁶ Some formulations, in addition, feature a quite limited content of silica, with a negative impact on the chemical durability of ‘100% ash-derived’ glasses or on the temperatures required for melting.³⁷ Composition corrections with more properly silica-rich wastes or pure silica provide a simple and effective solution,^{38, 39} with additional advantages, i.e. the possibility to extract low boiling point metals.⁴⁰

The high temperatures required by vitrification cause the destruction of many hazardous organic compounds,³ but gaseous emissions still need attention, especially concerning the presence of chloride salts and volatile heavy metal oxides.⁴¹ Chlorine has a very limited solubility in glasses⁴² and may lead, if uncontrolled, to the formation of hazardous species in the cooling step and to the corrosion of equipment. A preliminary washing treatment may be applied⁴³⁻⁴⁶ in order to remove all the water-soluble salts and

some heavy metals, but the aqueous by-product could determine a new disposal problem. A pre-stabilization with chemical agents, such as NaOH, Na₂S or phosphates,⁴⁷ may promote the formation of less volatile species. The controlled addition of chlorides (e.g. MgCl₂) may be considered, in some cases, as a strategy for the removal of heavy metals (particularly Zn) by the formation of low boiling point compounds, leaving a practically Cl-free ash, easier to reuse.⁴⁸

Ashes may derive from any process for energy recovery, reduction of waste volume and destruction of possible organic pollutants. The ashes produced vary in their composition according to the different waste incinerated. Rice husk ash, produced in biomass power plants that use rice husk as fuel, has been used as a silica precursor since it contains around 85–90% of amorphous or crystalline silica depending on the combustion conditions.⁴⁹⁻⁵¹ Sewage sludge fly ash,⁵²⁻⁵⁵ paper sludge ash,⁵⁶ oil-shale ash⁵⁷ or meat and bone meal ashes⁵⁸ feature a lower content of silica, but they contain significant amounts of P₂O₅ (another glass forming oxide) and Al₂O₃ (‘intermediate’ glass-forming oxide, when combined with alkali or alkaline earth oxides).

Asbestos waste represents a further example of silica-rich waste, is mainly composed of magnesium silicates. The destruction of the characteristic fibrous structure, which constitutes the main health danger, as written above, generally implies very energetic procedures, such as Joule heating,⁵⁹ microwave irradiation,^{60, 61} plasma heating,⁶² with vitrification temperatures well exceeding 1500 °C.

I.2.2 - Iron-rich wastes

The most significant production of iron-rich wastes is associated with the iron and steel industry; different final products (cast iron or steel) and different processes reflect in important composition variations. Blast furnace (BF) slag is undoubtedly easier to convert into a glass (in turn further transformed into glass-ceramics)⁶³⁻⁶⁵ than other slags, due to the high contents of silica and alumina, usually accompanied by CaO and, in a lower amount, MgO, as reported in Table 3. However, being a well-known pozzolanic material^{66, 67} BF slag is often reused for not-glass-based products, such as concrete and geopolymers. Other slags, such as basic oxygen furnace slag (BOF) and electric arc furnace (EAF) slag, dust from electrostatic precipitators, on the contrary, richer in iron oxides, but poorer in glass-forming oxides, may find applications after composition correction and vitrification.⁶⁸⁻⁷²

The most recent research refers to iron-rich waste from non-ferrous metallurgy. As an example, obtaining copper from ores generates a slag that contains more than 40 wt% iron, present as non-magnetic iron silicate.⁷³ The slag also includes alumina, silica, calcium oxide etc. and oxides of heavy metals that make this waste hazardous. Due to the limited amount of glass-forming oxides the copper flotation waste is usually mixed with natural raw materials and other residues to achieve glasses to be further transformed.

Karamanov et al.⁷⁴ used an iron-rich copper flotation waste (Fe_2O_3 exceeding 67 wt%) with the addition of blast furnace slag and glass cullet to increase the silica content, lower the melting temperature of the batch and increase the durability of the final glass-ceramic obtained. Çoruh et al.⁷⁵ used a similar approach, adding fly ash and perlite to the copper flotation waste (Fe_2O_3 content approaching 70 wt%). Ponsot et al.⁷⁶ successfully prepared glass-ceramics by mixing crystalline residues of the copper metallurgy, comprising fayalite (Fe_2SiO_4), with recycled borosilicate glass.

	BF slag	BOF slag	EAF dust	Cu extraction waste	Red mud
SiO_2	34.4-37	10.3-13.7	4.4-5.94	24.87-24.93	7.8
Al_2O_3	14.8-14.5	1.1-3.9	0.65-1.48	0.88-0.92	17.1
CaO	26.7-41.7	38.7-40.4	7.5-20.69	0.69-0.72	11.7
MgO	6.5-6.7	7.4-8.2	5.21-9.6	0.36-0.43	0.6
Fe_2O_3	0.3-0.6	11.2-12.9	24.28-52.82	67.68-67.72	44.1
Na_2O	0.2-1.4	-	0.91-6.62	-	3.2
K_2O	0.3-0.6	-	1.01-1.76	0.46-0.48	0.1
SO_3	-	-	-	2.16	-
P_2O_5	-	2	-	-	-
Cl^-	-	-	-	-	-
Cr_2O_3	-	-	1.12-15.85	0.12	-
ZnO	-	-	7.57-13.80	2.78-2.82	-

Table 3. Typical chemical compositions of selected slags

The iron content may even be recovered, as recently proposed by Yang et al.,⁷⁷ who produced an iron-poor, light coloured glass-ceramic, as an effect of melting in reducing conditions (coke added to the waste batch, with results conditioned by the CaO/SiO_2 ratio).⁷⁸

Zinc hydrometallurgy is another important source of iron-rich waste, as raw material for glass-based materials. The process yields solid waste with jarosite and goethite, as major crystalline phases, both containing Fe_2O_3 in excess of 50 wt%. The recovery of iron is complicated, due to the substantial traces of other oxides, notably silica and heavy metal oxides. Both iron-rich hydrometallurgy wastes have been successfully employed in glasses later transformed into marble-like glass-ceramics, by the adoption of a sinter-crystallisation approach,⁷⁹⁻⁸³ described later in detail.

A third example of iron-rich waste, from the primary production of a non-ferrous metal is that of 'red mud', i.e. the residue from the well-known 'Bayer process', applied to bauxite in order to separate pure aluminium hydroxide, in turn, exploited to obtain both alumina and aluminium. This residue has a limited quantity of glass-forming oxides; it was successfully used for both dense and porous glass-ceramics,⁸⁴ by transformation of waste-derived glasses (comprising red mud and other waste as raw materials) or by direct sintering.

Finally, we should consider tailings from the extraction of other metal ores. Residues from the extraction of tungsten,⁸⁵ gold,⁸⁶ or rare earth metals⁸⁷ were also used as starting materials in the production of glass and glass ceramics; they feature a high content of glass forming compounds, but as in the previous cases the presence of heavy metals represents an environmental problem. Obviously, this is true for residues from the extraction of the same heavy metals, such as Pb;⁷⁶ the decreasing use of heavy metals in many engineering applications, reduces the availability of 'new' waste, but it does not affect the amounts of waste produced in the past and not reused.

I.3 - Overview of glass-based products

I.3.1 - Glasses from the vitrification of inorganic waste

Vitrification generally consists in the transformation of the waste in a stable and homogeneous (silicate) glass, with the dissolution of the of hazardous waste components in the molten glass, at high temperatures; the components are then incorporated homogeneously into the vitreous structure following the cooling of the melt. This is due to the fundamental characteristics of glass when adequately formulated, such as the high chemical stability and the possibility to contain a huge variety of oxides.^{2,3} Mixing with minerals or already formed glasses (e.g. recycled glasses) is generally performed, if the composition of waste does not contain enough silica, essential for glass formation and chemical stability (low-silica glasses can be formed, but they may exhibit inferior durability). In some cases the stabilization does not rely on the dissolution of waste, but simply in the thermal destruction, associated to the high temperatures required by glass processing: as an example, asbestos-containing waste do not contain significant traces of heavy metal oxides, with vitrification recommended essentially for the dismantling of the characteristic, and highly hazardous, fibrous structure.²

The main advantages of vitrification can be summarised as follows:

- the flexibility of the process, which allows treating many types of waste, such as sludge, contaminated soil, ash, slag from hazardous processing, wet and dry solids in large and variable proportions;

- destruction of all organics (including the most toxic substances such as dioxins and furans) with an efficiency exceeding 99.99%;
- excellent stabilization of hazardous inorganic substances (such as heavy metals, radioactive elements, etc..) within the glassy network in ionic form; consequently, low environmental impact and possibility of landfill disposal without any problem, because any inorganic contaminant is retained permanently (any leakage of contaminants is so slow that no detectable adverse environmental effects are produced);
- substantial reduction in volume of the treated waste (from 20 to 97%, depending on the type of waste);
- good mechanical and thermal properties of the vitreous product;

The advantages of vitrification are somewhat compensated by significant drawbacks, such as the high costs of plants and the energy consumption.^{2, 3, 41, 88} The overall sustainability of the process is quite disputable if the economic advantage relies on avoided disposal costs. The previously mentioned asbestos-containing materials, for their intrinsically high hazardousness, justify the adoption even of the most expensive technologies, such as plasma heating.⁸⁹ Other wastes, on the contrary, are less likely to be vitrified, with a much less favourable cost/benefits balance, even in a perspective of rising landfilling costs (for the exhaustion of available landfill sites and the hostility of the people towards the opening of new ones).

Fruergaard et al.,⁹⁰ as an example, applied a life-cycle assessment (LCA) analysis to several scenarios for the treatment of air pollution control (APC) residues from incineration of municipal solid waste and found that vitrification, followed by landfilling, compared poorly with other management options (including direct landfilling without treatment, backfilling in salt mines, neutralization of waste acid, use as filler material in asphalt, etc.). The issues are represented by the environmental load with regard to GW (global warming potential), in turn greatly affected by the energy consumption (in the order of 700 kW·h per tonne of APC residue), and also by the HTw and HTs (human toxicity potential via water and via soil, respectively), due to air emissions especially of Sb, Hg and As associated with the thermal process. A higher energy efficiency and a good stabilisation of pollutants were claimed by Park et al.,⁹¹ who reported the vitrification of incinerator residues by a special combustion furnace, using Brown's gas (a stoichiometric hydrogen/oxygen mixture supplied by water electrolysis), but this has not been confirmed by further literature. Concerning plasma heating, Sobiecka and Szymanski⁹² found that the processing temperature and energy consumption could be decreased significantly, passing from the vitrification of municipal solid waste incinerator fly ash to engineered mixtures of fly ash and chromium-rich sewage sludge (CRSS); the content of CRSS, however, must be controlled, since the secondary waste may impair the chemical stability of the vitrified mass.

The cost/benefits balance may be much more favourable if the glass produced could provide extra revenue, by fabrication of high-value products. More precisely, any vitrification approach should be evaluated in the light of a complex economic balance: according to Gomez et al.⁹³ specifically discussing plasma heating, the avoidance of landfill charges, the added value of the reuse of the vitrified product, the energy production from syngas and the recovery of metals together improve the commercial viability of the process. The vitrified product is the principal output of the thermal process, being less sensitive to particular conditions (syngas is a combustible gas from transformation of organics, by pyrolysis, i.e. by thermal treatment in non-oxidative atmosphere, recognized as a more environmentally friendly technology than incineration due to the higher energy recovery efficiency;⁹⁴ molten metals may separate, at the bottom of glass furnaces, under reducing conditions).³

I.3.2 - Conventional glass-ceramic monoliths

Glass-ceramics represent a vast range of materials obtained by controlled crystallization of a glass of selected composition; the products usually possess outstanding properties, such as high hardness and mechanical strength, a thermal expansion coefficient adjustable over a wide range of values (from negative to more than $12 \times 10^{-6} \text{ }^\circ\text{C}^{-1}$), high refractoriness, high chemical durability and excellent dielectric properties. Almost pore-free articles, starting from an almost pore-free parent glasses, are easily achieved, differently from other ceramic systems.⁹⁵

The technology of controlled crystallisation has been applied to waste glasses since the early 1960s, soon after the discovery of the very first glass-ceramics.⁹⁵ As a consequence, the manufacturing of glass-ceramics must be considered as the most established valorisation way for inorganic waste, as supported by an extremely vast literature (an excellent review was provided by Boccaccini and Rawlings),⁶ and by extensive industrial production, under trade names such as ‘Slagsitalls’ and ‘Slagceram’.

Sheeted and pressed Slagsitalls have been produced for the last 50 years, with more than 20 billion square meters used in construction, chemical, mining and other branches of industry. The base glasses for both Slagsitalls and Slagceram products belong to the systems $\text{CaO-Al}_2\text{O}_3\text{-SiO}_2$ (C-A-S) and $\text{CaO-MgO-Al}_2\text{O}_3\text{-SiO}_2$ (C-M-A-S) (e.g. for Slagsitalls, $\text{SiO}_2 = 50\text{-}63 \text{ wt}\%$, $\text{Al}_2\text{O}_3 = 5\text{-}11\%$, $\text{CaO} = 23\text{-}30\%$, $\text{MgO} = 1\text{-}12\%$)^{6,7} and are obtained from slags of ferrous and non-ferrous metallurgy, ashes and waste from mining and chemical industries, with minor compositional adjustments with glass-forming oxides.

Quite constant glass compositions may be achieved by adjusting the ratios between different waste materials, when variations in the composition of single components occur; in any case, changes in the overall glass composition are tolerated, considering the nature of the crystal phases developed. Calcium silicate (wollastonite, $\text{CaO}\cdot\text{SiO}_2$) and calcium

feldspar (anorthite, $\text{CaO} \cdot \text{Al}_2\text{O}_3 \cdot 2\text{SiO}_2$) are generally the main crystal phases, with other silicates and alumino-silicates (pyroxenes, melilites, i.e. rather complex chain silicates, or gehlenite $2\text{CaO} \cdot \text{Al}_2\text{O}_3 \cdot \text{SiO}_2$ and its solid solutions), present as secondary phases. Depending on the composition, different ions may be accommodated in the same crystal, by formation of quite complex solid solutions (e.g. pyroxenes expressed by the general formula $\text{XY}(\text{Si,Al})_2\text{O}_6$, where $\text{X} = \text{Na}^+, \text{Ca}^{2+}, \text{Fe}^{2+}, \text{Mg}^{2+}$, etc. and $\text{Y} = \text{Mg}^{2+}, \text{Fe}^{2+}, \text{Fe}^{3+}, \text{Al}^{3+}, \text{Cr}^{3+}, \text{Ti}^{4+}$ etc.),⁹⁶ and the secondary phases may in some cases replace the main ones and vice versa.⁹⁵ The high percentage of crystals, distributed uniformly in the whole volume, with sizes varying from 0.1 to 1 μm , leads to good mechanical strength and excellent abrasion resistance.

The classical glass-ceramic technology relies on a double step heat treatment (often termed ‘ceramization’) of a previously formed glass object (shaped into the desired form). The treatment provides the nucleation of crystals within the base glass, favoured by the separation of some glass components, known as ‘nucleating agents’ (such as Ag or Au colloids, or oxides like TiO_2 and ZrO_2), and the crystal growth. The base glass is heated first to the temperature of maximum nucleation and then to the temperature of maximum crystal growth (slightly higher than the previous one), with a holding time at each temperature, before cooling.

For non-waste-derived glasses, the nucleating agents are intentionally added to the formulation of the base glass; a key feature of waste-derived glasses, on the contrary, is the availability of nucleating agents from the same starting waste stream. Some oxides, in fact, present limited solubility in glasses; dissolved in the base glass, they may easily separate upon ceramization. The most significant example is undoubtedly that of iron oxides. Karamanov and Pelino observed the dependence of crystallisation on the ratio $\text{Fe}^{3+}/\text{Fe}^{2+}$.^{80, 97} They showed that the crystallization of iron-rich glasses begins with the separation of small magnetite (Fe_3O_4) crystals, but the surface oxidation of Fe^{2+} to Fe^{3+} causes a change in the chemical composition, with the formation of hematite (Fe_2O_3), thus decreasing the total amount of crystal phase and changing the reaction order of the crystallization process.

Fe_2O_3 is also interesting for its interaction with sulfur: Suzuki et al.⁵⁵ showed that, due to the presence of Fe_2O_3 , sulfur and carbon, iron sulfide, FeS , could be formed and favour the precipitation of anorthite. Sulfides also control the colour of glass-ceramics: in Slagsitalls, the addition of ZnO turns the colour of glass-ceramics from greyish black, given by FeS or MnS , to white, due to the formation of ZnS (together with FeO or MnO).⁹⁵

I.3.3 - Glass-ceramic monoliths from alternative routes

The above-described nucleation/crystal growth step may be difficult to control and economically expensive. The overall costs may be reduced by the application of two distinct processes:

- i. petrurgic process,
- ii. sinter-crystallisation process.

The petrurgic process resembles the process of crystallisation of natural rocks.⁹⁸ In this process (applied since the 1970s, with the development of ‘Silceram’ ceramics from metallurgical slags),⁶ crystals nucleate and grow directly upon cooling of the glass melt, with an intermediate temperature holding stage, which can sometimes be avoided. As an example, Francis et al.⁹⁸ reported the feasibility of crystallisation upon controlled cooling (from 1 to 10 °C min⁻¹) of glasses obtained from mixtures of coal ash and soda lime glass melted at 1500 °C, without any intermediate step. Nominally, the process is not ‘glass-ceramic’, since the base material is not available as an actual glass (material below the transition temperature) at any stage, but keeps the concept of finely controlling the microstructure by control of the heat treatment conditions, particularly the cooling rate. More precisely, in the paper by Francis et al.⁹⁸ faster cooling rates are found to promote magnetite, with samples exhibiting magnetic properties, while slow cooling rates cause the formation of plagioclase and augite.

The sinter-crystallisation process, consisting of the viscous flow sintering of glass frits with concurrent crystallisation, is somewhat more refined. Originally applied for the first time during the 1970s, for the manufacturing of the well-known Japanese ‘Neoparies’ tiles (used in the building industry)⁹⁵ the process has been successfully transferred to the valorisation of waste glasses.^{99, 100} It specifically provides valid solutions to the usual drawbacks of waste-derived glass-ceramics developed by traditional processes, i.e. the control of defects and the visual appearance.

The removal of gas bubbles from the glass melt requires high temperatures and long holding times, i.e. a carefully controlled refining step during vitrification. This operation may be difficult with waste glasses, which are usually dark and feature a low thermal conductivity by radiation, due to the amount of heavy metals, with the risk of leaving many pores in the base glass, later ‘frozen’ by ceramization. Concerning the visual appearance, that of waste-derived glass-ceramics is generally rather inferior to that of natural stones and traditional ceramics.^{2, 3}

When applying the sintering route, there is no need to refine the melt before casting into a frit, thus reducing cost and gaseous emissions. In fact, the vitrification may be conducted in small plants and in particularly short times, favouring the immobilisation of components which could vaporise with longer heat treatments. The ground glass powder is subsequently pressed and heated to a certain temperature, at which viscous flow densification occurs together with crystallisation. The crystallisation, generally starting at the contact points between adjacent glass granules,¹⁰⁰ gives a pleasant visual appearance to the products (Fig. 1a). More significantly, a relatively high degree of crystallisation may be achieved in very short times, the surface of the glass is a preferred site for nucleation.¹⁰¹⁻¹⁰⁴

In general, ground glass is easier to devitrify than bulk glass with the same composition, so that nucleating agents are not needed. In some cases, the holding time at the sintering temperature may not exceed 30 min, being also accompanied by very fast heating rates (even ‘direct heating’ is possible, that is the direct insertion of glass powder compacts in the furnace directly at the sintering temperature), thus configuring a ‘fast sinter-crystallization’.¹⁰⁵ Pyroxenes, wollastonite and anorthite (with solid solutions) are very common crystal phases (Fig. 3.b). However, the remarkable nucleation activity of fine glass powders (<40 µm) has been found to enable the quite unusual precipitation of alkali feldspars and feldspathoids, such as sanidine and nepheline, as main crystal phases.^{106, 107}

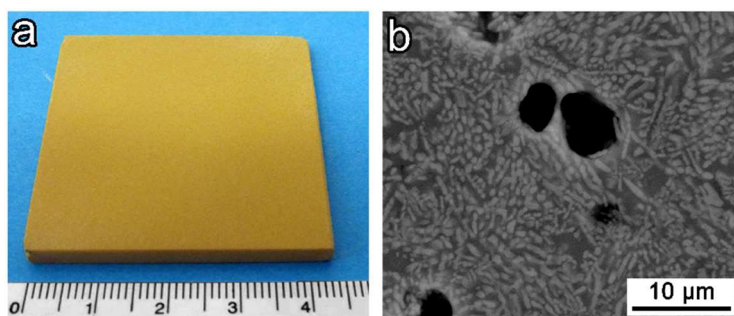


Figure 1. a) example of sintered glass-ceramic tile, obtained by use of powders <100 µm of a CAS glass (from the melting of a basalt rock/boron waste mixtures); b) example of the microstructure of a sintered glass-ceramic, with evidence of $\text{Ca}(\text{Mg,Zn})\text{Si}_2\text{O}_6$ pyroxene crystals.¹⁰⁸

The sinter-crystallisation process relies on a delicate balance between viscous flow sintering, surface crystallisation and even bulk crystallisation, i.e. crystallisation operated by the separation of components acting as nucleating agents. As shown in Figure 2, if the crystallisation at the glass surfaces is too intensive, the densification may be incomplete; on the contrary, for a glass not prone to surface crystallisation, the viscous flow sintering predominates, with the formation of a sintered glass body.

The viscous flow/crystallisation balance is sensitive to many conditions, e.g. the oxidation state and the heating rate. Starting from an iron-rich waste glass, Karamanov et al.¹⁰⁹ observed that the addition of C (1.5-2%) to the glass batch increased the magnetite phase and enhanced the crystallisation rate. Liu et al.¹¹⁰ found that iron oxidation, causing an increase of viscosity, reduced the crystal growth of silicates; this fact could be prevented by applying sintering in an inert (N_2) or reactive (CO) atmosphere. Bernardo et al.,⁸⁴ on the contrary, starting from a base waste glass with a low $\text{Fe}^{2+}/\text{Fe}^{3+}$ ratio, observed that magnetite was promoted by oxidation, more pronounced for fine glass powders (<40 µm) than for coarse ones (<80 µm). Karamanov et al.^{111, 112} reported that low heating rates favour bulk crystallisation, and sintering may be inhibited by the crystal phase, causing incomplete densification, whereas high heating rates favour sintering, with lower crystal phase formation, by reduction of glass surfaces.

It has been shown in many papers^{57, 84, 105-107} that, in the presence of fine glass powders (<40 μm), crystallisation may be achieved right at the temperature of the crystallisation exothermic peak in the DTA plot of the same powders. More recent investigations,¹¹³ however, highlighted that optimum crystallisation is achievable only if the crystallisation peak is located at a temperature suitably higher than that corresponding to the dilatometric softening point, i.e. the temperature at which viscous flow becomes appreciable.¹¹⁴ If the temperature difference is limited, the glass-ceramics obtained are remarkably porous (as illustrated by the lower part of Figure 2) and improvements in the densification are achievable only by increasing the sintering temperature and the heating rate.

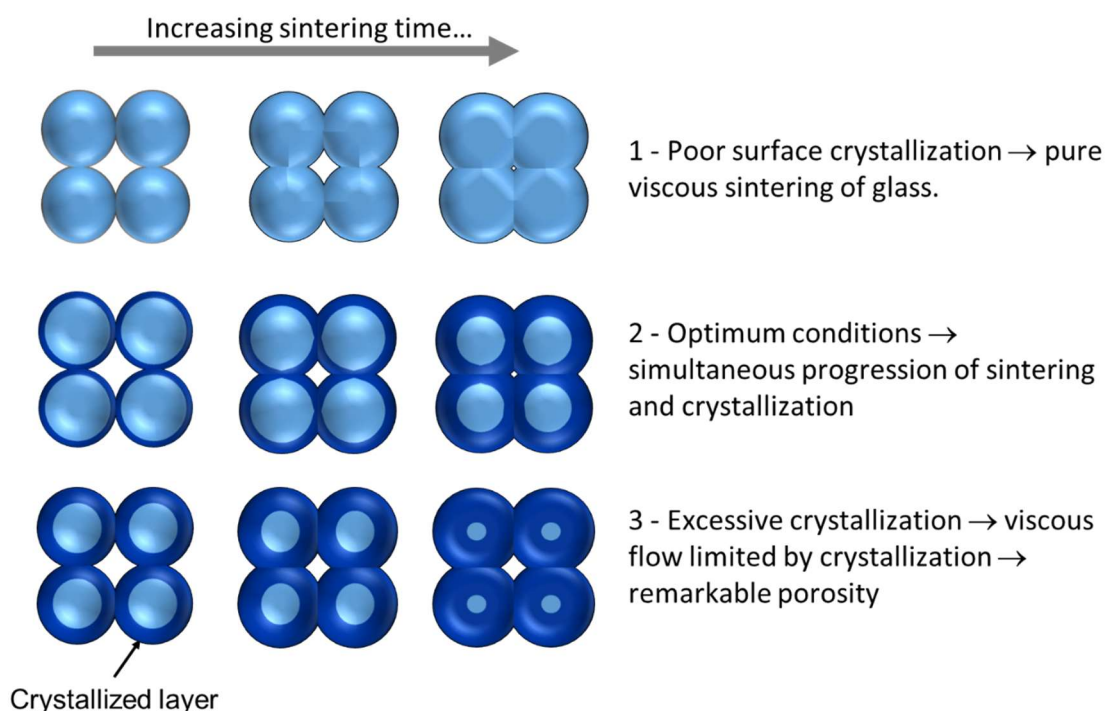


Figure 2. Schematic representation of the sinter-crystallisation process.

1.3.4 - Cellular glass-based materials

Cellular glasses generally offer high surface area, high permeability, low density, low specific heat, high thermal and acoustic insulation and high chemical resistance.¹¹⁵ When mostly closed-celled, they are referred to as ‘foams’.

In most cases, glass-based foams represent a further variant of glass sintering. If sinter-crystallised glass-ceramics depend on a delicate balance between viscous flow sintering and crystallisation, glass foams depend on a similarly delicate balance between viscous flow sintering and gas evolution. The crystallisation may occur as well, with contrasting effects, discussed later.¹¹⁶

Gas evolution depends on oxidation or decomposition reactions of additives mixed with glass powders.¹¹⁵ Oxidation reactions are in turn associated with the release of CO_x

gas (carbon monoxide or carbon dioxide) from C-containing compounds, e.g. carbon black, graphite, SiC, organic substances, reacting with oxygen from the atmosphere. Decomposition reactions are those provided by carbonates (mainly Na- and Ca-carbonates) or sulphates, leading to the release of CO₂ or SO_x; a particular variant comes from oxides of metals undergoing a transition from high to low valence state and releasing oxygen gas (e.g. MnO₂ being transformed into MnO).^{8, 115} Oxidation and decomposition may even overlap, as in the case of nitrides, being transformed into oxides and releasing nitrogen gas.¹¹⁵

Considering the difficulty of controlling both foaming and crystallisation of waste-derived glasses, the most suited starting materials for glass-based foams⁸ are the waste glasses (i.e. as previously discussed, ‘unemployed recycled glasses’) with limited tendency towards crystallisation. However, some crystals may form even in this case, owing to secondary reactions involving the glass and the additives. CRT glasses may form wollastonite (calcium silicate, CaSiO₃) or colloids of metallic lead, when foamed by decomposition of CaCO₃,⁶⁵ or by oxidation of SiC and TiN,^{116, 117} due to CaO/glass interaction ($\text{CaO} + \text{SiO}_{2(\text{glass})} \rightarrow \text{CaSiO}_3$) or reduction of PbO (yielding the oxygen necessary for the oxidation of carbides and nitrides). The crystallisation may be intentionally stimulated by using glass cullet mixed foaming agents as well as with glasses more prone to devitrification, waste-derived or not,^{118, 119} or directly with inorganic waste, mainly represented by fly ash.^{120, 121}

Foaming additives, such as SiC, may be quite expensive and have a negative impact on the overall cost/benefit balance. However, many recent investigations have demonstrated the effectiveness of foaming agents representing by themselves forms of inorganic waste. SiC could derive from the waste originated by the polishing of glass or traditional ceramics, i.e. a mixture of silicate residues (the abraded materials) and SiC (the abrasive medium),⁸ as well as from burned wastes of abrasive papers.¹²² Residues from glass polishing could consist of fine glass powders mixed with oil-based coolant;¹²³ also, in this case, the oxidation of the additive causes substantial foaming upon sintering. Carbonaceous residues, as foaming agents, may derive from common industrial waste, e.g. sawdust.¹²⁴ A further example is that of boron waste (mining residues from excavation of B-rich minerals), featuring a remarkable content of CaCO₃ and leading to foams with a complex distribution of crystal phases, when combined with soda-lime glass and clay.⁵⁸ ‘Mineral’ CaCO₃ can be replaced by ‘natural’ CaCO₃ in the form of egg-shell waste.¹⁶ It should be noted, in any case, that the foaming reaction must take place in a pyroplastic mass, determined by the softening of glass powders, with a specified viscosity (in the order of 10³–10⁵ Pa·s).¹¹⁵ While the decomposition of carbonates well matches with the softening of glasses from dismantled CRTs (known for their low characteristic temperatures),¹²⁵⁻¹³⁰ it may be more difficult to exploit with other glasses.

Special attention must be given again to iron oxides, in waste-derived glasses or slags. Fe₂O₃ (iron as Fe³⁺) is interesting for its reduction, at moderate temperatures (1000 °C),

into FeO (iron as Fe^{2+}) with the release of oxygen ($2 \text{Fe}_2\text{O}_3 \rightarrow 2 \text{FeO} + \text{O}_2$).¹³¹ The release is in turn exploited for foaming, both indirectly and directly. In the first case, the extra oxygen (in addition to that from the atmosphere) from Fe-rich glasses optimises the reaction of C-containing compounds or nitrides, as already done for the industrial process of commercial glass foams (the well-known Foamglas[®] by Pittsburgh Corning).¹³² In the second case, oxygen is by itself the foaming gas, as found by Appendino et al.¹³³ (condition known as ‘bloating’). The addition of soda-lime glass to waste-derived glass powders is currently under investigation in order to control the size and morphology of oxygen bubbles.¹⁰⁸ A fundamental alternative to iron-rich waste-derived glasses is provided by iron-rich minerals, such as basalt scoria (unemployed volcanic mineral)¹³⁴ (Fig. 5a), and metallurgical slags (e.g. slag from the refining of precious metals,¹³⁵ or from lead metallurgy, (see Fig. 3b). In the latter case, the crystallisation is proof of both glass/waste interaction and effectiveness of reduction (with hematite, Fe_2O_3 , available as major phase from the crystallisation of vitreous slag alone, replaced by calcium-iron silicates, with iron as Fe^{2+} , or magnetite, for glass/slag foams).

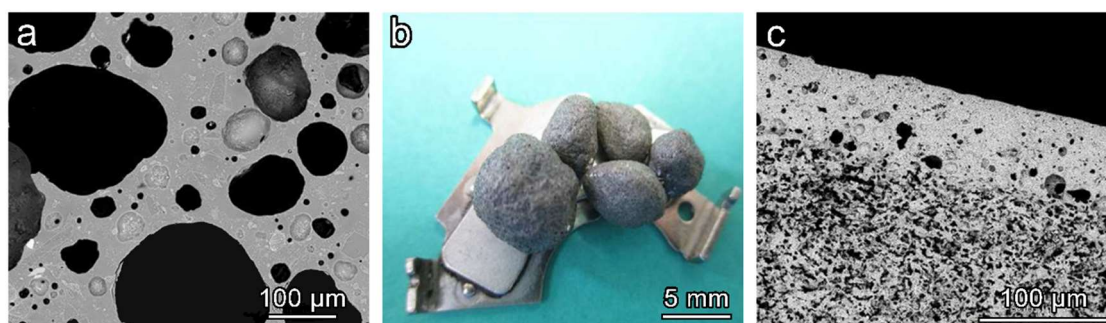


Figure 3. Examples of waste-derived porous glass-based materials: a) glass foam from cullet/basalt scoria mixture; b) magnetic glass foam granules from glass cullet/lead metallurgy slag attached to a permanent magnet; and c) example of layered glass-ceramic.

Substantial crystallisation, if negative for the development of highly porous foams, is an advantage for cellular structures, with open-cell morphology, with a process resembling that of crystalline ceramic foams, for which a three-dimensional, trabecular structure is templated by polyurethane (PU) sponges. The crystallisation of glass, deposited on the PU substrate, prevents collapse by viscous flow. As an alternative, sacrificial materials in the form of polymethylmethacrylate (PMMA) or polyethylene (PE) may be used to template the porosity: if the viscous flow of surrounding glass powder defines the cells, the cellular structure is again stabilized by the crystallization (a silicone resin may help as low-temperature binder, before sintering).^{59, 136}

I.3.5 - Hybrid glass-based materials

The viscous flow sintering approach can lead to monolithic materials with high Young's modulus, modulus of rupture, hardness and fracture toughness, suitable for structural applications, even avoiding the melting stage (at 1350-1400 °C), by sintering of mixtures comprising waste glasses, at moderate temperatures (generally not exceeding 1000-1100 °C). We can generally divide these materials into: (i) glass matrix composites; (ii) glass-ceramics from direct sintering; and (iii) hybrid glass-ceramics, from combinations of the first two classes.

The development of glass matrix composites from waste was pioneered by Boccaccini et al.¹³⁷ who reported the introduction of up to 20 vol% low-cost alumina platelets in a glass matrix developed by sintering borosilicate glass cullet mixed with fly ash. The particular reinforcement has been successfully proposed for other waste glasses, such as CRT glasses.¹³⁸ As in the case of glass foams, the additive can be a waste by itself, as shown by Ferraris et al.,¹³⁹ who reported the introduction of solid waste from an aluminium foundry. The concept of composites can also be transferred to glass foams, reinforced with particulates (e.g. TiO₂)¹⁴⁰ and fibres.^{141, 142} The foaming may be related to the nature of the reinforcement, operating with metal fibres (Hastelloy X fibres)¹⁴³ mixed with borosilicate glass, under microwave radiation. The fibres tips act as 'nucleating agents' for pores, since the higher local electric field strength in their vicinity, connected with their pronounced radius of curvature, enhances the power dissipation in the surrounding glass matrix, which overheats, releasing gasses. The metal fibres prevent cracking and disintegration of the composites during processing and favour the application of the cellular glass-based composites obtained as lightweight components for electromagnetic interference shielding.

Differently from composites, in which the mechanical properties are conditioned by a secondary phase, physically dispersed in a glass matrix (e.g. the brittleness of glass is reduced owing to crack deflection at glass/reinforcement interfaces or plastic deformation, in the case of metal reinforcement), glass-ceramics from direct sintering rely on the formation of silicate and alumino-silicate crystals, similar to those produced by crystallization of waste glasses. This fact supports the use of the term 'glass-ceramic', despite the absence of a vitrification step.^{3, 6}

In addition to the savings in energy required by the overall manufacturing process, direct sintering is advantageous for reducing the volatilization of some pollutants (e.g. fluorides);⁶ on the other hand, as previously stated, the products lack homogeneity, so that some pollutants could remain concentrated in some areas of the samples, although the leachability of sintered residues could be in any case lower than that of untreated waste (Zacco et al. specifically mention the viability of direct sintering of incinerator residues).³⁶ Finally, direct sintering can also be used for highly porous glass-ceramics,

with a glass phase originating from part of the waste or from fluxes, such as Na silicate and Na borate.^{128, 144-146}

‘Hybrid’ glass-ceramics are systems in which many features of the previously presented glass-based materials are successfully combined. As an example, platelets can be used as reinforcing phase both with waste-derived glasses unable to crystallize,¹⁴⁷ for glass matrix composites, as well as with glasses subjected to sinter-crystallisation, for glass-ceramic matrix composites: Bernardo et al.¹⁰⁶ prepared composites with a bending strength of 163 ± 14 MPa and a fracture toughness of 1.9 ± 0.1 MPa·m^{0.5}, by the addition of up to 15 vol% alumina platelets to a waste glass capable of sinter-crystallization and leading to a nepheline-based glass-ceramic matrix. Appendino et al.¹³³ and Aloisi et al.¹⁴⁸ found similar results with a glass from MSW incinerator fly ash mixed with alumina waste.

Layered glass-ceramics, object of more recent investigations, are even more complicated. They refer to a specific market need, in the field of building materials, i.e. that for lightweight tiles, with low water absorption (below 2%, for optimised frost resistance), to be placed vertically. Anchored to metal frames, in turn, fixed on main building walls, these tiles constitute the so-called ventilated façades. The air gap between the tiles and the wall contributes positively to the thermal insulation (minimising thermal losses, in winter, and minimising overheating, in summer). A solution may come from traditional porcelain stoneware tiles with an engineered porosity, but they are obtained by using expensive foaming agents (SiC, CeO₂; the foaming of porcelain stoneware must be matched with sintering, as in glass foams, but at much higher temperatures).¹⁴⁹ In layered glass-ceramics, a single-step treatment causes the direct sintering of a base body formed by a glass/waste mixture and the sinter-crystallisation of a glaze, obtained from a glass in turn derived from the same starting materials.^{150, 151} The high residual porosity (in the order of 30-35%), the high water absorption, the poor visual appearance and the limited chemical homogeneity of the base body are not significant issues, since mechanical strength, colour and stabilization of pollutants depend on the much denser glaze (the glazed side is the one to be exposed directly to the environment). Strength, colour and shrinkage of the glaze can be adjusted by using secondary phases and waste glasses. Vittrification of waste is reputed to be sustainable since it is applied only to a limited amount of starting materials; the single firing reduces the costs associated with the deposition of a glaze.

I.4 - Main properties of waste-derived glass-based materials

I.4.1 - Structural and functional properties

The replacement of natural stones, such as granite and marble, has been a fundamental aim of waste-derived glass-ceramics, since the 1960s, with the first examples of

Slagsitalls.⁹⁵ As discussed above, the process conditions (sinter-crystallization instead of conventional treatments, application of glazes) may provide a solution to the general problem of poor visual appearance or unpleasant colouration of waste-derived materials, compared with natural stones or high-quality traditional ceramics, like porcelain stoneware; the mechanical properties, on the contrary, have always been considered a strength of glass-ceramics compared with other materials.^{152, 153} Many authors claim that high strength materials are associated with the precipitation of very fine silicate and alumino-silicate crystals; just to cite some examples, Boccaccini et al.¹⁵⁴ showed an almost 3-fold increase of bending strength (from 90 to 240 MPa) and fracture toughness (from 0.6 to 1.7 MPa·m^{0.5}) for a glass-ceramic with respect to the parent glass, produced from vitrification of MSW ash; Oveçoglu¹⁵⁵ produced slag-based glass-ceramics with a high bending strength (>300 MPa) and excellent fracture toughness (5.2 MPa m^{0.5}); Peng et al.¹⁵⁶ demonstrated the feasibility of glass-ceramics with nano-sized crystals (<200 nm), from the controlled crystallization of a glass from high alumina coal fly ash. A collection of mechanical data is presented in the review paper by Rawlings et al.⁶

The strength data may lead to some misunderstandings. Brittle materials are well known for the sensitivity of strength on the dimension of samples; strength data (typically bending strength data), consequently must refer to samples with standardised dimensions. Alternative approaches correspond to the application of Weibull's statistics or to the assumption of a benchmark. In the first case, strength data of laboratory scale samples can be converted into strength data for samples of standardised dimensions, using scaling equations based on Weibull's modulus,¹⁵⁷ as done by Bernardo et al.⁵³ for glass-ceramics from vitrified sewage sludge pyrolysis residues, compared with traditional ceramics. In the second case, waste-derived glass-ceramics may be compared with traditional ceramics (the benchmark) using samples of the same dimensions.¹⁵⁸

The mechanical properties of highly porous glasses and glass-ceramics are generally expressed in terms of compressive strength, practically not sensitive to the dimension of samples (provided that the dimensions of test samples are adequately bigger than pore size, and buckling is avoided),¹⁵⁹ but they must be discussed in the light of the main applications, in the field of thermal and acoustic insulation. Figure 4 demonstrates that glass-based cellular materials can be considered as 'thermo-structural materials' for their distinctive combination of thermal properties and strength.

The thermal conductivity can be lowered (solution placed at the left of the trade-off curve) only operating with less stable polymeric foams; in fact, contrary to polymeric cellular materials, glass-based cellular materials are non-flammable and flame resistant, chemically inert and not toxic (even if waste-derived), rodent and insect resistant, bacteria resistant, water and vapour resistant.¹¹⁵ In selected cases, the thermal conductivity of glass-based cellular materials may be particularly low, in the order of 0.05 W mK⁻¹. Among stable, inorganic cellular materials (coloured 'bubbles' in Fig. 4), glass foams express the best compromise between low thermal conductivity and high specific strength

(ratio between compressive strength and density, of vital importance for lightweight components). As an example, ‘Misapor’ foams (commercial glass foams from recycled soda-lime glass foamed with SiC additive)¹⁶¹ represent a ‘non-dominated’ solution: with the same thermal conductivity, no material exists with a higher specific strength (or lower density/compressive strength ratio); with the same specific strength, no material exists with a lower thermal conductivity.

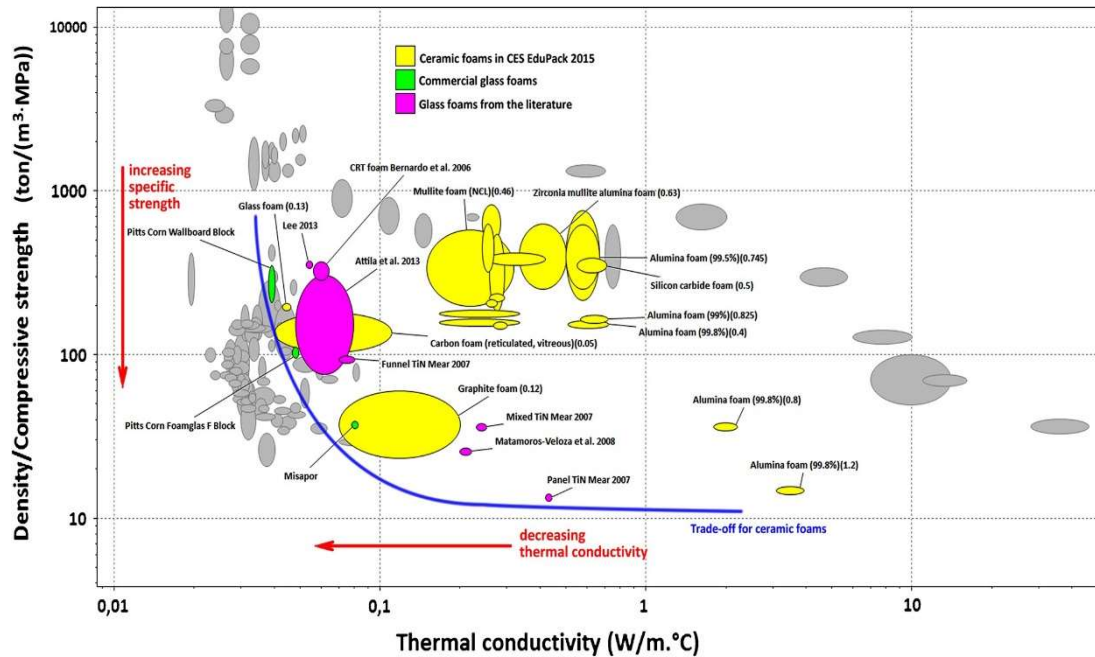


Figure 4. Specific strength-thermal conductivity trade-off plot for foams (non-ceramic foams are shown in grey colour) - figure and basic data derived from CES EduPack 2015 program package,¹⁶⁰ extra data inferred from the literature.^{123, 125, 161-163}

Most ceramic foams (in yellow in Fig. 4) are quite far from the trade-off curve; the superiority of glass foams can be justified on the basis of the distinctive closed-cell morphology. In general, the crushing strength of a cellular material derives from the bending strength of the solid, with a scaling factor in turn associated with the relative density (ρ_r , ratio between density of the porous body and density of the solid phase, or ‘true density’), according to the equation (derived from the well-known Ashby model):¹⁵⁹

$$\frac{\sigma_{cr}}{\sigma_{fs}} \approx 0.2(\phi\rho_r)^{3/2} + (1-\phi)\rho_r$$

where ϕ defines the fraction of solid at the cell edges ($1-\phi$ obviously stands for the fraction of solid at the cell faces), σ_{cr} is the compressive strength and σ_{fs} is the bending strength of the solid. A closed-cell morphology corresponds to a significant contribution from the linear term, absent for open-celled foams (or ‘sponges’, with $\phi = 1$). Any glass-based cellular material, however, is not ‘ideally closed-celled’ in its mechanical behaviour; in fact, if closed walls between adjacent pores are in turn porous, their

contribution to the strength is quite poor, despite the positive contribution to the minimization of thermal insulation; in addition, as brittle foams, porous glasses are subjected to a size effect, so that beyond differences in the distribution of solid phase between cell and faces (ϕ ratio), the strut strength increases with decreasing cell size; finally, pores without uniform shape and dimensions lead to low strength, as an effect of non-homogenous stress distribution (and local stress concentration).¹²⁵

The effect of partial crystallisation (in glass-ceramic foams) on crushing strength is not straightforward. On the one hand, it increases the bending strength of the solid phase (high strength foams are actually partially crystallised)^{118, 119} on the other hand; the crystallisation may strongly increase the apparent viscosity of the glass, limiting foaming and hindering the formation of well-defined, solid walls. In other words, potential improvements may be counterbalanced by the weakening effect of inhomogeneous microstructures.¹¹⁶ Surface nucleation is even enhanced with a porous body, owing to the higher specific surface: Bernardo¹²⁵ has shown that a foam from a given waste-derived glass reached the same crystallisation degree in 1 hour as a monolith in 2 hours at 880 °C.

I.4.2 - Magnetic properties

Iron-rich ceramic phases, such as magnetite and other ferrites (oxides with the general formula $M^{2+}Fe_2O_4$, or $M^{2+}O \cdot Fe_2O_3$; magnetite, Fe_3O_4 , may be expressed as $FeO \cdot Fe_2O_3$) are well known for their ferrimagnetic behaviour.¹⁶⁴ Considering the great availability of iron in waste-derived glasses, and the limited solubility of iron oxides in glasses, as stated above, it is not surprising to find ferrimagnetic phases in waste-derived glass-ceramics. The magnetic behaviour achieved may be tuned by changing composition, processing temperature, annealing time, particle size (for frit-derived glass-ceramics), heating and cooling rates.

Romero et al.⁹⁹ from a glass derived from the combination of goethite, dolomite and soda-lime glass cullet, found that the magnetic properties are directly correlated with the iron oxide: low concentrations (15.6-18 wt%) lead to a paramagnetic behaviour, with iron ions distributed in solid solutions, whereas high concentrations (18.4-25.8 wt%), exceeding the solubility limit, lead to the precipitation of magnetite particles (Fe_3O_4). The magnetic clusters obtained, provide a superparamagnetic behaviour, but the behaviour may turn into ferrimagnetic when the precipitates are close enough to exhibit fully magnetic behaviour (iron oxide content above 22.9 wt%).

Min'ko et al.¹⁶⁵ studied the separation of magnetite in more detail. The crystallisation of magnetite particles may take place at relatively low temperature, starting from 700–800 °C; higher temperatures favour the formation of non-magnetic species and the magnetic susceptibility decreases. This was confirmed by Francis,¹⁶⁶ who studied the annealing of a glass, from the melting of furnace slag and flue dust, for 2 h at 800 to 1000 °C, and found that saturation magnetisation decreases as a consequence of the

transformation of the magnetic species (magnetite or γ -maghemite) into non-magnetic phases. The magnetic susceptibility is also maximized for smaller particle sizes: as an example, Lorenzi et al.,⁷¹ who used dust from an electrostatic precipitator as iron source (combined with glass cullet), obtained a ferromagnetic material after direct casting of the melt and explained the increase of saturation magnetization in terms of higher content of ferrimagnetic species (magnetite/maghemite) and a peculiar size distribution of the particles (nanometric or micrometric crystals) within the samples.

The energy losses associated with hysteresis cycles of ferro- and ferrimagnetic materials may lead to substantial heating of samples under alternating magnetic field, as widely shown for iron-containing biocompatible glass-ceramics, generally exploited for hyperthermia cancer therapy.¹⁶⁷ The concept of indirect heating has been applied even to iron-rich waste-derived glass-ceramics, for the same medical application or not. In fact, Abbasi et al.¹⁶⁸ obtained a biocompatible glass-ceramic material from the direct sintering of soda-lime-silica waste glass and strontium hexaferrite particles: with an optimised hexaferrite content of 20 wt%, the energy loss could exceed $75000 \text{ erg}\cdot\text{g}^{-1}$, in agreement with the requirements of hypothermia therapy. As an alternative, Ponsot et al.,⁷⁶ obtained ferrimagnetic glass-ceramics from the sintering of borosilicate waste glass with iron-rich slags (from copper and lead metallurgy), reaching high temperatures (exceeding $300 \text{ }^\circ\text{C}$) after the application of an alternating magnetic field for very limited times (60 s), that could be good candidates for innovative heating elements (e.g. in cooking tops), considering the resistance to thermal shock (no cracks are developed upon sudden cooling, as an effect of the low expansion coefficient of the borosilicate glass matrix) and the chemical stability (confirmed by cytotoxicity studies). Further applications, e.g. in the field of electromagnetic shielding (the energy losses associated with magnetisation hysteresis could be exploited to reduce the intensity of low-frequency electromagnetic waves).¹⁶⁹

I.4.3 – Electric properties

Like most glasses, waste-derived glasses exhibit low electronic conductivity; the overall electric conductivity and the polarizability, however, are conditioned by the ionic mobility.¹⁷⁰ Saccani et al.¹⁷¹ studied the electrical behaviour of different glasses derived from the melting of municipal solid waste incinerator grate ash and soda-lime cullet and observed that with increasing content of incinerator waste the electrical conductivity decreased (conductivity below $10^{-14} \text{ S}\cdot\text{cm}^{-1}$ at room temperatures), as a consequence of increased content of alkaline-earth ions, strengthening the silicate network and hindering the motion of alkali metal ions. This is accompanied by low values of dielectric permittivity and loss factor as well as by significant chemical durability, so that the materials developed could be a valid alternative to E-glass (for fibres) for insulators. Similar results were described by Elalaily et al.,¹⁷² who reported a conductivity of about

$10^{-8} \text{ S}\cdot\text{cm}^{-1}$ (at room temperatures) for glasses derived from blast furnace slag, that could be increased significantly by γ -irradiation, as a consequence of an increasing number of vacancies and vacancy interstitials recombining or migrating to the glass surface.

The multiple valence states of iron (Fe^{2+} , Fe^{3+}) represent a fundamental factor for the conductivity of waste-derived glasses, as evidenced by Min'ko et al.,¹⁷³ on glasses prepared using mining overburden (sand, chalk, marl and crystalline shale) and ore-dressing wastes of iron quartzite. A wide range of electrical resistivity (1011–1014 $\Omega\cdot\text{cm}$) may be achieved, depending on the ratio $\text{Fe}^{3+}/\text{Fe}^{2+}$ (Fe^{3+} acts as glass former so that it favours high resistivity). In a more recent study¹⁶⁵ the same authors, using the same raw materials, showed that crystallisation had a dramatic impact on electrical properties, passing from magnetite to pyroxene with increasing annealing temperature. A maximum conductivity of $4.1 \times 10^{-5} \text{ S}\cdot\text{m}^{-1}$ was detected at 800 °C, in the presence of magnetite precipitates.

Lorenzi et al.⁷¹ recently reported that iron-rich glasses may lead to glass-ceramics with low electrical resistivity, in the order of 20 $\Omega\cdot\text{m}$, attributed to the fact that iron oxide nanoclusters, when their density exceeds a certain threshold value, can give rise to percolation effects that can strongly reduce the resistivity of the material, up to values that make it suitable for applications in antistatic surfaces.

I.4.4 - Other properties

A high infrared radiance glass-ceramic was obtained by Wang et al.¹⁷⁴ using coal fly ash and titanium slag with MgCO_3 additives. They studied the nucleation and the crystallisation process and concluded that enhanced infrared radiance performance was achieved due the iron impurities of the initial materials, leading to the formation of iron-substituted cordierite ($\text{Mg, Fe}_2\text{Al}_4\text{Si}_5\text{O}_{18}$). The specific phase, even non-substituted, is effectively interesting for its emissivity,¹⁷⁵ which could be exploited for panels placed in building façades heavily exposed to the sun, in order to minimize the absorbed heat (at least a small fraction of radiation, in an opaque material, is not reflected) and the consequent so-called 'heating island effect'.¹⁷⁶

An open-celled glass foam (open porosity exceeding 70%), coated with TiO_2 , prepared by Lebullenger et al.¹⁷⁹ using glass waste from the automobile industry mixed with AlN , recently exhibited significant potential for photo-catalysis. In particular, foam glasses with specific coatings may present photocatalytic activity in the UV region and can be used for toluene decomposition in the gas phase, as an alternative to cellulose/titania commercial supports, with the fundamental advantage of being more easily reusable (the restoration of photocatalysis power, by heat treatment or any other cleaning process, is obviously more difficult to realize with an organic support).

Additional catalytic supports were developed by Dominguez et al.,¹⁷⁷ who developed reticulated ceramic foams by replication of sacrificial PU templates with slurries

comprising waste glass, dust and reduction slag from stainless steel production and Portland cement. The catalytic activity (particularly for the CO oxidation reaction) was due to the application of coatings consisting of Al_2O_3 , CeO_2 and gold, but the metal content of the wastes was found to have a positive influence on the activity of the foams. Glass-ceramic foams, developed in a similar way and featuring the separation of iron oxide phases, considering the well-known activity of these compounds (particularly in thermochemical water splitting)¹⁷⁸ could constitute an interesting extension of the approach.

Highly porous materials from the sintering of glass mixed with as received or weathered volcanic ash may constitute valid humidity control devices, as shown by Vu et al.¹⁷⁹ The characteristic low temperatures (not exceeding 820 °C) required by viscous flow sintering of glass make it a good ‘glue’ for minerals from volcanic ash. Hydrated alumino-silicates with distinctive moisture retention (mordenite and allophane) did not decompose completely, keeping a substantial micro-porosity, despite infiltration of softened glass. As an example, a mixture comprising 30 wt% weathered volcanic ash and 70 wt% waste glass, sintered at 800 °C, with a holding time of only 5 min, led to ceramics with a BET surface area and porosity exceeding $160 \text{ m}^2 \cdot \text{g}^{-1}$ and 50%, respectively, with a pore size of approximately 9 nm in diameter.

I.5 - Methodology

A new technique for the production of glass foams to obtain thermal insulator materials was developed and constituted a fundamental focus of the PhD studies; it consists in a combination of the alkali-activation of glass waste and gel casting. The new process is less expensive and more environmentally sustainable than the current procedures based on glass powders mixed with foaming agents, which decompose and release gases at a temperature well exceeding the softening glass point.

The new approach to glass foams implies a substantial revision of the foaming process, starting from alkali activation of soda-lime glass powders. The alkali-activation is receiving growing interest in the fields of ceramics. Usual alkali-activated materials, generally known as ‘geopolymers’, are produced through the reaction of an alumino-silicate raw material with an alkaline compound, which is typically a concentrated aqueous solution of alkali hydroxide or silicate.¹⁸⁰ The dissolution of the alumino-silicate component determines the release of ‘inorganic oligomers’ (molecules with few Si^{4+} and Al^{3+} ions mutually bonded by bridging oxygens, with OH terminations) in the aqueous solution, later subjected to condensation reactions, with water release and formation of a gel at low temperature (room temperature or typically a temperature below 100 °C). Alumino-silicate raw materials, such as metakaolin, are known to yield to a ‘zeolite-like’ gel, consisting of a continuous, three-dimensional alumino-silicate network, amorphous or crystalline.¹⁸⁰ The network features the bridging of $[\text{SiO}_4]$ and $[\text{AlO}_4]$ tetrahedra, the

latter being formed by the presence of alkali ions in the surrounding spaces, for the charge compensation. The alkali ions remain substantially ‘trapped’ in the alumino-silicate network, for an optimum $\text{Al}_2\text{O}_3/\text{SiO}_2$ balance in the raw materials, with the achievement of chemically stable products. The stability is further confirmed by the possible entrapment of pollutants, starting from industrial by-products as part of the raw materials.¹⁸¹

It should be noted that the formation of a gel is possible even from formulations with different $\text{Al}_2\text{O}_3/\text{SiO}_2$ balances; as an example, CaO-rich formulations do not yield to a ‘zeolite-like’ gel, but provide a condensation product that could be termed ‘tobermorite-like’ gel, given the analogy with the products of cement hydration.¹⁸⁰ The term ‘inorganic polymer’ may be used to identify the products, independently from the structure.¹⁸²

The concept of alkali activation and ‘inorganic polymerisation’ is open also to glasses, as raw materials. Glasses with engineered chemical composition (alumino-silicate glasses) can be used as precursors for geopolymer-like materials¹⁸³⁻¹⁸⁵ which can then be employed as new binders in the building industry, thanks to the formation of sodium alumino-silicate hydrate (N-A-S-H) and calcium alumino-silicate hydrate (C-A-S-H) gels. With proper molecular balances between different oxides, both strength and chemical stability are maximised. Recycled glass can be used as a component of mixtures yielding geopolymers,¹⁸⁶⁻¹⁸⁸ if a zeolite-like gel is not the target, soda lime-glass cullet, activated with sodium or potassium hydroxide solutions, can be used as the only component. The so-obtained ‘glass-based mortars’, cured at 40-60 °C, achieve good mechanical strength (e.g. compressive strength of 50 MPa), but limited durability.¹⁸⁹

The alkali activation of the silica-rich material allows the realisation of well-dispersed concentrated suspensions, undergoing gelation by treatment at low temperature (40-80°C), owing to the formation of silicate hydrates. The formation of the cellular structure is obtained by the entrapment of air at the first stages of gelification, by mechanical stirring with the support of a surfactant. The obtained wet foam is stabilised by the progressive hardening (‘gelation’) of the starting slurry.

However, the alkali-activated silicate gels based on waste glass powder, when exposed to water, showed a high solubility, with the leaching of alkali ions that compromise the durability of these materials. For this reason, a sintering treatment, at relatively low temperature, was finally applied to stabilise the hardened foams, regarding leaching of alkaline ions.^{190, 191}

The production of glass foams by this innovative process was initially optimised for waste glass cullet (Chapter II). The method is more environmentally friendly as it does not need a previous melting step to adjust the composition, uses lower temperatures in the stabilisation process and avoids the use of foaming agents that decompose with the production of CO_2 . This foaming agents are usually expensive and need an inconvenient milling step; replacing them with a surfactant, these problems are avoided.

Furthermore, the process is easier to control, leading to more flexibility in the production, as the final properties of the product are not correlated with the composition of the starting raw materials. The approach proved to be extendible to different glasses and industrial waste mixtures leading to different gels after alkali activation (Chapters III and IV). For this reason, the alkali activation of soda-lime waste glass was exploited through mixing with iron-rich inorganic waste from a copper slag and fly ash from coal combustion. The approach was also extended to different glass-based material coming from waste, such as an alumino-boro-silicate glass from the recycling of pharmaceutical vials and vitrified bottom ashes from municipal solid waste incinerators.

Apart from waste-derived materials and applications in the building industry, the technique was also applied to create highly porous bioactive glass-ceramics scaffolds (Chapter V); the successful production of highly homogeneous foams can be seen as a proof of versatility within the approach.

A considerable number of processing parameters combinations (such as surfactants, activating solution, curing times, conditions for heating treatments etc.) were explored and studied, and a similar production route was followed to prepare all glass-ceramic foams using the innovative technique for all the compositions studied.

The original raw materials, when received as small fragments, were firstly ground into fine powders using dry ball milling (Pulverisette 7 planetary ball mill, Fritsch, Idar-Oberstein, Germany) and then were manually sieved; only particles with a diameter below 75 μm were kept.

Fine powders of the different raw materials were placed in a NaOH or KOH (reagent grade, Sigma – Aldrich, Gillingham, UK), aqueous solution 2-5M for a solid loading from 60-70 wt%. The glass powders were subjected to alkaline attack for 1-4 hours, under low-speed mechanical stirring. (500 rpm; ArgoLab AM 20-D mixer, Test Srl, Perugia, Italy).

Silica-rich materials are soluble in an alkaline media and in low basic conditions (pH < 11) the formation of silicate ions is in equilibrium with the solid phase. However, at values higher than 11, the amorphous silica in the solid phase dissolves to form a soluble silicate.^{192, 193} However, major obstacles were slow dissolution and reactivity, which could be overcome by selecting small particle sizes together with long reaction times.

Clearly, high alkali concentrations would lead to higher dissolution rates, but they would compromise the economic viability of the process. A weak alkali activation strategy was followed (molarities between 2-5M were studied) as its only purpose is to dissolve the initial components partially, in order to produce the silicate and aluminate ions and cause their gelification in a sufficient extent to change the rheology of the suspension.

Afterwards, the obtained activated suspensions were cast in closed polystyrene cylindrical moulds (60 mm diameter) and cured at low temperature (40-75 °C). Different curing times were tested according to the different compositions, in this stage the

condensation reactions between the ‘inorganic oligomers’ take place, with the formation of a gel, leading to a noticeable increase in the suspension viscosity by the formation of calcium alumino-silicate hydrate (C-S-H), sodium alumino-silicate hydrate (N-A-S-H) and calcium alumino-silicate hydrate (C-A-S-H).¹⁹⁴

The gelified suspensions at different curing times were foamed with the help of a surfactant by vigorous mechanical mixing (2000 rpm; ArgoLab AM 20-D mixer, Test Srl, Perugia, Italy). Different surfactants were studied; non-ionic surfactants that do not interfere with ceramic dispersions¹⁹⁵ such as Triton X-100 (polyoxyethylene octyl phenyl ether; $C_{14}H_{22}O(C_2H_4O)_n$, $n = 9-10$, Sigma-Aldrich, Gillingham, UK); and Tween-80 (Polyethylene glycol sorbitan monooleate; $C_{32}H_{60}O_{10}$; Sigma-Aldrich, Gillingham, UK) or an inexpensive ionic surfactant; sodium dodecyl sulphate (SLS; $(CH_3(CH_2)_{11}OSO_3Na$ (Carlo Erba, Cornaredo, Milan, Italy) that was prepared in an aqueous solution 1/10 in weight.

The surfactants were always added in an 4 wt% as this amount is considered to be in high excess. Therefore the amount of surfactant added is not a parameter that influences the foaming process.

Foamed gels were kept in the same moulds at 40-80 °C for 24-48 h, for curing and completing the hardening of wet foams, before being demoulded. Finally, 60 mm diameter hardened foamed gels were fired at temperatures between 800 and 1000 °C, with 1h holding time, and heating rates from 1-10 °C/min were investigated.

A schematic representation of the process can be seen in Figure 5.

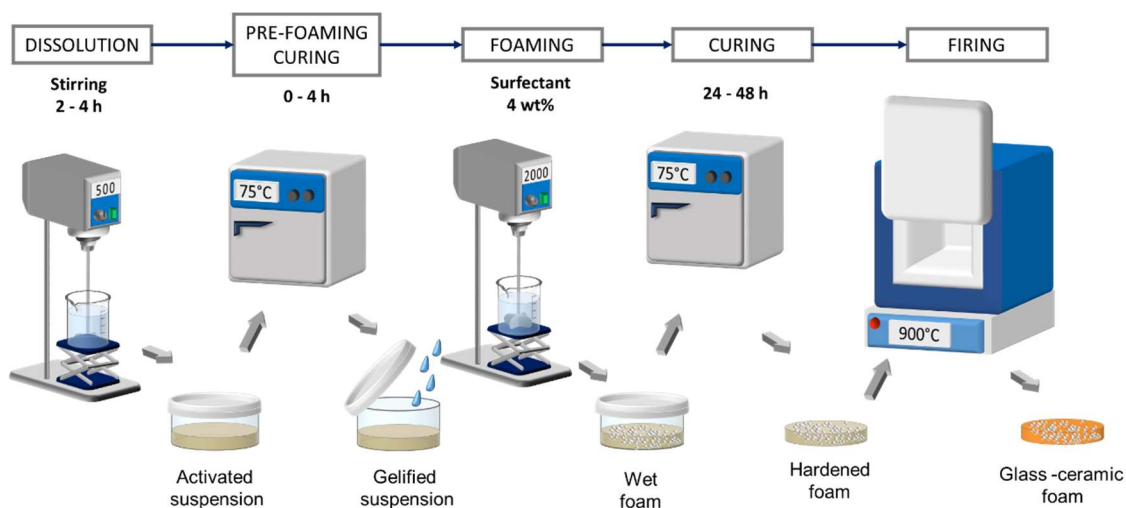


Figure 5. Processing scheme for the production of glass-ceramic foams by the combination of alkali activation, gel casting and sintering.

The progressive hardening associated with inorganic polymerisation configuring an ‘inorganic gel casting’ has also been used to produce advanced ceramics, such as mullite and cordierite foams and scaffolds described in Chapter VI. These materials were obtained through the thermal treatment of engineered alkali activated suspensions

consisting of a Na-geopolymer enriched with reactive γ - Al_2O_3 powders in the case of mullite, and reactive γ - Al_2O_3 and talc in the synthesis of cordierite. The gelification was studied in order to have a proper viscosity for trapping air during vigorous mechanical stirring or maintaining the shape of the scaffold struts derived from direct ink writing. After the hardened samples were obtained, sodium ions were extracted through ion exchange in ammonium nitrate solution. Finally, the ion-exchanged foams were successfully converted into pure mullite or cordierite foams and scaffolds with the application of a firing treatment.

A distinctive character of waste glasses is the transformation into glass-ceramics through crystallisation, favoured by specific compositions (glasses of the $\text{CaO-Al}_2\text{O}_3\text{-Fe}_2\text{O}_3\text{-SiO}_2$ system), overlapping with viscous flow sintering (sinter-crystallisation). The significant increase of viscosity due to crystallisation was found helpful, for foams from alkali activation and mechanical foaming, in maintaining the open-celled structure developed at low temperature.

The sinter-crystallisation was the basis for the manufacturing of glass-ceramic proppants, useful for oil extraction. Prototypes were obtained according to a 'spheroidisation technique' previously developed at the University of Padova, consisting in the casting of fine glass powders (together with a liquid binder) on a rotary drum, before firing.

The spheroidisation actually opened the way to new glass-ceramic materials for thermal and acoustic insulation, in the form of granules. Hardened suspensions of soda-lime glass, after the above described alkaline activation, were reduced into fragments and cast on a rotary drum with dry glass. The firing of green granules was accompanied by a significant foaming, through decomposition of hydrated compounds. These alternative conformation techniques are described in Chapter VII.

I.6 - Characterization techniques

All the studied systems were characterised using some common techniques and applying the same methodology in the sample characterisation. The standard procedure used in the characterisation is described in the following paragraphs. Additional tests were carried out in the different systems as needed to understand the process fully, and they are explained in each chapter.

Selected samples were subjected to thermogravimetric analysis (TGA, STA409, Netzsch Gerätebau GmbH, Selb, Germany) operated at $10\text{ }^\circ\text{C}/\text{min}$ in static air from room temperature up to $1000\text{ }^\circ\text{C}$. Fourier-transform infrared spectroscopy (FTIR, FTIR model 2000, Perkin Elmer Waltham, MA) was conducted on solid discs (with 13 mm diameter), prepared by mixing $\approx 1\text{ wt}\%$ (2 mg dispersed in 200 mg of KBr) from the finely powdered sample with KBr operating in absorbance mode with a 4 cm^{-1} resolution for 32 scans in the $4500\text{--}400\text{ cm}^{-1}$ region.

The morphological and microstructural characterisations were performed with optical stereomicroscopy (AxioCam ERc 5s Microscope Camera, Carl Zeiss Microscopy, Thornwood, New York, US) and scanning electron microscopy (FEI Quanta 200 ESEM, Eindhoven, The Netherlands). The pore size distribution of the foams was evaluated by means of image analysis using the Image J software.

The mineralogical analysis was conducted by X-Ray Diffraction analysis (XRD) on powdered samples (Bruker D8 Advance, Karlsruhe, Germany – CuK α radiation, 0.15418 nm, 40 kV–40 mA, $2\theta = 10\text{--}70^\circ$, step size 0.05° , 2 s counting time). The phase identification was performed with the Match![®] software suite (Crystal Impact GbR, Bonn, Germany), supported by data from PDF-2 database (ICDD-International Centre for Diffraction Data, Newtown Square, PA).

The geometric density (ρ_g) of fired foams was evaluated by considering the mass to volume ratio. The apparent (ρ_a) and true density (ρ_t) were measured using a helium pycnometer (Micromeritics AccuPyc 1330, Norcross, GA), operating on bulk or finely crushed samples, respectively. The three density values (ρ_g , ρ_a , and ρ_t) were used to compute the amounts of open and closed porosity.¹⁹⁶

The obtained foams were subjected to compression tests by using an Instron 1121 UTS (Instron, Danvers, MA) machine, with a crosshead speed of 1 mm/min, employing samples of about 10 mm \times 10 mm \times 10 mm, cut out from larger specimens (each data point corresponding to 10-12 samples).

References

- 1 Chartier, Y. (Ed.). (2014). *Safe management of wastes from health-care activities*. World Health Organization.
- 2 Bernardo, E., Scarinci, G., & Colombo, P. (2012). Vitrification of waste and reuse of waste-derived glass. In *Encyclopedia of Sustainability Science and Technology* (pp. 11581-11613). Springer, New York, NY.
- 3 Colombo, P., Brusatin, G., Bernardo, E., & Scarinci, G. (2003). Inertization and reuse of waste materials by vitrification and fabrication of glass-based products. *Current Opinion in Solid State and Materials Science*, 7(3), 225-239.
- 4 Ferraris, M., Salvo, M., Ventrella, A., Buzzi, L., & Veglia, M. (2009). Use of vitrified MSWI bottom ashes for concrete production. *Waste Management*, 29(3), 1041-1047.
- 5 Bassani, M., Santagata, E., Baglieri, O., Ferraris, M., Salvo, M., & Ventrella, A. (2009). Use of vitrified bottom ashes of municipal solid waste incinerators in bituminous mixtures in substitution of natural sands. *Advances in Applied Ceramics*, 108(1), 33-43.
- 6 Rawlings, R. D., Wu, J. P., & Boccaccini, A. R. (2006). Glass-ceramics: their production from wastes—a review. *Journal of Materials Science*, 41(3), 733-761.

- 7 Chinnam, R. K., Francis, A. A., Will, J., Bernardo, E., & Boccaccini, A. R. (2013). Functional glasses and glass-ceramics derived from iron rich waste and combination of industrial residues. *Journal of Non-Crystalline Solids*, 365, 63-74.
- 8 Bernardo, E., Cedro, R., Florean, M., & Hreglich, S. (2007). Reutilization and stabilization of wastes by the production of glass foams. *Ceramics International*, 33(6), 963-968.
- 9 Butler, J., & Hooper, P. (2005). Dilemmas in optimising the environmental benefit from recycling: A case study of glass container waste management in the UK. *Resources, Conservation and Recycling*, 45(4), 331-355.
- 10 Vellini, M., & Savioli, M. (2009). Energy and environmental analysis of glass container production and recycling. *Energy*, 34(12), 2137-2143.
- 11 Meylan, G., Ami, H., & Spoerri, A. (2014). Transitions of municipal solid waste management. Part II: Hybrid life cycle assessment of Swiss glass-packaging disposal. *Resources, Conservation and Recycling*, 86, 16-27.
- 12 The European Container Glass Federation (FEVE) Environmental, social and economic contribution of the Container Glass sector in Europe Final Report (February 2015).
- 13 2008 Review of Directive 2002/96 on Waste Electrical and Electronic Equipment (WEEE), Final Report (August 2007)
- 14 Bernardo, E., Scarinci, G., Hreglich, S., & Zangiacomi, G. (2007). Effect of time and furnace atmosphere on the sintering of glasses from dismantled cathode ray tubes. *Journal of the European Ceramic Society*, 27(2-3), 1637-1643.
- 15 Andreola, F., Barbieri, L., Corradi, A., Lancellotti, I., Falcone, R., & Hreglich, S. (2005). Glass-ceramics obtained by the recycling of end of life cathode ray tubes glasses. *Waste Management*, 25(2), 183-189.
- 16 Mugoni, C., Montorsi, M., Siligardi, C., Andreola, F., Lancellotti, I., Bernardo, E., & Barbieri, L. (2015). Design of glass foams with low environmental impact. *Ceramics International*, 41(3), 3400-3408.
- 17 Lin, K. L., Chang, W. K., Chang, T. C., Lee, C. H., & Lin, C. H. (2009). Recycling thin film transistor liquid crystal display (TFT-LCD) waste glass produced as glass-ceramics. *Journal of Cleaner Production*, 17(16), 1499-1503.
- 18 Fan, C. S., & Li, K. C. (2014). Glass-ceramics produced from thin-film transistor liquid-crystal display waste glass and blast oxygen furnace slag. *Ceramics International*, 40(5), 7117-7123.
- 19 Lee, C. T. (2013). Production of alumino-borosilicate foamed glass body from waste LCD glass. *Journal of Industrial and Engineering Chemistry*, 19(6), 1916-1925.
- 20 Bernardo, E., & Scarinci, G. (2004). Sintering behaviour and mechanical properties of Al₂O₃ platelet-reinforced glass matrix composites obtained by powder technology. *Ceramics international*, 30(5), 785-791.
- 21 Rocchetti, L., & Beolchini, F. (2014). Environmental burdens in the management of end-of-life cathode ray tubes. *Waste management*, 34(2), 468-474.
- 22 Cox, M., Nugteren, H., & Janssen-Jurkovičová, M. (Eds.). (2008). *Combustion residues: current, novel and renewable applications*. John Wiley & Sons.
- 23 Mohapatra, R., & Rao, J. R. (2001). Some aspects of characterisation, utilisation and environmental effects of fly ash. *Journal of Chemical Technology & Biotechnology: International Research in Process, Environmental & Clean Technology*, 76(1), 9-26.

- 24 Erol, M., Küçükbayrak, S., & Ersoy-Meriçboyu, A. (2007). Characterization of coal fly ash for possible utilization in glass production. *Fuel*, 86(5-6), 706-714.
- 25 Erol, M., Küçükbayrak, S., & Ersoy-Meriçboyu, A. (2008). Comparison of the properties of glass, glass-ceramic and ceramic materials produced from coal fly ash. *Journal of Hazardous Materials*, 153(1-2), 418-425.
- 26 Leroy, C., Ferro, M. C., Monteiro, R. C. C., & Fernandes, M. H. V. (2001). Production of glass-ceramics from coal ashes. *Journal of the European Ceramic Society*, 21(2), 195-202.
- 27 Zhang, J., Dong, W., Li, J., Qiao, L., Zheng, J., & Sheng, J. (2007). Utilization of coal fly ash in the glass-ceramic production. *Journal of hazardous materials*, 149(2), 523-526.
- 28 Park, J. S., Taniguchi, S., & Park, Y. J. (2009). Alkali borosilicate glass by fly ash from a coal-fired power plant. *Chemosphere*, 74(2), 320-324.
- 29 Barbieri, L., Manfredini, T., Queralt, I., Rincón, J. M., & Romero, M. (1997). Vitrification of fly ash from thermal power stations. *Glass technology*, 38(5), 165-170.
- 30 Barbieri, L., Lancellotti, I., Manfredini, T., Pellacani, G. C., Rincón, J. M., & Romero, M. (2001). Nucleation and crystallization of new glasses from fly ash originating from thermal power plants. *Journal of the American Ceramic Society*, 84(8), 1851-1858.
- 31 Kim, J. M., & Kim, H. S. (2004). Processing and properties of a glass-ceramic from coal fly ash from a thermal power plant through an economic process. *Journal of the European Ceramic Society*, 24(9), 2825-2833.
- 32 Vasilopoulos, K. C., Tulyaganov, D. U., Agathopoulos, S., Karakassides, M. A., Ferreira, J. M. F., & Tspas, D. (2009). Bulk nucleated fine grained mono-mineral glass-ceramics from low-silica fly ash. *Ceramics International*, 35(2), 555-558.
- 33 Chimenos, J. M., Segarra, M., Fernández, M. A., & Espiell, F. (1999). Characterization of the bottom ash in municipal solid waste incinerator. *Journal of hazardous materials*, 64(3), 211-222.
- 34 Bethanis, S., Cheeseman, C. R., & Sollars, C. J. (2002). Properties and microstructure of sintered incinerator bottom ash. *Ceramics International*, 28(8), 881-886.
- 35 Schabbach, L. M., Andreola, F., Karamanova, E., Lancellotti, I., Karamanov, A., & Barbieri, L. (2011). Integrated approach to establish the sinter-crystallization ability of glasses from secondary raw material. *Journal of non-crystalline solids*, 357(1), 10-17.
- 36 Zacco, A., Borgese, L., Gianoncelli, A., Struis, R. P., Depero, L. E., & Bontempi, E. (2014). Review of fly ash inertisation treatments and recycling. *Environmental chemistry letters*, 12(1), 153-175.
- 37 Frugier, P., Godon, N., Vernaz, E., & Larché, F. (2002). Influence of composition variations on the initial alteration rate of vitrified domestic waste incineration fly-ash. *Waste Management*, 22(2), 137-142.
- 38 Park, Y. J., & Heo, J. (2002). Vitrification of fly ash from municipal solid waste incinerator. *Journal of Hazardous Materials*, 91(1-3), 83-93.
- 39 Yang, J., Xiao, B., & Boccaccini, A. R. (2009). Preparation of low melting temperature glass-ceramics from municipal waste incineration fly ash. *Fuel*, 88(7), 1275-1280.
- 40 Kuo, Y. M., Huang, K. L., & Lin, C. (2012). Metal behavior during vitrification of municipal solid waste incinerator fly ash. *Aerosol Air Qual. Res*, 12, 1379-1385.
- 41 Margallo, M., Taddei, M. B. M., Hernández-Pellón, A., Aldaco, R., & Irabien, A. (2015). Environmental sustainability assessment of the management of municipal solid waste

- incineration residues: a review of the current situation. *Clean Technologies and Environmental Policy*, 17(5), 1333-1353.
- 42 Siwadamrongpong, S., Koide, M., & Matusita, K. (2004). Prediction of chloride solubility in CaO–Al₂O₃–SiO₂ glass systems. *Journal of non-crystalline solids*, 347(1-3), 114-120.
- 43 Kim, J. M., & Kim, H. S. (2004). Glass-ceramic produced from a municipal waste incinerator fly ash with high Cl content. *Journal of the European Ceramic Society*, 24(8), 2373-2382.
- 44 Dimech, C., Cheeseman, C. R., Cook, S., Simon, J., & Boccaccini, A. R. (2008). Production of sintered materials from air pollution control residues from waste incineration. *Journal of Materials Science*, 43(12), 4143-4151.
- 45 Chiang, K. Y., & Hu, Y. H. (2010). Water washing effects on metals emission reduction during municipal solid waste incinerator (MSWI) fly ash melting process. *Waste management*, 30(5), 831-838.
- 46 Liu, H., Wei, G., & Zhang, R. (2013). Effect of water washing pre-treatment on the properties of glass-ceramics from incinerator fly ash using electronic arc furnace. *Journal of Wuhan University of Technology-Mater. Sci. Ed.*, 28(1), 62-68.
- 47 Wu, S., Xu, Y., Sun, J., Cao, Z., Zhou, J., Pan, Y., & Qian, G. (2015). Inhibiting evaporation of heavy metal by controlling its chemical speciation in MSWI fly ash. *Fuel*, 158, 764-769.
- 48 Nowak, B., Rocha, S. F., Aschenbrenner, P., Rechberger, H., & Winter, F. (2012). Heavy metal removal from MSW fly ash by means of chlorination and thermal treatment: Influence of the chloride type. *Chemical Engineering Journal*, 179, 178-185.
- 49 Tuscharoen, S., Kaewkhao, J., Limsuwan, P., & Chewpraditkul, W. (2012). Structural, optical and radiation shielding properties of BaO-B₂O₃-rice husk ash glasses. *Procedia Engineering*, 32, 734-739.
- 50 Lee, T., Othman, R., & Yeoh, F. Y. (2013). Development of photoluminescent glass derived from rice husk. *Biomass and bioenergy*, 59, 380-392.
- 51 Andreola, F., Martín, M. I., Ferrari, A. M., Lancellotti, I., Bondioli, F., Rincón, J. M., ... & Barbieri, L. (2013). Technological properties of glass-ceramic tiles obtained using rice husk ash as silica precursor. *Ceramics International*, 39(5), 5427-5435.
- 52 Park, Y. J., Moon, S. O., & Heo, J. (2003). Crystalline phase control of glass ceramics obtained from sewage sludge fly ash. *Ceramics International*, 29(2), 223-227.
- 53 Bernardo, E., & Dal Maschio, R. (2011). Glass–ceramics from vitrified sewage sludge pyrolysis residues and recycled glasses. *Waste Management*, 31(11), 2245-2252.
- 54 Zhang, Z., Li, A., Yin, Y., & Zhao, L. (2013). Effect of crystallization time on behaviors of glass-ceramic produced from sludge incineration ash. *Procedia Environmental Sciences*, 18, 788-793.
- 55 Suzuki, S., Tanaka, M., & Kaneko, T. (1997). Glass-ceramic from sewage sludge ash. *Journal of materials science*, 32(7), 1775-1779.
- 56 Toya, T., Kameshima, Y., Nakajima, A., & Okada, K. (2006). Preparation and properties of glass-ceramics from kaolin clay refining waste (Kira) and paper sludge ash. *Ceramics International*, 32(7), 789-796.
- 57 Marangoni, M., Ponsot, I., Kuusik, R., & Bernardo, E. (2014). Strong and chemically inert sinter crystallised glass ceramics based on Estonian oil shale ash. *Advances in Applied Ceramics*, 113(2), 120-128.
- 58 Bernardo, E., & Bingham, P. A. (2011). Sintered silicophosphate glass ceramics from MBM ash and recycled soda–lime–silica glass. *Advances in Applied Ceramics*, 110(1), 41-48.

- 59 Dellisanti, F., Rossi, P. L., & Valdrè, G. (2009). Remediation of asbestos containing materials by Joule heating vitrification performed in a pre-pilot apparatus. *International Journal of Mineral Processing*, 91(3-4), 61-67.
- 60 Leonelli, C., Veronesi, P., Boccaccini, D. N., Rivasi, M. R., Barbieri, L., Andreola, F., ... & Pellacani, G. C. (2006). Microwave thermal inertisation of asbestos containing waste and its recycling in traditional ceramics. *Journal of hazardous materials*, 135(1-3), 149-155.
- 61 Boccaccini, D. N., Leonelli, C., Rivasi, M. R., Romagnoli, M., Veronesi, P., Pellacani, G. C., & Boccaccini, A. R. (2007). Recycling of microwave inertised asbestos containing waste in refractory materials. *Journal of the European Ceramic Society*, 27(2-3), 1855-1858.
- 62 Bernardo, E., Esposito, L., Rambaldi, E., & Tucci, A. (2011). Sintered glass ceramic articles from plasma vitrified asbestos containing waste. *Advances in Applied Ceramics*, 110(6), 346-352.
- 63 Fredericci, C., Zanotto, E. D., & Ziemath, E. C. (2000). Crystallization mechanism and properties of a blast furnace slag glass. *Journal of non-crystalline solids*, 273(1-3), 64-75.
- 64 Francis, A. A. (2004). Conversion of blast furnace slag into new glass-ceramic material. *Journal of the European Ceramic Society*, 24(9), 2819-2824.
- 65 Francis, A. A. (2005). Non-isothermal crystallization kinetics of a blast furnace slag glass. *Journal of the American Ceramic Society*, 88(7), 1859-1863.
- 66 Pal, S. C., Mukherjee, A., & Pathak, S. R. (2003). Investigation of hydraulic activity of ground granulated blast furnace slag in concrete. *Cement and Concrete Research*, 33(9), 1481-1486.
- 67 Cheng, T. W., & Chiu, J. P. (2003). Fire-resistant geopolymer produced by granulated blast furnace slag. *Minerals engineering*, 16(3), 205-210.
- 68 Ferreira, E. B., Zanotto, E. D., & Scudeller, L. A. (2002). Glass and glass-ceramic from basic oxygen furnace (BOF) slag. *Glass Science and Technology*, 75(2), 75-86.
- 69 Proctor, D. M., Fehling, K. A., Shay, E. C., Wittenborn, J. L., Green, J. J., Avent, C., ... & Zak, M. A. (2000). Physical and chemical characteristics of blast furnace, basic oxygen furnace, and electric arc furnace steel industry slags. *Environmental science & technology*, 34(8), 1576-1582.
- 70 Pelino, M., Karamanov, A., Piscicella, P., Crisucci, S., & Zonetti, D. (2002). Vitrification of electric arc furnace dusts. *Waste Management*, 22(8), 945-949.
- 71 Lorenzi, A., Rastelli, D., Biavati, A., Poncini, M., Alfieri, I., Albertini, F., ... & Montenero, A. (2015). Immobilization of iron rich steel industry waste and products characterization. *Journal of Environmental Chemical Engineering*, 3(1), 196-201.
- 72 Gomes, V., De Borba, C. D. G., & Riella, H. G. (2002). Production and characterization of glass ceramics from steelwork slag. *Journal of materials science*, 37(12), 2581-2585.
- 73 Sarrafi, A., Rahmati, B., Hassani, H. R., & Shirazi, H. H. A. (2004). Recovery of copper from reverberatory furnace slag by flotation. *Minerals Engineering*, 17(3), 457-459.
- 74 Karamanov, A., Aloisi, M., & Pelino, M. (2007). Vitrification of copper flotation waste. *Journal of hazardous materials*, 140(1-2), 333-339.
- 75 Çoruh, S., Ergun, O. N., & Cheng, T. W. (2006). Treatment of copper industry waste and production of sintered glass-ceramic. *Waste management & research*, 24(3), 234-241.
- 76 Ponsot, I., Pontikes, Y., Baldi, G., Chinnam, R., Detsch, R., Boccaccini, A., & Bernardo, E. (2014). Magnetic glass ceramics by sintering of borosilicate glass and inorganic waste. *Materials*, 7(8), 5565-5580.

- 77 Yang, Z., Xia, J., He, Y., Liao, G., & Ke, Y. (2013). Preparation and crystallization of glass-ceramics derived from iron-rich copper slag. *Journal of Alloys and Compounds*, 574, 354-360.
- 78 Yang, Z., Lin, Q., Lu, S., He, Y., Liao, G., & Ke, Y. (2014). Effect of CaO/SiO₂ ratio on the preparation and crystallization of glass-ceramics from copper slag. *Ceramics International*, 40(5), 7297-7305.
- 79 Pelino, M. (2000). Recycling of zinc-hydrometallurgy wastes in glass and glass ceramic materials. *Waste management*, 20(7), 561-568.
- 80 Karamanov, A., Cantalini, C., Pelino, M., & Hreglich, A. (1999). Kinetics of phase formation in jarosite glass-ceramic. *Journal of the European Ceramic Society*, 19(4), 527-533.
- 81 Karamanov, A., & Pelino, M. (1999). Evaluation of the degree of crystallisation in glass-ceramics by density measurements. *Journal of the European Ceramic Society*, 19(5), 649-654.
- 82 Karamanov, A., Taglieri, G., & Pelino, M. (1999). Iron-rich sintered glass-ceramics from industrial wastes. *Journal of the American Ceramic Society*, 82(11), 3012-3016.
- 83 Piscicella, P., & Pelino, M. (2005). FTIR spectroscopy investigation of the crystallisation process in an iron rich glass. *Journal of the European Ceramic Society*, 25(11), 1855-1861.
- 84 Bernardo, E., Esposito, L., Rambaldi, E., Tucci, A., Pontikes, Y., & Angelopoulos, G. N. (2009). Sintered esseneite-wollastonite-plagioclase glass-ceramics from vitrified waste. *Journal of the European Ceramic Society*, 29(14), 2921-2927.
- 85 Zhao, T., Li, B. W., Gao, Z. Y., & Chang, D. Q. (2010). The utilization of rare earth tailing for the production of glass-ceramics. *Materials Science and Engineering: B*, 170(1-3), 22-25.
- 86 Peng, K., Lv, C., & Yang, H. (2014). Novel preparation of glass ceramics from amorphized tungsten tailings. *Ceramics International*, 40(7), 10291-10296.
- 87 Shao, H., Liang, K., Peng, F., Zhou, F., & Hu, A. (2005). Production and properties of cordierite-based glass-ceramics from gold tailings. *Minerals engineering*, 18(6), 635-637.
- 88 Lam, C. H., Ip, A. W., Barford, J. P., & McKay, G. (2010). Use of incineration MSW ash: a review. *Sustainability*, 2(7), 1943-1968.
- 89 <http://www.europlasma.com/> (Accessed July 2018)
- 90 Fruergaard, T., Hyks, J., & Astrup, T. (2010). Life-cycle assessment of selected management options for air pollution control residues from waste incineration. *Science of the Total Environment*, 408(20), 4672-4680.
- 91 Park, K., Hyun, J., Maken, S., Jang, S., & Park, J. W. (2005). Vitrification of municipal solid waste incinerator fly ash using Brown's gas. *Energy & fuels*, 19(1), 258-262.
- 92 Sobiecka, E., & Szymanski, L. (2014). Thermal plasma vitrification process as an effective technology for fly ash and chromium-rich sewage sludge utilization. *Journal of Chemical Technology & Biotechnology*, 89(7), 1115-1117.
- 93 Gomez, E., Rani, D. A., Cheeseman, C. R., Deegan, D., Wise, M., & Boccaccini, A. R. (2009). Thermal plasma technology for the treatment of wastes: a critical review. *Journal of hazardous materials*, 161(2-3), 614-626.
- 94 Zaman, A. U. (2010). Comparative study of municipal solid waste treatment technologies using life cycle assessment method. *International Journal of Environmental Science & Technology*, 7(2), 225-234.

- 95 Beall, G. H. (2012). *Glass Ceramic Technology*. Wiley.
- 96 Morimoto, N. (1988). Nomenclature of pyroxenes. *Mineralogy and Petrology*, 39(1), 55-76.
- 97 Karamanov, A., & Pelino, M. (2001). Crystallization phenomena in iron-rich glasses. *Journal of Non-Crystalline Solids*, 281(1-3), 139-151.
- 98 Francis, A. A., Rawlings, R. D., & Boccaccini, A. R. (2002). Glass-ceramics from mixtures of coal ash and soda-lime glass by the peturgic method. *Journal of materials science letters*, 21(12), 975-980.
- 99 Romero, M., & Rincón, J. M. (1999). Surface and Bulk Crystallization of Glass-Ceramic in the Na₂O-CaO-ZnO-PbO-Fe₂O₃-Al₂O₃-SiO₂ System Derived from a Goethite Waste. *Journal of the American Ceramic Society*, 82(5), 1313-1317.
- 100 Gutzow, I., Pascova, R., Karamanov, A., & Schmelzer, J. (1998). The kinetics of surface induced sinter crystallization and the formation of glass-ceramic materials. *Journal of materials science*, 33(21), 5265-5273.
- 101 Müller, R., Zanotto, E. D., & Fokin, V. M. (2000). Surface crystallization of silicate glasses: nucleation sites and kinetics. *Journal of non-crystalline solids*, 274(1-3), 208-231.
- 102 Prado, M. O., & Zanotto, E. D. (2002). Glass sintering with concurrent crystallization. *Comptes Rendus Chimie*, 5(11), 773-786.
- 103 Francis, A. A., Rawlings, R. D., Sweeney, R., & Boccaccini, A. R. (2004). Crystallization kinetic of glass particles prepared from a mixture of coal ash and soda-lime cullet glass. *Journal of non-crystalline solids*, 333(2), 187-193.
- 104 Hernández-Crespo, M. S., Romero, M., & Rincon, J. M. (2006). Nucleation and crystal growth of glasses produced by a generic plasma arc-process. *Journal of the European Ceramic Society*, 26(9), 1679-1685.
- 105 Bernardo, E. (2008). Fast sinter-crystallization of a glass from waste materials. *Journal of Non-Crystalline Solids*, 354(29), 3486-3490.
- 106 Bernardo, E., Andreola, F., Barbieri, L., & Lancellotti, I. (2005). Sintered glass-ceramics and glass-ceramic matrix composites from CRT panel glass. *Journal of the American Ceramic Society*, 88(7), 1886-1891.
- 107 Bernardo, E., Castellan, R., Hreglich, S., & Lancellotti, I. (2006). Sintered sanidine glass-ceramics from industrial wastes. *Journal of the European Ceramic Society*, 26(15), 3335-3341.
- 108 Authors' previously unpublished data
- 109 Karamanov, A., Piscicella, P., Cantalini, C., & Pelino, M. (2000). Influence of Fe³⁺/Fe²⁺ ratio on the crystallization of iron-rich glasses made with industrial wastes. *Journal of the American Ceramic Society*, 83(12), 3153-3157.
- 110 Liu, Z., Zong, Y., & Li, H. (2015). Preparation and characterization of glass-ceramic under various sintering atmospheres. *Materials Letters*, 159, 122-125.
- 111 Karamanov, A., Pelino, M., & Hreglich, A. (2003). Sintered glass-ceramics from Municipal Solid Waste-incinerator fly ashes—part I: the influence of the heating rate on the sinter-crystallisation. *Journal of the European Ceramic Society*, 23(6), 827-832.
- 112 Karamanov, A., Aloisi, M., & Pelino, M. (2005). Sintering behaviour of a glass obtained from MSWI ash. *Journal of the European Ceramic Society*, 25(9), 1531-1540.
- 113 Bernardo, E., Scarinci, G., Edme, E., Michon, U., & Planty, N. (2009). Fast-Sintered Gehlenite Glass-Ceramics from Plasma-Vitrified Municipal Solid Waste Incinerator Fly Ashes. *Journal of the American Ceramic Society*, 92(2), 528-530.

- 114 Ray, A., & Tiwari, A. N. (2001). Compaction and sintering behaviour of glass–alumina composites. *Materials chemistry and physics*, 67(1-3), 220-225.
- 115 Scarinci, G., Brusatin, G., & Bernardo, E. (2005). Cellular Ceramics. Structure, Manufacturing, Properties and Applications, M. Scheffler and P. Colombo.
- 116 Mear, F., Yot, P., Cambon, M., & Ribes, M. (2005). Elaboration and characterisation of foam glass from cathode ray tubes. *Advances in Applied Ceramics*, 104(3), 123-130.
- 117 Méar, F., Yot, P., & Ribes, M. (2006). Effects of temperature, reaction time and reducing agent content on the synthesis of macroporous foam glasses from waste funnel glasses. *Materials Letters*, 60(7), 929-934.
- 118 Bernardo, E., Scarinci, G., Bertuzzi, P., Ercole, P., & Ramon, L. (2010). Recycling of waste glasses into partially crystallized glass foams. *Journal of Porous Materials*, 17(3), 359-365.
- 119 Tulyaganov, D. U., Fernandes, H. R., Agathopoulos, S., & Ferreira, J. M. F. (2006). Preparation and characterization of high compressive strength foams from sheet glass. *Journal of Porous Materials*, 13(2), 133-139.
- 120 Fernandes, H. R., Tulyaganov, D. U., & Ferreira, J. M. F. (2009). Preparation and characterization of foams from sheet glass and fly ash using carbonates as foaming agents. *Ceramics International*, 35(1), 229-235.
- 121 Wu, J. P., Boccaccini, A. R., Lee, P. D., Kershaw, M. J., & Rawlings, R. D. (2006). Glass ceramic foams from coal ash and waste glass: production and characterisation. *Advances in Applied Ceramics*, 105(1), 32-39.
- 122 Fernandes, H. R., Tulyaganov, D. U., & Ferreira, J. M. F. (2009). Production and characterisation of glass ceramic foams from recycled raw materials. *Advances in Applied Ceramics*, 108(1), 9-13.
- 123 Attila, Y., Güden, M., & Taşdemirci, A. (2013). Foam glass processing using a polishing glass powder residue. *Ceramics International*, 39(5), 5869-5877.
- 124 Francis, A. A., & Abdel Rahman, M. K. (2013). Formation of cellular-structure material from automotive glass waste and sawdust. *Materials and Manufacturing Processes*, 28(6), 616-620.
- 125 Bernardo, E., & Albertini, F. (2006). Glass foams from dismantled cathode ray tubes. *Ceramics international*, 32(6), 603-608.
- 126 König, J., Petersen, R. R., & Yue, Y. (2014). Influence of the glass–calcium carbonate mixture's characteristics on the foaming process and the properties of the foam glass. *Journal of the European Ceramic Society*, 34(6), 1591-1598.
- 127 Benzerga, R., Laur, V., Lebullenger, R., Le Gendre, L., Genty, S., Sharaiha, A., & Queffelec, P. (2015). Waste-glass recycling: a step toward microwave applications. *Materials research bulletin*, 67, 261-265.
- 128 Guo, Y., Zhang, Y., Huang, H., Meng, K., Hu, K., Hu, P., ... & Meng, X. (2014). Novel glass ceramic foams materials based on red mud. *Ceramics International*, 40(5), 6677-6683.
- 129 König, J., Petersen, R. R., & Yue, Y. (2015). Fabrication of highly insulating foam glass made from CRT panel glass. *Ceramics international*, 41(8), 9793-9800.
- 130 Sasmal, N., Garai, M., & Karmakar, B. (2015). Preparation and characterization of novel foamed porous glass-ceramics. *Materials Characterization*, 103, 90-100.
- 131 García-Ten, J., Saburit, A., Orts, M. J., Bernardo, E., & Colombo, P. (2011). Glass foams from oxidation/reduction reactions using SiC, Si₃N₄ and AlN powders. *Glass Technology-European Journal of Glass Science and Technology Part A*, 52(4), 103-110.

- 132 Foamglas. [Online]. Available: <http://www.foamglas.com> [July 2018].
- 133 Appendino, P., Ferraris, M., Matekovits, I., & Salvo, M. (2004). Production of glass–ceramic bodies from the bottom ashes of municipal solid waste incinerators. *Journal of the European Ceramic Society*, 24(5), 803-810.
- 134 Marangoni, M., Secco, M., Parisatto, M., Artioli, G., Bernardo, E., Colombo, P., ... & Binhussain, M. (2014). Cellular glass–ceramics from a self foaming mixture of glass and basalt scoria. *Journal of Non-Crystalline Solids*, 403, 38-46.
- 135 Ponsot, I., & Bernardo, E. (2013). Self glazed glass ceramic foams from metallurgical slag and recycled glass. *Journal of cleaner production*, 59, 245-250.
- 136 Bernardo, E. (2007). Micro-and macro-cellular sintered glass-ceramics from wastes. *Journal of the European ceramic Society*, 27(6), 2415-2422.
- 137 Boccaccini, A. R., Bücken, M., Bossert, J., & Marszalek, K. (1997). Glass matrix composites from coal flyash and waste glass. *Waste management*, 17(1), 39-45.
- 138 Bernardo, E., Scarinci, G., & Hreglich, S. (2005). Development and mechanical characterization of Al₂O₃ platelet-reinforced glass matrix composites obtained from glasses coming from dismantled cathode ray tubes. *Journal of the European Ceramic Society*, 25(9), 1541-1550.
- 139 Ferraris, M., Salvo, M., Smeacetto, F., Augier, L., Barbieri, L., Corradi, A., & Lancellotti, I. (2001). Glass matrix composites from solid waste materials. *Journal of the European Ceramic Society*, 21(4), 453-460.
- 140 Bento, A. C., Kubaski, E. T., Sequinel, T., Pianaro, S. A., Varela, J. A., & Tebcherani, S. M. (2013). Glass foam of macroporosity using glass waste and sodium hydroxide as the foaming agent. *Ceramics International*, 39(3), 2423-2430.
- 141 Guo, H. W., Wang, X. F., Gong, Y. X., Liu, X. N., & Gao, D. N. (2010). Improved mechanical property of foam glass composites toughened by glass fiber. *Materials Letters*, 64(24), 2725-2727.
- 142 Ayadi, A., Stiti, N., Boumchedda, K., Rennai, H., & Lerari, Y. (2011). Elaboration and characterization of porous granules based on waste glass. *Powder technology*, 208(2), 423-426.
- 143 Minay, E. J., Veronesi, P., Cannillo, V., Leonelli, C., & Boccaccini, A. R. (2004). Control of pore size by metallic fibres in glass matrix composite foams produced by microwave heating. *Journal of the European Ceramic Society*, 24(10-11), 3203-3208.
- 144 Espejel-Ayala, F., Ramírez-Zamora, R. M., González-Barceló, O., & Schouwenaars, R. (2013). Novel self-foaming cellular composites produced from recycled water potabilisation sludge. In *Proceedings of the 8th Pacific Rim International Congress on Advanced Materials and Processing* (pp. 269-275). Springer, Cham.
- 145 Chen, X., Lu, A., & Qu, G. (2013). Preparation and characterization of foam ceramics from red mud and fly ash using sodium silicate as foaming agent. *Ceramics International*, 39(2), 1923-1929.
- 146 Chen, B., Luo, Z., & Lu, A. (2011). Preparation of sintered foam glass with high fly ash content. *Materials Letters*, 65(23-24), 3555-3558.
- 147 Bernardo, E., Castellan, R., & Hreglich, S. (2007). Al₂O₃-platelet reinforced glass matrix composites from a mixture of wastes. *Journal of materials science*, 42(8), 2706-2711.

- 148 Aloisi, M., Karamanov, A., Taglieri, G., Ferrante, F., & Pelino, M. (2006). Sintered glass ceramic composites from vitrified municipal solid waste bottom ashes. *Journal of hazardous materials*, 137(1), 138-143.
- 149 García-Ten, J., Saburit, A., Bernardo, E., & Colombo, P. (2012). Development of lightweight porcelain stoneware tiles using foaming agents. *Journal of the European Ceramic Society*, 32(4), 745-752.
- 150 Binhussain, M. A., Marangoni, M., Bernardo, E., & Colombo, P. (2014). Sintered and glazed glass-ceramics from natural and waste raw materials. *Ceramics International*, 40(2), 3543-3551.
- 151 Cetin, S., Marangoni, M., & Bernardo, E. (2015). Lightweight glass-ceramic tiles from the sintering of mining tailings. *Ceramics International*, 41(4), 5294-5300.
- 152 Hernández-Crespo, M. S., & Rincón, J. M. (2001). New porcelainized stoneware materials obtained by recycling of MSW incinerator fly ashes and granite sawing residues. *Ceramics International*, 27(6), 713-720.
- 153 Cheng, T. W., Huang, M. Z., Tzeng, C. C., Cheng, K. B., & Ueng, T. H. (2007). Production of coloured glass-ceramics from incinerator ash using thermal plasma technology. *Chemosphere*, 68(10), 1937-1945.
- 154 Boccaccini, A. R., Köpf, M., & Stumpfe, W. (1995). Glass-ceramics from filter dusts from waste incinerators. *Ceramics International*, 21(4), 231-235.
- 155 Öveçoğlu, M. L. (1998). Microstructural characterization and physical properties of a slag-based glass-ceramic crystallized at 950 and 1100 C. *Journal of the European Ceramic Society*, 18(2), 161-168.
- 156 Peng, F., Liang, K. M., & Hu, A. M. (2005). Nano-crystal glass-ceramics obtained from high alumina coal fly ash. *Fuel*, 84(4), 341-346.
- 157 Quinn, G. D. (2003). Weibull strength scaling for standardized rectangular flexure specimens. *Journal of the American Ceramic Society*, 86(3), 508-510.
- 158 Bernardo, E., Esposito, L., Rambaldi, E., Tucci, A., & Hreglich, S. (2008). Recycle of waste glass into “glass-ceramic stoneware”. *Journal of the American Ceramic Society*, 91(7), 2156-2162.
- 159 Gibson, L. J., & Ashby, M. F. (1999). *Cellular solids: structure and properties*. Cambridge university press.
- 160 CES EduPack 2015 materials education software supports teaching for real-world engineering. [Online]. Available: <http://www.grantadesign.com/news/2015/edupack2015.shtml> [July 2018].
- 161 Hurley, J. (2009). Glass research and development final report: a UK market survey for foam glass.(WRAP, The Waste and Resources Action Programme, 2003).
- 162 Méar, F., Yot, P., Viennois, R., & Ribes, M. (2007). Mechanical behaviour and thermal and electrical properties of foam glass. *Ceramics international*, 33(4), 543-550.
- 163 Matamoros-Veloza, Z., Rendón-Angeles, J. C., Yanagisawa, K., Cisneros-Guerrero, M. A., Cisneros-Guerrero, M. M., & Aguirre, L. (2008). Preparation of foamed glasses from CRT TV glass by means of hydrothermal hot-pressing technique. *Journal of the European Ceramic Society*, 28(4), 739-745.
- 164 Sandu, V., Nicolescu, M. S., Kuncser, V., Damian, R., & Sandu, E. (2012). Magnetic glass-ceramics. *Journal of Advanced Ceramics*, 1(2), 138-143.

- 165 Min'ko, N. I., & Koval'chenko, N. A. (2002). Electrical and magnetic characteristics of iron-containing glass in crystallization. *Glass and ceramics*, 59(9-10), 296-298.
- 166 Francis, A. A. (2007). Magnetic characteristics of iron-containing glass originated from the mixture of various wastes. *Ceramics international*, 33(2), 163-168.
- 167 Jordan, A., Wust, P., Föhling, H., John, W., Hinz, A., & Felix, R. (2009). Inductive heating of ferrimagnetic particles and magnetic fluids: physical evaluation of their potential for hyperthermia. *International Journal of Hyperthermia*, 25(7), 499-511.
- 168 Abbasi, M., Hashemi, B., & Shokrollahi, H. (2014). Investigating in vitro bioactivity and magnetic properties of the ferrimagnetic bioactive glass–ceramic fabricated using soda-lime–silica waste glass. *Journal of Magnetism and Magnetic Materials*, 356, 5-11.
- 169 Sulaiman, H. A., Othman, M. A., Aziz, M. Z. A. A., & Malek, M. F. A. (2015). *Theory and Applications of Applied Electromagnetics*. Springer International Publishing: Imprint: Springer,.
- 170 Roling, B., & Ingram, M. D. (2000). Mixed alkaline–earth effects in ion conducting glasses. *Journal of non-crystalline solids*, 265(1-2), 113-119.
- 171 Saccani, A., Sandrolini, F., Barbieri, L., Corradi, A., & Lancellotti, I. (2001). Structural studies and electrical properties of recycled glasses from glass and incinerator wastes. *Journal of materials science*, 36(9), 2173-2177.
- 172 Elalaily, N. A., Khalil, M. M., & Ahmed, L. S. (2007). Effect of γ -irradiation on the electrical conductivity of some soda lime silicate glass containing blast furnace slag. *Physica B: Condensed Matter*, 390(1-2), 236-244.
- 173 Min'ko, N. I., Koval'chenko, N. A., Pavlenko, Z. V., & Zhernovaya, N. F. (1997). Raw materials from the Kursk magnetic anomaly region: the basis of glass materials for electrical engineering. *Glass and ceramics*, 54(7-8), 202-204.
- 174 Wang, S., & Liang, K. (2007). High infrared radiance glass–ceramics obtained from fly ash and titanium slag. *Chemosphere*, 69(11), 1798-1801.
- 175 Wang, S., & Liang, K. (2008). Crystallization behavior and infrared radiation property of nickel–magnesium cordierite based glass–ceramics. *Journal of Non-Crystalline Solids*, 354(14), 1522-1525.
- 176 Doulos, L., Santamouris, M., & Livada, I. (2004). Passive cooling of outdoor urban spaces. The role of materials. *Solar energy*, 77(2), 231-249.
- 177 Domínguez, M. I., Sánchez, M., Centeno, M. A., Montes, M., & Odriozola, J. A. (2006). CO oxidation over gold-supported catalysts-coated ceramic foams prepared from stainless steel wastes. *Applied Catalysis A: General*, 302(1), 96-103.
- 178 . Gokon, N., Murayama, H., Nagasaki, A., & Kodama, T. (2009). Thermochemical two-step water splitting cycles by monoclinic ZrO₂-supported NiFe₂O₄ and Fe₃O₄ powders and ceramic foam devices. *Solar Energy*, 83(4), 527-537
- 179 Vu, D. H., Wang, K. S., & Bac, B. H. (2011). Humidity control porous ceramics prepared from waste and porous materials. *Materials Letters*, 65(6), 940-943.
- 180 Provis, J. L. (2014). Geopolymers and other alkali activated materials: why, how, and what?. *Materials and Structures*, 47(1-2), 11-25.
- 181 Lancellotti, I., Kamseu, E., Michelazzi, M., Barbieri, L., Corradi, A., & Leonelli, C. (2010). Chemical stability of geopolymers containing municipal solid waste incinerator fly ash. *Waste Management*, 30(4), 673-679.

- 182 Garbev, K., Black, L., Beuchle, G., & Stemmermann, P. (2002). Inorganic polymers in cement based materials. *Wasser-und Geotechnologie*, 1(2), 19-30.
- 183 Garcia-Lodeiro, I., Fernández-Jimenez, A., Pena, P., & Palomo, A. (2014). Alkaline activation of synthetic aluminosilicate glass. *Ceramics International*, 40(4), 5547-5558.
- 184 Garcia-Lodeiro, I., Aparicio-Rebollo, E., Fernández-Jimenez, A., & Palomo, A. (2016). Effect of calcium on the alkaline activation of aluminosilicate glass. *Ceramics International*, 42(6), 7697-7707.
- 185 Ruiz-Santaquiteria, C., Fernández-Jiménez, A., & Palomo, A. (2016). Alternative prime materials for developing new cements: Alkaline activation of alkali aluminosilicate glasses. *Ceramics international*, 42(8), 9333-9340.
- 186 Puertas, F., & Torres-Carrasco, M. (2014). Use of glass waste as an activator in the preparation of alkali-activated slag. Mechanical strength and paste characterisation. *Cement and Concrete Research*, 57, 95-104.
- 187 Redden, R., & Neithalath, N. (2014). Microstructure, strength, and moisture stability of alkali activated glass powder-based binders. *Cement and Concrete Composites*, 45, 46-56.
- 188 Torres-Carrasco, M., & Puertas, F. (2015). Waste glass in the geopolymer preparation. Mechanical and microstructural characterisation. *Journal of cleaner production*, 90, 397-408.
- 189 Cyr, M., Idir, R., & Poinot, T. (2012). Properties of inorganic polymer (geopolymer) mortars made of glass cullet. *Journal of Materials Science*, 47(6), 2782-2797.
- 190 Al Saadi, T. H. A., Badanoiu, A. I., Nicoara, A. I., Stoleriu, S., & Voicu, G. (2017). Synthesis and properties of alkali activated borosilicate inorganic polymers based on waste glass. *Construction and Building Materials*, 136, 298-306.
- 191 Bădănoiu, A. I., Al-Saadi, T. H. A., & Voicu, G. (2015). Synthesis and properties of new materials produced by alkaline activation of glass cullet and red mud. *International Journal of Mineral Processing*, 135, 1-10.
- 192 Paul, A. (1977). Chemical durability of glasses; a thermodynamic approach. *Journal of materials science*, 12(11), 2246-2268.
- 193 Torres-Carrasco, M., Palomo, J. G., & Puertas, F. (2014). Sodium silicate solutions from dissolution of glasswastes. Statistical analysis. *Materiales de Construcción*, 64(314), 014.
- 194 Marchand, B., Lanier, S., Davy, C. A., Albert-Mercier, C., & Tricot, G. (2018). Are calcium silicate hydrates (CSH) present in alkali-activated glass cullet cement?. *Materials Letters*, 219, 104-108.
- 195 Wang, X., Ruan, J. M., & Chen, Q. Y. (2009). Effects of surfactants on the microstructure of porous ceramic scaffolds fabricated by foaming for bone tissue engineering. *Materials Research Bulletin*, 44(6), 1275-1279.
- 196 Martín-Márquez, J., Rincón, J. M., & Romero, M. (2008). Effect of firing temperature on sintering of porcelain stoneware tiles. *Ceramics International*, 34(8), 1867-1873.

CHAPTER II

Glass foams from cullet produced by inorganic gel casting

II.1 - Aim of the study

Glass foams are a valuable product used as thermal insulator in the building industry. The increasing demand for net-zero energy buildings along with their non-flammable properties make glass foams the perfect candidate to be used in the near future. However, their production is still expensive and quite difficult to control, and for this reason, new and alternative fabrication techniques are needed to reduce production cost and increase environmental sustainability.

In this chapter, a new technique for the production of glass foam is described. In order to maintain a zero-waste approach the raw material selected was glass cullet that cannot be used for manufacturing the initial products where it comes from (technically known as ‘closed loop recycling’).

The new method is based on alkali activation inorganic gel casting and heat treatment. The alkali activation of soda-lime waste glass powders allowed to obtain well-dispersed concentrated suspensions, and later the products of alkali activation were subject to a gelation process with a treatment at low temperature (75 °C). The partially gelified suspensions can be foamed through mechanical stirring, also comprising a surfactant. The suspensions were carefully studied with respect to their rheological behaviour so that the

final microstructure (total amount of porosity and cell size) could be directly related to the degree of gelation.

A sintering treatment, at 700-800 °C, was applied to stabilise the foams as regards the leaching of alkaline ions. The newly obtained foam, considering the high overall porosity (88-93%), exhibited a remarkable compressive strength, in the range of 1.7-4.8 MPa.

In Section 2.2 the approach previously applied at a laboratory scale is extended to the semi-industrial production of lightweight panels. The main objective of this part of the study is to validate the foaming technique and demonstrate the viability of the process.

II.2 - Production of glass foams through inorganic gel casting *

II.2.1 - Introduction

The recovery of glass through the differentiated urban waste collection, in order to manufacture new glass containers ('closed-loop recycling'), has been successfully implemented in the last few years, reaching a rate of 73% of the overall volume of glass packaging in the European Union in 2015.¹ The recovery approach is undoubtedly beneficial, due to the significant savings in terms of raw materials and energy consumption upon melting (pre-formed glass acts as a flux for the reaction of mineral raw materials),² albeit with significant limitations. In fact, an 'ideal' recycling, i.e. a complete reuse of glass cullet in the manufacturing of the original glass articles, technically known as 'closed loop recycling', is far from being feasible. It was estimated that the savings of embodied energy (energy to be used to create a mass of usable material) using recycled material instead of 'virgin' raw materials are just about 20% for glass, versus 90% for aluminium.³

The controversy of glass recycling basically concerns the quality of resulting glass articles, which may be significantly degraded, when employing not properly purified glass cullet. Crushed glass from municipal waste collection is typically subjected to an expensive and difficult sorting process of the collected cullet, aimed at separating glass pieces with different colours, and removing metal, plastic or ceramic impurities. A glass fraction, in which these impurities are concentrated, remains practically useless and is mostly landfilled.^{4,5} Even in the case of limited impurities, some glass may be discarded if the original glass articles are no longer produced, as is the case of glasses from

* *The following text, data and images are an adaptation of the results that were published in the article: "Rincón, A., Giacomello, G., Pasetto, M., & Bernardo, E. (2017). Novel 'inorganic gel casting' process for the manufacturing of glass foams. Journal of the European Ceramic Society, 37(5), 2227-2234". It is reproduced in this chapter with the incorporation of more results and slight modifications.*

dismantled cathode ray tubes (TV and PC screens abandoned the CRT technology more than a decade ago).⁶⁻⁸ It is not surprising, as a consequence, that glass cullet should also be considered in a condition of ‘open loop recycling’, i.e. re-use in articles different from the original ones, also called ‘down-cycling’.⁹

Glass foams (or cellular glasses) represent a fundamental class of glass-based building materials. They offer high surface area, high permeability, low density, low specific heat, high thermal and acoustic insulation and high chemical resistance. Unlike polymeric cellular materials, glass foams are non-flammable and flame resistant, chemically inert and non-toxic (even if waste-derived), rodent and insect resistant, bacteria resistant, water and vapour resistant.^{10, 11}

Unlike most glass-based objects, glass foams are not manufactured by means of a melting process, but generally depend on the sintering of recycled glass powders. The current procedure is based on mixing glass powders with foaming agents, which decompose and release gases at temperature well exceeding the glass softening point. The appropriate foaming depends on a delicate balance between viscous flow sintering and gas evolution, which is determined by oxidation or decomposition reactions of additives mixed with glass powders.^{11, 12} On occasion, heat treatment involves some degree of crystallisation of the initial glass. All these complex processes lead to an exhaustive compositional control of the initial materials, involving the addition of natural raw minerals and limiting the use of recycle glass. As a result, the process may require a further melting step for the production of homogeneous glass for use in the initial mixture.

As thermally insulating materials, glass foams positively contribute to energy saving and reduction of CO₂ emissions, but the same foaming reactions have a disputable environmental effect since they occur at temperatures generally exceeding 850 °C (for common soda-lime glass), and imply energy dissipations in order to be effective. In the case of oxidation reactions, as an example, the homogeneity of foaming depends on the availability of oxygen, not only from the atmosphere, but also ‘in situ’ (as done by Pittsburgh Corning for the production of the well-known Foamglas[®], from glass powders mixed with carbon black.^{11, 13} This can be achieved by mixing recycled glass with an ‘oxidised glass’, rich in ferric and manganic oxides (releasing oxygen upon firing, by conversion into ferrous and manganous oxides), which must be specifically prepared (with significant energy consumption associated with glass melting). Oxidising compounds represent an alternative as additives in mixtures of glass and foaming agent.¹⁴

The building and construction industry segment was dominant in the global foam insulation market in 2016, in terms of value and volume. The use of insulation materials is expected to increase due to the rising concerns relating to greenhouse gas emissions and the growing demand for net-zero energy buildings in countries like Germany, U.K., France, and U.S. The various legislations regulating residential and commercial buildings in countries such as U.S., U.K., Germany, China, Japan, and South Korea are also expected to drive the demand for foam insulation. The civil engineering sector covers

about 80% of the heat insulating market. European demand will reach 213 million m³ of insulation materials in 2017, despite the decline in the construction sector caused by the recent economic crisis. This conflicting trend in the two markets is influenced by the recent housing-efficiency concerns raised after the Kyoto Protocol. Another reason for this change is the increasing energy costs and, consequently, the general awareness towards the benefits of energy savings. The European thermal insulation demand is expected to grow by 2.2% per year, corresponding to a market value of 10.6 billion euro in 2017.^{15, 16}

A substantial change in the production approach of glass foams is offered by the separation of foaming and sintering steps, obtainable by gel casting technology,¹⁷ that may be applied to solutions (from sol-gel processing),¹⁸ as well as to suspensions of glass powders.^{19, 20} In the present investigation, the gel provided by the alkali activation of soda-lime glass powders is used as an intermediate product for the foaming. As previously shown for highly porous geopolymers, air may be trapped by mechanical stirring of mixtures at the first stages of gelation, with the support of a surfactant; the setting of the mixtures determines the ‘freezing’ of the cellular structure. In other words, inorganic polymers may replace the complex mixture of organic compounds typically applied for the setting of aqueous slurries, in ‘conventional’ gel casting (also applied to glass powders, for the manufacturing of bioactive glass-ceramic foams). A sintering treatment, at 700-800 °C, was finally applied to convert highly porous ‘glass-based mortars’ into glass foams, limiting the leaching of alkaline ions.

II.2.2 - Experimental process

Soda-lime glass (later referred to as ‘SLG’) from municipal waste collection of glass containers was used as starting material. It was provided by the company SASIL S.r.l. (Brusnengo, Biella, Italy) in the form of fine powders (mean particle size of 75 µm). It comes from crushed bottles that the glass container industry sent to landfill due to impurities present in the cullet after colour selection and removal of metallic and polymeric residues. Adapting a series of original physical treatments employed for natural minerals, SASIL S.r.l. performs a secondary washing process on this cullet to further recover the reject glass inside it creating a product that could be melted seamlessly during glass container manufacturing. A by-product of this process is the fine glass fraction used in this study that remains practically unusable due to the presence of metallic and ceramic contaminations. The chemical composition²¹ of the starting glass is shown in Table 1.

Oxide (wt%)	SiO ₂	Na ₂ O	CaO	MgO	Al ₂ O ₃	Fe ₂ O ₃	K ₂ O
SLG	71.9	14.4	7.5	4.0	1.2	0.4	0.4

Table 1. Chemical composition (expressed in wt%) of the starting glass.

The initial fine powders were added to an aqueous solution containing 2.5 M KOH (reagent grade, Sigma-Aldrich, Gillingham, UK), at a solid loading of 65 wt%. The glass powders were subjected to alkaline attack for 3 hours, under low-speed mechanical stirring (500 rpm). After alkaline activation, the obtained suspension of partially dissolved glass powders was cast in closed polystyrene cylindrical moulds (60 mm diameter), and cured at 75 °C for 0-4 hours.

The gelation process was evaluated at different times by controlling the rheological behaviour.* Suspensions were extracted from the moulds and analysed by means of a plate-plate rheometer (Anton Paar MCR 302, Paar Physica, Austria), operating with a controlled shear rate (increase from 0 to 500 s⁻¹ in 3 min, stabilization at 500 s⁻¹ for 1 min and decrease from 500 to 0 s⁻¹ in 3 min), at room temperature. Regression analyses were performed considering only the up-curves of the corresponding rheograms.

The gels obtained at different curing times were first added with 4 wt% Triton X-100 then foamed by vigorous mechanical mixing (2000 rpm). Foamed gels were kept at 75 °C for 24 hours, in order to complete the curing, before demould. Finally, hardened foamed gels were fired at 700 and 800 °C for 1 hour with a heating rate of 1 °C/min or 10 °C/min. A schematic representation of the process is shown in Figure 1.

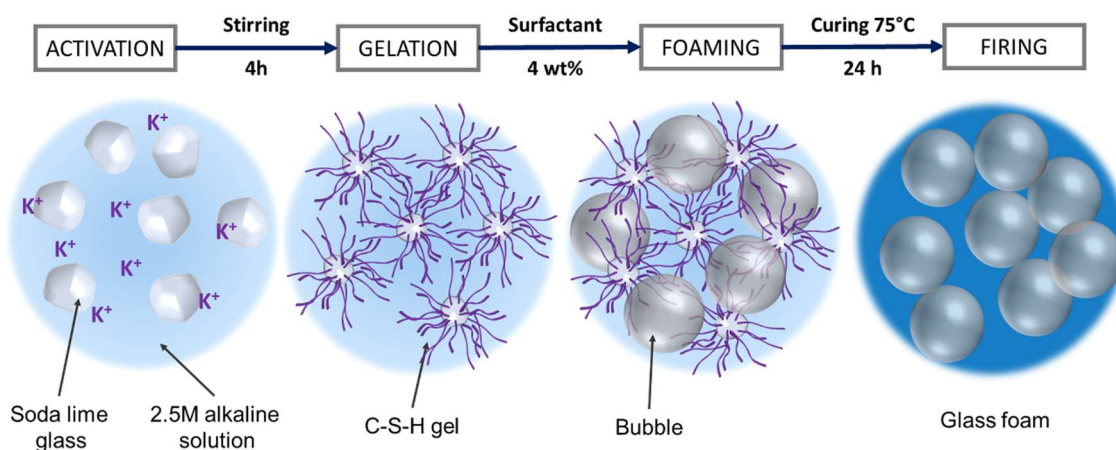


Figure 1. Processing scheme to obtain glass foams, combining alkali activation, gel casting and sintering.

The characterisation of the obtained foams was carried out through the standard methods and equipment described in Chapter I. The geometric density, the apparent and the true density of the samples were measured, and with such data the porosity of the samples was evaluated. Morphological and microstructural characterisations were

* The rheological measures were carried out at the Department of Civil, Environmental and Architectural Engineering (ICEA), University of Padova, Italy with the support of Giovanni Giacomello.

performed by optical stereomicroscopy and scanning electron microscopy. The mineralogical analysis was conducted by x-ray diffraction analysis, and the resulting foams were subjected to compression tests to evaluate their mechanical performance. The pore size distribution of the foams was evaluated by means of image analysis using the Image J software.²²

The thermal conductivity of the processed samples** was measured using the xenon light flash technique (LFT) (Netzsch LFA 467 Hyperflash, Selb, Germany). The samples were cut in disks with a diameter of 5 mm, and the measurements were carried out in a special in-plane sample holder, where the sample is heated in the central region, and the temperature rise measured on the outer ring of the sample. Measurements were carried out twice using different samples, each measured three times.

II.2.3 - Results and discussion

The gelation process that takes place in the suspension after alkali activation was studied concerning its rheological behaviour. The flow curves of the process, plotted in Figure 2, were obtained just after 3 hours from the alkali activation of the SLG and then every hour of permanence in the furnace at 75 °C.

The suspension prepared after 3 hours of mechanical stirring, before its gelation at low temperature (denoted as 0h), presents a narrow thixotropic cycle and low viscosity, both indicating well-dispersed particles in the suspension. Once the gelation process started, the flow curves presented a typical pseudoplastic behaviour, the thixotropic cycle became gradually more significant, and the viscosity increased. The viscous resistance is the result of the formation of gel structures, which enhance the particle interaction and produce viscous resistance to the flow.

After 1 hour of gelation at 75 °C, the production of a hardened foamed body is not possible since the wet cellular structure determined by air incorporation collapsed after the interruption of the mechanical stirring, due to the progressive coalescence of the bubbles before the complete setting of the foam. In contrast, with curing times of at least 2 hours, the shear-thinning behaviour is more pronounced. Higher values of shear stress are obtained at a fixed shear rate, with significant thixotropic cycles and the development of a yield point in the suspension. The transition from continuous mechanical stirring (high shear rate) to interrupted mechanical stirring (a shear rate equal to 0) determined an increase of viscosity that prevented the coalescence of bubbles and allowed to maintain the air trapped, following the foaming process with the surfactant during the complete setting of the wet foam.

** *The thermal diffusivity measures were carried out at the Dipartimento di Scienza Applicata e Tecnologia, Politecnico di Torino supported by Samuele Colonna.*

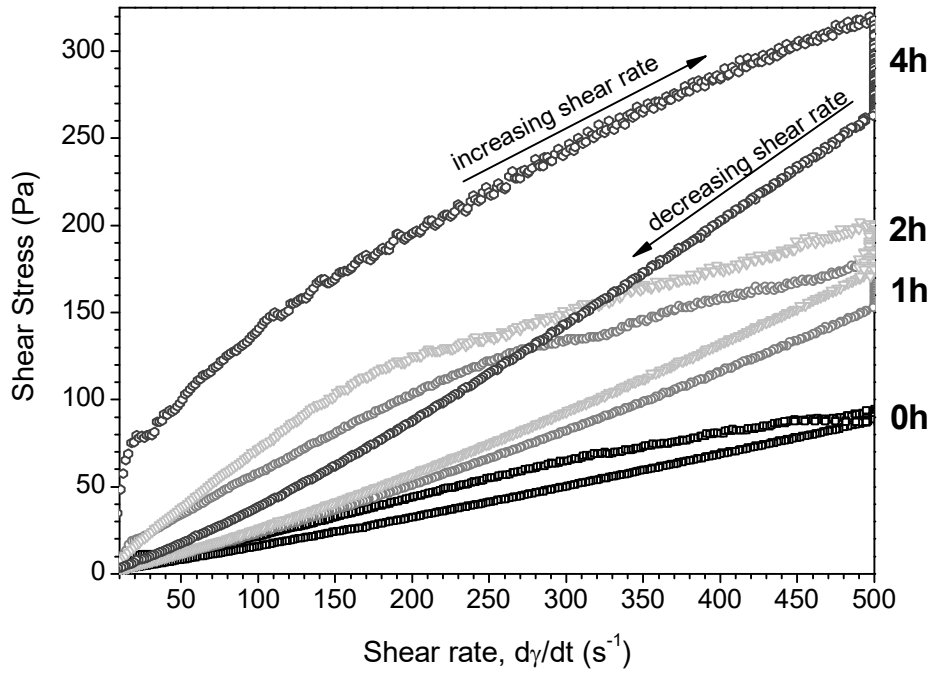


Figure 2. Flow curves of suspensions of SLS glass (65 wt% solids) with different gelation times.

This shear-thinning behaviour can be better understood from the viscosity plot in Figure. The flow curves were analysed considering different regression models; the best fitting results were provided by the Herschel–Bulkley model, as follows:

$$\tau = \tau_0 + K \cdot \dot{\gamma}^n \quad (\text{Eq. 1})$$

Where the shear stress (τ) is given by the sum of yield stress (τ_0) and a factor of shear rate ($\dot{\gamma}$), with K being a consistency factor and n the flow index correlated with pseudoplasticity.^{23, 24} For a Newtonian fluid, the flow index is 1, whereas, for a non-Newtonian pseudoplastic fluid, n is lower than 1. If we consider the viscosity, η , as the ratio between shear stress and shear rate, we can divide the exponential term of Eq.1 by the shear rate:

$$\eta = \frac{\tau}{\dot{\gamma}} = K \cdot \dot{\gamma}^{n-1} \quad (\text{Eq. 2})$$

This can be rewritten as:

$$\text{Log } \eta = \text{Log } K + (n - 1) \cdot \text{Log } \dot{\gamma} \quad (\text{Eq. 3})$$

The data obtained after fitting to the Herschel-Bulkley model are shown in Table 2. The regression analyses were performed only considering the up-curves of the corresponding rheograms. The viscosity at the representative shear rate of 500 s^{-1} and the thixotropy values, calculated as the area enclosed between the up-ramp and the down-ramp of the flow curves, are also given in the table.

Curing time (h)	Thixotropy (Pa·s ⁻¹)	$\eta_{500} \text{ s}^{-1}$ (Pa·s)	τ_o (Pa)	K (Pa·s ⁿ)	n
0	5162	0.191	3.3	0.31	0.93
2	23033	0.403	5.3	4.86	0.66
4	44949	0.637	30.2	6.37	0.61

Table 2. Rheological parameters measured at different curing times.

The thixotropy is related with the energy needed for breaking the structures formed during gelation, and it increases with the curing time, meaning that more complex structures are being formed over time, requiring higher energy to be broken up.

The linearity between viscosity and shear rate, in logarithmic scale, is confirmed by the viscosity plot showed in Fig. 3. We can notice the difference between the mixture just after the alkali activation, practically a Newtonian fluid, with $n = 0.93$, leading to $1 - n \approx 0$ corresponding to an almost horizontal line, and after 2 and 4 hours of curing where n is equal to 0.66 and 0.61 respectively.

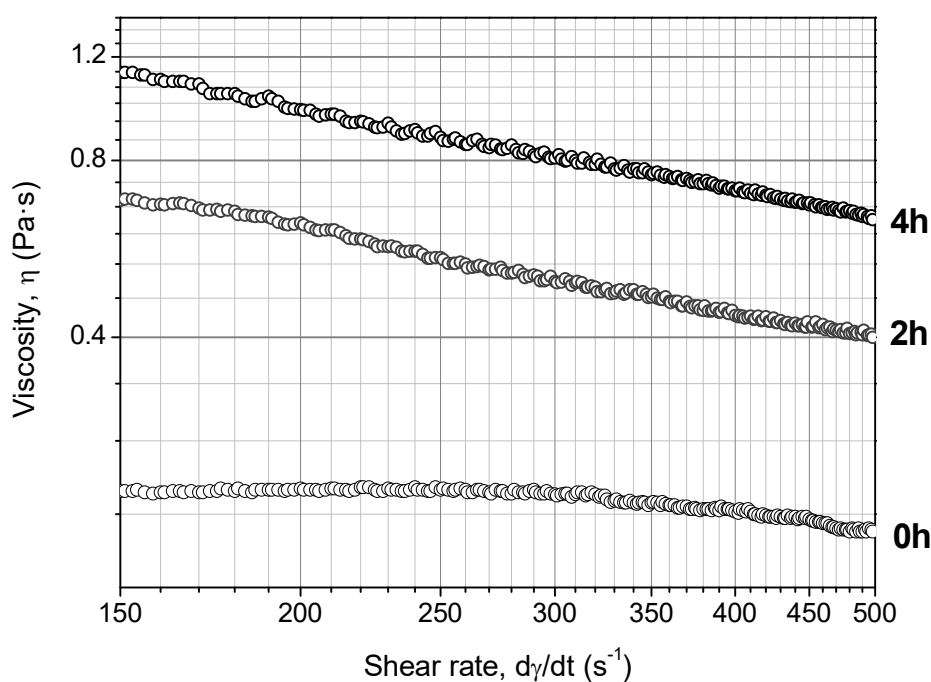


Figure 3. Viscosity plot for selected curing times

After prolonged curing the mixture corresponds, according to Figure 3, to a ‘Bingham-pseudoplastic’ fluid, since the interaction between surface gels formed at the surface of glass particles was so intense that shear rate increased only after the shear stress passed yield stress of about 30 Pa. After the yield point, the decrease of viscosity with increasing shear rate is similar to the one for 2h curing (Fig. 3 actually refers to an interval of shear rate values above the yield point).

The suspensions, before foaming, due to the gelation process at low temperature, present a different rheological behaviour, which can be seen as a tuning parameter for the microstructure of the hardened foams as shown Figure 4, where the optical images of the green foams produced at different gelation times and the pore size distribution calculated by image processing are presented.

The hardened bodies obtained with no curing treatment and after 1 hour of gelation are not presented here. As explained, the limited pseudoplasticity of the suspension does not allow to retain the air incorporated in the wet foam. Subsequently, the progressive coalescence of bubbles leads to the collapse of the foam before the complete setting. In contrast, the foams obtained after longer curing times, thanks to a higher pseudoplasticity of the slurries, where the coalescence phenomena is not so significant, and the wet foams, reach the complete setting before the collapse of the structure. The hardened foams obtained after 2 hours exhibited a quite coarse microstructure, with many big interconnect pores surrounded by smaller ones, as an effect of a limited coalescence between adjacent bubbles (Fig. 4a). The higher pseudoplasticity of the suspension after a longer curing step, of 3 and 4 hours, progressively reduces the coalescence, and the hardened foams obtained (Fig. 4b,c) present further spherical cells in a more homogeneous cell structure. In particular, a curing step of 4 h was found to enhance the uniformity of foams (Fig. 4c).

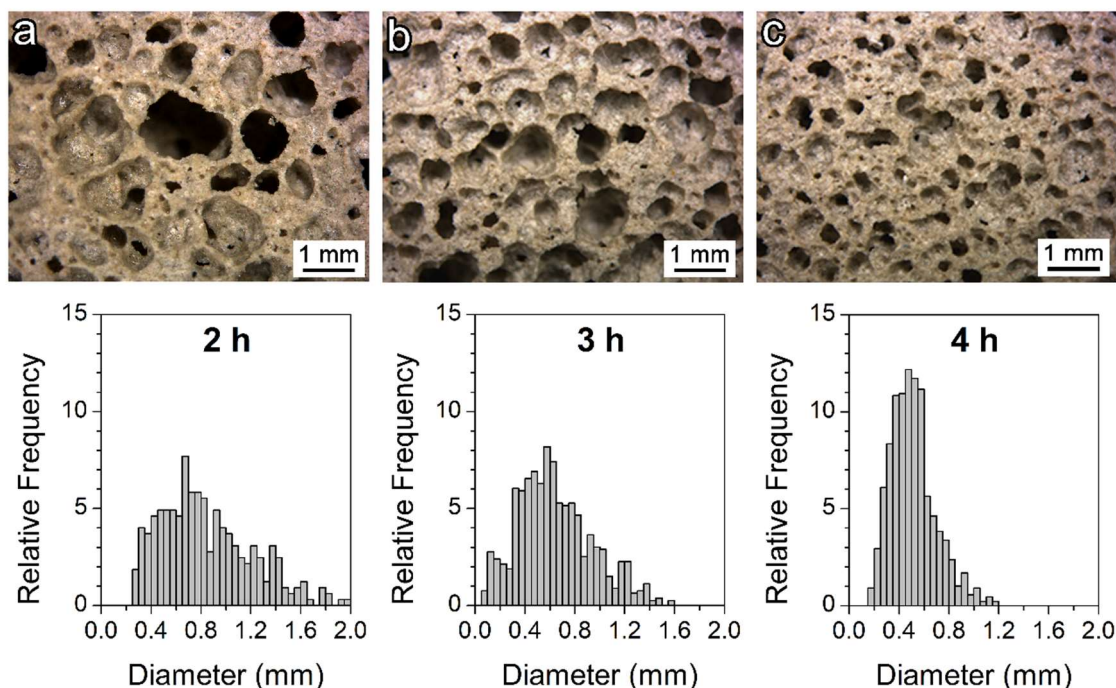


Figure 4. Microstructural details and pore size distribution (bottom) of hardened foamed gels after different gelation times.

The pore size distribution of the foams in Fig. 4c (bottom) shows that the optimised curing time led to a quite narrow pore size distribution centred at 500 μm , with a very limited fraction of pores having a diameter above 1 mm. Samples produced from shorter

curing (Fig. 4a, b), on the contrary, are evidently not uniform, presenting a significant fraction of pores above 1 mm in diameter.

Pre-curing time (hours)	Density, ρ (g/cm ³)			Porosity (%)			Strength σ_{comp} (MPa)
	geometric	apparent	true	total	open	closed	
2	0.74 ± 0.02	2.08 ± 0.03	2.11 ± 0.02	65 ± 4	64 ± 5	1 ± 3	0.8 ± 0.5
3	0.67 ± 0.01	2.14 ± 0.06	2.22 ± 0.02	70 ± 5	69 ± 6	1 ± 2	1.2 ± 0.6
4	0.57 ± 0.01	2.29 ± 0.04	2.31 ± 0.02	75 ± 5	75 ± 4	0.2 ± 0.1	1.3 ± 0.8

Table 3. Density, porosity and mechanical properties of the hardened foams.

The density and porosity values of hardened foams reported in Table 3 shows a porosity increase with the pre-gelation time from 65 to 75%, with all samples practically having a fully open porosity. This increment is due to a better homogenization and distribution of the cells in the foams and the reduction of the thickness of the cell walls because of a limited coalescence with the longer pre-curing times

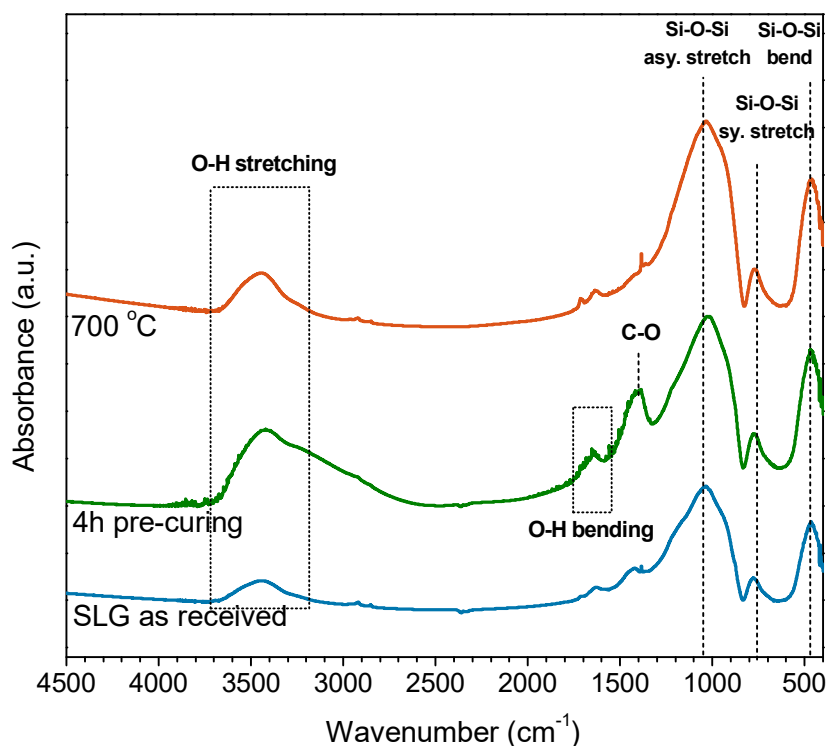


Figure 5. FTIR spectra of selected materials

As expected, the materials after the post-foaming curing step were not chemically stable. When placed in distilled water, the foams led to a quite rapid increase of pH (up to ≈ 12), reasonably due to the release of alkali from the gels that previously caused the

setting. Even though the mechanical strength, also reported in Table 3, is high enough to permit the easy manipulation of the green bodies.

Some indications relating to the nature of the compounds developed upon curing and the related transformations, upon firing, may come from the FTIR spectra of selected samples shown in Figure 5. The initial glass presents the characteristic symmetric and asymmetric stretch as well as the bending bands of Si-O groups centred at 1000, 700 and 450 cm^{-1} respectively.

A broad band in the 3000-3500 cm^{-1} interval is also detected in the initial glass, and corresponds to the O-H symmetric stretch, which is probably the result of atmospheric moisture. In the hardened foams, this band becomes broader and more intense. In addition, the band at 1625 cm^{-1} generated by the bending vibrations of the OH groups indicate the presence of hydrated compounds after alkali activation.

On the other hand, the band generated by the SiO_4 groups at around 1000 cm^{-1} in the hardened foam is slightly shifted to lower wavenumbers, which is consistent with the formation of C-S-H gels in the presence of alkali.^{25, 26} A new band centred at 1450 cm^{-1} is produced by the stretching vibrations of O-C-O groups, as also observed in C-S-H gels, and indicates a slight formation of carbonate compounds.²⁷

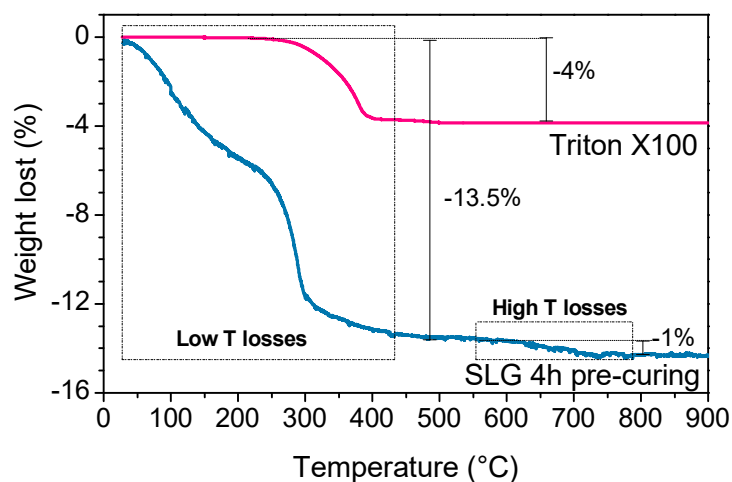


Figure 6. Thermogravimetric plot of surfactant and gelified glass-based mixture.

The thermogravimetric analysis (TGA) of the hardened foam after activation and the complete setting is shown in Figure 6. The graph also shows the weight loss of pure Triton X-100, normalised according to the actual 4 wt% content, which represents the amount of additive used in the foaming process. The weight loss of the hardened foam can be separated into two well-distinct ranges of weight loss, respectively at a temperature below 500 °C, and above 600 °C.

Nearly a 14 wt% of weight loss is generated at low temperature; with a loss of around 5 wt% below 200 °C, attributable to the loss of physically bonded water. The further weight losses, around 9 wt%, occurring between 200 and 500 °C could not be attributed to the burn-out of surfactant, added in a content of 4 wt%, and they are in agreement with the formation of hydrated compounds, known to lead to water releases with higher temperatures.²⁸ The weight losses above 600 °C can be attributed to the decomposition of hydrated compounds, with the release of water from the removal of -OH groups.

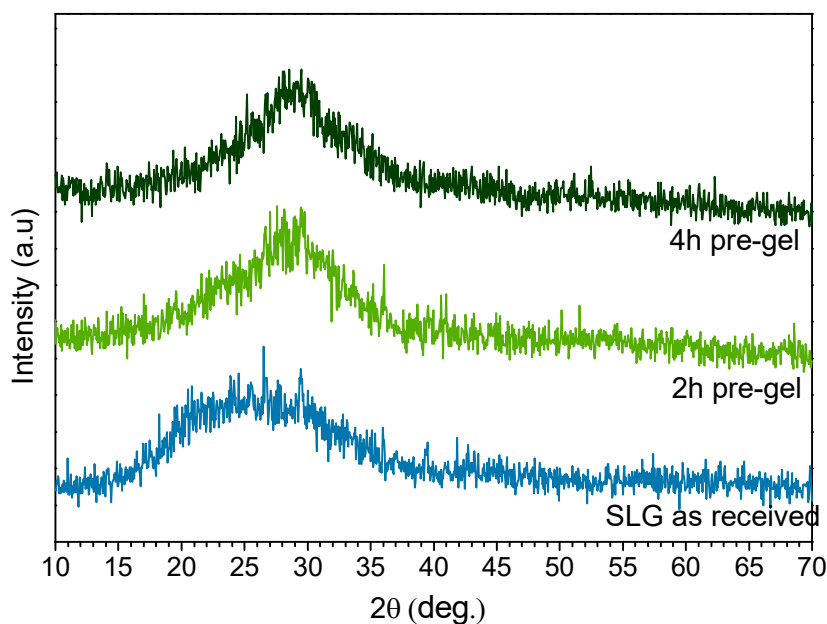


Figure 7. X-ray diffraction patterns of SLG as received and glass foams in the hardened state

Figure 7 represents the diffraction patterns of as-received soda-lime glass and hardened foams foamed after 2 and 4 hours of pre-gelation at 75°C. The XRD patterns of the initial SLG and those of the unfired foams present a broad halo attributed to the glassy phase, which does not permit the identification of crystalline phases. Nonetheless it could be noticed the shifting of halo peak for glass powder from around $2\theta = 24-26^\circ$, representative of SiO_2 [PDF#82-1575], for the initial glass powders, to $2\theta = 28-30^\circ$, in the activated samples, specific for potassium sodium silicate hydrate [PDF#47-1837], potassium hydrogen silicate [PDF#43-0629] or sodium hydrogen silicate hydrate [PDF#80-0698].²⁹ This shift indicates the different structural features determined by the alkaline activation of glass powder; in fact, the shift at higher angles is known to be correlated, in a glass, with the incorporation of network modifiers. In addition it can be seen as a clear indication of the compositional changes determined by the alkaline activation of glass powder, and the formation of a tobermoritic type gel, which always remains in an amorphous phase.

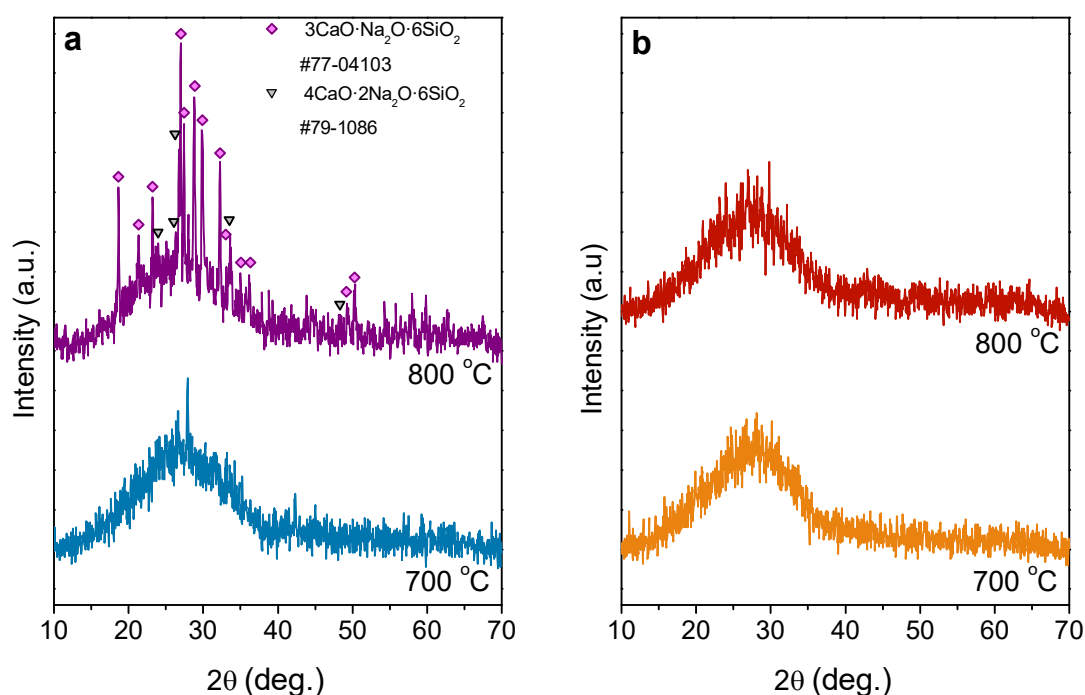


Figure 8. Diffraction patterns of foamed samples after heat treatment at different heating rates; a) slow heating rate (1 °C/min); b) fast heating rate (10 °C/min)

Figure 8 represents the diffraction patterns after the heat treatment at different heating rates. Working at a low heating rate of 1 °C/min (Fig. 8a), significant changes can be noticed in the crystallisation at 700 °C: the structure remains amorphous, and the ‘halo’ shifts back to lower angles. In this perspective, this is consistent with the decomposition of the hydrated compounds and the dissolution of oxides in the new glass matrix, so that only the shift from alkali incorporation remains.^{30, 31}

On the contrary, the heat treatment at 800 °C determined significant precipitation of sodium-calcium silicates (mainly 3CaO·Na₂O·6SiO₂ [PDF#77-0410], with traces of 4CaO·2Na₂O·6SiO₂ [PDF#79-1086]). These phases are well-known crystal phase from the devitrification of soda-lime glass, but at higher temperatures;³² the formation of an alkali-rich glass, from the decomposition of gels, evidently promoted the devitrification. The significant devitrification in the samples treated could be seen as an effect of ionic inter-diffusion from the original glass and the low viscosity glassy coating phase formed by the decomposition of gels.

When the samples are treated at a fast heating rate of 10 °C/min, to reproduce the condition of industrial production (Fig. 8b). The x-ray diffraction patterns do not allow the detection of any phase, the halo shifts again to lower angles, as in the case of the samples treated at 700 °C with low heating rate, confirming the incorporation of the alkali in the glass structure.

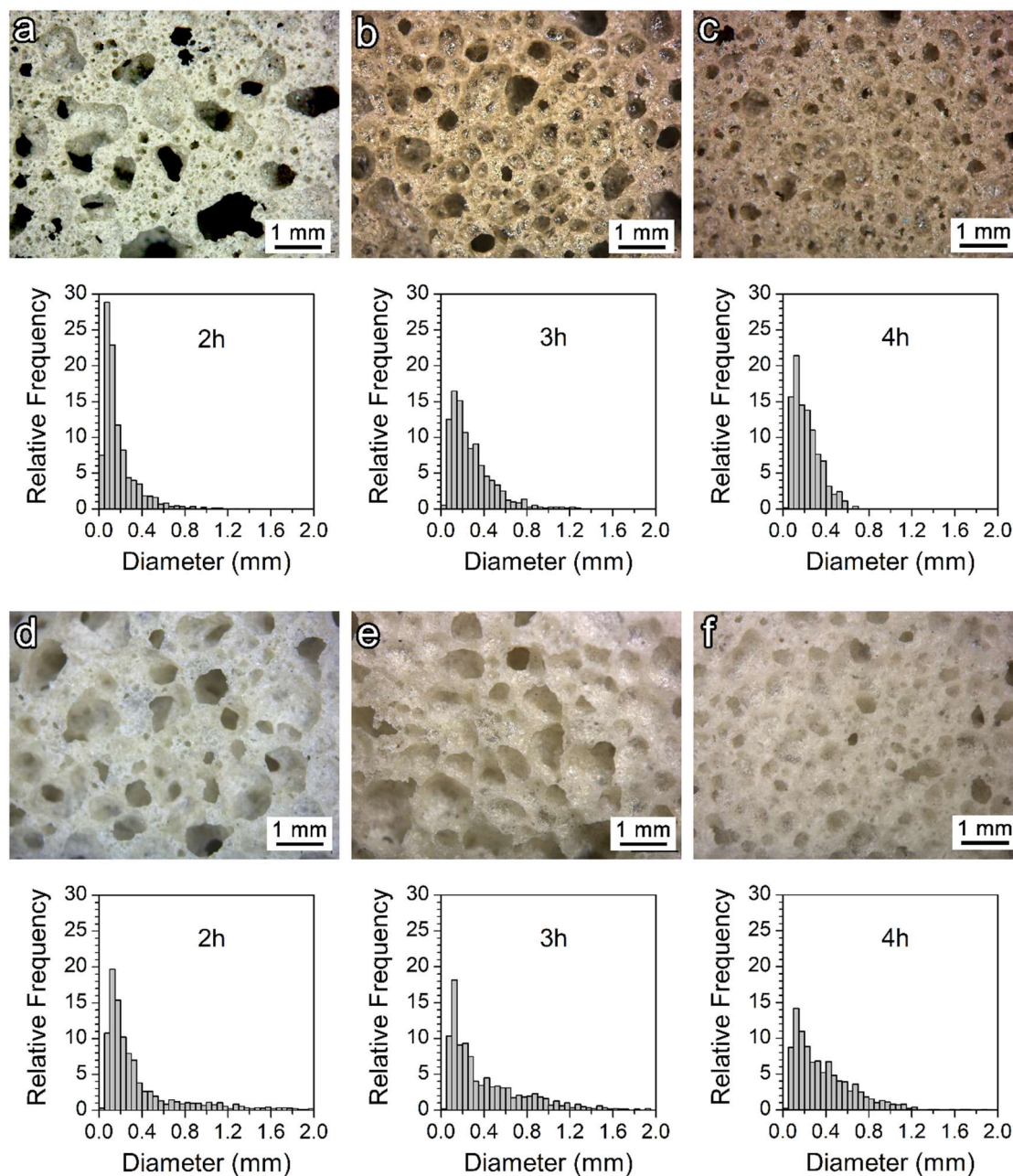


Figure 9. Microstructural details and pore size distribution of glass foams after firing at 700 °C (a-c) and 800 °C (d-f) [heating rate of 1 °C/min].

The heat treatment at 700 and 800 °C - after slow heating at 1 °C/min (aimed at the burn-out of the surfactant) - caused significant transformations in the cellular structures, especially for foams produced with short pre-foaming curing times. It can be seen in the optical images of the heat treated foams produced at different gelation times and the pore size distributions presented in Figure 9.

In these cases, the foams after firing are much more uniform than the hardened foams, and they present a narrower pore size distribution. The foam produced at 700 °C with 2h curing, as shown by Fig. 9a, features big pores surrounded by thick, micro-porous struts;

the foam produced with 3h curing, shown in Fig. 9b becomes quite similar in morphology to the foam produced with 4h curing, presented in Fig. 9c. Moreover, its pore structure remains similar to the hardened samples. The foam with 4h curing maintains a higher homogeneity, with only a limited fraction of pores with a diameter above 400 μm . The pore size distributions of foams after firing, shown below the corresponding image proves this evolution quantitatively. Analogous observations can be done on foams after firing at 800 $^{\circ}\text{C}$, as shown in Figure 5. In this samples, a wider pore distribution could be observed, with an increase of the mean pore size.

The transformations of the cellular structure are likely due to the decomposition mentioned above of hydrated compounds, which determined a ‘secondary foaming’. At 700 $^{\circ}\text{C}$, as firing temperature, the pore structure transformations would be low, for the foaming of soda-lime glass, but we must take into account the effect of alkali incorporation. Alkali-rich surface gels surrounding glass powders are reasonably transformed into a low viscosity glass phase, acting as a ‘glue’ for undissolved material, promoting ionic inter-diffusion and finally favouring the secondary foaming by water release. The pronounced devitrification at 800 $^{\circ}\text{C}$ could be seen as an effect of ionic inter-diffusion from the original glass and the low viscosity glassy coating phase formed by decomposition of gels.

It is interesting to note that, from the reflected light in optical images, the foams after treatment at 700 $^{\circ}\text{C}$ feature closed ‘membranes’ between adjacent pores: the release of water vapour evidently led to closed pores, in analogy with the conventional sintering technology of glass foams (gas evolution upon sintering).

The samples produced after 4 hours of pre-gelation present the narrowest pore distribution and a very homogeneous pore structure, and therefore they were also treated at a fast heating rate at 10 $^{\circ}\text{C}/\text{min}$ in order to reproduce the firing process at an industrial scale. The pore structures that were obtained after treatment at 700 and 800 $^{\circ}\text{C}$ and produced with a faster heating rate are shown in Figure 10. In both samples an enlargement of the pores can be noticed, and the sample treated at 700 $^{\circ}\text{C}$ (Fig. 10a) shows a more homogeneous structure presenting cells with spherical shape in a narrower pore distribution, meanwhile the distortion of the initial pore structure in the samples treated at 800 $^{\circ}\text{C}$ (Fig. 10b) is much more evident, showing very large cells that lost their spherical form

The secondary foaming process also determines the enlargement of the pore structure. At a faster heating rate, the gases produced due to the decomposition of the hydrated compounds remain trapped inside the low viscosity glass phase, which is formed before the complete water release, producing this reshaping. The effect is more evident in the foams treated at 800 $^{\circ}\text{C}$, as no crystallisation occurs at a faster heating rate (see the X-ray diffraction pattern in Fig. 3); the higher temperature produces a lower viscosity phase increasing the bubble coalescence.

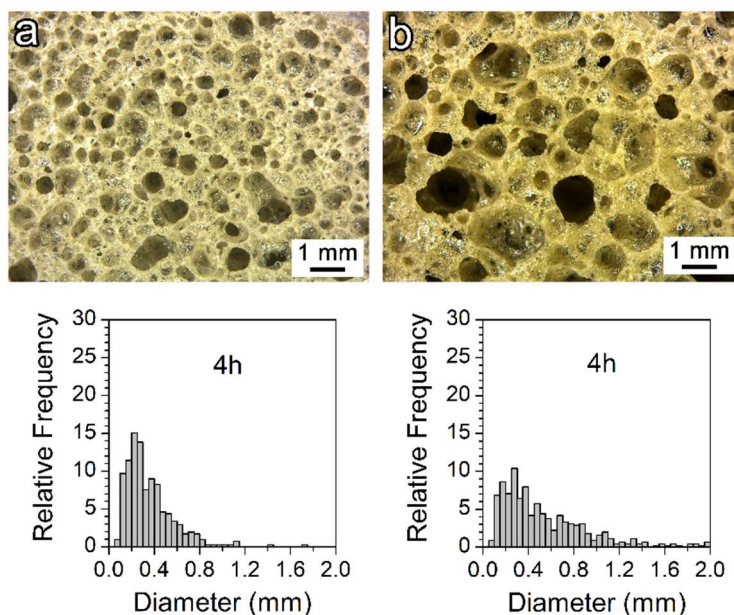


Figure 10. Microstructural details and pore size distribution of glass foams after firing at 700 °C (a) and 800 °C (d) [heating rate of 10 °C/min].

Pre-curing (hours)	Firing T ^a (°C)	Density, ρ (g/cm ³)			Porosity (%)			Strength σ_{comp} (MPa)
		geometric	apparent	true	total	open	closed	
Slow heating rate (1 °C/min)								
2	700	0.26 ± 0.03	0.55 ± 0.03	2.50 ± 0.01	90 ± 2	52 ± 1	37 ± 2	1.8 ± 0.7
	800	0.21 ± 0.03	2.73 ± 0.05	2.89 ± 0.01	92 ± 2	92 ± 1	1 ± 2	1.0 ± 0.2
3	700	0.27 ± 0.02	0.45 ± 0.02	2.44 ± 0.05	89 ± 1	39 ± 2	50 ± 1	2.0 ± 0.4
	800	0.27 ± 0.01	2.42 ± 0.02	2.73 ± 0.01	89 ± 1	88 ± 1	1 ± 1	2.4 ± 0.7
4	700	0.30 ± 0.01	0.43 ± 0.06	2.50 ± 0.02	88 ± 1	31 ± 2	57 ± 1	4.8 ± 0.3
	800	0.28 ± 0.01	2.41 ± 0.05	2.66 ± 0.03	89 ± 1	88 ± 2	1 ± 1	2.9 ± 0.4
Fast heating rate (10 °C/min)								
4	700	0.34 ± 0.03	0.48 ± 0.08	2.48 ± 0.08	86 ± 1	29 ± 2	57 ± 3	3.3 ± 0.5
	800	0.17 ± 0.01	2.41 ± 0.06	2.66 ± 0.04	93 ± 2	84 ± 4	9 ± 2	0.4 ± 0.1

Table 4. Density, porosity and mechanical properties of the fired treated foams at different heating rates.

The density data in Table 4 confirm the microstructural changes that occur upon firing. After the thermal treatment, all the samples present an increment of the total porosity achieving values close to 90%, and this increase could be explained by the decomposition

of the hydrates compounds with gas evolution, which promotes the foaming of the softening glass. The open porosity returned dominant at 800 °C, however, after the heat treatment at 700 °C, some closed porosity is formed. This is not a contradiction because the foaming of glass is not a ‘static’ process, simply involving cell nucleation, in the pyroplastic mass of softened glass, and growth. Bubbles may collapse and be replaced by new ones, formed later.

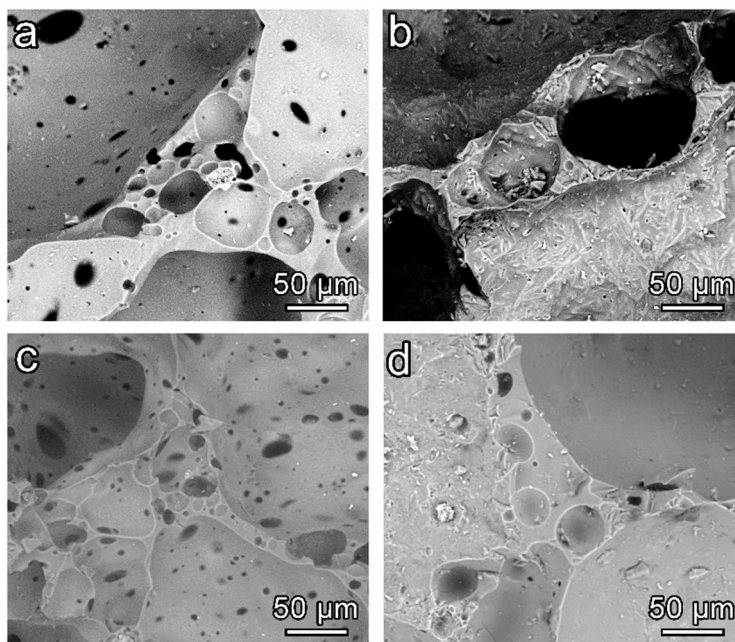


Figure 11. High magnification details of glass foams after firing at: a) 700 °C; b) 800 °C [low heating rate] c) 700 °C; c) 800 °C [fast heating rate]

Figure 11 shows a comparison between struts after firing at 700 (Fig. 11a) and 800 °C (Fig. 11b) with a slow heating rate, and those treated at 700 (Fig. 11c) and 800 °C (Fig. 11d) with a fast heating rate. In both samples treated at 700 °C, the struts contain several small pores, with small openings; the low open porosity could be ascribed to the fact that the openings did not determine continuous paths.

The small pores at the struts are likely to merge with increasing firing temperature, forming bigger pores like the one shown in Fig. 11b and 11d. Meanwhile in the sample treated with a slow heating rate the crystallisation blocked the re-shaping of pores, due to local increase of viscosity (softened glass turned into a suspension with rigid inclusions, represented by crystals), impeding the formation of continuous walls and leaving the pore structure mostly open. With a higher heating rate (10 °C/min), the foams treated at 800 °C remained practically amorphous (see the X-ray diffraction pattern in Fig. 3); however, the effect of remodelling by viscous flow was so intensive that cells had a significant coarsening (see Fig. 7). The high amount of open porosity could be an artefact, i.e. it could be due not to a system of interconnecting pores, but to gas occupying very large bubbles on the surface of tested samples.

The different microstructures had an impact on the mechanical properties. The compressive strength of a glass foam is typically a function of the relative density, according to the well-known Gibson and Ashby model:

$$\sigma_f \approx \sigma_{\text{bend}} \cdot f(\Phi, \rho_{\text{rel}}) = \sigma_c = \sigma_{\text{bend}} [C \phi (\rho_{\text{rel}})^{3/2} + (1 - \phi) \rho_{\text{rel}}] \quad (\text{Eqn. 4})$$

Where f is a ‘structural function’, depending on the relative density (ρ_{rel} , the ratio between the measured density of the foams and the true density, i.e. the density of the solid phase) and its distribution (open or closed porosity). The quantity $(1 - \Phi)$ expresses the fraction of solid positioned at the cell faces; if the foam is open-celled, the pores are fully interconnected with material only on the cell edges, so that $\Phi = 1$ ($1 - \Phi = 0$). For closed-cell foam, Φ is lower, with the solid phase constituting mostly cell walls and thus enhancing the linear term. C is a dimensionless calibration constant (~ 0.2). The reference soda lime glass bending strength σ_{fs} is 70 MPa, a typical value for the container glass employed as commercial material.¹⁴

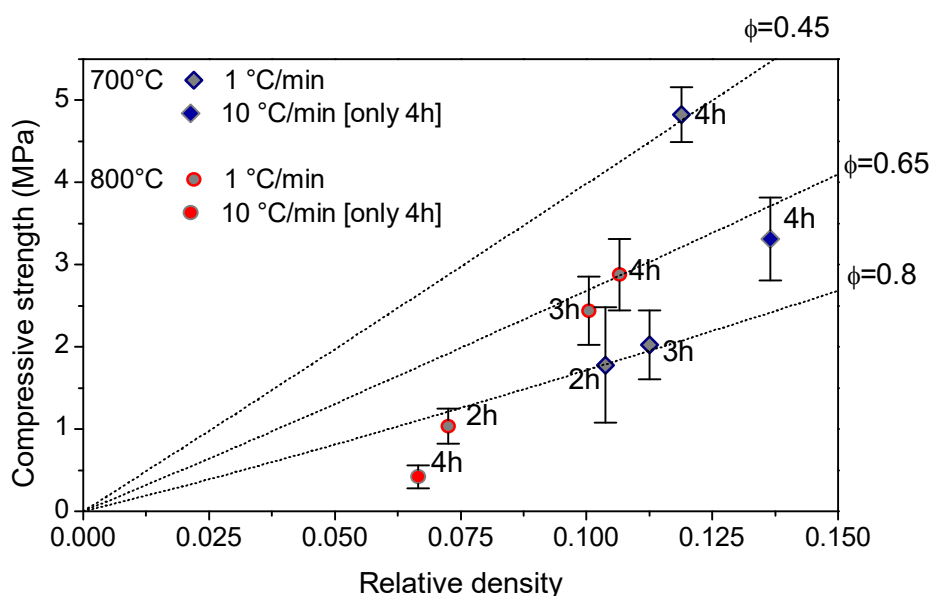


Figure 12. Strength/relative density correlation for selected glass foams.

From figure 12 the more homogeneous samples, with 4h pre-foaming curing, fired at 700 °C in both heating modes, can be considered ideal since they exhibited a crushing strength of more than 3 MPa with an overall porosity well above 85%. Although microporous, the membranes between adjacent cell walls were mechanically collaborating, so that the data are fitted by Φ well below 1. Firing at 800 °C had contrasting effects: while foams fired at slow heating rates were still particularly strong, given the high porosity (nearly 90%), as a consequence of the crystallisation. The foams fired at high heating rate were quite weak (Φ above 0.8), owing to the very coarse cellular structure.

Firing treatments at low heating rate are probably difficult to be applied at an industrial scale. In any case, the foams corresponding to the firing at 700 °C, with a more industrially viable heating rate of 10 °C/min, compare favourably with commercial products. In particular, the specific strength (σ_f / ρ) of these foams approaches 10 MPa·cm³/g, a level exhibited only by the best variant of commercial Foamglas®.³³ The weak foams fired at 800 °C actually are still comparable to other commercial foams (foams of similar density have a compressive strength of 400–800 kPa).^{34, 35}

In order to evaluate the viability of glass foams production at an industrial scale, further studies were conducted on the foam produced after 4h of pre-gelation and fired at 700 °C (10 °C/min), since the glass foams obtained with these process parameters are the more promising to be applied in commercial products.

Concerning the durability, the samples were immersed in distilled water and, after 10 days of immersion, no increase in pH, as a result of the incorporation of alkali in the glass structure, was observed (the pH, from a neutral value of 7, actually decreased to 6.5 after 10 days of immersion due to CO₂ dissolution from the atmosphere).

The thermal conductivity measured at 25 °C was $0.0926 \pm 0.0005 \text{ W}\cdot\text{m}^{-1}\cdot\text{K}^{-1}$. Although the high amount of open porosity observed in this foams, open porosity reduces the thermal insulation ability.³⁶ The cellular structure formed by small pores in the cell walls had probably an advantageous effect, by reducing the solid fraction between the main cells, leading to lower conductivity.

Even if the thermal conductivity test needs to be extended to all the processing conditions, to fully understand their correlation, the achieved values are quite promising, since they are close to the values reported for commercial foams^{33, 34} and in the range of other glass foams described in the literature.³⁷

II.3 - Semi-industrial production of glass foam lightweight panels by inorganic gel casting.

II.3.1 - Experimental process

The semi-industrial production of lightweight panels was developed according to the initial studies carried out in the laboratory. The optimum performance and most suitable processing conditions were obtained for the samples treated at 700 °C and with a fast heating rate (10 °C/min). Therefore these conditions were taken as the initial approach in the upscale of the process. Additionally, the many combinations of processing parameters were explored (e.g. processing times and temperatures, heating rates, concentration and type of surfactant, solid content and glass composition), and the variations arising in the samples produced during the upscaling process were optimised to achieve foams with a better performance.

The alkali activation process was conducted in the same manner as the foams produced in the laboratory. However, a relatively significant amount of activated suspension was prepared, around 5kg for each batch. The process was optimised with technical grade reagents; the alkaline activator was changed from KOH to NaOH as the latter presents economic advantages. Fine powders of waste SLG were placed in a NaOH (technical grade) 2.5M aqueous solution for a solid loading of 70 wt%. The glass powders were exposed to alkaline attack for 4 hours, under low-speed mechanical stirring, and the alkali-activated suspension was cured at 70 °C for 2 hours in the same closed mixing container, The resulting gels were foamed in the same container where the gelation takes place by adding 4wt% of sodium lauryl sulphate (SLS) and then foamed by vigorous mechanical mixing (2000 rpm). Afterwards, the resulting wet foam was cast in bigger polystyrene moulds (15 x 20 cm) and cured at 70 °C for 24 hours in order to complete the curing and hardening, before being demoulded.

Finally, hardened foamed gels were fired at temperatures between 700 and 800 °C for 1 hour with a heating rate of 1-10 °C/min, using a pilot scale continuous tunnel furnace (Nanetti ER-15S) at SASIL S. p. a. (Brusnengo, Biella, Italy). The research samples were fired in a muffle furnace, with heating and cooling rates defined 'statically'. The actual industrial firing should be performed in continuous tunnel furnaces, with heating/cooling rates and holding times that are set by controlling the temperature profile in the same tunnel and the transport speed from one end to the other. The samples were fed directly into the furnace with no preheating step, and the whole treatment lasted 1 hour.

The mechanical and physical characterisation of the foamed panels was conducted using the same procedure as the samples produced in the laboratory. Thermal conductivity* tests on the lightweight panels were performed using a Fox 50 Heat Flow Meter by TA Instruments (New Castle, DE, USA) operating at 25 °C. By cutting cylindrical samples from the panels with 50 mm diameter and 10 mm thickness, three replicated tests were performed on samples taken from different panels.

II.3.2 - Results and discussion

The overall aspect of the hardened lightweight panels produced with SLG, after 24 hours of post-foaming, is illustrated in Figure 13.a. The panels show a good consistency with no cracks and acceptable mechanical properties, which make them easy to handle. After firing at 700 °C (Fig. 13b), some reshaping of the panel takes place as a consequence of the viscous flow, but the overall structure remains unaltered (the sample shown here was not grind cut or rectified) and the fast heat treatment does not produce any visible

* *The thermal conductivity measures were carried out at Element Materials Technology, (Hitchin, United Kingdom) supported by Matteo Cavasin.*

cracks, even if no preheating was applied to the samples and they were inserted directly into the furnace. It can be observed an outer vitreous skin in the surface of the panel.

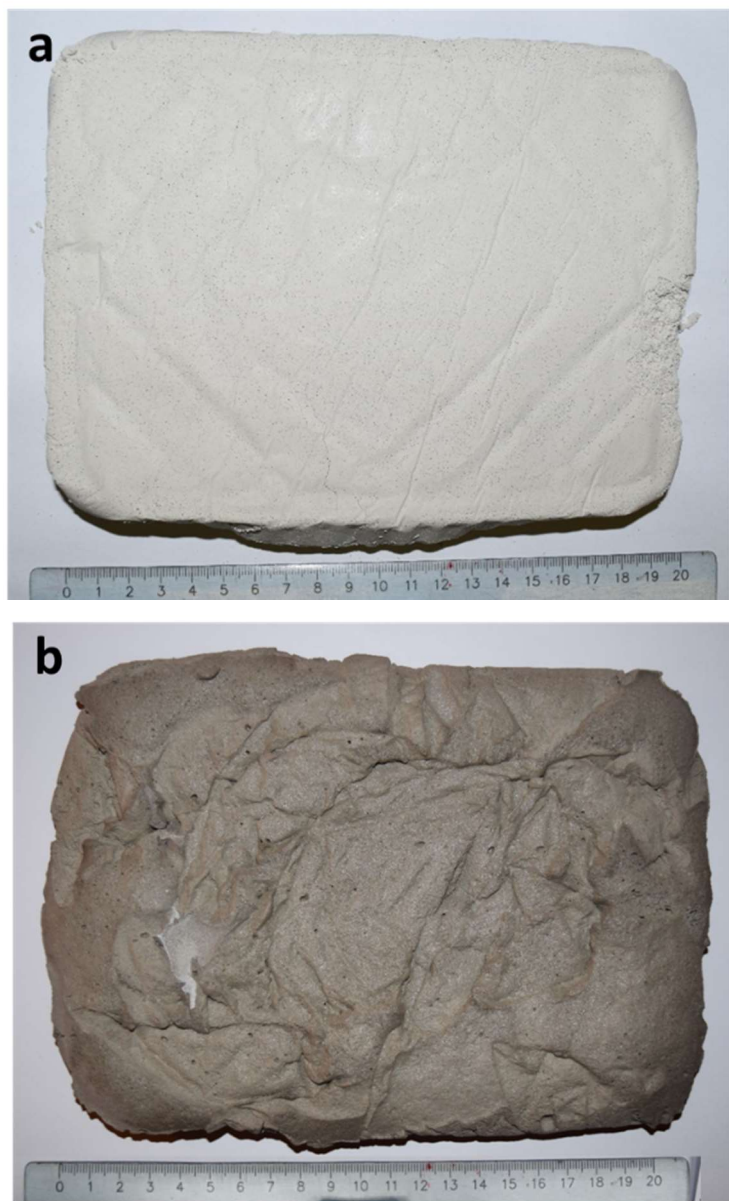


Figure 13. a) General view of a hardened lightweight panel; b) heat treated panel at 700 °C

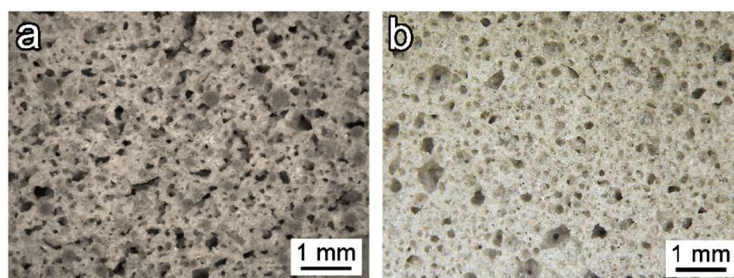


Figure 14. Microstructural details of hardened foamed after curing and after fire treatment at 700 °C

The microstructure of the hardened foam panels and heat treated panels at 700 °C is shown in Figure 14. The hardened panels present a high uniformity of the cellular structure, which is consistent in the whole panel, and no differences in the pore distribution were observed, even with larger sizes. The high uniform cellular structure is maintained in the heat treated samples, and some reshaping arises from the decomposition of the hydrated compounds, formed with the alkali activation process in the softened glass. This secondary foaming, like in the case of the samples produced on a laboratory scale, generates more spherical shaped pores and a slight increase in the pore diameter. The cells obtained are mostly in the 10-30 μm diameter range, although there is evidence of some larger pores. The panels present some closed ‘membranes’ between adjacent pores, and are morphologically similar to the previous foams produced in the laboratory, despite the latter showed bigger pores (Fig. 10a)

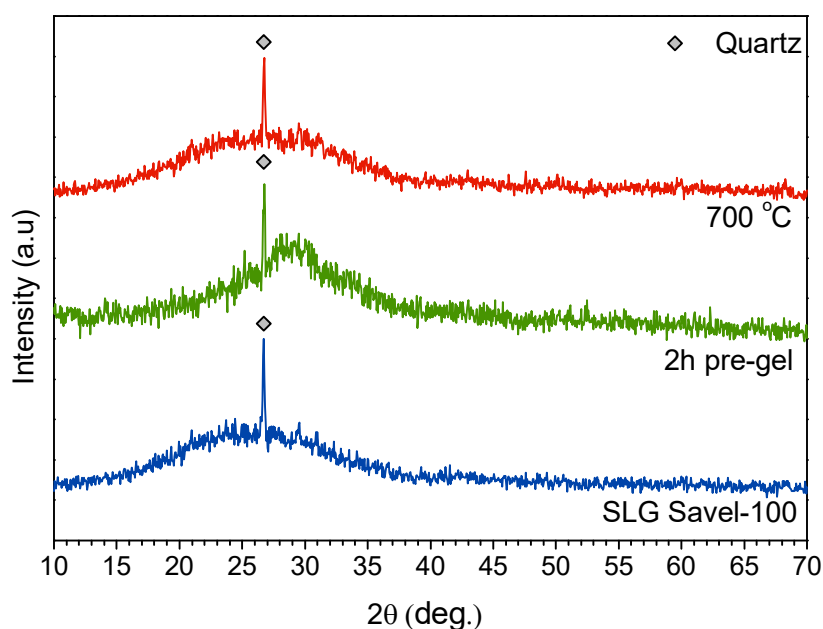


Figure 15. Diffraction patterns of initial SLG and lightweight panels after alkali activation and heat treatment at 700 °C

The x-ray powder diffraction pattern of the original waste glass and the panels produced after hardening and heat treatment at 700 °C are represented in Figure 15. The initial SLG shows the typical diffused halo between 20° and 35°, and a peak that corresponds to quartz (SiO₂ [PDF#85-0335]) is detected, where the crystalline phase remains apparently unaltered with activation. The different glass batches used in this study revealed the presence of quartz, which in previous samples was not detected.

The hardened samples present a shift of the amorphous halo to higher angles, which, as previously described, may be considered a proof of the formation of hydrated compounds with alkali activation. After heat treatment at 700 °C, the lightweight panel remained amorphous, as the fast heat treatment applied did not allow the formation of crystalline phases and the ‘halo’ shifted back to lower angles. In this perspective, this is consistent with the decomposition of the hydrated compounds and dissolution of alkali in new glass matrices. Like this the produced panels present the same behaviour as the samples produced in the laboratory fired at 700 °C with a fast heating rate of 10 °C/min.

Firing T ^a (°C)	Pre- curing (hours)	Density, ρ (g/cm ³)			Porosity (%)			Strength σ _{comp} (MPa)
		geometric	apparent	true	total	open	closed	
700	Panel	0.49 ± 0,01	0.94 ± 0.04	2.45 ± 0.01	80 ± 2	47 ± 6	36 ± 4	5.9 ± 0.3
	Lab	0.34 ± 0.03	0.48 ± 0.08	2.48 ± 0.08	86 ± 1	29 ± 2	57 ± 3	3.3 ± 0.5

Table 5. Density, porosity and mechanical properties of the fired treated panels (the properties of the samples produced in the laboratory are also reported with comparative proposes).

The density and porosity data presented in Table 5 confirm the microstructural changes that occur in the process upscale with variable parameters. The smaller pore size obtained in the lightweight panels led to an increase of the geometric density. However, the total porosity does not undergo substantial changes, remaining over 80%. A ratio of open porosity, which is higher than the one in the laboratory scale samples, can be seen in the panels. This increase can be explained considering the fast heat treatment applied to the panels, which limits the viscous flow of the samples.

The lightweight panels present excellent mechanical properties higher than the analogous samples produced at a laboratory scale, reaching values of 5.9 MPa. The high homogenous structure can explain this significant difference along with the smaller pore diameter presented by the foamed panels

The thermal conductivity measured at 25 °C was 0.079 ± 0.006 W·m⁻¹·K⁻¹. Such a relatively low value could be explained due to the low density and the particular cellular structure developed in the panels. It can be noticed that the lightweight panels present a lower thermal conductivity than the samples produced in the laboratory. Even if they have

a higher open porosity degree, the thermal insulation capacity in the small pore had probably an advantageous effect, by reducing the convection of air in the cells and leading to lower conductivity.³⁶

The excellent combination of mechanical properties and thermal insulation capacity proves the flexibility of the technique. Unlike commercial foams, the newly developed ones do not need any machining after firing. While Foamglas® is cut into regular panels starting from big blocks, foams from our ‘inorganic gel casting’ process may be shaped directly operating on the geometry of moulds; in addition, ‘green’ foams can be machined easily before firing.

II.4 - Conclusions

We may conclude that:

- A novel technique for the production of glass foams from alkali activation of glass suspensions, with subsequent inorganic gel casting and sintering, was successfully developed
- The hardening of glass-based suspensions is caused by the formation of calcium-silicate-hydrate (C-S-H), sodium alumino-silicate-hydrate (N-A-S-H) and calcium alumino-silicate-hydrate (C-A-S-H) gels, (‘inorganic gel-casting’).
- The cellular structure can be tuned depending on the rheology of gelified suspensions, adjusting viscosity with gelation time.
- Surfactants affect the morphology of ‘green’ foams but do not determine ‘secondary foaming’, which depends on the decomposition of hydrated compounds (and possibly other compounds developed upon hardening, e.g. minor traces of carbonate compounds).
- The firing treatments can be used to advance tune the porous structure and the ratio between open and closed porosity. Further, the heating rates used can promote crystallisation.
- A significant number of combinations of processing parameters can be modified (surfactants, activating solution, curing times or heat treatment conditions) allowing to tune and obtain the desired final properties of the resulting glass-ceramic foams.
- The upscaling of the process in the production of the lightweight panel with similar characteristics to the samples produced in the laboratory validates the innovative foaming process.
- The process is easier to control, leading to more flexibility in the production, since the final properties of the product are not correlated with the composition

of the starting raw materials. A homogeneous product is obtained even if the initial source presents some fluctuations in the chemical composition, as is the case of waste materials.

- The excellent mechanical properties along with the thermal insulator capacity demonstrate that the new process can be used as an alternative to the traditional method for the production of glass foams.

References

- 1 Press release European Container Glass industry welcomes long awaited circular economy package. Using waste as a secondary raw material in a closed loop is key Brussels, 02 December 2015.
- 2 Beerkens, R., Kers, G., & van Santen, E. (2011, January). Recycling of post-Consumer glass: energy savings, CO2 emission reduction, effects on glass quality and glass melting. In *Ceramic Engineering and Science Proceedings* (Vol. 32, pp. 167-194). American Ceramic Society, Inc., 735 Ceramic Place Westerville OH 43081 United States.
- 3 Gibson, L. J., & Ashby, M. F. (1999). *Cellular solids: structure and properties*. Cambridge university press.
- 4 Bonifazi, G., & Serranti, S. (2006). Imaging spectroscopy based strategies for ceramic glass contaminants removal in glass recycling. *Waste Management*, 26(6), 627-639.
- 5 Farcomeni, A., Serranti, S., & Bonifazi, G. (2008). Non-parametric analysis of infrared spectra for recognition of glass and glass ceramic fragments in recycling plants. *Waste Management*, 28(3), 557-564.
- 6 Rincón, A., Marangoni, M., Cetin, S., & Bernardo, E. (2016). Recycling of inorganic waste in monolithic and cellular glass-based materials for structural and functional applications. *Journal of Chemical Technology & Biotechnology*, 91(7), 1946-1961.
- 7 Rawlings, R. D., Wu, J. P., & Boccaccini, A. R. (2006). Glass-ceramics: their production from wastes—a review. *Journal of Materials Science*, 41(3), 733-761.
- 8 Yao, Z., Ling, T. C., Sarker, P. K., Su, W., Liu, J., Wu, W., & Tang, J. (2018). Recycling difficult-to-treat e-waste cathode-ray-tube glass as construction and building materials: A critical review. *Renewable and Sustainable Energy Reviews*, 81, 595-604.
- 9 Meylan, G., Ami, H., & Spoerri, A. (2014). Transitions of municipal solid waste management. Part II: Hybrid life cycle assessment of Swiss glass-packaging disposal. *Resources, Conservation and Recycling*, 86, 16-27.
- 10 Tulyaganov, D. U., Fernandes, H. R., Agathopoulos, S., & Ferreira, J. M. F. (2006). Preparation and characterization of high compressive strength foams from sheet glass. *Journal of Porous Materials*, 13(2), 133-139.
- 11 Scarinci, G., Brusatin, G., & Bernardo, E. (2005). Glass foams. *Cellular ceramics: structure, manufacturing, properties and applications*, 158-176.
- 12 Fedorov, A. G., & Pilon, L. (2002). Glass foams: formation, transport properties, and heat, mass, and radiation transfer. *Journal of Non-Crystalline Solids*, 311(2), 154-173.

- 13 <https://uk.foamglas.com/en-gb/products/foamglas-the-product/production-fabrication> (Accessed July 2018).
- 14 Llaudis, A. S., Tari, M. J. O., Ten, F. J. G., Bernardo, E., & Colombo, P. (2009). Foaming of flat glass cullet using Si₃N₄ and MnO₂ powders. *Ceramics international*, 35(5), 1953-1959.
- 15 Jelle, B. P. (2011). Traditional, state-of-the-art and future thermal building insulation materials and solutions—Properties, requirements and possibilities. *Energy and Buildings*, 43(10), 2549-2563.
- 16 Galbraith, C. (2000). The European Market for Thermal Insulation Products. *Materials Technology*, 15(1), 103-105.
- 17 Sepulveda, P., Jones, J. R., & Hench, L. L. (2002). In vitro dissolution of melt-derived 45S5 and sol-gel derived 58S bioactive glasses. *Journal of Biomedical Materials Research: An Official Journal of The Society for Biomaterials, The Japanese Society for Biomaterials, and The Australian Society for Biomaterials and the Korean Society for Biomaterials*, 61(2), 301-311.
- 18 Jones, J. R., & Hench, L. L. (2003). Effect of surfactant concentration and composition on the structure and properties of sol-gel-derived bioactive glass foam scaffolds for tissue engineering. *Journal of Materials Science*, 38(18), 3783-3790.
- 19 Wu, Z. Y., Hill, R. G., Yue, S., Nightingale, D., Lee, P. D., & Jones, J. R. (2011). Melt-derived bioactive glass scaffolds produced by a gel-cast foaming technique. *Acta Biomaterialia*, 7(4), 1807-1816.
- 20 Novajra, G., Perdika, P., Pisano, R., Miola, M., Bari, A., Jones, J. R., ... & Vitale-Brovarone, C. (2015). Structure optimisation and biological evaluation of bone scaffolds prepared by co-sintering of silicate and phosphate glasses. *Advances in Applied Ceramics*, 114(sup1), S48-S55.
- 21 Marangoni, M., Ponsot, I., Kuusik, R., & Bernardo, E. (2014). Strong and chemically inert sinter crystallised glass ceramics based on Estonian oil shale ash. *Advances in Applied Ceramics*, 113(2), 120-128.
- 22 <https://imagej.nih.gov/ij/>. (Accessed July 2018).
- 23 Bergstrom, L. (2017). *Surface and colloid chemistry in advanced ceramics processing*. Routledge.
- 24 Vieira Jr, L. E., Rodrigues Neto, J. B., Klein, A. N., Moreno, R., & Hotza, D. (2011). Rheological and structural characterization of Ni–SiO₂ nanocomposites produced by aqueous colloidal processing. *Journal of the American Ceramic Society*, 94(12), 4179-4183.
- 25 Lodeiro, I. G., Fernández-Jiménez, A., Palomo, A., & Macphee, D. E. (2010). Effect on fresh CSH gels of the simultaneous addition of alkali and aluminium. *Cement and Concrete Research*, 40(1), 27-32.
- 26 Fernández-Jiménez, A., Puertas, F., Sobrados, I., & Sanz, J. (2003). Structure of calcium silicate hydrates formed in alkaline-activated slag: influence of the type of alkaline activator. *Journal of the American Ceramic Society*, 86(8), 1389-1394.
- 27 Vafaei, M., & Allahverdi, A. (2017). High strength geopolymer binder based on waste-glass powder. *Advanced Powder Technology*, 28(1), 215-222.
- 28 Zhang, Q., & Ye, G. (2012). Dehydration kinetics of Portland cement paste at high temperature. *Journal of thermal analysis and calorimetry*, 110(1), 153-158.

- 29 Dimas, D., Giannopoulou, I., & Papias, D. (2009). Polymerization in sodium silicate solutions: a fundamental process in geopolymerization technology. *Journal of materials science*, 44(14), 3719-3730.
- 30 Cyr, M., Idir, R., & Poinot, T. (2012). Properties of inorganic polymer (geopolymer) mortars made of glass cullet. *Journal of Materials Science*, 47(6), 2782-2797.
- 31 Hemmings, R. T., & Berry, E. E. (1987). On the glass in coal fly ashes: recent advances. *MRS Online Proceedings Library Archive*, 113.
- 32 Hrma, P., Smith, D. E., Matyáš, J., Yeager, J. D., Jones, J. V., & Boulos, E. N. (2006). Effect of float glass composition on liquidus temperature and devitrification behaviour. *Glass Technology-European Journal of Glass Science and Technology Part A*, 47(3), 78-90.
- 33 http://uk.foamglas.com/__/frontend/handler/document.php?id=131&type=42 [accessed July 2018]
- 34 <http://www.misapor.ch/>. (Accessed July 2018).
- 35 <http://www.glapor.de/>. (Accessed July 2018).
- 36 Petersen, R. R., König, J., & Yue, Y. (2015). The mechanism of foaming and thermal conductivity of glasses foamed with MnO₂. *Journal of Non-Crystalline Solids*, 425, 74-82.
- 37 Méar, F., Yot, P., Viennois, R., & Ribes, M. (2007). Mechanical behaviour and thermal and electrical properties of foam glass. *Ceramics international*, 33(4), 543-550.

CHAPTER III

Glass-ceramic foams through inorganic gel casting from industrial waste and glass cullet

III.1 - Aim of the study

In this chapter, the production of glass-ceramic foams from glass cullet and different industrial wastes, such as copper slag and fly ash, is described applying the same method developed in Chapter II, where soda-lime glass was used as the only waste material.

The technique, as previously described, is based on the alkali-activation of glass particles, and subsequent gel casting foaming with a surfactant. Finally, a sintering treatment to produce stable foams is conducted. As this technique relies on the separation of the foaming and the sintering process, the exhaustive compositional control of the initial materials required by the traditional methods used to produce glass foams is not necessary. The final microstructure (total amount of porosity, cell size) can be directly correlated with the degree of gelification. As a result, the tuning of the cellular structure is relatively easy to control by changing the parameters that affect the gelification process after alkali activation. Consequently, the possibility of incorporation of other industrial wastes along with the glass in the original process is promising. It was conceived not only for environmental and economic purposes but also to modify the mechanical properties and functionalities of the final products.

The final sintering treatment applied to stabilise the hardened foam structures is based on a sinter-crystallisation process, where the viscous flow sintering of glass is concurrent

with the crystallisation. The introduction of waste with selected compositions will induce the precipitation of crystals, by enhancing the apparent viscosity of the glass mass during sintering, then leading to the ‘freezing’ of the initial cell structure. The crystalline phases developed by the glass-waste interaction upon firing could present interesting properties, e.g., magnetism.

The investigation reported in Section III.2 was essentially aimed at offering a strategy that could combine the stabilisation of copper slag with its re-utilisation in the manufacturing of highly porous glass-ceramic foams, as a way to up-cycle this waste material in the building industry as thermal and acoustic insulators.

Soda-lime glass and slag powders mixtures (with slag content ranging from 10 to 30 wt%), when suspended in alkaline aqueous solution, are expected to experience a progressive hardening at low temperature (75 °C), owing to the formation of hydrated calcium silicate compounds (C-S-H) as was proved before only for glass. The cellular structure could be achieved with the help of a surfactant, before the complete setting of the mixture, whereas extensive foaming could be achieved by vigorous mechanical stirring of the partially gellified alkali activated suspensions

After foaming, the hardened foam structure should be stabilised with a sintering treatment at 800-1000 °C; the mutual interaction between glass and slag caused an extensive crystallization, with precipitation of Ca-Fe silicates and iron oxides (hematite and magnetite), enhancing the mechanical properties (up to 4.4 MPa, with a porosity of about 80%). The newly obtained foams exhibited a ferrimagnetic behaviour that could be exploited in electromagnetic shielding applications. The stabilisation of pollutants, from the slag, in the final ceramics allows the production of a highly valuable product.

The next study (Section III.3) extends the new foaming approach to geopolymer-based materials by the incorporation of fly ash into soda lime glass. Fly ash was selected as initial waste material as it is a well-established precursor in the production of geopolymer materials. A ‘weak alkali activation’ of glass mixtures is not aimed at the complete dissolution of components, but rather at developing gels on the surface of particles. This configures a fundamental difference with the so-called ‘geopolymers’, in which the complete dissolution of the alumino-silicate component determines the release of ‘inorganic oligomers’ (molecules with few Si^{4+} and Al^{3+} ions mutually bonded by bridging oxygens, with -OH terminations) in the aqueous solution, later subjected to condensation reactions, in turn leading to a three-dimensional hydrated alumino-silicate network structure.

In recent investigations aimed at the production of dense geopolymer materials with fly ash and waste glass, also performed during the PhD, it was found that the samples activated at low molarity prove less stable due to the restricted dissolution of the initial raw materials and the limited formation of the geopolymeric gel. This phenomenon is

exploited in this part of the work to develop the cellular structure according to the low-temperature foaming method.

However, using weaker alkali activator concentrations, far from the conditions to the development of stable geopolymers, allows the formation of a geopolymer-like gel; the pseudoelasticity developed by this reaction products after alkali activation allows the formation of a hardened foam, by intensive mechanical stirring of alkali-activated suspensions (with the help of a surfactant). Successively the geopolymeric reaction retains the air into the hardened foamed body.

Finally, the hardened geopolymer-like foam structure was stabilised by ceramisation with a heat treatment, between 700-900 °C; the mutual interaction between fly ash/glass caused an extensive crystallisation, promoting the mechanical properties (reaching values around 5 MPa with a porosity of about 70%).

III.2 - Functional Glass-ceramic foams from copper slag and glass cullet*

III.2.1 - Introduction

About 30 million tonnes of copper slag are produced annually worldwide. Considering that 2.2-3 tons of slag are generated for each ton of metal obtained,¹ this by-product can lead to significant ecological and financial problems, in particular, the heavy metals present in the slag could be leached away and dispersed in the environment if a proper disposal or stabilisation treatment is not applied.

Contaminations represent a fundamental issue for the reuse of copper slag, also known as ‘fayalite slag’ (owing to the presence of a specific iron silicate, FeSiO_3) since the heavy metals could leach if a proper disposal or stabilisation treatment is not applied to them limiting its up-cycling.^{2,3} As an example, fayalite slag can be reused only in limited quantity, as a pozzolanic material, due to the potential leaching of heavy metals.⁴ It may be used in concrete, as coarse aggregate,⁵⁻⁷ or outside the building industry, as low cost abrasive.⁸

A recently proposed approach, for the up-cycling of copper slag in building applications, is represented by ‘geopolymer-like’ inorganic polymers, approaching conventional Portland concrete in terms of strength and durability,⁹ but with a reduced

* *The following text, data and images are an adaptation of the results that were published in the article: “Rincón, A., Desideri, D., & Bernardo, E. (2018). Functional glass-ceramic foams from ‘inorganic gel casting’ and sintering of glass/slag mixtures. Journal of Cleaner Production, 187, 250-256.”. It is partially reproduced in this chapter with the incorporation of more results and slight modifications.*

CO₂ footprint.^{10,11} The literature suggests a strong dependence between the characteristics of the activating solution and the formation of a truly geopolymeric (zeolite-like) network. A proper reactivity, in fact, is achieved with sodium hydroxide solutions (possibly replaced by sodium silicate) at high molarity.¹² Other studies prove the evolution of the geopolymeric reaction for the production of geopolymer mortars from fayalitic slag, by increasing temperature and curing times.¹³

Few studies were actually performed taking into account the possible leaching of heavy metals from inorganic polymers made from fayalitic slag. It was established that curing conditions play a direct effect on the mechanical properties, but do not directly affect leachability;¹⁴ even if the geopolymer matrix presents good immobilisation of most of the heavy metals, the leaching of Cr ions is still possible.

In general, glass-ceramics represent the most established valorisation strategy for inorganic waste,^{15,16} but we must observe that the melting of waste ('vitrification') and the subsequent thermal treatment for the transformation of glass into partially crystallised products imply extra costs. The situation is even more complicated for cellular materials, in which the gas evolution, from selected additives, should be carefully coupled with viscous flow sintering and crystallisation.¹⁷

The approach adopted in the research reported here actually combined several strategies for energy saving. First, glass-ceramics were obtained by direct sintering of recycled glass and slag. The direct treatment relies on the formation of silicate and alumino-silicate crystals, similar to those produced by crystallisation of waste glasses, through the interaction of recycled glasses with inorganic waste upon heat treatment. This fact supports the use of the term 'glass-ceramic', despite the absence of any melting step.¹⁶ Secondly, a cellular structure was developed according to recent experiences on the low-temperature foaming of geopolymers, by intensive mechanical stirring of alkali-activated suspensions (with the help of a surfactant),¹⁸ although with a significantly weaker alkali concentration and far from the conditions for the development of inorganic polymers.

Operating with soda-lime glass, the hardening process corresponds to the development of calcium silicate hydrates (C-S-H type) on the surfaces of particles, later subjected to viscous flow sintering upon firing. As discussed in previous chapters, since the cellular structure is already available, there is no need for any foaming agent (e.g. C or SiC), and the sintering temperature should only be controlled to promote the appropriate sinter-crystallisation of the hardened green bodies.¹⁹

Mixing soda-lime glass with copper slag determines the need for higher sintering temperatures (at least 800 °C), than in the case of pure recycled soda-lime glass. The heat treatment at temperatures between 800-1000 °C led to complex glass-slag interactions. These interactions were based on the oxidative decomposition of fayalite, and led to a

significant crystallisation of the foamed products, with precipitation of CaFe silicates and iron oxides (hematite and magnetite).

The glass-ceramic products exhibited the desired stabilisation of heavy metals, essential for the application of foams in thermal and acoustic insulation. Under selected conditions, the precipitation of iron oxides led to a ferri-magnetic behaviour, configuring ‘multifunctional’ porous glass-ceramics.

III.2.2 - Experimental process

In this study the waste materials used were: iron-rich slag coming from copper metallurgy (later referred to as ‘CS’), provided by KU Leuven (Leuven, Belgium) with a mean particle size of 45 μm , and waste soda-lime glass (SLG), which comes from the same fraction of waste glass used in Chapter II, provided by SASIL S.r.l (Brusnengo, Biella, Italy) with a mean particle size of 75 μm . The chemical composition of the two starting waste materials is shown in Table 1.

Oxide (wt%)	SiO ₂	FeO	Al ₂ O ₃	Na ₂ O	K ₂ O	MgO	CaO	ZnO
CS	29	52	4	< 1	< 1	1	2	7
SLG	71.6	-	1	13.5	0.4	3.9	9	-

Table 1. Chemical composition (expressed in wt%) of the starting materials.

Mixtures of fine powders of SLG and CS were designed by replacing the SLG with increasing proportions of CS, leading to compositions of SLG/CS with the following proportions: 10/90, 80/20 and 70/30 wt%. The initial waste powders were mixed in a 2.5 M KOH aqueous solution (reagent grade, Sigma-Aldrich, Gillingham, UK), with a final solid loading of 65 wt%, and subjected to alkaline attack for 2 hours, under low-speed mechanical stirring.

After alkaline activation, the obtained suspensions were cast in closed polystyrene cylindrical moulds (60 mm diameter) and cured at 75 °C. Based on previous tests with pure soda lime glass the gelation process was maintained only for 2 hours, as it was noticed that at this point the suspension presented a marked pseudoplastic behaviour.

After adding a non-ionic surfactant Triton X-100 (Sigma-Aldrich, Gillingham, UK), with an amount of 4 wt%, the partially hardened suspensions were foamed by vigorous mechanical mixing. Foamed wet foams were kept in the same moulds at 40 °C for 24 h, in order to allow curing and complete hardening, before being demoulded. Finally, 60 mm diameter hardened ‘green’ foams were fired at temperatures between 800 and 1000 °C, for 1 hour, with a heating rate of 10 °C/min. A diagram of the whole process could be seen in Figure 1.

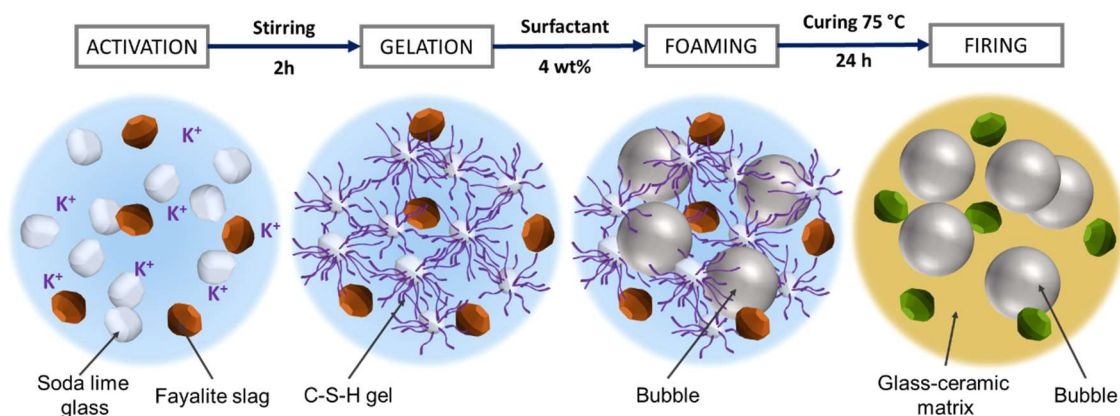


Figure 1. Processing scheme for the production of glass-ceramic foams by the combination of alkali activation, gel casting and sintering.

The characterisation of the obtained foams was carried out through the standard methods and equipment described in Chapter I section 1.6. The geometric, apparent and true density of the samples were measured, and with such data, the porosity of the samples was evaluated. Morphological and microstructural characterisations were performed by optical (AxioCam ERc 5s Microscope Camera, Carl Zeiss Microscopy, Thornwood, New York, US) and scanning electron microscopy (FEI Quanta 200 ESEM, Eindhoven, The Netherlands). The mineralogical analysis was conducted by x-ray diffraction analysis (Bruker D8 Advance, Karlsruhe), and the resulting foams were subjected to compression tests to evaluate their mechanical performance (Instron, Danvers, MA).

Electromagnetic shielding effectiveness was measured* with a coaxial waveguide, initially developed for thin films, and already proven to be appropriate for porous ceramics.²⁰ Measures were taken in the range of 0 to 3 GHz.

The release of heavy metals was evaluated by application of a toxicity control leaching procedure prepared according to European Standard for waste toxicity evaluation (EN 12457-2). Fragments below 4 mm were placed in an extraction solution consisting of distilled water, with a pH value of ~ 7 , for a liquid/solid ratio of 10, and softly stirred at 25°C for 24h. The resulting solutions were filtered through a 0.6 μm filter and analysed using inductively coupled plasma (ICP; SPECTRO Analytical Instruments GmbH, Kleve, Germany).

III.2.3 - Results and discussion

Figure 2 illustrates the microstructure of the hardened foams after the activation and gelification process, for the mixtures SLG/CS 90/10, 80/20 and 70/30 (Fig. 2a, 2b and 2c

* The Electromagnetic shielding measures were conducted by Prof. Daniele Desideri at the Dipartimento di Ingegneria Industriale, University of Padova; Padova, Italy.

respectively). The hardened foams after 24 h of curing feature a high microstructural uniformity showing slightly bigger pores as the proportion of slag increases in the mixture. The pore diameter is around 80 μm in SLG/CS 90/10, 100 μm in SLG/CS 80/20, and 250 μm in SLG/CS 70/30.

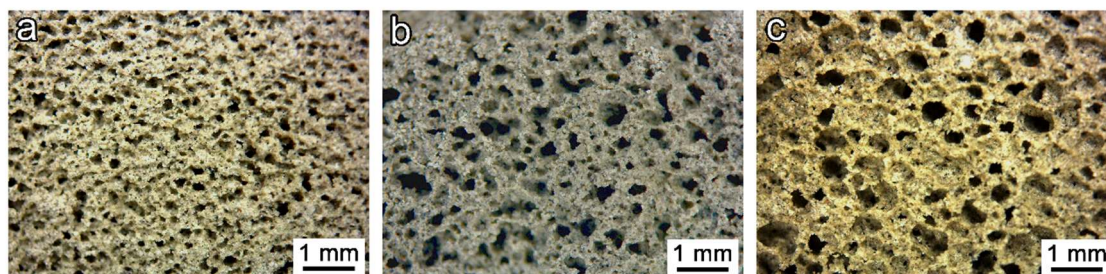


Figure 2. Microstructural details of the SLG/CS foams in the hardened state: a) SLG/CS 90/10; b) SLG/CS 80/20; c) SLG/CS 70/30

The difference in pore size can be attributed to an effect of the ‘dilution’ of soda-lime glass operated by the slag. With a lower soda lime glass content, the formation of C-S-H compounds is limited, and the gelation of the mixtures induced by these compounds is restricted, leading to a more limited pseudoplasticity and lower viscosities of the starting suspensions. The lower gelation degree of the mixtures will produce higher cell coalescence in the wet foams, and bigger pores in the hardened foams. In contrast, in the 90/10 mixture, the larger formation of C-S-H compounds enhanced gelification and led to many small pores.

The effect is analogous to the SLG foams described in the previous chapter, where a higher gelation degree enhances the formation of C-S-H compounds, resulting in a higher pseudoplasticity of the suspension, and producing hardened foams with smaller pore size distributions.

Figure 3a shows the thermogravimetric plot analysis of the glass-slag mixtures after activation and gelation; the surfactant Triton-X100, normalised according to the actual content of 4 wt% added to the foams, is also included with the aim to evaluate its influence. The weight losses around 2-3 wt% below 200 °C that could be noticed for all the SLG/CS compositions could be attributed to the loss of physically bonded water, also corroborated by the endothermic peak in the DTA plot (Fig. 3b).

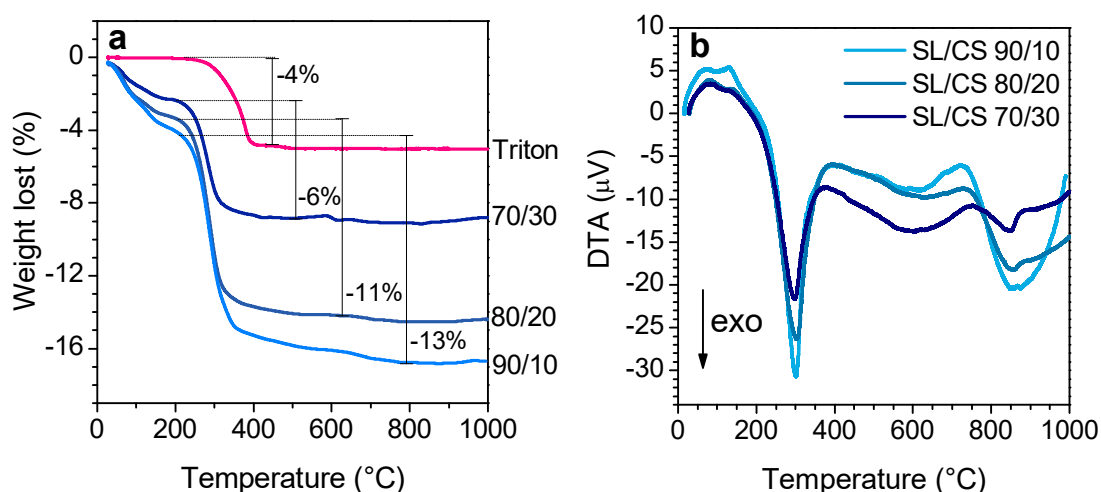


Figure 3. a) Thermogravimetric analysis and b) DTA plots of surfactant and hardened glass-slag mixtures.

The further significant weight losses detected in all the samples between 200-600 °C could not be merely attributed to the surfactant burn-out. The specific plot of the surfactant Triton X-100 alone demonstrates that its decomposition is complete at 450-450 °C. Nonetheless, these losses cannot be attributed only to the burn-out of the surfactant as they are higher (>6 wt%) than the amount of surfactant added. After the loss of physically bonded water and burn out of surfactant, weight losses of 6, 11 and 13 wt% for SLG/CS 70/30, 80/20 and 90/10 mixtures respectively in this temperature range could be attributed only to the dehydroxylation of the above-mentioned C-S-H compounds formed after the alkali activation.²¹

The difference amongst the mixtures is consistent with this attribution as the more significant losses are detected in the mixtures with higher soda-lime glass content, as in these mixtures the formation of C-S-H after the alkali activation is favoured.²² These results are in agreement with the microstructures obtained in the hardened foams; more C-S-H compounds produce higher gelation degrees and more homogenous pore structures. In addition, they also indicate a preferential activation of the SLG, suggesting a higher formation of C-S-H compounds from the SLG in comparison with CS. In other words, the activation of the SLG is more favourable than the activation of the CS.

The slight weight increase from 800 °C to 1000 °C could be attributed to oxidation reactions, produced in the slag at high temperature, i.e. changes in the valence state of iron ions.²³ In this temperature range in the DTA analysis, it could be detected a crystallisation peak roughly at around 900 °C.

The hydrated compounds formed after the alkali activation and subsequent curing of the hardened foams, and their transformation after the heat treatment could be studied using infrared spectroscopy. Figure 4 reports the FTIR spectra of SL glass and CS slag at the starting stage; along with the spectra after alkali activation and thermal treatment at

900 °C for the mixture SL/CS 70/30; this composition was selected because it represents the mixture where the influence of the Cu slag is more evident.

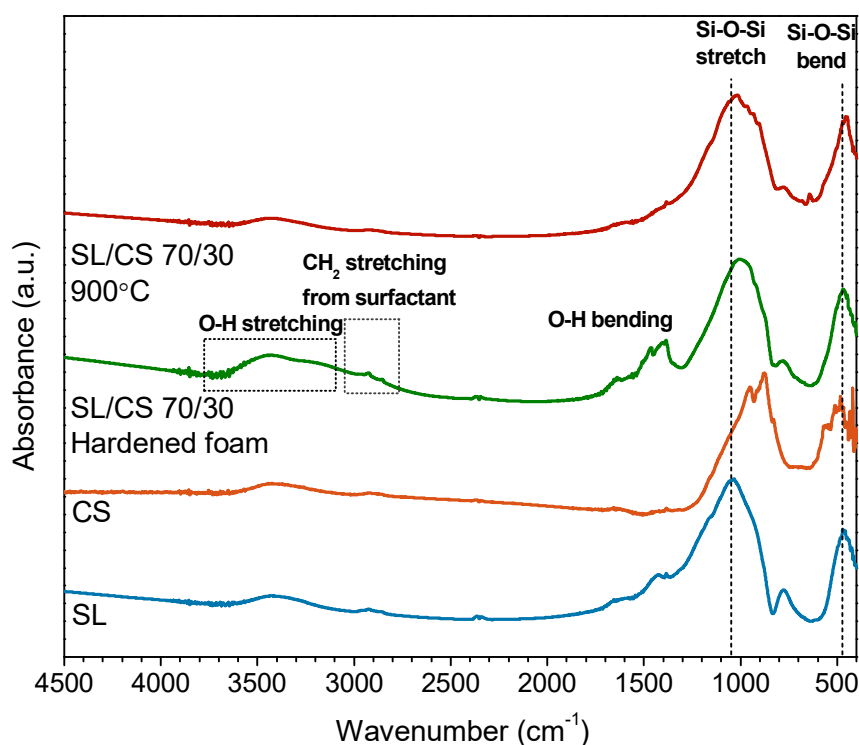


Figure 4. FTIR spectra of selected samples.

Soda lime glass cullet presents its typical absorption bands, i.e. Si-O-Si asymmetrical stretching at 1050 cm^{-1} , and the bands at 800 and 450 cm^{-1} are identified as a result of rocking and bending of the Si-O-Si group.^{24, 25} As expected, the CS presents the characteristic bands of fayalite slags with bands at 955 , 910 and 877 cm^{-1} corresponding to the asymmetric stretching vibrations of SiO_4 and the corresponding symmetric stretch at 828 cm^{-1} ,¹² where the bands that appear between $600\text{--}400\text{ cm}^{-1}$ are identified with the rotations of SiO_4 and transitions of the iron cations in the structure.²⁶

In the hardened state, the so mentioned bands remain unaltered, and the main difference arises from a broad absorption band between 3000 and 3700 cm^{-1} , which could be assigned to stretching vibration of O-H groups, as a consequence of hydration processes. While the weak signals detected in CS and SLG could be attributed to atmospheric hydration of the samples during their preparation, the same band in the hardened foam is more intense and is related to the presence of C-S-H products, formed after alkali activation. The C-S-H compounds are also indicated by a weaker band around 1650 cm^{-1} , assigned to the deformation mode of O-H groups. On the hardened foam, the organic surfactant is also detected from the bands attributable to C-H₂ stretch centred at 2900 cm^{-1} , assigned to C-H vibrations.

After heat treatment, the bands assigned to the C-S-H compounds are not present as a result of its decomposition. The other bands present in the hardened and fired foams are in the range $1000\text{-}850\text{ cm}^{-1}$ attributed to Si-O asymmetric stretching vibrations. In the range between $450\text{-}500\text{ cm}^{-1}$, bands associated with the O-Si-O bending vibration can be observed.²⁷

The substantial foam microstructural changes after the heat treatment could be seen in Figure 5, where the foam microstructures of the samples with ratios SL/CS 90/10 (Fig. 5a-c), 80/20 (Fig. 5d-f) and 90/10 (Fig. 5g-i) are shown after heat treatment at 800, 900 and 1000 °C.

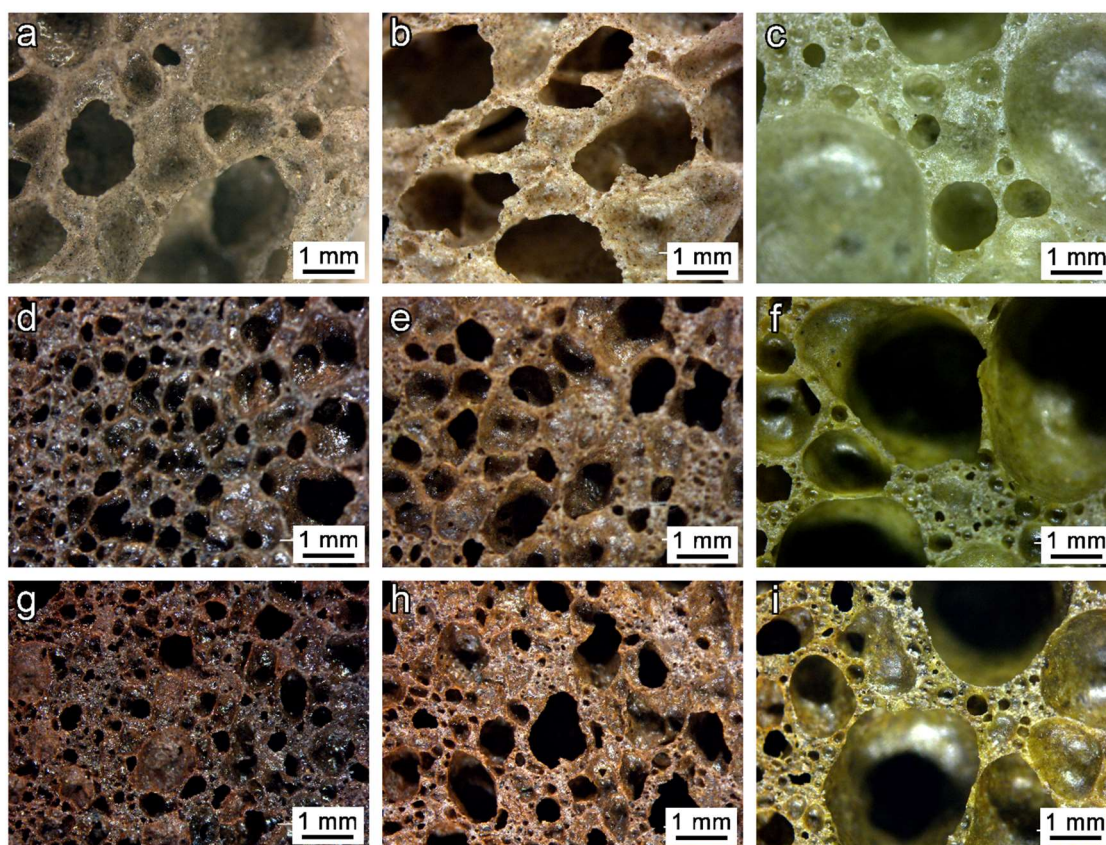


Figure 5. Microstructural details of glass ceramic foams after heat treatment: a–c) SLG/CS 90/10; d–f) SLG/CS 80/20; g–i) SLG/CS 70/30; a, d and g) 800 °C; b, e and h) 900 °C; c, f and i) 1000 °C.

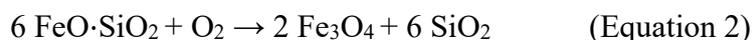
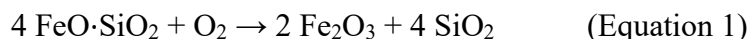
An intense change in the foam structure could be noticed in the SLG/CS 90/10 samples due to a considerable enlargement of the pores for all the treated temperatures. This reshaping of the pores, caused by excessive viscous flow is similar to the samples of pure soda-lime glass foams, studied previously in Chapter II. As explained, this reshaping is attributed to the decomposition of the hydrated phases formed upon hardening, and it is more significant in the SLG/CS 90/10, where the C-S-H compounds are formed in a

higher proportion as previously discussed, and the higher glass content reduces the temperature softening point of the mixture.

Meanwhile, in the SLG/CS 80/20 and 70/30 samples, this reshaping process, even if still present, is not so intense. After firing at 800 °C (Figs. 5d, 5g), both foams feature slightly bigger pores in comparison with the initial hardened foams. Several larger pores are detected after heat treatment at 900 °C (Figs. 5e, 5h), indicating some cell coalescence, but the foams maintain a homogeneous cellular structure. Finally, in foams obtained at 1000 °C (Figs. 5d, 5h), a significant coalescence results in big pores surrounded by thick walls, as the temperature is well above the softening point of the glass.

This minor pore reshaping upon firing in the SLG/CS 80/20 and 70/30 CS samples could not be explained only through the limited formation and later decomposition of C-S-H compounds in the samples. The glass-slag interactions play a crucial role in the sinter-crystallisation process and subsequently in the final pore structure of the sintered foams.

The observed significant pore reshaping upon firing could be due to glass-slag reactions, as a result of the instability of fayalite, which, in an oxidative atmosphere, goes through oxygenolysis according to the following reactions, forming hematite (Fe_2O_3) and magnetite (Fe_3O_4) respectively.²⁸



The by-product of slag oxygenolysis consists of amorphous silica, reasonably dissolved in softened soda-lime glass.²⁹ The oxidation could justify the slight weight increase detected in the thermogravimetric plots of Figure 3a. However, it should be noted that thermal analysis does not take into account any effects that may arise with time. In particular, it has been already shown that iron oxides may transform, with increasing firing temperature, from the variant with ferric ions (Fe^{3+} , in Fe_2O_3) to variants with ferrous ions (both Fe^{2+} and Fe^{3+} , in $\text{Fe}_3\text{O}_4 = \text{FeO} \cdot \text{Fe}_2\text{O}_3$; only Fe^{2+} , in FeO), with oxygen release exploited for foamed materials:^{30, 31}



In other words, the thermal treatment probably determined a reaction chain, with an oxidation phase (decomposition of fayalite, known to start above 400 °C,²³ possibly occurring during the heating step) followed by a reduction phase (release of oxygen, possibly occurring upon holding at the firing temperature).

The above-described phenomenology was confirmed by the X-ray diffraction analysis shown in Figure 6. Only the SLG/CS 70/30 mixture is discussed in this section as the higher proportion of CS induces a higher crystallisation and simplify the phase

identification. The other samples present similar patterns and the same crystalline phases with more amorphous phase due to the higher SLG content.

The diffraction patterns of as-received SLG and CS hardened foams after curing are displayed in Figure 6.a. The CS, in the as-received conditions, contains mainly fayalite, (Fe_2SiO_4 , PDF#87-0317) with a very limited fraction of the amorphous phase. The starting glass remains almost completely amorphous but presents weak traces of calcium silicate hydrated phases (CSH#1, $\text{Ca}_{1.5}\text{SiO}_{3.5}\cdot x\text{H}_2\text{O}$, PDF#33-0306; CSH#2, suolonite, $\text{CaSiO}_3\cdot\text{H}_2\text{O}$, PDF#74-2248), likely due to surface reaction with environmental humidity.

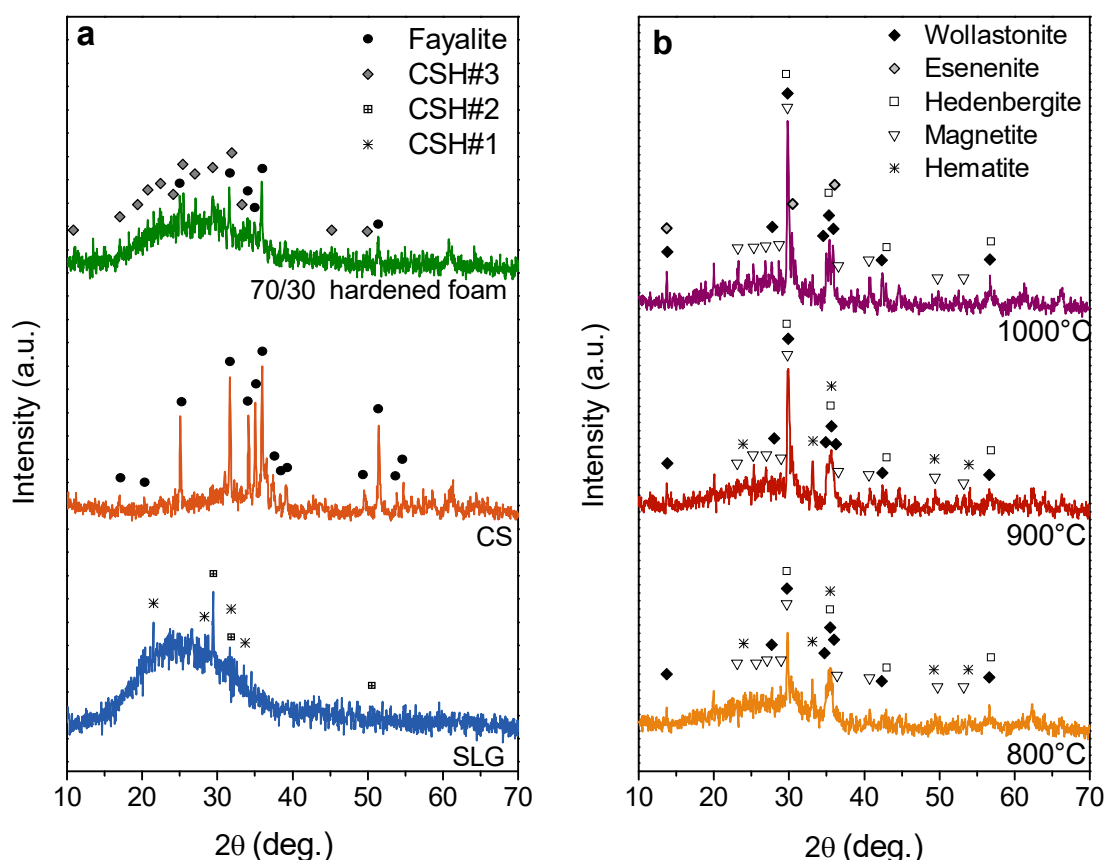


Figure 6. X-ray diffraction patterns of SLG/CS foams (70% soda-lime glass-30% copper slag) a) in the hardened state; b) and after firing.

In the hardened foam, after alkali activation of glass-slag mixture, the crystalline fayalite phase remains unaltered as the amorphous phase undergoes a preferential dissolution with alkaline activation, in agreement with previous studies on inorganic polymers.^{14, 32} The amorphous halo, at the background, appears shifted to higher 2θ values, compared to as received glass, in agreement with the compositional changes associated to the incorporation of network modifiers with alkaline attack.^{33, 34} Traces of another calcium silicate hydrated phase (CSH#3), attributable to a riversideite-type structure ($2\text{CaSiO}_3\cdot 3\text{H}_2\text{O}$, PDF# 02-0600), were also detected.

Figure 6.b shows the comparison of XRD patterns after heat treatment at 800, 900 and 1000 °C for the SLG/CS 70/30 mixture. Fayalite is no longer detected at any temperature as its oxidation is complete at 400°C, as predicted by equations 1 and 2. The firing treatments lead to glass-slag interactions and the precipitation of Ca-Fe silicates, with iron in both Fe²⁺ and Fe³⁺ oxidation states. The main peaks were ascribed to esseneite (CaFe_{0.6}Al_{1.3}Si_{1.08}O₆, PDF#84-1206), featuring ferric ions; however, both ‘pure’ hedenbergite (CaFeSi₂O₆, PDF#87-1704) and iron-doped wollastonite (Ca_{2.87}Fe_{0.13}Si₃O₉, PDF#83-2198), featuring ferrous ions, could not be excluded. Hematite (featuring only Fe³⁺ ions, Fe₂O₃, PDF#89-0691) was detected only below 1000 °C, whereas magnetite (Fe₃O₄, PDF#89-0691) was found at all temperatures.

The crystallisation is known to increase the mechanical properties of glass-ceramics, compared to the starting glasses, however, in the studied foams, its effect is quite controversial. The formation of crystal inclusions upon firing determines a dramatic increase of viscosity in the softened glass, impeding the viscous flow, which has fundamental consequences on the ratio between open and closed porosity. As previously observed in Chapter II, the reshaping of porosity in alkali-activated soda-lime glass foams, not particularly prone to crystallisation, favoured the formation of closed cells. On the other side, in a glass sensitive to crystallisation, the open-celled structure obtained after low-temperature foaming could remain practically unaltered.³⁵

Slag (%)	Firing T ^a (°C)	Density, ρ (g/cm ³)			Porosity (%)			Strength σ _{comp} (MPa)
		geometric	apparent	true	total	open	closed	
10	800	0.34 ± 0.03	1.10 ± 0.09	2.51 ± 0.01	86 ± 2	66 ± 3	19 ± 2	1.4 ± 0.5
	900	0.35 ± 0.02	2.44 ± 0.03	2.57 ± 0.01	86 ± 4	85 ± 3	1 ± 2	1.8 ± 0.6
	1000	0.60 ± 0.05	1.60 ± 0.3	2.58 ± 0.01	77 ± 3	62 ± 4	14 ± 2	1.5 ± 0.8
20	800	0.55 ± 0.02	1.63 ± 0.08	2.64 ± 0.01	79 ± 4	66 ± 8	12 ± 5	1.6 ± 0.8
	900	0.47 ± 0.02	1.90 ± 0.10	2.63 ± 0.01	82 ± 4	75 ± 9	6 ± 5	1.3 ± 0.1
	1000	0.59 ± 0.02	1.13 ± 0.06	2.75 ± 0.01	78 ± 3	47 ± 8	30 ± 5	2.2 ± 0.4
30	800	0.62 ± 0.02	1.57 ± 0.02	2.67 ± 0.01	76 ± 4	60 ± 4	16 ± 2	4.3 ± 0.9
	900	0.59 ± 0.02	1.99 ± 0.01	2.71 ± 0.01	78 ± 3	70 ± 4	8 ± 1	2.3 ± 0.4
	1000	0.69 ± 0.05	1.33 ± 0.03	2.83 ± 0.01	72 ± 7	48 ± 9	27 ± 2	3.3 ± 0.9

Table 2. Density, porosity and mechanical properties of the developed glass ceramic foams

From the density and porosity data reported in Table 2, we can assume that the ratio open/closed porosity, in our system, could be effectively tuned depending on the balance between crystallisation and viscous flow. The higher rates of closed porosity are

correlated with the lowest temperature (800 °C), at which crystallisation was limited (see Fig. 4b), and with the highest temperature (1000 °C), at which the enhanced crystallisation could be compensated by the reduced viscosity of the residual glass phase. For the intermediate temperature (900 °C), the porosity remained mostly open.

Table 2 also reports data concerning the compressive strength of the developed foams. Given the particular microstructures, the strength values are quite promising. In fact, the compressive strength of foams (σ_c) is generally expressed by the Gibson-Ashby equation:³⁶

$$\sigma_c = \sigma_{\text{bend}} [C \varphi (\rho_{\text{rel}})^{3/2} + (1 - \varphi) \rho_{\text{rel}}] \quad (\text{Equation 5})$$

where σ_{bend} is the bending strength of the solid phase, C is a dimensionless constant (being ~ 0.2), ρ_{rel} is the relative density ($\rho_{\text{rel}} = 1 - P/100$, where P is the total porosity) and φ is the material fraction at the cell edges. If we consider the foams fired at 900 °C as mostly open-celled, φ could be assumed to be equal to 1: with the observed compressive strength, and the bending strength of the solid phase (σ_{bend}) should be above 110 MPa (for the sample with 30% slag), in line with the bending strength of dense glass-ceramics.

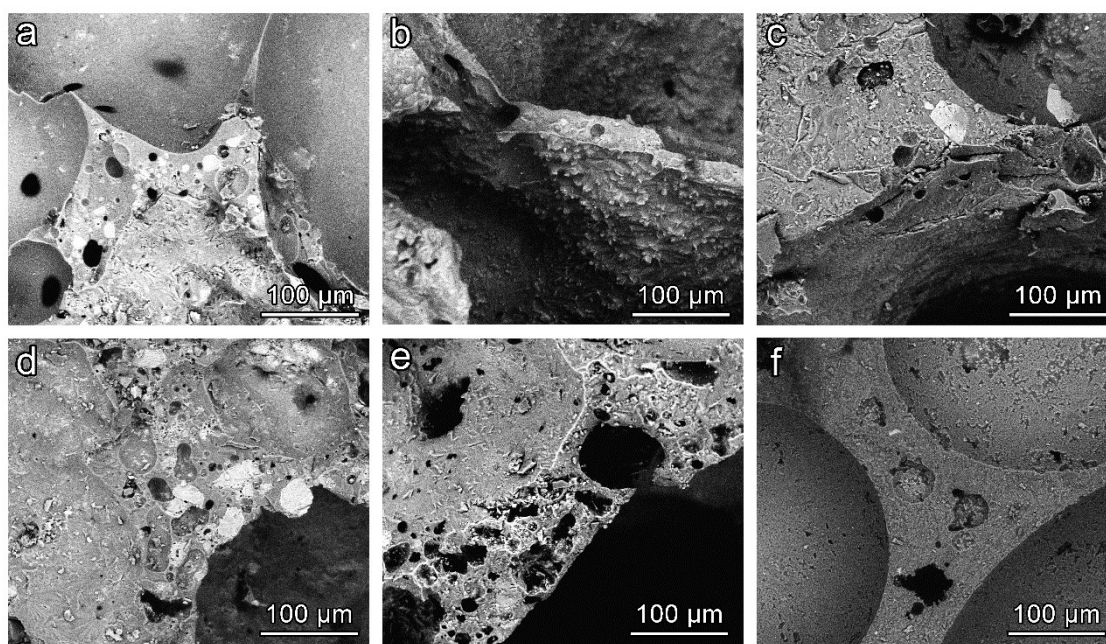


Figure 7. High magnification details of SL/CS 80/20 glass ceramic foams after firing at a) 800°C; b) 900 °C and c) 1000 °C and SL/CS 70/30 samples after firing at d) 800°C; e) 900 °C and f) 1000 °C.

The microstructural details provide a further understanding of the porosity and the mechanical properties. Figures 7a, b and c show the 80/20 mixture after heat treatment at 800, 900 and 1000 °C, meanwhile Figures 7d, e and f show the 70/30 mixture after sintering at 800, 900 and 1000 °C respectively. After heat treatment at 800 °C, smooth cell struts with some close micro-pores are observed for both compositions (Figs. 7a and

c). These morphologies could be seen as an evidence of the decomposition of the C-S-H compounds inside the softened glass, producing closed cells.

After heat treatment at 900 °C, the cell struts present a reshaping with a more interconnected structure, also confirmed by the porosity data. It could be explained as a consequence of the iron oxide reduction that takes place at this temperature with oxygen evolution. The crystallisation is evident from the observation of cell struts, where many acicular crystals are detected embedded into an amorphous glassy phase. When the samples are treated at 1000 °C, well above the softening point of the glass, a coarsening of the cell struts occurs as a result of the bubble coalescence that takes place.

The sample 70 SL-30 CS treated at 900 °C presents the best mechanical performance. Some bright particles are detected embedded in foam struts, and since fayalite is no longer present in the x-ray diffraction patterns, they should be attributed to particles of reacted slag that are richer in iron than the glass.

Element (ppm)	SLG/CS 80/20		SLG/CS 70/30		Limits [UE] (ppm)	
	800°C	900°C	800°C	900°C	Inert material	Non- hazardous material
As	0.0180	<0.0225	<0.0205	<0.0016	0.05	0.2
Ba	0.0148	<0.0141	<0.0160	0.0044	2	10
Cd	<0.002	<0.0271	<0.0272	<0.0066	0.004	0.1
Cr	0.4419	0.2953	0.1104	0.1200	0.05	1
Cu	0.0666	<0.0453	<0.0326	<0.0134	0.2	5
Mo	0.1177	0.0253	0.0279	0.0351	0.04	1
Ni	0.0018	<0.0443	<0.0439	<0.0237	0.05	1
Pb	0.0293	<0.0100	<0.0101	0.0129	0.006	0.07
Se	0.0122	<0.0280	<0.0260	<0.0045	0.01	0.05
Zn	0.1694	<0.0612	<0.0642	<0.0195	0.4	5
Final pH	9.46	9.73	9.26	9.58		

Table 3. Chemical analysis of the leachate of selected samples

The glass-ceramic foams developed present good strength-to-density ratios so that they could be applied in buildings for thermal and acoustic insulation. Also, the open cell structure that they present opens the way to further applications, such as catalytic supports or filters. However, their use is only possible after controlling the possible toxicity and guaranteeing the absolute safety of the waste-derived materials.

The leaching data of the glass-ceramic foams that present the best performance are reported in Table 3; antimony (Sb) was not measured, owing to problems of instrument calibration. The leaching data provided for all the samples show that all the metal ions are well below the thresholds for non-hazardous materials, according to EN 12457. It can be assumed that the desired chemical stability was achieved, thanks to the liquid phase provided by the softening of soda-lime glass, which incorporates the slag particles and possible pollutants, confirming that the simple sintering with soda-lime glass is a valid waste stabilisation method.^{37, 38} With regards to the thresholds for inert materials, a good chemical stabilisation is also presented, except in the case of the 80/20 sample treated at 800 °C, where molybdenum ions are above the limit. The findings are particularly significant since the leaching test, which is designed for dense materials, could be considered extremely severe. Taking into consideration the high specific area of porous materials, a superior stabilisation of the potential pollutants can be expected.

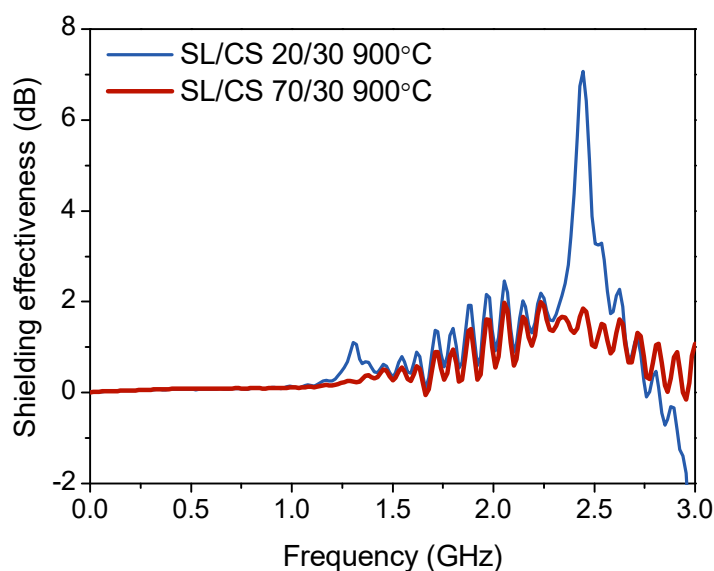


Figure 8. Shielding effectiveness of 80 SLG – 20 CS and 70 SLG – 30 CS samples (about 6 mm thick) in the range from 0.1 MHz to 3 GHz.

The obtained foams showed interesting magnetic properties that could be exploited in electromagnetic shielding applications. In the best samples (fired 900 °C, showing both good mechanical properties and chemical resistance), due to the presence of magnetite, a ferri-magnetic behaviour on the sample is detected. Ferri-magnetic materials may dissipate electromagnetic energy upon magnetisation hysteresis.³¹ The measures done with a transverse electromagnetic mode (TEM) field within a coaxial waveguide, for frequencies from 0.1 MHz up to 3 GHz (Figure 8) reveal that the 80/20 sample has a non-negligible value of shielding effectiveness (SE) in the 2–2.6 GHz range, with a marked peak (about 7 dB) near 2.4 GHz. Oscillations in the data (of about 1 dB), already shown in past experiments, are probably due to the particular test set-up.²⁰

The development of lightweight glass-ceramic panels, combining good thermal and acoustic insulation properties (associated to the high porosity) with electromagnetic shielding, is encouraging for the development of low-cost, waste-derived electromagnetic shields alternative to those already reported, depending on specific additives (e.g. carbon fibres in cement-based composites).^{39, 40}

III.2.4 - Conclusions

We may conclude that:

- The novel technique developed for the production of glass foams from alkali activation of glass suspensions/mechanical foaming/sintering was successfully transferred to a mixture of glass and fayalite slag from copper metallurgy.
- The introduction of slag determined a ‘dilution’ of the calcium silicate hydrated compounds, responsible for low-temperature hardening of glass-slag suspensions and attributable to the alkaline attack of the soda lime glass fraction; coarser pores could be observed with increasing slag content.
- The sintering at 800-1000 °C led to a substantial ‘reshaping’ of pores, already produced from the mechanical stirring of partially gelified glass/slag suspensions. The reshaping is mainly attributable to transformations reactions of the slag, implying the precipitation of iron oxides, in the form of hematite and magnetite; transitions in the valence state of iron ions determined the evolution of oxygen, acting as a foaming agent.
- Glass-slag interaction upon firing led to the crystallisation of Ca-Fe silicate (pyroxene), coupled with Fe-doped wollastonite.
- The ratio between open and closed porosity can be tuned depending on the firing temperature and slag concentration; despite a substantial amount of open porosity, the developed glass-ceramics exhibited a remarkable compressive strength.
- Despite the absence of a preliminary melting phase, leading to a homogeneous glass, the direct sintering of glass/slag mixtures led to the stabilisation of pollutants from the same slag; the release of heavy metals was particularly limited, even in severe conditions (tests applied to foamed samples, with high specific surface);
- The ferri-magnetic behaviour associated with the presence of magnetite gave additional functionalities to the developed materials; in particular, preliminary tests showed the potential of glass-ceramics regarding electromagnetic shielding.

III. 3 - Soda-lime waste glass and fly ash-based glass ceramic foams*

III.3.1 - Introduction

Fly ash is a by-product generated in coal power stations; it is a fine particulate material with fluctuating chemical and phase compositions depending on the original coal and burning conditions. The increasing demand of energy generates about 900 million tonnes of fly ash worldwide, and is expected to increase up to 2 billion tons in 2020.⁴¹ Coal fly ash is mainly landfilled, producing significant environmental problems such as the potential leaching of heavy metals or polycyclic aromatic hydrocarbons.⁴²⁻⁴⁴ Therefore its utilisation in new valuable materials is a critical issue for a sustainable society.

A significant amount of fly ashes are being used in the building industry due to their pozzolanic properties, and, also when mixed with cement, they can improve concrete durability.^{43, 45, 46} Fly ash valorisation has also been proposed for the production of dense glass-ceramic materials where the addition of glass cullet to modify the sintering temperatures plays a fundamental role in the process.^{47, 48}

Lightweight glass-ceramic foams represent a more valuable product, whose formulation incorporates fly ash and glass cullet. They have been produced from a mixture of glass waste and fly ash using a powder sintering route with the addition of different foaming agents, such as SiC.⁴⁹ Many authors used the same foaming strategy adding waste glass to reduce the treatment temperature.^{50, 51}

Alternative and more environmental friendly foaming agents have been also studied. Carbonates such as dolomite ($\text{CaMg}(\text{CO}_3)_2$), and sludge from a marble cutting-polishing plant containing mainly calcite (CaCO_3) were also used as foaming agents to obtain foams with low apparent density ($0.36\text{--}0.41\text{ g/cm}^3$) and relatively high compressive strength values ($2.40\text{--}2.80\text{ MPa}$). However only a 20 wt% of fly ash was the highest possible amount that could be incorporated for the foam production.⁴³ Calcium carbonate can also be used as a foaming agent to produce glass-ceramic foams with a higher amount of coal fly ash 40 wt%, but 30 wt% borax has to be added as a fluxing agent to lower the softening temperature of the mixture.

Some attempts have been made to produce lightweight aggregates avoiding the use of any foaming agents by mixing the fly ash (75 wt%) and waste window panes (25 wt%) exploiting the bloating of the fly ash at high temperature.⁵²

In addition, fly ash is rich in amorphous alumina and silica in a proper chemical balance and can be used as a potential raw material in the formulation of waste derived

* *The experimental work leading to this results was carried out at the Institute of Biomaterials, University of Erlangen-Nuremberg, in collaboration with Nicoletta Toniolo and Professor Dr. Aldo R. Boccaccini.*

geopolymers.⁵³ Geopolymer materials are a class of inorganic polymers synthesised through the reaction of solid aluminosilicate precursor with a highly concentrated alkali solution. Subject to strong alkali conditions, the aluminosilicate-reactive materials are dissolved, leading to the formation of free SiO_4 and AlO_4 tetrahedral units. The following co-polymerisation of individual alumino and silicate species creates a highly stable three-dimensional network structure where the SiO_4 and AlO_4 tetrahedra are linked together by sharing oxygen atoms. This structure reflects the one of zeolites, but it reveals an amorphous nature.⁵⁴

The use of fly ash in the geopolymer formulation was widely studied and is proposed as an alternative binder to cement in the building industry. In the geopolymer formulation, it can be used alone or mixed with other natural sources or industrial wastes.⁵⁵⁻⁵⁷ Its use can generate some potential economic and environmental benefits, as its production does not require the huge energy consumption needed in the production of Portland cement, with the advantage of lower CO_2 emissions and a reduced use of natural materials.^{58, 59}

However, the standard reagents used as alkali activator in fly ash geopolymer-based materials are expensive, such as sodium silicate (also known as water glass) and sodium or potassium hydroxide.^{60, 61} Some efforts have recently been made to substitute them with low cost and more environmental friendly activators such as industrial residues of discarded cleaning solutions for aluminium moulds.⁶²

Another recent approach is to use waste glass as partial replacement of water glass in alkali-activated slag/fly ash systems for the production of alkaline cement.⁶³ The use of glass can bring several advantages, is expected to reduce the energy demand and CO_2 emissions associated with sodium silicate production, where temperatures around 1300 °C are required, in order to melt sodium carbonate and silica mixtures.⁶⁴

In recent investigations, we proposed the synthesis of dense fly ash⁶⁵ or red mud⁶⁶ based geopolymers using waste glass from municipal waste collection, for replacement of water glass, like silica source in the geopolymeric formulation. It was established that, despite the alternative formulation, by mixing fly ash and waste glass in an appropriate ratio and using NaOH in relatively low molarities (NaOH 8M), it is possible to produce stable and chemically resistant geopolymeric gels. This section is conceived as an extension of that work, but in this case much lower alkali activation is used, as the aim of the study is to develop a geopolymeric gel that could be foamed directly with the help of a surfactant, applying a similar workflow including inorganic gel casting, foaming and heat treatment, as described in previous chapters.

III. 3. 2 - Experimental process

The initial raw materials used in this study were low calcium fly ash (FA) class F (ASTM C 618),⁶⁷ with a mean particle size of 20 μm , provided by Steag Power Minerals (Dinslaken, Germany), and soda-lime glass waste (SLG), provided by SASIL S.r.l.

(Brusnengo, Biella, Italy) in the form of fine powders with a particle size $< 30 \mu\text{m}$. The waste glass used in this part of the work is a finer fraction that is also produced during the purification process of glass cullet carried out in the company. Its only possible use is in the ceramic industry for the production of tiles. It was selected with the aim of producing higher dissolution rates of the glass, which are due to the higher reactivity of the finer particles.

Table 1 summarises the chemical composition reported in previous studies of the fly ash and waste glass used.

Oxide (wt%)	SiO ₂	Al ₂ O ₃	Na ₂ O	K ₂ O	CaO	MgO	Fe ₂ O ₃	TiO ₂
FA	54.36	24.84	0.83	3.03	2.56	2.06	8.28	1.07
SLG	70.5	3.2	12	1	10	2.3	0.42	0.07

Table 1. Chemical composition (expressed in wt%) of the starting materials.

This investigation follows a similar experimental programme used in previous studies,^{65, 66} varying the theoretical molar ratio between SiO₂ and Al₂O₃ but keeping the concentration of NaOH solution to lower concentrations at 3M.

The mixtures were prepared with FA and SLG in proportions of 76/24, 64/36, 54/46, which represent a SiO₂/Al₂O₃ theoretical molar ratio in the final geopolymers of 5, 6 and 7 respectively. The liquid/solid ratio was fixed at 0.45, for all the samples to obtain good workability. As in previous studies, the mixture was kept under mechanical stirring (500 rpm) at room temperature for 4h, to achieve the maximum possible dissolution of the initial material and a good dispersion of the remaining undissolved particles in the slurry.

The direct foaming of the partially dissolved glass suspension was achieved by the addition of 4 wt% of sodium lauryl sulphate (SLS) (CH₃(CH₂)₁₁OSO₃Na (Carlo Erba, Cornaredo, Milan, Italy) in an aqueous solution 1/10 in weight and then subjected to intensive mechanical stirring (2000 rpm, for 10 min). The prepared wet foams were kept at 70 °C for 24h inside sealed moulds to complete the hardening, before being demoulded. Finally, a thermal treatment at 800, 900 and 1000 °C for 1h (10 °C/min heating rate) was applied to hardened foams for stabilisation. A schematic representation of the process could be seen in Figure 1.

The mineralogical analysis was conducted by X-Ray Diffraction analysis (XRD) on powdered samples (Bruker D8 Advance, Karlsruhe, Germany; CuK α radiation, 0.15418 nm, 40 kV-40mA, $2\theta = 10-70^\circ$), a step size of 0.02° and 2s counting time was set for the initial materials and the hardened foams analysis, and a step size of 0.02° and 0.5s for the fired samples. The phase Identification was performed using the Match!® suite (Crystal Impact GbR, Bonn, Germany), supported by data from PDF-2 database (ICDD-International Centre for Diffraction Data, Newtown Square, PA).

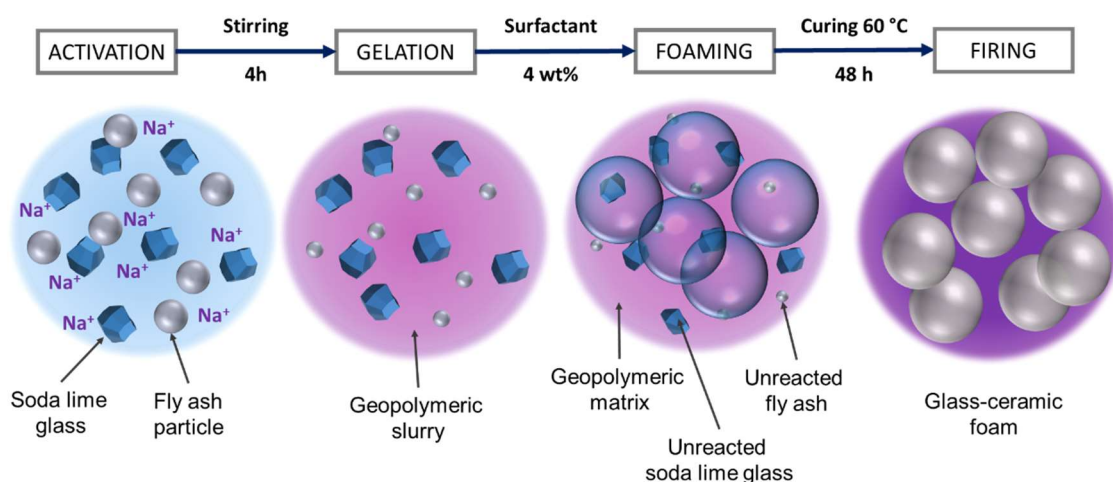


Figure 1. Processing scheme for the production of glass-ceramic foams.

The geometric density was evaluated considering the mass by volume ratio. The apparent and true densities were measured by using a helium pycnometer (Micromeritics AccuPyc 1330, Norcross, GA), on bulk or finely crushed samples, respectively. The three density values were used to compute the amounts of open and closed porosity.

Compression tests were done using an Instron 1121 UTS (Instron, Danvers, MA) machine, with a crosshead speed of 0.5 mm/min, employing foam samples of about 10 mm × 10 mm × 10 mm, cut from larger specimens. Each data point corresponds to 9-10 samples.

The release of heavy metals was evaluated according to the European Standard for the compliance test for leaching of granular waste materials and sludge (EN 12457-2). Fragments under 4 mm were placed in an extraction solution consisting of distilled water, with a pH value of ~7 and a liquid/solid ratio of 10, and softly stirred at 25 °C for 24h. The resulting solutions were filtered through a 0.6 µm filter and analysed using inductively coupled plasma (ICP; SPECTRO Analytical Instruments GmbH, Kleve, Germany).

The semi-industrial production of lightweight panels was developed for selected samples. The alkali activation process was conducted in the same way. However, a relatively significant amount of activated suspension was prepared for each batch (around 5kg), and the process was carried out with technical grade reagents. The hardened foamed panels were obtained after casting in bigger moulds (15 x 20 cm). Finally, hardened foamed gels were fired at temperatures between 800 °C for 1 hour, using a pilot scale tunnel furnace (Nanetti ER-15S) at SASIL S. p. a. (Brusnengo, Biella, Italy).

Thermal conductivity* tests on the lightweight panels were performed using a Fox 50 Heat Flow Meter by TA Instruments (New Castle, DE, USA) operating at 25 °C. By cutting cylindrical samples from the panels with 50 mm diameter and 10 mm thickness, three replicated tests were performed on samples taken from different panels.

III.3.3 - Results and discussion

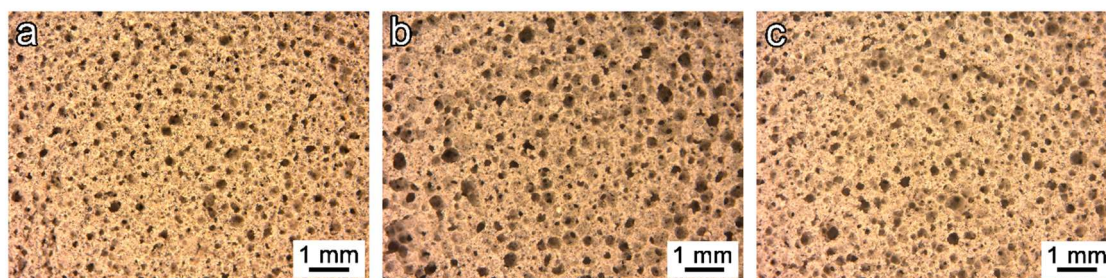


Figure 2. Microstructural details of the SLG/FA foams in the hardened state; a) 5S; b) 6S and c) 7S.

Figure 2. shows the microstructure for the geopolymer foam after 24 h of curing for the mixtures 5S, 6S and 7S (Fig. 2a, b and c respectively). The hardened foams reveal a high microstructural uniformity, presenting pores in a range from 10 to 30 μm diameter. No significant changes in the pore distribution between samples with different compositions can be detected, even if the viscosity of the initial slurries was different.

The spherical morphology of the FA ensures good workability and low viscosity of the slurries, whereas it was observed a viscosity increase with a higher amount of glass content in the formulation.⁶⁸ According to the previous experiences, higher viscosity slurries lead to smaller pores; however, at present, all the samples have similar porosities independently from their initial formulation. As explained in previous chapters the foam microstructure is affected by a vast number of physical influences and processing factors. In this case, the great homogeneity presented between the samples can be explained thanks to the rapid setting of the wet foam, which does not allow any coalescence effect.⁶⁹

The X-ray diffraction analyses of the initial materials are presented in Figure 3; a different intensity scale was selected for each material in order to highlight the crystalline phases present. The starting waste SLG (Fig. 3a) presents an amorphous halo centred approximately at $2\theta = 24\text{-}26^\circ$. Some weak traces of silicate hydrated phases such as calcium aluminium silica hydrate (CASH#1, gismondine $\text{CaAl}_2\text{Si}_2\text{O}_8 \cdot 4\text{H}_2\text{O}$, PDF#020-0452), calcium silica hydrate (CSH#1, $\text{Ca}_{1.5}\text{SiO}_{3.5} \cdot x\text{H}_2\text{O}$, PDF#033-0306), and sodium aluminium silica hydrate (NASH#1, $\text{K}_2\text{NaAl}_3\text{Si}_9\text{O}_{24} \cdot 7\text{H}_2\text{O}$, PDF#022-0773), are also

* The thermal conductivity measures were carried out at Element Materials Technology, (Hitchin, United Kingdom) supported by Matteo Cavasin.

detected. These hydrated phases are formed probably due to surface reaction of the fine glass particles with environmental humidity during storage.

The original fly ash (Fig. 3b) shows a characteristic diffraction pattern with quartz (SiO_2 , PDF#083-0539) and mullite (Al_4SiO_8 , PDF#079-1275) as the main phases, moreover minor traces of hematite (Fe_2O_3 , PDF#033-0664) are also detected. In the pattern, it is also possible to detect an amorphous halo at around $24\text{-}26^\circ$.

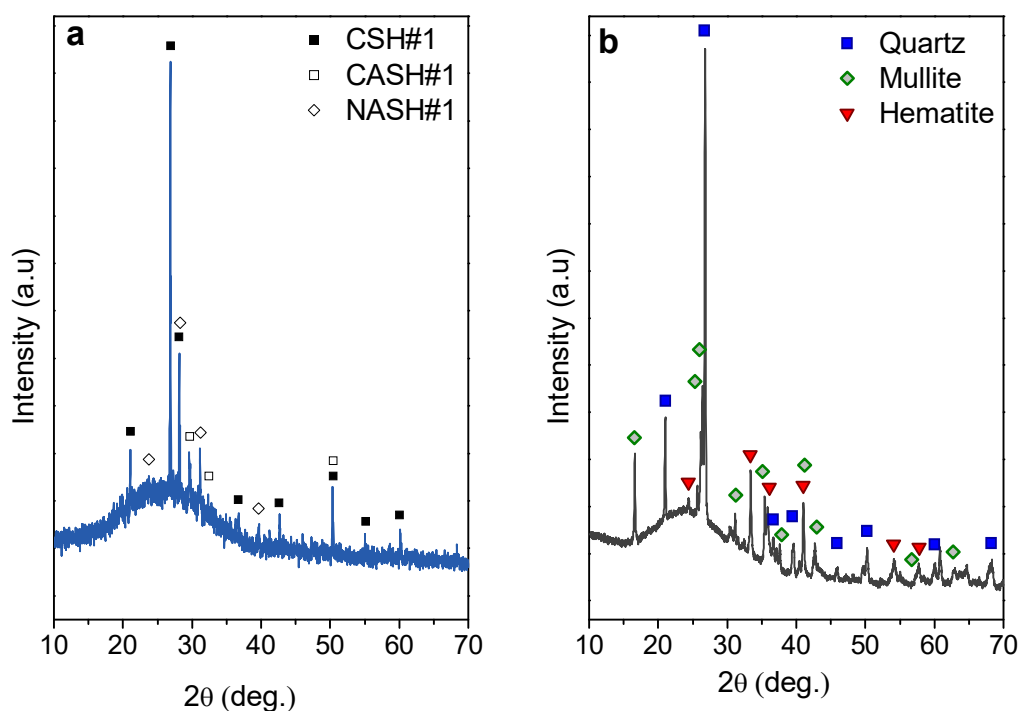


Figure 3. X-ray diffraction patterns of the initial materials: a) waste soda lime glass; and b) fly ash.

The x-rays diffraction patterns of the hardened geopolymeric foams represented in Figure 4 show that quartz (SiO_2 ; PDF#083-0539) and mullite (Al_4SiO_8 ; PDF#079-1275), from the initial fly ash, have been not affected by the alkali activation process, and they remain apparently unaltered. The intensity of these peaks decreases as the amount of glass increase in the formulation of the samples; as a result of this dilution effect, hematite (Fe_2O_3 , PDF#033-0664) is not visible.

The amorphous silica peak from around 24° in the original raw materials is shifted to higher 2θ angles (close to 30°) after the alkali activation. This suggests the formation of a geopolymeric-like gel in the hardened foam, as this shift is perceived as an indication of an alkaline aluminosilicate (N-A-S-H) gel as a reaction product.⁷⁰⁻⁷²

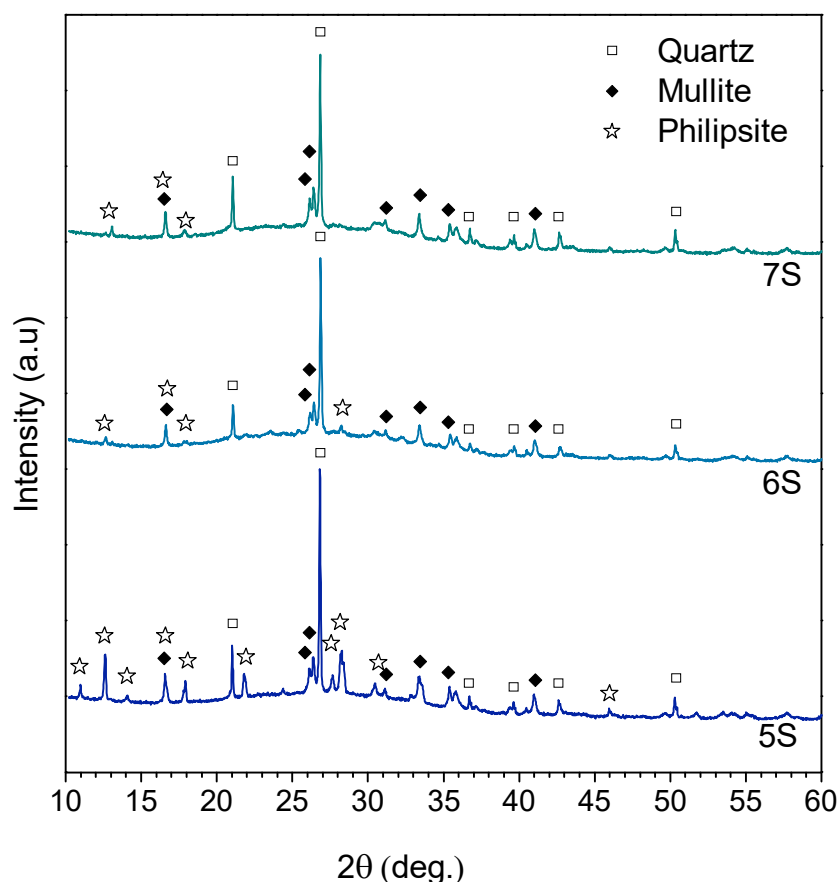


Figure 4. X-rays diffraction patterns of the hardened geopolymeric foams

Some minor new formed crystalline phases after the alkali activation could be identified in the hardened foams. The presence of philipsite ($\text{Na}_4\text{KAl}_5\text{Si}_{11}\text{O}_{32}(\text{H}_2\text{O})_{10}$, PDF#073-1419) confirms the reaction of the initial raw materials even the low molarity of the initial activator.^{73, 74} Philipsite, a sodium potassium aluminium silicate hydrate with a zeolite-type structure is present in all the compositions, especially when the formulation is enriched with fly ash, suggesting its formation from them.

The microstructural details of the cell struts from hardened sample 5S were studied using SEM (Figure 5). Low magnification image (Figure 5a) reveals the spherical shape of the fly ash blended with irregular shape particles of SLG. The low activator molarity does not allow the formation of a continuous geopolymeric gel. Still, the reaction products developed are enough to promote the formation of the geopolymeric-like gel on the surface of the unreacted particles allowing the cohesion between them.

At higher magnification, zeolite crystals were detected some of these reaction products could be seen (Figure 5b) where a fly ash particle, with its characteristic spherical shape, is covered with some crystals; they are typically associated with the formation of zeolite compounds after the alkali activation of fly ashes.^{75, 76}

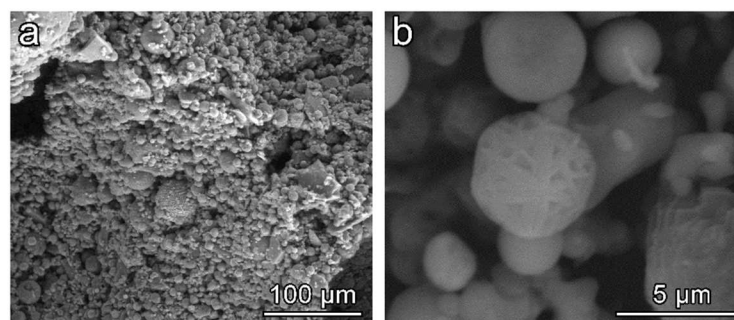


Figure 5. High magnification morphology of 5S hardened state foam: a) low magnification; b) high magnification.

The hardened geopolymeric foams keep their structural integrity, and a good consistency which make them easy to handle. However, when they are immersed in boiling water, the water becomes turbid, and pH rises to values close to thirteen. This fact, reveals poor chemical stability of the hardened samples when activated at low molarity. For this reason, a heat treatment is required to stabilise the foams.

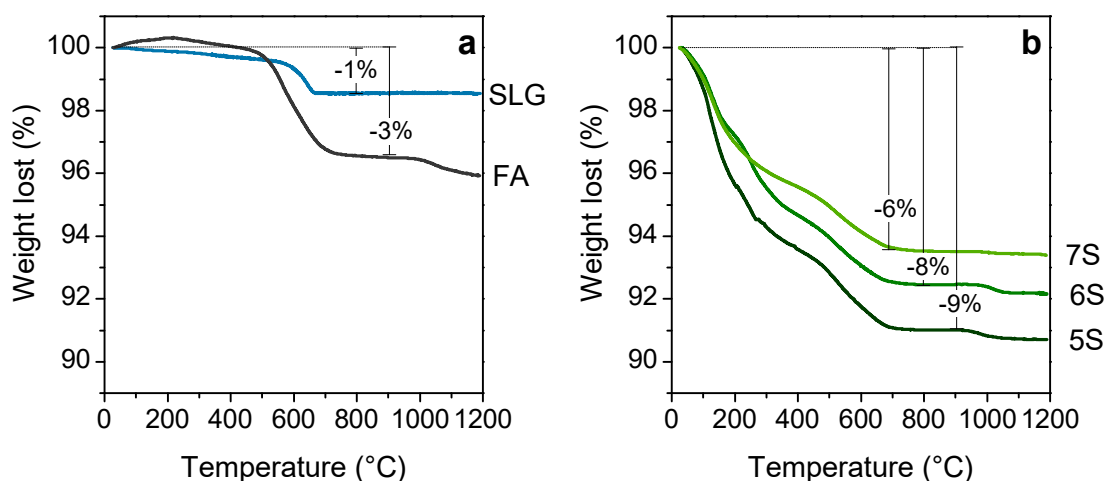


Figure 6. Differential thermal analysis plots; a) initial soda lime glass cullet and fly ash; b) hardened geopolymeric like foams.

The weight losses of the initial SLG waste and FA are presented in Figure. 4a. The waste glass presents a negligible loss of weight around 1 wt% at 700 °C, which is attributed to the burn-out of the plastic impurities inside the waste glass fraction. The weight losses of the FA are approximately 4 wt% from room temperature to 1200 °C. Losses between 200 and 800 °C are associated with the combustion of carbon present in the FA, and marginal loss of near 1wt% at 1000 °C is associated with sulphate decomposition.⁷⁷

The TGA results of the hardened samples showed in Figure 4b reveal a higher weight loss with the increase of fly ash content in the initial formulation. The surfactant influence

is not taken into account as it is added in an aqueous solution 1/10 so the total weight loss attributed to it could not exceed 0.4%.

It is quite challenging to identify the weight losses in the geopolymeric-like hardened foams as they are the result of many compounds decompositions, however it is possible to recognise two principal changes, a gradual weight loss till 500 °C, which is attributed mainly to the evaporation of physical bonded and combined water in the geopolymeric-like gel; and a loss of weight between at 500-700 °C, which corresponds mainly to the carbon combustion mentioned before and secondly to the final dehydration of the C-S-H and N-A-S-H compounds.⁷⁸ Beyond 700 °C, the weight losses are stabilised in all the samples, and only the sulphate decomposition from the initial fly ash can be noticed.⁷⁷

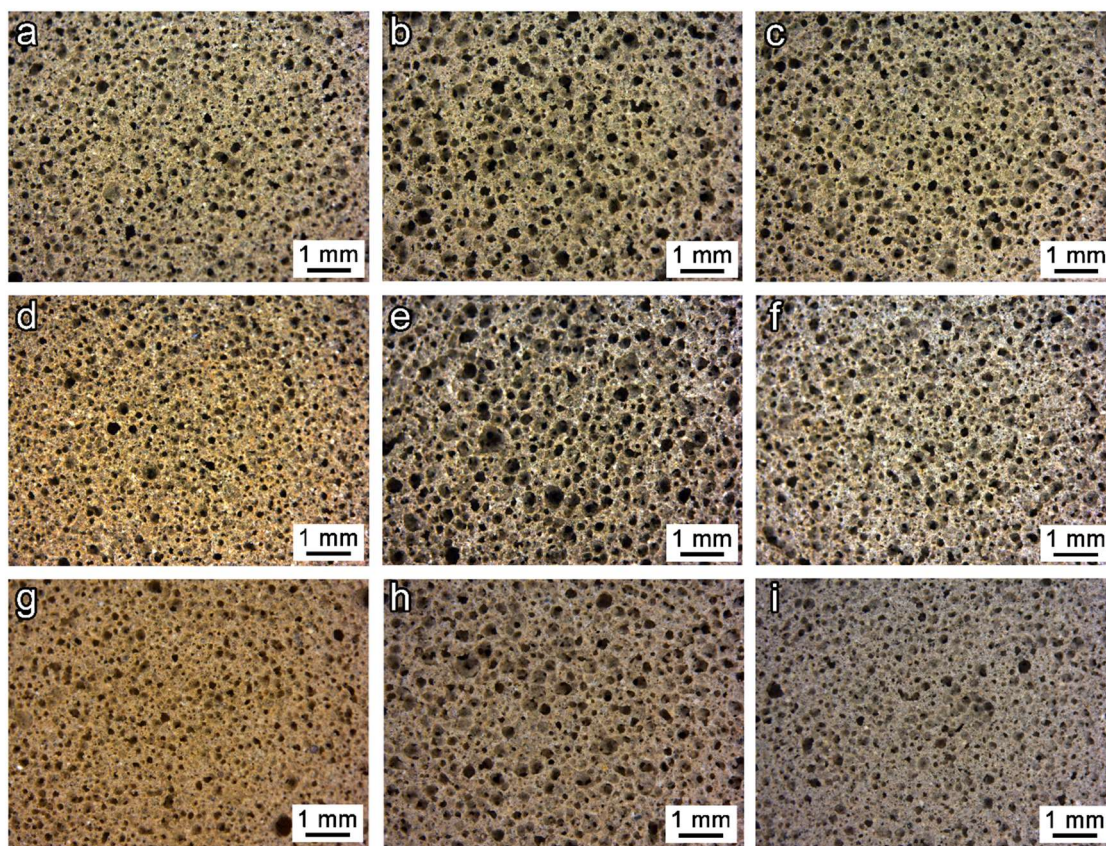


Figure 7. Morphological characterisation of the fired foams with different $\text{SiO}_2/\text{Al}_2\text{O}_3$ molar ratio; a, b and c) 5S; d, e and f) 6S; g, h and i) 7S fired at 700, 800 and 900 °C respectively.

After the heat treatment, all the samples resulted in well-sintered bodies; the porous structure is illustrated in Figure 7. Homogeneous well distributed round shaped pores with diameters from 10-30 μm are detected where the initial structure of the hardened foam remains after the heat treatment process, maintaining high uniformity. Even if the treatment temperature between 700-900 °C was far beyond the softening point of glass (around 650 °C) leading to low viscosity upon firing, no coalescence of the cells is

observed, with all the samples having the same pore microstructure as the hardened foams.

The evolution of the crystalline phases upon firing is evident from the x-ray diffraction patterns represented in Figure 8. It can be noticed that crystallisation degree is correlated not only with the thermal treatment temperature, but also with the FA/SLG proportion of the initial mixtures. The samples treated at 700 °C (Fig. 8a) show that quartz (SiO_2 ; PDF#083-0539) and mullite (Al_4SiO_8 ; PDF#079-1275) as the only identifiable phases. At this temperature, just above the softening point of the SLG glass, the phases initially present in the fly ash do not seem to be altered with the heat treatment, and only a limited viscous flow occurs. The absence of philipsite ($\text{Na}_4\text{KAl}_5\text{Si}_{11}\text{O}_{32}(\text{H}_2\text{O})_{10}$, PDF#073-1419) is noticeable.

The intensity of quartz and mullite from the original raw materials decrease with the increasing sintering temperature. After treatment at 800 °C (Fig. 8b) they are still the predominant crystalline phases, then at 900 °C (Fig. 8b) a significant intensity decrease in these phase reflections is noticed. It can also be appreciated that these peaks decrease with increasing waste glass addition in the original mixture. This result revealed that the waste glass might react with fly ash at high temperature.

The increase of temperature also determines the crystallisation of new phases, and the fly ash/glass interaction caused an extensive crystallisation of iron oxides, hematite (Fe_2O_3 , PDF#89-0691) and magnetite (Fe_3O_4 , PDF#89-0691) are also detected. Its relative abundance is difficult to quantify. However, it can be noticed a significant increase of the magnetite after the heat treatment at 900°C

The presence of nepheline ($\text{Na}_{6.65}\text{Al}_{6.24}\text{Si}_{9.76}\text{O}_{32}$, PDF#083-2372) in the samples treated at 800 and 900 °C also demonstrates the effective formation of an alumino-silicate tridimensional structure in the hardened foams, as this crystalline phase is usually present in the transformation of geopolymers at high temperature.⁷⁹⁻⁸¹

The modifications that occur in the samples upon firing are reflected in the density and porosity data shown in Table 2. For all the compositions the geometrical, apparent and true density increase with the firing temperature; the liquid phase produced by the melting of the waste glass enhances the viscous flow that enhances the density of the cell struts.

These changes are also noticeable in the porosity data. The samples that present higher porosities are those treated at the lowest temperature, 700 °C, achieving porosity values above 70%; this high values gradually decrease with the firing temperature. In addition, it can be observed that the porosity is predominantly open in all the composition for all the treated temperatures. This can be explained thanks to the delicate balance between crystallisation and viscous flow in the samples, as the liquid glass simultaneously increases the density of the samples and promotes crystallisation.

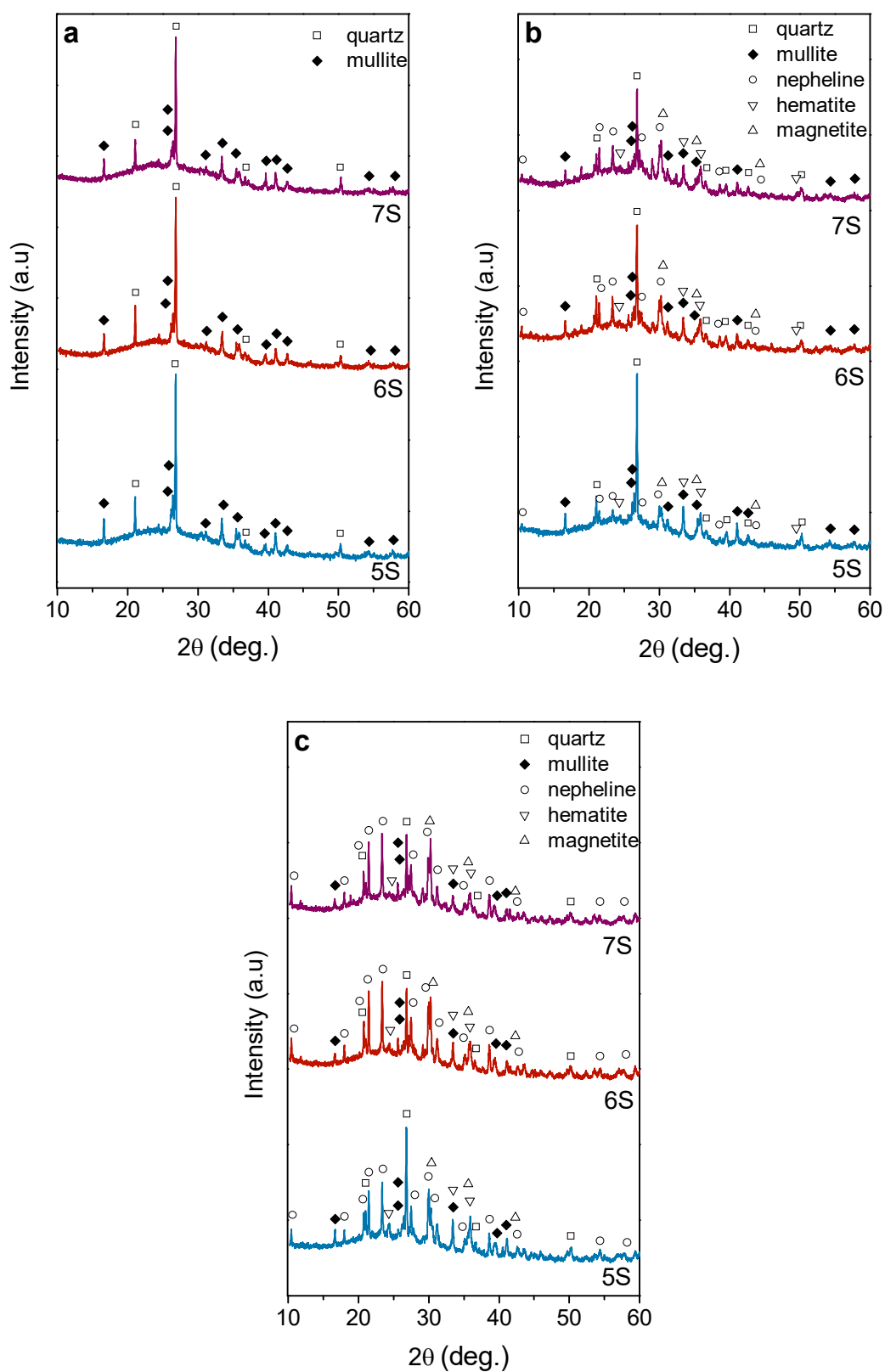


Figure 8. X-ray diffraction patterns of the fired foams with different compositions; a) 700 °C; b) 800 °C and c) 900 °C.

Sample	Firing T ^a (°C)	Density, ρ (g/cm ³)			Porosity (%)			Strength σ_{comp} (MPa)
		geometric	apparent	true	total	open	closed	
5	700	0.71 ± 0,01	2.28 ± 0.03	2.46 ± 0.01	71 ± 1	68 ± 2	2 ± 1	1.8 ± 0.2
	800	0.82 ± 0.01	2.32 ± 0.01	2.49 ± 0.01	67 ± 1	64 ± 1	2 ± 1	5.1 ± 0.3
	900	0.87 ± 0.01	2.36 ± 0.01	2.51 ± 0.01	65 ± 1	62 ± 1	2 ± 1	7.4 ± 0.3
6	700	0.54 ± 0.08	2.25 ± 0.02	2.42 ± 0.01	78 ± 2	75 ± 3	2 ± 1	1.9 ± 0.2
	800	0.66 ± 0.01	2.26 ± 0.02	2.43 ± 0.01	72 ± 1	70 ± 2	2 ± 1	4.5 ± 0.2
	900	0.71 ± 0.01	2.26 ± 0.01	2.45 ± 0.01	70 ± 3	68 ± 3	2 ± 1	5.4 ± 0.4
7	700	0.71 ± 0.01	2.31 ± 0.06	2.46 ± 0.01	71 ± 1	69 ± 2	2 ± 1	3.8 ± 0.2
	800	0.83 ± 0.01	2.13 ± 0.05	2.49 ± 0.01	66 ± 2	61 ± 2	6 ± 1	5.3 ± 0.4
	900	1.02 ± 0.3	2.08 ± 0.02	2.44 ± 0.01	58 ± 3	50 ± 4	7 ± 2	8.7 ± 0.6

Table 2. Density, porosity and mechanical properties of the fired treated foams at different heating temperatures.

The viscous flow and crystallisation effects also have a consequence in the mechanical properties of the foamed samples, also reported in Table 2. The increasing temperature promotes the densification of the samples, and the reaction between the glass cullet and the fly ash promotes the crystallisation of the samples presenting a better mechanical performance at higher temperature treatment. The highest values are reached by sample 7S treated at 900 °C. However, this sample presents the higher amount of glass cullet in its formulation, and at this temperature the viscous flow is promoted, reducing the porosity of the samples significantly. The samples that present the best performances are 5S and 6S as they maintain high rates of porosity and reach mechanical properties between 4.5 -7.4 MPa.

According to the Gibson-Ashby model⁸² the shape factor ϕ for open cells (quantity of solid at the cell walls) was assumed to be equal to 1. The bending strength, for the 5S and 6S samples fired at 800 and 900 °C is above the strength values of most glasses.⁸³

Figure 9 reports the microstructure of the geopolymeric-like foams after the heat treatment process. Initially, the foam microstructures revealed that the samples with different SiO₂/Al₂O₃ molar ratio and treated at different temperatures have similar pore morphology approximately (see Fig. 7). However, the SEM analysis reveals many changes such as strut thickness, the interconnection between pores and roundness, all of which behaved consistently with sintering temperature and can be correlated with the mechanical properties described before.

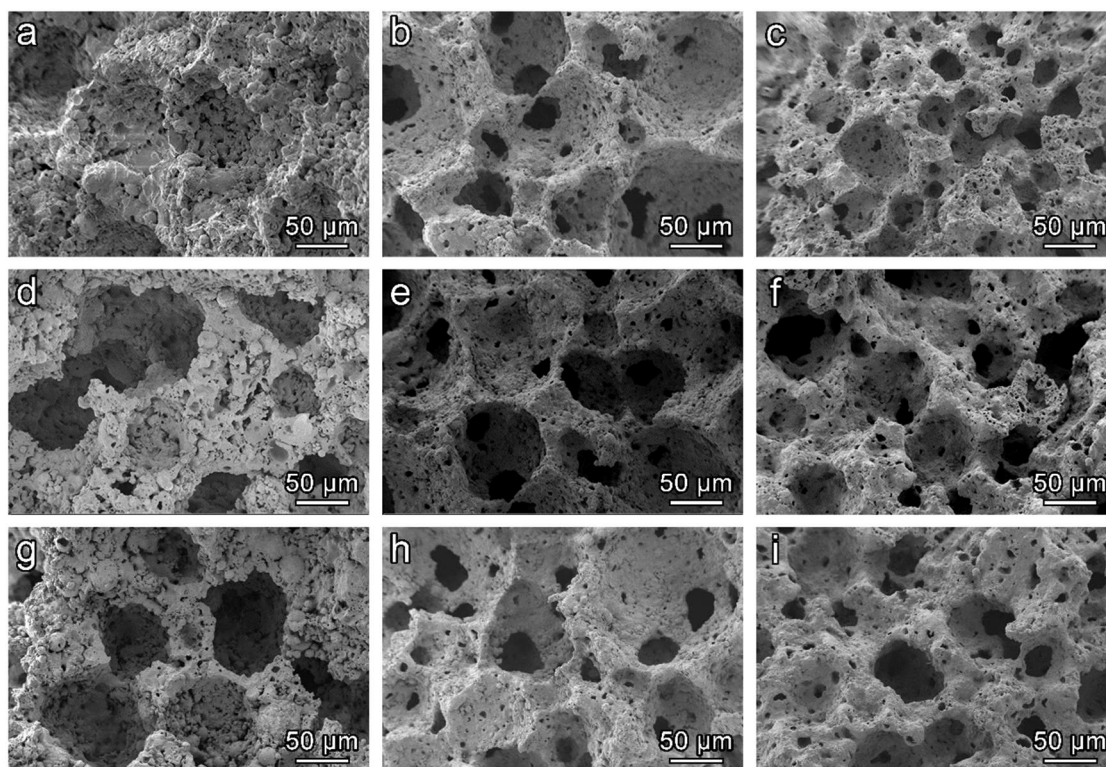


Figure 9. Microstructure of glass-ceramic foams with different $\text{SiO}_2/\text{Al}_2\text{O}_3$ molar ratio; a, b and c) 5S; d, e and f) 6S; g, h and i) 7S fired at 700, 800 and 900 °C respectively

In the samples treated at 700 °C (Figure 9 a, b and c) the struts contain several small pores, with small openings. The high open porosity could be related to the fact that the openings determine continuous paths, since the samples treated at this temperature, just above the softening point of the glass cullet, maintain a high porosity. The limited viscous flow acts just as a bonding agent between the particles without producing any reshaping. After heat treatment at 800 °C, (Figure 9 d, e and f) the cell struts present a reshaping with lower interconnections between them; this effect is more evident from the samples treated at 900 °C, also confirmed by the porosity data. With the increasing firing temperature, the small pores at the struts are likely to disappear, due to local decrease of viscosity of softened glass, leading to the formation of continuous walls and reducing the total porosity of the samples. In addition, this phenomenon produces a densification of the cell struts, which is reflected in the superior mechanical properties of this samples. Still, at this temperature, the crystallisation produced in the foam matrix keeps the pore structure mostly open.

In the pictures at higher magnification (Figure 10), the cell struts of the samples with different $\text{SiO}_2/\text{Al}_2\text{O}_3$ molar ratio treated at 800 °C are shown. It can be appreciated that in the sample with lower glass amount, sample 5S (Fig. 10a) the viscous flow is not so intense, while in cell struts some spherical particles, recognised as fly ash, are partially

embedded with fused waste glass; the struts remain quite porous as the amount of glass is not enough to produce the densification of the whole pore wall. In the samples treated at 800 and 900 °C (Fig.10 b and c) the densification of the struts is more visible, the fused glass occupies most of the struts, no fly ash can be noticed, and an intensive crystallisation occurs.

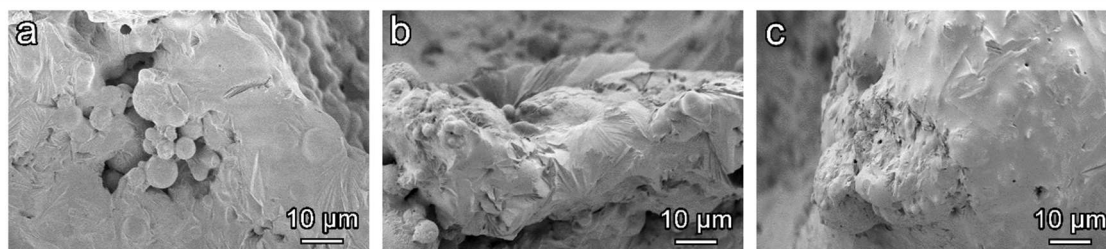


Figure 10. High magnification details of the foams struts after firing at 800 °C; a) 5S, b) 6S and c) 7S

Element (ppm)	5S3M		6S3M		7S3M		Limits [UE] (ppm)	
	800	900	800	900	800	900	Inert material	Non- hazardous material
As	0.0316	0.0635	0.068	0.0503	0.0491	0.0795	0.5	2
Ba	> adl	> adl	> adl	> adl	0.0672	0.1108	20	100
Cd	<0.0002	<0.0002	<0.0002	<0.0002	<0.0002	<0.0002	0.04	1
Cr	0.3406	0.0805	0.0255	0.0598	0.0689	0.3001	0.5	10
Cu	0.0029	0.0183	0.0024	0.0065	0.0053	0.0207	2	50
Hg	0.0032	<0.0004	0.0006	<0.0004	0.0020	0.0017	0.01	0.2
Mo	0.5324	0.0472	0.2107	0.0087	0.1973	0.2435	0.5	10
Ni	<0.0014	<0.0014	<0.0014	<0.0014	<0.0014	<0.0014	0.4	10
Pb	<0.0047	<0.0047	<0.0047	<0.0047	<0.0047	<0.0047	0.5	10
Se	0.0133	<0.0122	0.0255	<0.0122	0.0226	<0.0122	0.1	0.5
Zn	<0.0203	<0.0203	<0.0203	<0.0203	<0.0203	<0.0203	4	50
pH	9.4	8.6	8.2	7.7	8.0	7.6		

Abbreviation: >al, above detection limit

Table 3. Leachate chemical analysis of selected samples

The chemical analysis of the leachate of the glass-ceramic foams with compositions 5S and 6S after firing at 800 and 900 °C are shown in Table 3 and they were selected for their better overall performance. According to EN-12457, the leachates of the selected

samples are well below the thresholds for non-hazardous materials in all the analysed metal ions.

Meanwhile, regarding the limits for inert materials, a suitable chemical stabilisation is also reached in all the samples, except in the case of the 5S sample treated at 800°C, where molybdenum ions are slightly above the limit. Even though these foam products can be considered as safe since the leaching normative is designed for dense materials and can be considered extremely severe when applied to porous materials.

The stabilisation of the potential pollutants present in the initial waste materials supports the possible use of the glass-ceramic foams as eco-friendly thermal and acoustic insulation materials. For this reason, selected samples were produced in a semi-industrial scale, given that the proposed alkali activation and foaming method is undoubtedly beneficial to the manufacturing of large panels and low-temperature foaming does not imply any geometrical limitation.

The overall aspect of the 5S hardened lightweight panels produced with, after 24 hours of post-foaming, is illustrated in Figure 11a. The panels show good consistency with no cracks and acceptable mechanical properties, which make them easy to handle. After firing at 800 °C (Fig. 11b), no reshaping of the panel takes place due to the intense crystallisation, and the overall structure remains unaltered (the sample shown here was not cut or rectified) and the fast heat treatment does not produce any visible cracks, even if no preheating was applied to the samples and they were inserted directly into the furnace.

The thermal conductivity measured at 25 °C in the samples treated at 800 °C was 0.163 ± 0.005 , 0.983 ± 0.003 and $0.968 \pm 0.006 \text{ W}\cdot\text{m}^{-1}\cdot\text{K}^{-1}$ for the samples 5S, 6S and 7S respectively. Such a relatively low value could be explained due to the low density and the particular cellular structure developed in the panels. Even if they have a higher open porosity degree, the small and well distributed pores had probably an advantageous effect, by reducing the convection of air in the cells and leading to lower conductivity.⁸⁴

This optimised foam panels could find applications in buildings, as thermal insulators, and the open-celled morphology along with the abundant content of iron oxide could favour additional application, e.g. as catalytic supports.



Figure 11. General view of lightweight panels; a) 6S hardened panel; b) heat treated panel at 700 °C.

III.3.4 - Conclusions

We may conclude that:

- The technique ensures an excellent approach to produce glass-ceramic foams allowing the incorporation of high proportions of fly ash.

- This new approach provides an interesting way for recycling a fraction of glass currently landfilled, offering a big economic advantage as well as an environmentally friendly solution to the landfill problems.
- The possibility to replace the water glass normally used in geopolymer production with soda-lime glass, to produce fly ash-based geopolymers like gels, is demonstrated.
- The formation of zeolite crystalline phases confirms the formation of the geopolymeric gel, detected by the XRD analysis.
- The developed geopolymer foams have high porosity, low density and reasonable mechanical properties to be applied as thermal insulation materials.
- The leaching of heavy metals from selected compositions meets the current regulatory thresholds for non-hazardous materials, indicating that pollutants can be successfully stabilised in the glass-ceramic.

References

- 1 Gorai, B., & Jana, R. K. (2003). Characteristics and utilisation of copper slag—a review. *Resources, Conservation and Recycling*, 39(4), 299-313.
- 2 Lottermoser, B. G. (2002). Mobilization of heavy metals from historical smelting slag dumps, north Queensland, Australia. *Mineralogical Magazine*, 66(4), 475-490.
- 3 Van der Sloot, H. A., & Dijkstra, J. J. (2004). Development of horizontally standardized leaching tests for construction materials: a material based or release based approach?: Identical leaching mechanisms for different materials.
- 4 Zain, M. F. M., Islam, M. N., Radin, S. S., & Yap, S. G. (2004). Cement-based solidification for the safe disposal of blasted copper slag. *Cement and Concrete Composites*, 26(7), 845-851.
- 5 Moura, W. A., Gonçalves, J. P., & Lima, M. B. L. (2007). Copper slag waste as a supplementary cementing material to concrete. *Journal of Materials Science*, 42(7), 2226.
- 6 Najimi, M., Sobhani, J., & Pourkhorshidi, A. R. (2011). Durability of copper slag contained concrete exposed to sulfate attack. *Construction and Building materials*, 25(4), 1895-1905.
- 7 Al-Jabri, K. S., Hisada, M., Al-Saidy, A. H., & Al-Oraimi, S. K. (2009). Performance of high strength concrete made with copper slag as a fine aggregate. *Construction and building materials*, 23(6), 2132-2140.
- 8 Kambham, K., Sangameswaran, S., Datar, S. R., & Kura, B. (2007). Copper slag: optimization of productivity and consumption for cleaner production in dry abrasive blasting. *Journal of Cleaner Production*, 15(5), 465-473.

- 9 Mithun, B. M., & Narasimhan, M. C. (2016). Performance of alkali activated slag concrete mixes incorporating copper slag as fine aggregate. *Journal of Cleaner Production*, *112*, 837-844.
- 10 Provis, J. L., & Van Deventer, J. S. J. (Eds.). (2009). *Geopolymers: structures, processing, properties and industrial applications*. Elsevier.
- 11 Peys, A., Arnout, L., Blanpain, B., Rahier, H., Van Acker, K., & Pontikes, Y. (2018). Mix-design parameters and real-life considerations in the pursuit of lower environmental impact inorganic polymers. *Waste and Biomass Valorization*, *9*(6), 879-889.
- 12 Onisei, S., Lesage, K., Blanpain, B., & Pontikes, Y. (2015). Early age microstructural transformations of an inorganic polymer made of fayalite slag. *Journal of the American Ceramic Society*, *98*(7), 2269-2277.
- 13 Nazer, A., Payá, J., Borrachero, M. V., & Monzó, J. (2016). Use of ancient copper slags in Portland cement and alkali activated cement matrices. *Journal of environmental management*, *167*, 115-123..
- 14 Iacobescu, R. I., Cappuyns, V., Geens, T., Kriskova, L., Onisei, S., Jones, P. T., & Pontikes, Y. (2017). The influence of curing conditions on the mechanical properties and leaching of inorganic polymers made of fayalitic slag. *Frontiers of Chemical Science and Engineering*, *11*(3), 317-327.
- 15 Rawlings, R. D., Wu, J. P., & Boccaccini, A. R. (2006). Glass-ceramics: their production from wastes—a review. *Journal of Materials Science*, *41*(3), 733-761.
- 16 Chinnam, R. K., Francis, A. A., Will, J., Bernardo, E., & Boccaccini, A. R. (2013). Functional glasses and glass-ceramics derived from iron rich waste and combination of industrial residues. *Journal of Non-Crystalline Solids*, *365*, 63-74.
- 17 Bernardo, E. (2007). Micro-and macro-cellular sintered glass-ceramics from wastes. *Journal of the European ceramic Society*, *27*(6), 2415-2422.
- 18 Cilla, M. S., Colombo, P., & Morelli, M. R. (2014). Geopolymer foams by gelcasting. *Ceramics International*, *40*(4), 5723-5730.
- 19 Scarinci, G., Brusatin, G., & Bernardo, E. (2005). Glass foams. *Cellular ceramics: structure, manufacturing, properties and applications*, WILEY-VCH Verlag GmbH & Co. KGaA, Weinheim, 158-176.
- 20 Maschio, A., Bernardo, E., Desideri, D., Marangoni, M., Ponsot, I., & Pontikes, Y. (2016). Shielding effectiveness of construction materials. *International Journal of Applied Electromagnetics and Mechanics*, *52*(1-2), 137-144.
- 21 Haq, E. U., Padmanabhan, S. K., & Licciulli, A. (2014). In-situ carbonation of alkali activated fly ash geopolymer. *Construction and Building Materials*, *66*, 781-786.
- 22 Tchakouté, H. K., Rüscher, C. H., Kong, S., Kamseu, E., & Leonelli, C. (2017). Thermal behavior of metakaolin-based geopolymer cements using sodium waterglass from rice husk ash and waste glass as alternative activators. *Waste and Biomass Valorization*, *8*(3), 573-584.
- 23 Marangoni, M., Arnout, L., Machiels, L., Pandelaers, L., Bernardo, E., Colombo, P., & Pontikes, Y. (2016). Porous, Sintered Glass-Ceramics from Inorganic Polymers Based on Fayalite Slag. *Journal of the American Ceramic Society*, *99*(6), 1985-1991.

- 24 Dussauze, M., Rodriguez, V., Lipovskii, A., Petrov, M., Smith, C., Richardson, K., ... & Kamitsos, E. I. (2010). How does thermal poling affect the structure of soda-lime glass?. *The Journal of Physical Chemistry C*, 114(29), 12754-12759.
- 25 Attila, Y., Güden, M., & Taşdemirci, A. (2013). Foam glass processing using a polishing glass powder residue. *Ceramics International*, 39(5), 5869-5877.
- 26 Lane, M. D., Glotch, T. D., Dyar, M. D., Pieters, C. M., Klima, R., Hiroi, T., ... & Sunshine, J. (2011). Midinfrared spectroscopy of synthetic olivines: Thermal emission, specular and diffuse reflectance, and attenuated total reflectance studies of forsterite to fayalite. *Journal of Geophysical Research: Planets*, 116(E8).
- 27 Tomozawa, M., Hong, J. W., & Ryu, S. R. (2005). Infrared (IR) investigation of the structural changes of silica glasses with fictive temperature. *Journal of non-crystalline solids*, 351(12-13), 1054-1060.
- 28 Gyurov, S., Rabadjieva, D., Kovacheva, D., & Kostova, Y. (2014). Kinetics of copper slag oxidation under nonisothermal conditions. *Journal of Thermal Analysis and Calorimetry*, 116(2), 945-953.
- 29 Brinkmann, U., & Laqua, W. (1985). Decomposition of fayalite (Fe₂SiO₄) in an oxygen potential gradient at 1,418 K. *Physics and Chemistry of Minerals*, 12(5), 283-290.
- 30 Ponsot, I., & Bernardo, E. (2013). Self glazed glass ceramic foams from metallurgical slag and recycled glass. *Journal of cleaner production*, 59, 245-250.
- 31 Ponsot, I., Pontikes, Y., Baldi, G., Chinnam, R., Detsch, R., Boccaccini, A., & Bernardo, E. (2014). Magnetic glass ceramics by sintering of borosilicate glass and inorganic waste. *Materials*, 7(8), 5565-5580.
- 32 Pontikes, Y., Machiels, L., Onisei, S., Pandelaers, L., Geysen, D., Jones, P. T., & Blanpain, B. (2013). Slags with a high Al and Fe content as precursors for inorganic polymers. *Applied Clay Science*, 73, 93-102.
- 33 Cyr, M., Idir, R., & Poinot, T. (2012). Properties of inorganic polymer (geopolymer) mortars made of glass cullet. *Journal of Materials Science*, 47(6), 2782-2797.
- 34 Hemmings, R. T., & Berry, E. E. (1987). On the glass in coal fly ashes: recent advances. *MRS Online Proceedings Library Archive*, 113.
- 35 Elsayed, H., Rincón Romero, A., Ferroni, L., Gardin, C., Zavan, B., & Bernardo, E. (2017). Bioactive glass-ceramic scaffolds from novel 'inorganic gel casting' and sinter-crystallization. *Materials*, 10(2), 171.
- 36 Gibson, L. J., & Ashby, M. F. (1999). *Cellular solids: structure and properties*. Cambridge university press.
- 37 Bontempi, E., Zacco, A., Borgese, L., Gianoncelli, A., Ardesi, R., & Depero, L. E. (2010). A new method for municipal solid waste incinerator (MSWI) fly ash inertization, based on colloidal silica. *Journal of Environmental Monitoring*, 12(11), 2093-2099.
- 38 Ponsot, I., Bernardo, E., Bontempi, E., Depero, L., Detsch, R., Chinnam, R. K., & Boccaccini, A. R. (2015). Recycling of pre-stabilized municipal waste incinerator fly ash and soda-lime glass into sintered glass-ceramics. *Journal of Cleaner Production*, 89, 224-230.
- 39 Zornoza, E., Catalá, G., Jiménez, F., Andión, L. G., & Garcés, P. (2010). Electromagnetic interference shielding with Portland cement paste containing carbon materials and processed fly ash. *Materiales de Construcción*, 60(300), 21-32.

- 40 Wang, Z., Zhang, T., & Zhou, L. (2016). Investigation on electromagnetic and microwave absorption properties of copper slag-filled cement mortar. *Cement and Concrete Composites*, 74, 174-181.
- 41 Blissett, R. S., & Rowson, N. A. (2012). A review of the multi-component utilisation of coal fly ash. *Fuel*, 97, 1-23.
- 42 Carlson, C. L., & Adriano, D. C. (1993). Environmental impacts of coal combustion residues. *Journal of Environmental quality*, 22(2), 227-247.
- 43 Fernandes, H. R., Tulyaganov, D. U., & Ferreira, J. M. F. (2009). Preparation and characterization of foams from sheet glass and fly ash using carbonates as foaming agents. *Ceramics International*, 35(1), 229-235.
- 44 Asokan, P., Saxena, M., & Asolekar, S. R. (2005). Coal combustion residues—environmental implications and recycling potentials. *Resources, Conservation and recycling*, 43(3), 239-262.
- 45 Kulasuriya, C., Vimonsatit, V., Dias, W. P. S., & De Silva, P. (2014). Design and development of alkali pozzolan cement (APC). *Construction and Building Materials*, 68, 426-433.
- 46 Bui, P. T., Ogawa, Y., Nakarai, K., & Kawai, K. (2016). Effect of internal alkali activation on pozzolanic reaction of low-calcium fly ash cement paste. *Materials and Structures*, 49(8), 3039-3053.
- 47 Leroy, C., Ferro, M. C., Monteiro, R. C. C., & Fernandes, M. H. V. (2001). Production of glass-ceramics from coal ashes. *Journal of the European Ceramic Society*, 21(2), 195-202.
- 48 Barbieri, L., Lancellotti, I., Manfredini, T., Queralt, I., Rincon, J., & Romero, M. (1999). Design, obtainment and properties of glasses and glass-ceramics from coal fly ash. *Fuel*, 78(2), 271-276.
- 49 Wu, J. P., Boccaccini, A. R., Lee, P. D., Kershaw, M. J., & Rawlings, R. D. (2006). Glass ceramic foams from coal ash and waste glass: production and characterisation. *Advances in Applied Ceramics*, 105(1), 32-39.
- 50 Bai, J., Yang, X., Xu, S., Jing, W., & Yang, J. (2014). Preparation of foam glass from waste glass and fly ash. *Materials Letters*, 136, 52-54.
- 51 Mi, H., Yang, J., Su, Z., Wang, T., Li, Z., Huo, W., & Qu, Y. (2017). Preparation of ultra-light ceramic foams from waste glass and fly ash. *Advances in Applied Ceramics*, 116(7), 400-408.
- 52 Wei, Y. L., Cheng, S. H., & Ko, G. W. (2016). Effect of waste glass addition on lightweight aggregates prepared from F-class coal fly ash. *Construction and Building Materials*, 112, 773-782.
- 53 Feng, J., Zhang, R., Gong, L., Li, Y., Cao, W., & Cheng, X. (2015). Development of porous fly ash-based geopolymer with low thermal conductivity. *Materials & Design (1980-2015)*, 65, 529-533.
- 54 Xu, H., & Van Deventer, J. S. J. (2000). The geopolymerisation of alumino-silicate minerals. *International journal of mineral processing*, 59(3), 247-266.
- 55 Palomo, A., Grutzeck, M. W., & Blanco, M. T. (1999). Alkali-activated fly ashes: a cement for the future. *Cement and concrete research*, 29(8), 1323-1329.
- 56 Toniolo, N., & Boccaccini, A. R. (2017). Fly ash-based geopolymers containing added silicate waste. A review. *Ceramics International*.

- 57 Swanepoel, J. C., & Strydom, C. A. (2002). Utilisation of fly ash in a geopolymeric material. *Applied geochemistry*, 17(8), 1143-1148.
- 58 Fernández-Jiménez, A., Palomo, A., & Criado, M. (2005). Microstructure development of alkali-activated fly ash cement: a descriptive model. *Cement and concrete research*, 35(6), 1204-1209.
- 59 Al Bakri, M. M., Mohammed, H., Kamarudin, H., Niza, I. K., & Zarina, Y. (2011). Review on fly ash-based geopolymer concrete without Portland Cement. *Journal of engineering and technology research*, 3(1), 1-4.
- 60 Komljenović, M., Bašćarević, Z., & Bradić, V. (2010). Mechanical and microstructural properties of alkali-activated fly ash geopolymers. *Journal of Hazardous Materials*, 181(1-3), 35-42.
- 61 Somna, K., Jaturapitakkul, C., Kajitvichyanukul, P., & Chindaprasirt, P. (2011). NaOH-activated ground fly ash geopolymer cured at ambient temperature. *Fuel*, 90(6), 2118-2124.
- 62 Fernández-Jiménez, A., Cristelo, N., Miranda, T., & Palomo, Á. (2017). Sustainable alkali activated materials: Precursor and activator derived from industrial wastes. *Journal of Cleaner Production*, 162, 1200-1209.
- 63 Zhang, S., Keulen, A., Arbi, K., & Ye, G. (2017). Waste glass as partial mineral precursor in alkali-activated slag/fly ash system. *Cement and Concrete Research*, 102, 29-40.
- 64 Puertas, F., & Torres-Carrasco, M. (2014). Use of glass waste as an activator in the preparation of alkali-activated slag. Mechanical strength and paste characterisation. *Cement and Concrete Research*, 57, 95-104..
- 65 Toniolo, N., Rincon, A., Roether, J.A., Ercole, P., Bernardo, E. and Boccaccini, A.R., 2018. Extensive reuse of soda-lime waste glass in fly ash-based geopolymers. *Construction and Building Materials*, 188,1077-1084.
- 66 Toniolo, N., Rincón, A., Avadhut, Y. S., Hartmann, M., Bernardo, E., & Boccaccini, A. R. (2018). Novel geopolymers incorporating red mud and waste glass cullet. *Materials Letters*, 219, 152-154.
- 67 ASTM Committee C-09 on Concrete and Concrete Aggregates. (2013). Standard specification for coal fly ash and raw or calcined natural pozzolan for use in concrete. ASTM International.
- 68 Ranjbar, N., Mehrali, M., Alengaram, U. J., Metselaar, H. S. C., & Jumaat, M. Z. (2014). Compressive strength and microstructural analysis of fly ash/palm oil fuel ash based geopolymer mortar under elevated temperatures. *Construction and building materials*, 65, 114-121.
- 69 Studart, A. R., Gonzenbach, U. T., Tervoort, E., & Gauckler, L. J. (2006). Processing routes to macroporous ceramics: a review. *Journal of the American Ceramic Society*, 89(6), 1771-1789.
- 70 Álvarez-Ayuso, E., Querol, X., Plana, F., Alastuey, A., Moreno, N., Izquierdo, M., ... & Barra, M. (2008). Environmental, physical and structural characterisation of geopolymer matrixes synthesised from coal (co-) combustion fly ashes. *Journal of Hazardous Materials*, 154(1-3), 175-183.
- 71 Torres-Carrasco, M., & Puertas, F. (2015). Waste glass in the geopolymer preparation. Mechanical and microstructural characterisation. *Journal of cleaner production*, 90, 397-408.

- 72 Rattanasak, U., & Chindaprasirt, P. (2009). Influence of NaOH solution on the synthesis of fly ash geopolymer. *Minerals Engineering*, 22(12), 1073-1078.
- 73 Desbats-Le Chequer, C., & Frizon, F. (2011). Impact of sulfate and nitrate incorporation on potassium-and sodium-based geopolymers: geopolymerization and materials properties. *Journal of materials science*, 46(17), 5657-5664.
- 74 Hu, N., Bernsmeier, D., Grathoff, G. H., & Warr, L. N. (2017). The influence of alkali activator type, curing temperature and gibbsite on the geopolymerization of an interstratified illite-smectite rich clay from Friedland. *Applied Clay Science*, 135, 386-393.
- 75 Fernández-Jiménez, A., & Palomo, A. (2005). Composition and microstructure of alkali activated fly ash binder: Effect of the activator. *Cement and concrete research*, 35(10), 1984-1992.
- 76 Katz, A. (1998). Microscopic study of alkali-activated fly ash. *Cement and Concrete Research*, 28(2), 197-208.
- 77 Li, J., Zhuang, X., Monfort, E., Querol, X., Llaudis, A. S., Font, O., ... & Izquierdo, M. (2018). Utilization of coal fly ash from a Chinese power plant for manufacturing highly insulating foam glass: Implications of physical, mechanical properties and environmental features. *Construction and Building Materials*, 175, 64-76.
- 78 ul Haq, E., Padmanabhan, S. K., & Licciulli, A. (2014). Synthesis and characteristics of fly ash and bottom ash based geopolymers—A comparative study. *Ceramics International*, 40(2), 2965-2971.
- 79 Bakharev, T. (2006). Thermal behaviour of geopolymers prepared using class F fly ash and elevated temperature curing. *Cement and Concrete Research*, 36(6), 1134-1147.
- 80 Dombrowski, K., Buchwald, A., & Weil, M. (2007). The influence of calcium content on the structure and thermal performance of fly ash based geopolymers. *Journal of Materials Science*, 42(9), 3033-3043.
- 81 Kuenzel, C., Grover, L. M., Vandeperre, L., Boccaccini, A. R., & Cheeseman, C. R. (2013). Production of nepheline/quartz ceramics from geopolymer mortars. *Journal of the European Ceramic Society*, 33(2), 251-258.
- 82 Gibson, L. J., & Ashby, M. F. (1999). *Cellular solids: structure and properties*. Cambridge university press.
- 83 Bernardo, E., Scarinci, G., Maddalena, A., & Hreglich, S. (2004). Development and mechanical properties of metal-particulate glass matrix composites from recycled glasses. *Composites Part A: Applied Science and Manufacturing*, 35(1), 17-22.
- 84 Petersen, R. R., König, J., & Yue, Y. (2015). The mechanism of foaming and thermal conductivity of glasses foamed with MnO₂. *Journal of Non-Crystalline Solids*, 425, 74-82.

CHAPTER IV

Extension of the ‘inorganic gel casting’ process to up-cycling of glass waste into glass and glass-ceramic foams

IV.1 - Aim of the study

In the previous chapters, glass-ceramic foams were obtained by alkali activation of aqueous suspensions of glass powders or glass-slag mixtures. As this technique avoids the comprehensive compositional control of the initial materials, the foaming process is particularly easy to control. In this chapter, the same method involving a combination of alkali activation, gel casting and sintering has been applied to the production of glass foams from other waste glass-based materials avoiding the addition of soda lime glass.

In the first section (Section IV.2) of the chapter, vitrified bottom ash from municipal waste incineration was selected as a raw material to produce glass-ceramic foams as a way to valorise this waste. The bottom ashes produce in the incinerators contain potentially toxic elements, which can leach into soils, so its vitrification offers the advantage of their complete immobilisation. However, this high energy consuming process could be compensated only in case of up-cycling of derived by-product in high-value components, such as lightweight glass-ceramics. The up-cycling is obviously convenient if the additional processing of waste-derived glass is inexpensive and straightforward.

This investigation on cellular glass-ceramics from vitrified bottom ash was essentially conceived to assess the suitability of the alternative method to produce glass and glass-

ceramic foams described before, based on the alkali activation of aqueous suspensions of glass powders or glass-slag mixtures. The suspensions undergo progressive hardening by partial dissolution of glass and formation of C-S-H (calcium-silicate-hydrated) compounds as a binding phase; before complete setting, the mixtures can be foamed by intensive mechanical stirring, with the help of a surfactant. “Green” foams are later subjected to viscous flow sintering, or sinter-crystallisation, for glasses sensitive to surface nucleation. The viscous flow, besides joining adjacent glass particles, has some potential in reshaping the pores obtained from low-temperature foaming, however, in case of significant crystallisation, the increase of viscosity of softened glass caused by crystal inclusions ‘freezes’ the microstructural evolution, so that open-celled structures remain substantially unaltered.

The optimised vitrified bottom ash foams feature an open cell structure with an overall porosity of 80% and remarkable compressive strength, above 6 MPa. The stabilisation of pollutants, pursued with the vitrification, remains unaltered and no practical leaching is observed after the production of the glass-ceramic foam. The successful production of highly homogeneous foams can be seen as a proof of the versatility of this approach.

To maintain the zero-waste approach, borosilicate glass from discarded pharmaceutical vials from the pharmaceutical packaging industry was studied in the second part of the chapter (Section IV.3). The possibility of developing borosilicate glass foams was considered, applying the same foaming technique described in previous chapters.

The gel determined by the formation of calcium hydrates, upon alkali activation of soda-lime glass, may be replaced by a truly “geopolymeric gel” in the case of the alkali activation of a CaO-free alumino-boro-silicate. Given the composition of BSG, the formation of sodium hydrated alumino-silicates is the most likely reason for the hardening during pre-foaming curing. BSG can provide the critical components of zeolitic networks for geopolymer production, such as amorphous silica and alumina, as well as boron which can contribute to the polycondensation process.

Different alkali activators were studied, and the hardened green foams obtained after alkali activation and gel casting were studied by means of NMR spectroscopy to explain the possible hardening mechanisms. Finally, the foam structure was stabilised through a sintered treatment at 700 °C, promoting the mechanical properties of the resulting glass foams up to 7 MPa, with a porosity of about 70%.

IV.2 - Up-cycling MSWI vitrified bottom ash into glass-ceramic foams*

IV.2.1 - Introduction

The total amount of municipal solid waste (MSW) generated in the EU-28 in 2016 was 246 million tonnes, of which up to 66 million tonnes were incinerated.¹ The main goals of incineration are the destruction of hazardous organic substances, the volume reduction of the initial waste, and the energy recovery. Bottom ash is one of the final residues from municipal solid waste incineration (MSWI); it represents about 10% of volume and approximately 20-30 wt% of the initial waste treated in the process.^{2,3}

Bottom ash presents a risk of heavy metals leaching so that before being landfilled or reused as secondary raw material, proper pre-treatments must be applied. In any case, the direct reuse is not feasible, and a delicate balance between stabilisation costs and economic benefits from using bottom ash as an alternative raw material must be carefully studied.^{4,5}

The building industry represents an excellent target for the valorisation of adequately treated bottom ash. Depending on formulations, bottom ash may be used in the form of aggregates, in road pavement^{6,7} and concrete production, replacing natural aggregates,⁸ or as a reactive component, in concretes, thanks to some pozzolanic characteristics.^{9,10} However, it should be observed that the presence of metallic aluminium or metallic zinc and chlorides leads to long-term degradation of concrete, and the heavy metals immobilisation could not be complete.^{11,12}

Waste vitrification is one the most effective techniques available to achieve the complete stabilisation of heavy metals.¹³ When applied to MSWI bottom ash, vitrification destroys dioxins and other organic hazardous components. Therein determines a significant reduction in volume (60%) and yields a highly homogeneous glass that can be used in many applications.^{14,15} The high energy demand could be a significant drawback of the process, but the transformation of the by-products into a more valuable product can compensate the cost and avoid the disposal fees.¹⁶

Vitrified bottom ash can be used as a further replacement of natural aggregates or as a pozzolanic additive in concrete,¹⁷⁻¹⁹ but the most interesting applications actually rely on

** The following text, data and images are an adaptation of the results that were published in the article: Acacio Rincon Romero, Milena Salvo, and Enrico Bernardo. "Up-cycling of vitrified bottom ash from MSWI into glass-ceramic foams by means of 'inorganic gel casting' and sinter-crystallization." Construction and Building Materials 192 (2018): 133-140. It is reproduced in this section with the incorporation of more results and some modifications.*

the glassy nature. Waste-derived glass could be used as raw material for traditional glass-based products, such as glass fibres,²⁰ ceramic glazes²¹ and, glass-ceramic tiles.^{22, 23}

Due to its aluminosilicate rich composition and its amorphous nature, the alkali activation of bottom ash it is also used alone,^{24, 25} or mixed with other minerals²⁶ in the production of alkali-activated materials (geopolymers).^{27, 28} Its use in aerated lightweight geopolymers has also been reported.²⁹ Whereas the inhomogeneous nature of the initial bottom ash can compromise the chemical stabilisation of the geopolymer products, as the reactive aluminosilicate phase could not be in a proper Si/Al ratio, essential parameters to control the geopolymer formulation.³⁰

Among waste-derived glass-based material, cellular glasses and glass-ceramics are particularly interesting for the unique combination of low thermal conductivity, high mechanical strength, and high chemical and thermal stability.³¹ Compared to polymeric insulators, glass-based foams are non-flammable but undoubtedly more expensive. The significant production costs are mostly due to the complex control required by the viscous flow sintering of the glass, with parallel gas evolution, owing to decomposition or oxidation reactions (Quiam et al., as an example, foamed vitrified bottom ash by decomposition of calcium carbonate additive).³² The balance is even more delicate in the case of waste-derived glasses, undergoing crystallisation upon sintering.

The specific glass used here presents a high chemical homogeneity. Glass suspensions could be consolidated even with limited formation of C-S-H compounds, using an activating solution of particularly low molarity compared to the ones used for geopolymers (also based on bottom ash).³³ VBA will be produced a different hardening mechanism, at a low temperature. Due to the substantial crystallisation, the obtained glass-ceramic foams exhibited particularly remarkable specific strength values.

IV.2.2 - Experimental process

The starting material used in this study consisted of vitrified bottom ash (VBA), coming from a north Italian municipal solid waste incinerator (MSWI), which was melted at 1450 °C without adding any vitrifying agent. The vitrification process and the characteristics of the final vitrified bottom ash (VBA) are reported elsewhere.³⁴ Table 1 summarises the chemical composition reported in previous studies of the VBA used.

Oxide (wt%)	SiO ₂	Al ₂ O ₃	CaO	Na ₂ O	Fe ₂ O ₃	MgO	K ₂ O	TiO ₂	BaO	ZnO	MnO
VBA	51.7	10.9	16.2	6.9	5.8	4.1	1.6	0.7	0.2	0.2	0.1

Table 1. Chemical composition (expressed in wt%) of the starting materials.

The VBA was milled and sieved under 75µm. The powders were suspended in an aqueous solution of 2.5 M NaOH (reagent grade, Sigma-Aldrich, Gillingham, UK), to a total solid loading of 70 wt%. The mixture was kept under mechanical stirring (500 rpm),

at room temperature, for 2 hours, to achieve the partial dissolution of the initial VBA and a good dispersion of the remaining undissolved particles in the slurry.

After, a 4wt% of surfactant Triton X-100 (polyoxyethylene octyl phenyl ether - $C_{14}H_{22}O(C_2H_4O)_n$, $n = 9-10$, Sigma-Aldrich, Gillingham, UK) was added to the suspension, which at that moment was subjected to intensive mechanical stirring (2000 rpm, for 10 min). Some samples were also obtained after a pre-curing step, keeping them in close polystyrene moulds for 1h at 70 °C; this step was previously found to increase the pseudoplasticity of glass slurries by promoting the gelation. The partially gellified samples were followed by the same direct foaming process described before

Wet foams were kept at 70 °C for 24 h in sealed polystyrene cylindrical moulds, to complete the hardening. After demoulding, a thermal treatment at 800, 900 and 1000 °C for 1h in air (10 °C/min heating rate) was finally applied. A schematic representation of the whole production process could be seen in Figure 1.

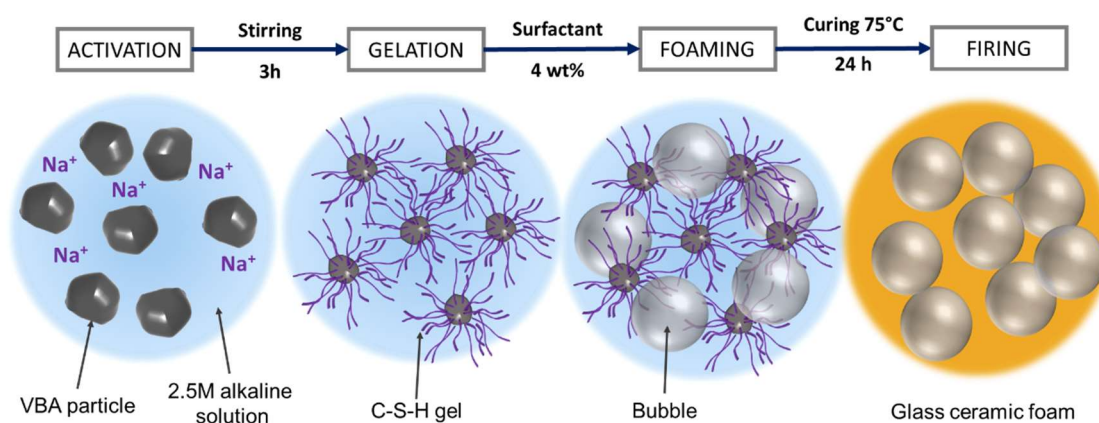


Figure 1. Processing scheme for the production of glass-ceramic foams

Samples were characterised through the standard methodology described in Chapter I. The morphological and microstructural characterisations were executed by optical stereomicroscopy (AxioCam ERc 5s Microscope Camera, Carl Zeiss Microscopy, Thornwood, New York, US) and scanning electron microscopy (FEI Quanta 200 ESEM, Eindhoven, The Netherlands). The mineralogical analysis was conducted by means of X-ray diffraction (XRD) (Bruker D8 Advance, Karlsruhe, Germany).

Selected samples were subjected to thermal analysis (TGA, Mettler Toledo TGA/DSC 3+, Zurich, Switzerland) operating at 10 °C/min, in static air, from room temperature up to 800-900°C. Fourier-transform infrared spectroscopy (FTIR, FTIR model 2000, Perkin Elmer Waltham, MA, USA). The geometric density (ρ_g) of fired foams was evaluated by considering the mass to volume ratio. The apparent (ρ_a) and the true density (ρ_t) were measured by using a helium pycnometer (Micromeritics AccuPyc 1330, Norcross, GA), operating on bulk or finely crushed samples, respectively. Compression tests were done using an Instron 1121 UTS (Instron, Danvers, MA) machine.

The heavy metal release was evaluated according to the leaching procedure in the European Standard for waste toxicity evaluation (EN 12457-2). Fragments below 4 mm were placed in distilled water, with a pH value of ≈ 7 , for a liquid/solid ratio of 10, and softly stirred at 25°C for 24 hours. The solutions were filtered through a 0.6 μm filter and analysed using inductively coupled plasma (ICP; SPECTRO Analytical Instruments GmbH, Kleve, Germany).

IV.2.3 - Results and discussion

Figure 2 reports the FTIR spectra of VBA at the as-received state, after hardening and sintering. The two plots for activated VBA correspond to the hardened foams after the activation (no pre-curing step), and after a pre-curing of 1 hour; the plots for sintered VBA relate to thermal treatments at 800, 900 and 1000 °C.

The FTIR spectrum of the initial VBA presents a broad band between 950 and 1050 cm^{-1} , attributed to the asymmetric tension of Si-O-Si and Al-O-Si groups. This band, in the hardened foams, is shifted to lower wavenumber values, becoming narrower and more intense; this effect could be associated with the polycondensation products after the alkali activation responsible for the gelation of the suspension and foam hardening.^{35, 36} After sintering at 800 °C, this band resembled the shape of the VBA in starting conditions, whereas the treatment at 900 and 1000 °C led to the splitting of the band in several peaks, caused by the overlapping of several bands reasonably due to crystallisation, i.e. more ordered structures.

After alkali activation in the hardened foams, bands corresponding to the stretching O-H modes (centred at about 3400 cm^{-1}) and to the O-H bending vibration (around 1638 cm^{-1}) were detected, but they are poorly visible. However the band is not visible in the initial VBA and is also lacking after the firing treatment, this suggests the formation of hydrated calcium silicate compounds (C-S-H) in the hardened state but in a more limited extend, compared to previous experiences.³⁷⁻³⁹

Nonetheless, the quite strong band at around 1458 cm^{-1} only present in the hardened foams corresponds to the C-O stretching vibration. In addition, the sharp band at 875 cm^{-1} attributed to the out-of-plane bending of CO_3^{2-} is also detected in the hardened state. Altogether, these findings indicate the presence of carbonate groups, suggesting that the hardening of VBA was mostly due to carbonation. The formation of carbonates finds some analogies in previous studies and could be responsible for the fast setting of the wet foams.^{40, 41}

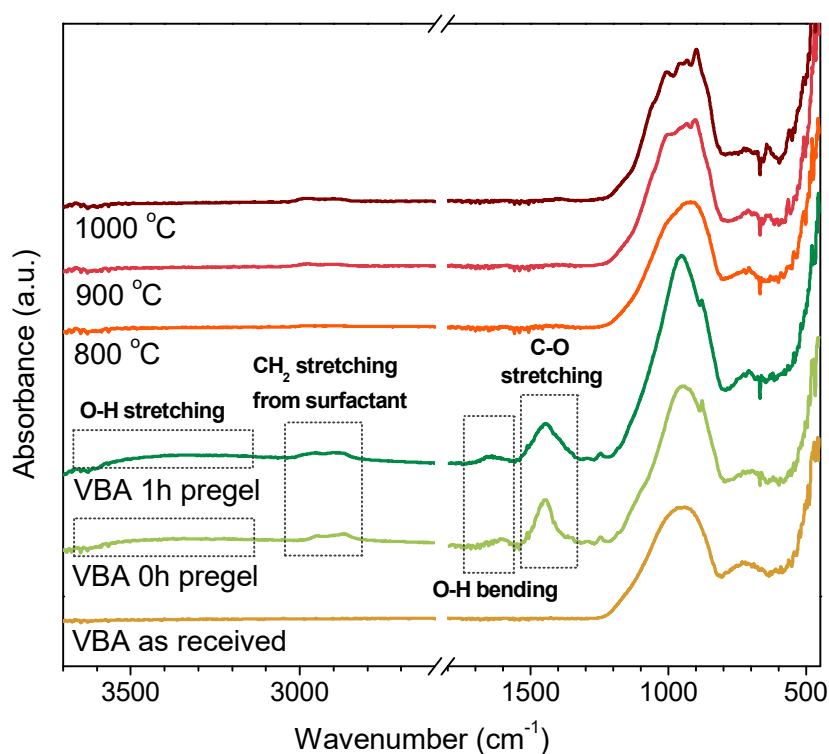


Figure 2. FTIR analysis of initial VBA glass, before and after foaming (with and without a pre-curing step at 70°C for 1h) and after heat treatments at 800, 900 and 1000 °C.

Finally, only for the hardened VBA, it is also possible to identify a band at about 2800 cm^{-1} attributable to CH_2 stretch vibrations of the surfactant. This band is not present in the fired samples as the surfactant decomposes at lower temperatures as shown by the TGA analysis (see Fig. 3a).

The new hardening mechanism from carbonatation was interestingly confirmed by thermal analysis. The thermogravimetric analysis (TGA) of the initial VBA and hardened foam after activation and the complete setting is shown in Figure 3a. The graph also reports the weight losses of the surfactant used (Triton X-100) normalised at 4% which represents the amount of additive employed in the foaming process. The weight loss below 200 °C on the hardened foam, around 2wt%, could be attributed to the loss of physically bonded water, consistent with the wide endothermic bands in the DTA plot (Fig. 3b). This loss is much lower, compared to the cases of glass suspensions hardened by C-S-H formation in previous studies. The further weight loss, around 5.8 wt%, that occurs between 200 and 500 °C could be mostly attributed to the surfactant burn-out ($\approx 4\%$ as shown in Fig. 2a) indicated by the sharp exothermic peak at 300 °C in Fig. 2b. A contribution loss of nearly 1.8 wt% should be attributed to the dehydroxylation of C-S-H compounds formed and to the decomposition of the carbonate species detected by the FTIR. Above 500 °C, the thermal effects are hardly distinguishable. Considering the

complete burn-out of the surfactant the detected changes should be attributed to the overlapping of oxidation reactions, causing a slight weight increase in both starting VBA and hardened samples.

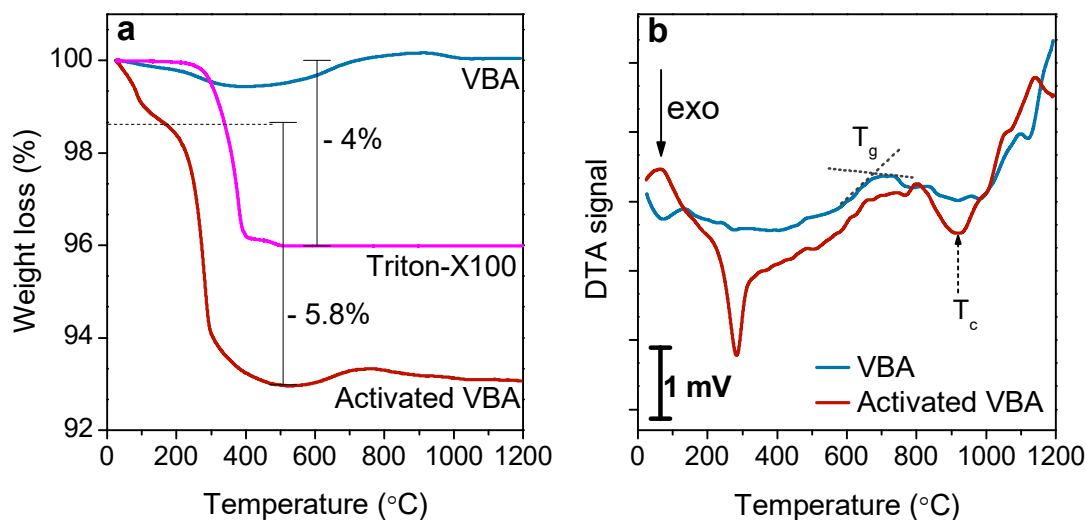


Figure 3. Thermal analysis of VBA glass before and after gel-casting foaming; (a) Thermo-gravimetric plot of VBA, alkali-activated hardened foams and normalised Triton X-100; (b) Differential thermal analysis of VBA glass powder and hardened glass foam after alkali activation and direct foaming.

From the DTA analysis (Figure 3b) the glass transition of was interpreted to occur at 660 °C (T_g). Moreover, a clear crystallisation exothermic effect can be detected centred at about 900 °C (see arrow in Fig. 2b) in the sample after alkali activation, and the peak is not present in the initial VBA. This crystallisation effect could be attributed to the formation of a low viscosity alkali-rich glass phase, after the decomposition of the phases developed upon low-temperature hardening. Alkali-enriched glasses are known to feature lower apparent activation energy of crystal growth.^{42, 43}

Figure 4 shows the overall pore structure developed in the hardened foams, by means of optical stereomicroscopy: Fig. 4a after 24h of curing with no pre-curing step, and Fig 4b after 1 hour of pre-curing step. Foams after activation and hardening feature a high microstructural uniformity, with a significant change in the pore size due to the application of the pre-curing step: while the foams not subjected to a pre-curing step presented pores with a diameter of $940 \pm 40 \mu\text{m}$, foams produced after 1h of pre-curing are characterised by much smaller cells, with a diameter of $330 \pm 10 \mu\text{m}$. The reduction in the pore size can be attributed to the increase of the viscosity of the glass suspension during the curing step, which prevents cell coalescence, and the subsequent enlargement of the pores through the setting process.

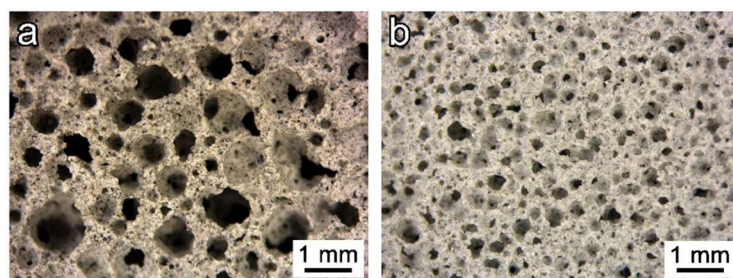


Figure 4. Microstructural morphology of VBA foams in the hardened state: a) 0h pre-curing; b) 1h pre-curing.

Figure 5 shows the final microstructural appearance of the foams after the heat treatment, Fig. 5a-c with no pre-curing step and Fig. 5d-f, after 1h of pre-curing step at 800, 900 and 1000 °C respectively. The firing treatment had no substantial effects on the microstructure or pore distribution, and the fired samples retain an overall structure similar to the original hardened foam. The cells were not subjected to any coarsening, and the openings between adjacent cells were not sealed by any thin membrane, formed by viscous flow (as observed for soda-lime glass).

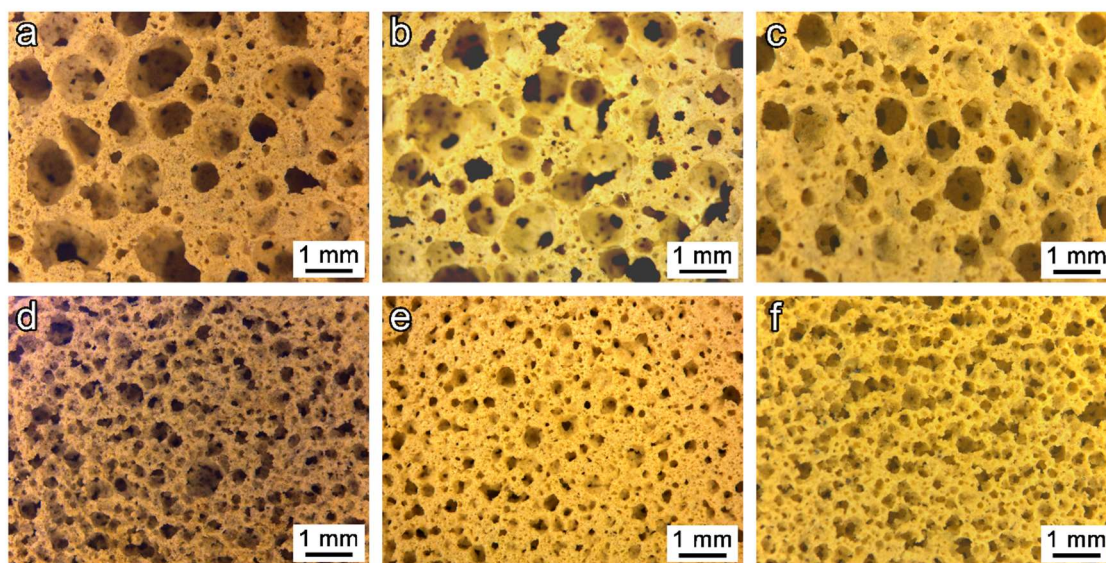


Figure 5. Microstructural morphology of VBA foams after firing treatment: a-c) 0h pre-curing; d-e) 1h pre-curing; 800 °C, 900 °C and 1000 °C respectively (actual colours).

The ‘freezing’ of the microstructure developed upon low-temperature foaming was attributed to the control of viscous flow operated by crystallisation, implying that during the heat treatments the crystallisation has a more notable effect on the microstructure than the viscous flow, preventing the remodelling of the cell structure. This behaviour was also found with bioglass foams transformed into wollastonite and diopside glass-ceramic foams, discussed in Chapter V.

The evolution of samples upon firing was further investigated by scanning electron microscopy, as shown by Figure 6, for foams fired at 900 °C, with no pre-gelation (Fig. 6a) and after 1h of pre-gelation (Fig. 6b). The differences in cell size, without or with the application of pre-curing step are again evident showing a significant size difference in the macropores detected in the optical microscope depending on the curing step. In addition, as can be noticed, the struts between adjacent cells contain several small pores.

Higher magnifications offer some additional specifications: first, as shown by Fig. 6c, (sample after 1h of pre-gelation) the obtained foams feature a ‘hierarchical’ porosity, and the macro-pores formed by gel-casting present in the cell struts some smaller pores due to gas release occurring during the decomposition of hydrated compounds and carbonates; secondly, as shown by Fig. 6d, an intensive crystallisation occurred.

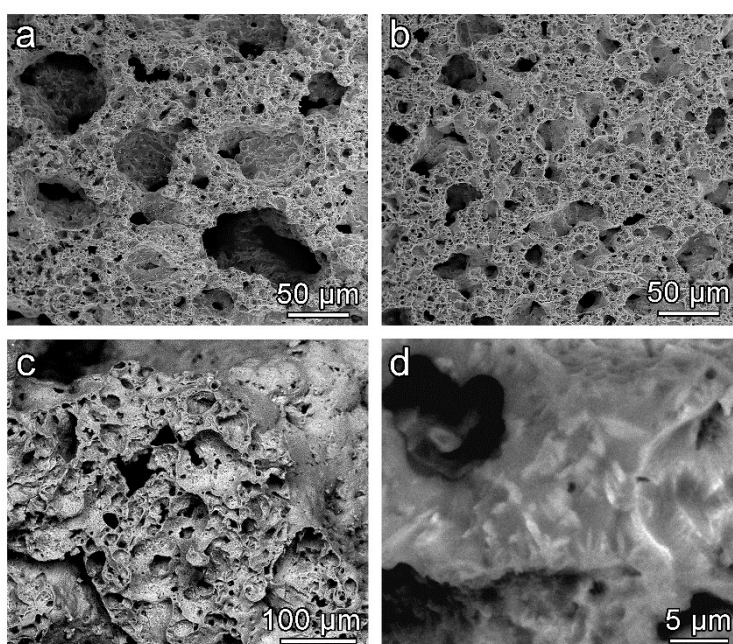


Figure 6. High magnification morphology of VBA foams in the hardened state and after firing treatment at 900 °C: a) 0h pre-curing; b) 1h pre-curing; c,d) details of strut structure; c) and solid phase; d) of a foam treated at 900 °C after 1h pre-curing.

X-ray diffraction confirmed the formation of carbonates as main binding phases formed after alkali activation. In particular, as shown by Fig. 7b, traces of calcium carbonate (CaCO_3 , PDF#29-0305), calcium sodium carbonate (shortite, $\text{Ca}_2\text{Na}_2(\text{CO}_3)_3$, PDF#72-1026) and sodium carbonate hydrate ($\text{Na}_2\text{CO}_3 \cdot 7\text{H}_2\text{O}$, PDF#76-1108) were detected, in the samples processed by application of the pre-curing step.

Sintering, starting at 800 °C, led to a substantial glass devitrification. Foams treated at 800 °C exhibited the formation of wollastonite (CaSiO_3 , PDF#43-1460) as well as quite complex solid solutions of the pyroxene ($\text{Mg}_{0.89}\text{Fe}_{0.08}\text{Al}_{0.20}\text{Cr}_{0.04}\text{Ti}_{0.01}\text{Ca}_{0.76}\text{Na}_{0.10}\text{Si}_{1.92}\text{O}_6$, PDF#85-1827) and melilite ($(\text{Ca}_{1.96}\text{Na}_{0.05})(\text{Mg}_{0.24}\text{Al}_{0.64}\text{Fe}_{0.12})(\text{Si}_{1.39}\text{Al}_{0.61}\text{O}_7)$, PDF#72-2128) groups. Interestingly, increasing the firing temperature to 900 °C the melilite solid

solution practically disappeared, which can be explained with the transformation of melilite into additional wollastonite and pyroxene solid solution, consistent with the increase of the related peaks. The transformation of the melilite solid solution could be due to the interaction with silica from the residual glass phase (if we consider phases containing only CaO and MgO, besides SiO₂, akermanite, Ca₂MgSi₂O₇ - a melilite solid solution end-member -, reacting with silica, may turn into a mixture of wollastonite and diopside, CaMgSi₂O₆ - a pyroxene end-member -, as follows: Ca₂MgSi₂O₇ + SiO₂ → CaSiO₃ + CaMgSi₂O₆).

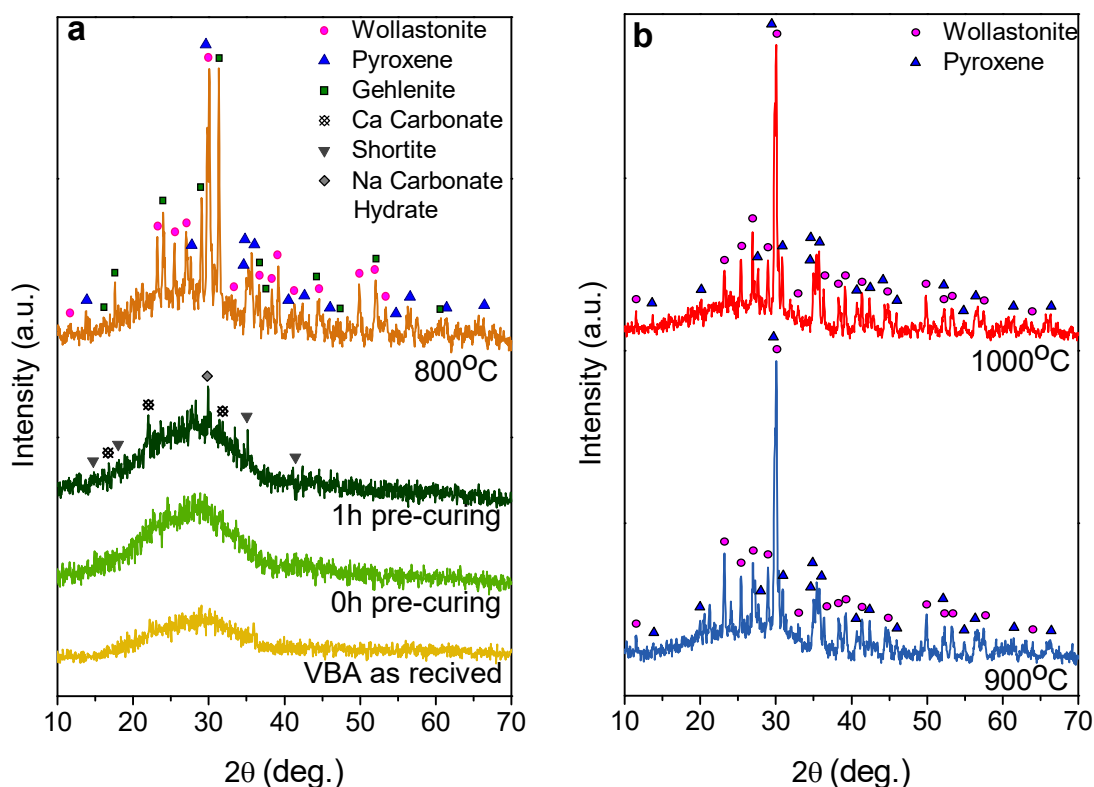


Figure 7. X-ray diffraction patterns of the initial VBA the foams in the hardened state and after firing at 800 and 900 °C.

The density and porosity data of the fired treated foams with no pre-curing step (0h pre-curing) and after 1h of pre-curing step are reported in Table 2. The compressive strength of the fired foams is also reported there. It reveals that despite the different microstructure and pore size distribution between the foams observed with the curing step, the density present similar values and tendencies after the different heat treatments. Both samples are subject to an increase of the geometrical and true density with the increase of the heat treatment temperature. This fact can be correlated with higher densification and an increase of the crystalline phases found in the glass-ceramic foams at higher temperatures.

The higher total porosity, exceeding 80%, relates to the lowest sintering temperature (800 °C), but these samples are characterised by the most reduced mechanical properties. The increase of firing temperature from 800 to 900 °C had slight effects on the overall porosity and balance between open and closed porosity, as a further confirmation of the reduction of viscous flow caused by the strong tendency to crystallisation. The viscous flow is very limited in the samples, producing only a sintering effect between glass particles and not affecting the overall porosity significantly. Meanwhile, some close porosity is detected after the treatment at 1000 °C as supplementary viscous flow is expected at higher temperatures leading to the closure of some of the cells.

Curing (hours)	Firing T(°C)	Density, ρ (g/cm ³)			Porosity (%)			Strength, σ_{comp} (MPa)
		geometric	apparent	true	total	open	closed	
0 h	800	0.43 ± 0.01	2.11 ± 0.01	2.64 ± 0.01	83 ± 2	79 ± 2	4.1 ± 0.5	2.2 ± 0.1
	900	0.45 ± 0.01	2.43 ± 0.05	2.78 ± 0.01	83 ± 2	81 ± 4	2 ± 2	2.7 ± 0.2
	1000	0.59 ± 0.01	2.25 ± 0.03	2.89 ± 0.04	79 ± 4	73 ± 4	6 ± 3	4 ± 0.3
1 h	800	0.48 ± 0.001	2.55 ± 0.05	2.66 ± 0.01	82 ± 2	81 ± 4	0 ± 2	1.5 ± 0.1
	900	0.59 ± 0.02	2.72 ± 0.02	2.85 ± 0.01	79 ± 2	78 ± 3	1.0 ± 0.8	6.2 ± 0.7
	1000	0.58 ± 0.01	2.39 ± 0.001	2.90 ± 0.01	79 ± 2	75 ± 2	4.3 ± 0.2	3.3 ± 0.4

Table 2. Physical and mechanical properties of the heat treated VBA foams.

The increase of the heat treatment temperature till 1000 °C is not justified since the foams sintered at 900 °C reached an excellent crushing strength. If we consider the classical model proposed by Gibson and Ashby⁴⁴ for an open-celled structure, the crushing strength (σ_c) depends on the bending strength (σ_{bend}) of the solid phase and on the relative density (ρ_{rel} , defined as $\rho_{\text{rel}}=1-P/100$, where P is the total porosity) according to an exponential correlation:

$$\sigma_c = \sigma_{\text{bend}} C \rho_{\text{rel}}^{3/2}$$

where C is a dimensionless constant (being ≈ 0.2). This equation may be used to assess, from experimental values of σ_c and ρ_{rel} , the strength of the solid phase. The calculated bending strength for foams treated with no pre-curing and fired at 900 °C exceeded 190 MPa, which is in good agreement with the bending strength of monolithic glass-ceramics.⁴⁵ The increase of crushing strength (corresponding to a calculated bending strength above 320 MPa) for foams fired at 900 °C, but processed with 1 h pre-curing, is consistent with the observed decrease in cell size (see Figure 5). The cell size is not included in the model from Gibson and Ashby, but it is well known that, at a given relative density, the strength of ceramic foams increases significantly with decreasing cell size.⁴⁶ The unusually high strength, combined with open porosity, makes the developed

materials ideal for many structural applications (e.g. thermal insulators in buildings or filters).

Element (ppm)	VBA as received (ppm)	900 °C (ppm)		Limits [2003/33/EC, 2003] (ppm)	
		0h gel	1h gel	Inert material	Non-hazardous material
As	<0.0049	<0.0049	<0.0049	0.5	2
Ba	<0.0000	<0.0000	<0.0000	20	100
Cd	<0.0002	0.0006	0.0004	0.04	1
Cr	<0.0004	0.0011	0.0008	0.5	10
Cu	<0.0001	0.0125	0.0003	2	50
Mo	<0.0033	<0.0033	<0.0033	0.5	10
Ni	<0.0014	<0.0014	<0.0014	0.4	10
Pb	<0.0047	0.0125	0.0157	0.5	10
Se	<0.0122	0.0617	0.0526	0.1	0.5
Zn	<0.0203	0.0146	<0.0203	4	50

Table 3. Results of the leaching tests from selected glass ceramic foams

Waste-derived materials, before any application, should undergo to a careful analysis of the chemical stability. In this investigation, foams fired at 900 °C were compared to the as-received VBA according to EN 12457-2 leaching test. According to the European Norm 2003/33/EC, 2003 (Table 3).

The heavy metals present in the initial bottom ash were initially stabilised by vitrification, with all the analysed metal ions below the detection limit of the ICP device. The leaching of VBA after transformation into glass-ceramic foams was mostly above the detection limits. In fact, due to the complex redistribution of ions in the crystal phases and the residual glass phase (with a new chemical composition)⁴⁷ each possessing a different chemical resistance. Even if these finds suggest some destabilisation of the VBA after its conversion to glass-ceramic foams, the leachates of glass-ceramics remained well below the limits for inert materials; the foams may be considered as safe, also taking into account that they were tested in the form of porous fragments, featuring a much-enhanced specific surface compared to solid fragments of as-received VBA.

IV.2.4 - Conclusions

We may conclude that:

- The approach to glass-ceramic foams through weak alkali activation of glass suspensions/mechanical foaming/sintering can be extended to vitrified bottom ash (VBA).
- Unlike previously investigated glasses, suspensions of powdered vitrified bottom ash were subject to hardening mainly by formation of carbonate phases, later decomposed upon firing.
- The sintering at 800-900 °C did not lead to any substantial ‘reshaping’ of the pores formed upon low-temperature mechanical foaming, due to the significant crystallisation, stimulated by the same alkali activation.
- The pore size can be adjusted operating on the low-temperature mechanical foaming step, with the simple application of a ‘pre-curing’ step; with the adopted solid/liquid ratio, the porosity remained practically constant at about 80% (mostly open).
- The crystallisation of VBA led to porous glass-ceramics with excellent crushing strength for the given substantial porosity, with no significant degradation of chemical stability, compared to the parent glass.

IV. 3 - Borosilicate glass foams from discarded pharmaceutical vials

IV.3.1 - Introduction

Borosilicate glasses present low thermal expansion coefficient, high electrical resistance, as well as a high resistance to chemical attack, which make them suitable for plenty of applications, including laboratory glassware, optical glasses, nuclear waste immobilisation, etc.⁴⁸⁻⁵⁰

Borosilicate glass (BSG) is also widely used in the pharmaceutical packaging industry, where products need to comply with strict quality control, maintaining accurate dimensions and tolerances; any piece proving faulty or incompatible is excluded from the process and disposed of. A direct recycling of the original vials is not practicable due to technical issues. It is estimated that above 1000 tonnes/year of pharmaceutical borosilicate glass are rejected, ending up into landfills.

Therefore, several ways to safely transform such BSG waste into high-value materials for different applications have so far been proposed, with significant environmental and economic benefits. Above the softening temperature, BSG can form a reasonably low viscosity viscous fluid and, for this reason, it has been used to produce lightweight glass-ceramic combined with iron-rich slags coming from non-ferrous metallurgy⁵¹ or residues

from the recycling of aluminium salt slags.⁵² The direct sintering and sinter-crystallisation processes is a way to avoid high-temperature treatment, achieve good mechanical properties, and ensure minimum water absorption and optimal chemical stability. In this composites, the Fe-rich phases interact upon firing with the glass resulting in the formation of magnetite crystals; this effect was also exploited to produce glass-ceramic tiles with electromagnetic applications.⁵³ The obtained glass ceramics foams also had some magnetic properties due to the presence of a ferrite type phase produced.

Borosilicate glass foams were obtained through conventional methods involving foaming agents such as SiC and or Si₃N₄.⁵⁴ Other alternative foaming agents have also been investigated, including carbon black, CaCO₃ and H₃BO₃ or Sb₂O₃ of different particle sizes.⁵⁵⁻⁵⁷

The direct sintering of fine particle BSG waste powder was used as an alternative technique to produce glass foams. Fine glass particles show a self-foaming behaviour and the viscous phase is formed upon firing. The gases released by the evaporation of boron, together with the moisture trapped during powder compaction, lead to the final glass foam.⁵⁸ The same approach was followed by other researchers, mixing BSG waste with other waste-derived materials.^{59, 60} Other foaming techniques were also explored, such as microwave radiation (leading to borosilicate glass foams reinforced by metallic fibres),^{61, 62} or melting of molten glass under pressurised argon.⁶³

Alkali-activated binders or geopolymers represent an excellent alternative to valorise wastes and stabilise the possible pollutants present in the waste source.⁶⁴⁻⁶⁶ The primary production of geopolymers usually involves the dissolution of alumina and silica-rich sources with an alkali activating solution; their condensation products lead to a stable alumino-silicate tridimensional network. The incorporation of boron in the geopolymer structure resulted in a new kind of geopolymers known as boroaluminosilicate geopolymers, where boron atoms can be found on trigonal or tetrahedral coordination, and Al-O bonds can be substituted to some extent by B-O bonds in the geopolymeric structure.⁶⁷ This incorporation proved extremely efficient for increasing the compressive strength and fracture mechanism.⁶⁸

To obtain these geopolymers, also featuring other interesting properties, boron is preferably sourced from anhydrous borax and is usually dissolved in sodium hydroxide or sodium silicate solution, also involving a new eco-friendlier alkaline activator.^{69, 70} The addition of borax was also exploited to increase the setting time and the workability of fly ash geopolymer, with no significant reduction in terms of mechanical properties.^{71, 72}

High flexural strengths were also obtained in unreinforced, and steel fibre-reinforced boroaluminosilicate geopolymers from fly ash, using a sodium hydroxide solution and anhydrous borax (Na₂B₄O₇) as alkaline activating solution.^{73, 74}

Metallurgical slag was also successfully used, through the activation with sodium hydroxide and borax in order to produce boroaluminosilicate geopolymers with enhanced tensile strength properties.⁷⁵

The direct alkali activation of borosilicate waste glass with highly concentrated NaOH solution was also proposed as a boron source in the production of fly ash geopolymers. Due to its composition, borosilicate glass can provide the fundamental components of geopolymeric networks contributing to the polycondensation reactions.⁷⁶

The alkali activation of BSG waste was also used in combination with plasmastone, a vitreous by-product of plasma gasification process of municipal solid waste, in order to produce highly porous foams, which were obtained through the combined techniques of inorganic gel-casting and sintering described in previous chapters, achieving a full stabilisation of the pollutants present in the waste material.⁷⁷

The investigation here presented was principally aimed at extending the inorganic gel casting approach to glass foams with the above mentioned boro-alumino-silicate pharmaceutical glass, known to feature a minimal CaO content⁷⁸ and thus expected to lead to different gels. In particular, alkali activation was expected to generate a truly ‘zeolite-like’ gel (instead of a ‘tobermorite-like’ (C-S-H) gel), determined by the bridging of [SiO₄] and [AlO₄] tetrahedra, in analogy with the usual alkali-activated materials, generally known as ‘geopolymers’.⁷⁹ The significant content of boron oxide was considered favourable, since it is well known to contribute to ‘zeolite-like’ networks, in the form of [BO₄] units.⁷⁶ Although its origin is still unclear, gelation effectively occurred, and the resulting open-celled glass foams present good strength-to-density ratios and a good microstructure ‘tunability’ based on the processing conditions.

IV.3.2 - Experimental process

Waste borosilicate glass coming from discarded pharmaceutical vials provided by Nuova OMPI (Piombino Dese, Padova, Italy) shows the overall composition⁵³ reported in Table 1.

Oxide (wt%)	SiO ₂	B ₂ O ₃	Al ₂ O ₃	Na ₂ O	K ₂ O	CaO	BaO
BSG	72	12	7	6	2	1	< 0.1

Table 1. Chemical composition (expressed in wt%) of the starting materials.

The initial material, received in the form of coarse fragments, was ground by ball milling into powders and sieved below 75 µm. Glass foams were obtained through a procedure similar to the one used in previous experiments. Firstly, a glass slurry was prepared for a solid loading of 68 wt% with the alkali activating solution. Different alkali solutions were used: NaOH, KOH and a mixture 1:1 of both of them. A 2.5M concentration was maintained in all the cases. The glass powders were subjected to

alkaline attack for 4h, under low-speed mechanical stirring (500 rpm) and then placed in sealed moulds at 75 °C for 4 hours, in order to induce the gelation of the mixture.

After pre-gelation, the foam was achieved by the addition of 4 wt % of surfactant and subsequent intensive mechanical stirring at 2000 rpm, until no increase in volume was observed. Triton x-100 was used as surfactant for all the compositions; selected samples were also foamed using Tween 80 or sodium lauryl sulphate (SLS; $\text{CH}_3(\text{CH}_2)_{11}\text{OSO}_3\text{Na}$ (Carlo Erba, Cornaredo, Milan, Italy) in an aqueous solution 1/10 in weight. The resulting wet foams were kept at 75 °C in close moulds in order to activate the final gelation. After that, it was observed that, when kept in closed moulds, the samples remained wet for long periods (3-4 days). So standard curing procedure was set at 75 °C for 72 hours in closed moulds, followed by a second curing step at 40 °C for 48 hours. The moulds were then opened to allow the slow evaporation of residual water and obtain the hardened foams. Finally, the so obtained samples were treated at 700 °C, using a heating rate of 10 °C/min and a holding time of 1 hour.

The characterisation of the obtained foams was carried out through the standard methods and equipment described in Chapter I (Section 1.6). The geometric density of both hardened foamed gels and fired glass foams was evaluated considering the mass to volume ratio. The apparent and true densities were measured using a helium pycnometer (Micromeritics AccuPyc 1330, Norcross, GA), operating on bulk and finely crushed samples, respectively. The three density values were used to compute the value of open and closed porosity.

Morphological and microstructural characterisations were performed by optical (AxioCam ERc 5s Microscope Camera, Carl Zeiss Microscopy, Thornwood, New York, US) and scanning electron microscopy (FEI Quanta 200 ESEM, Eindhoven, The Netherlands). The mineralogical characterisation was conducted by x-ray diffraction analysis (Bruker D8 Advance, Karlsruhe), and the resulting foams were subjected to compression tests to evaluate their mechanical performance (Instron, Danvers, MA).

NMR analysis consisted of ^{29}Si , ^{27}Al , and ^{11}B studies. ^{29}Si and ^{27}Al spectra* were collected on a Bruker AVANCE III spectrometer 300 (Bruker, Karlsruhe, Germany, magnetic field of 7.0 T corresponding to ^{29}Si and ^{27}Al Larmor frequencies of 59.623 and 78.066 MHz respectively) equipped for solid-state analysis in 4 mm diameter zirconia rotors. The magic angle was accurately adjusted prior to data acquisition using KBr. ^{29}Si chemical shifts were externally referenced to solid tetrakis(trimethylsilyl)silane at -9.8 ppm (in relation to TMS) and ^{27}Al chemical shifts were externally referenced to $\text{AlCl}_3 \cdot 6\text{H}_2\text{O}$ (0 ppm). The quantitative ^{29}Si single-pulse experiments were collected at a

* The ^{27}Al , and ^{11}B RMN measures were conducted by Michele Secco and Sergio Tamburini at the National Research Council of Italy (CNR), Institute of Condensed Matter Chemistry and Technologies for Energy (ICMATE), Padova, Italy.

spinning frequency of 6 kHz, a recycling delay of 100 s, and 2000 transients. ^{27}Al experiments were collected at a spinning frequency of 13 kHz with a recycle time of 2 s. About 4000 scans were needed using a single pulse experiment. ^{11}B NMR spectra** were obtained using a Bruker Avance-500 spectrometer (Bruker BioSpin, Billerica, MA, USA), operating at 14 kHz. A recycle delay of 5 s was used for both measurements and error tolerance was estimated at about ± 1 ppm.

IV.3.3 - Results and discussion

The x-ray diffraction patterns presented in Figure 1 do not allow the detection of any crystalline phase, and all the samples remain entirely amorphous. Considering that the patterns are nearly identical, independently from the state (as received, hardened and fired), no crystallisation was observed even in the heat-treated samples. Here, due to the relatively low sintering temperature, even common devitrification products of borosilicate glass such as cristobalite were not detected.⁸⁰

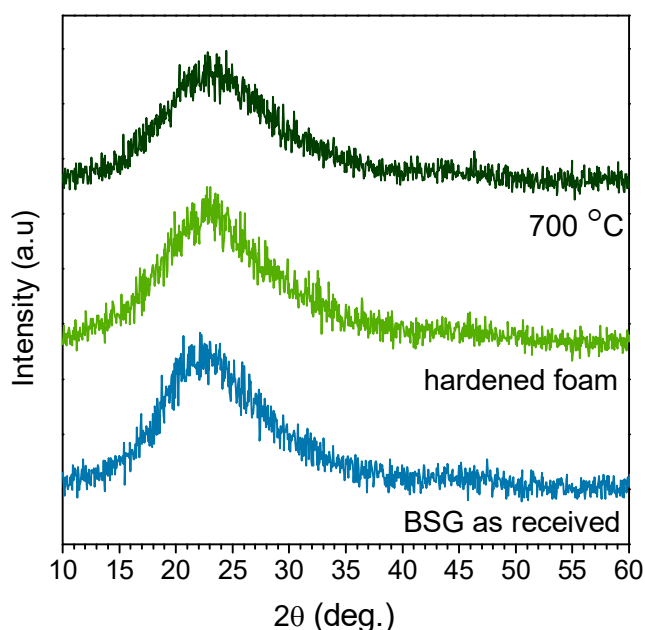


Figure 1. X-ray diffraction patterns of initial BSG, hardened samples after alkali activation and after firing

Given the composition of BSG, the formation of sodium hydrated alumino-silicates is the most likely reason behind hardening upon curing. However, the X-ray diffraction

*** The ^{11}B RMN measures were conducted in the collaboration framework of the CoACH-etn project by Gianmarco Taveri at the Institute of Physics of Materials (IPM), Brno, Czech Republic.*

analysis did not clarify the nature of the gel, and no traces of any geopolymeric related compound is distinguishable, as occurs after the alkali activation of soda lime glass and fly ash (Chapter III.3). Looking at the X-ray patterns, the only possible interpretation is that the gel was formed in limited quantities and it is amorphous, unlike soda-lime glass and other CaO rich glasses^{81, 82} where the typical shape of amorphous ‘halo’ presents some variations (i.e. clearly visible 2θ displacements).

As previously mentioned, the alkali activation determined the gelation of glass suspensions, exploited for low-temperature foaming. The nature of the resulting gel, which was responsible for the subsequent hardening, could be better understood using the FTIR analysis shown in Figure 2, where the spectra of the initial glass, the hardened foam produced with the activating solution of 2.5 M NaOH/ KOH, as well as the heat treated foam are reported.

In all the spectra, an intense high band centred around $1000\text{-}1050\text{ cm}^{-1}$ is attributed to the asymmetric stretching vibrations generated by Si-O and Al-O in tetrahedral coordination. This main band is accompanied by two broad shoulders, one around 1200 cm^{-1} , attributed to asymmetric stretching of B-O in trigonal BO_3 , and the other one around 900 cm^{-1} , attributed to the stretching vibrations of B-O bonds in BO_4 tetrahedral.^{83, 84} The band at around 800 cm^{-1} reflects the Si-O-Si symmetric stretching vibration, and remains almost unaltered throughout the process.

The alkali activation determined some broadening and shifting at lower wavenumbers; this is interpreted as the effects of the formation of a gel with mixed ions. In geopolymers the displacement of the band is correlated with an increase of Al or B in the network structure; the incorporation of different atoms in the structure reduces its homogeneity and produces a broadening of the band.^{67, 85} In addition, the shoulder at 1200 cm^{-1} correlated with boron in trigonal groups almost disappear, while the band at 900 cm^{-1} associated with the amount of boron in tetragonal conformation increases in intensity.

The bands around 700 and 1400 cm^{-1} are attributed to the B-O bond bending vibration and asymmetric stretching vibration of the trigonal boron units respectively;⁸⁶⁻⁸⁸ show a slight decrease in intensity in the hardened foam, and retain a lower intensity compared to the original glass in the fired foams.

Exclusively in the hardened foams, some additional bands are also present. A sharp absorption band at around 1600 cm^{-1} (ascribed to SiO-H stretching vibration of silanol groups), together with the band at 3430 cm^{-1} (attributed to stretching vibration of H_2O) and the band at 1 cm^{-1} (attributed to bending vibration of H_2O) are an indication of the reaction of the initial glass, leading to the formation of hydrated groups through the alkali activation process.⁸¹ Finally, the band at about 2800 cm^{-1} was attributed to C-H₂ stretch vibrations caused by the surfactant (subject to complete decomposition upon heating).

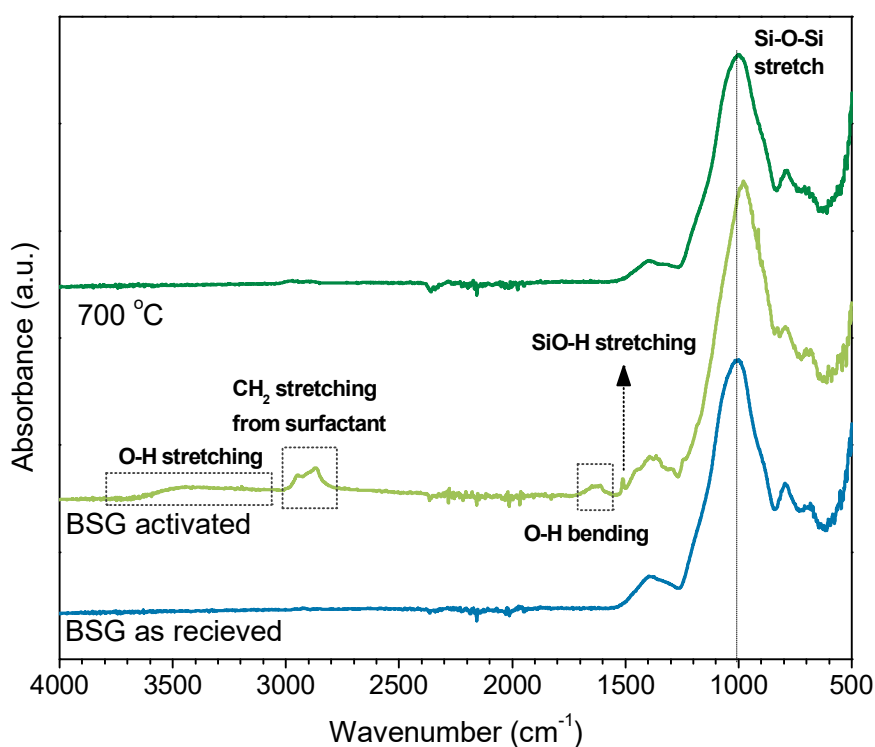


Figure 2. FTIR analysis of BSG glass in the as-received state, after alkali activation (in 'green' foams, NaOH/KOH activation) and after firing (in final foams).

Samples from NaOH/KOH activation were subjected to ^{29}Si and ^{27}Al NMR studies which led to interesting observations on the coordination of Si, Al and B ions, caused by the alkali activation and kept in the material after firing. In particular, from the ^{29}Si spectra in Fig.4a we can observe that BSG in the initial state presented a peak centred at about -105 ppm, composed by two equivalent peaks at -107.4 and -101.7 consistent with a mixed glass network (pure silica glass exhibits a peak centred at about -110 ppm, attributed to Q_4 silicons, SiO_4).^{89, 90}

The formation of silanol groups, observed with FTIR, in the alkali-activated BSG, is confirmed by the study that shows the presence of the peak at higher chemical shift can be attributed to the new hydrated specie, $\text{SiO}_2(\text{OH})_2$, that is known to provide signals at circa -89 ppm.⁹⁰ The peak returned quite symmetrical after firing, which caused dehydration but with increased upshifting respect the initial state, compared to pure silica glass, attributed to the incorporation of AlO_4 and BO_4 units (as observed in geopolymers, the chemical shifts decrease with increasing Al/Si ratio with the formation of $\text{Q}_4(1\text{Al})$ species).⁹¹

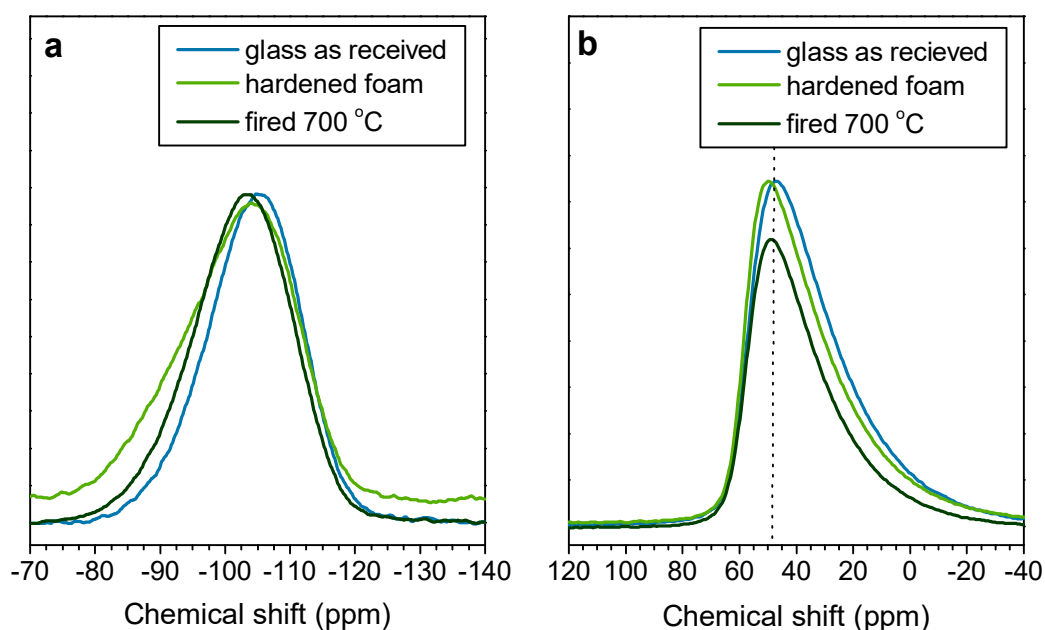


Figure 4. NMR studies BSG glass in the as-received state, after alkali activation (in 'green' foams, NaOH/KOH activation) and after firing (in final foams); a) ^{29}Si NMR and b) ^{27}Al NMR.

In Fig. 4b, the ^{27}Al spectra reveal a slight change in the coordination of aluminium ions, passing from the as-received state to the hardened and fired states: the main peak became more symmetrical at about 47 ppm, possibly due to an increase of the tetrahedral coordination (signals for 5- and 6-fold coordinations are known to prevail at lower chemical shifts).⁹²

Finally, significant evidence of the structural transformations with alkali activation and firing were provided by ^{11}B NMR spectroscopy. The ^{11}B NMR spectra of the initial BSG hardened foam after the alkali activation and fired samples are reported in Figure 4. The signals are at around 0 and 11 ppm and represent the fraction of boron in tetrahedral coordination (here denoted as $^{[4]}\text{B}$) and boron species in trigonal coordination (denoted as $^{[3]}\text{B}$) respectively, including symmetric and asymmetric configurations.

The spectrum reveals the presence of both trigonal and tetrahedral boron structural units in all the samples but their relative concentration changes with the alkali activation process and the subsequent firing. Comparing the signals of the initial glass with the hardened foam spectrum, an intensity variation between the signals is evident. After alkali activation, the intensity of the $^{[3]}\text{B}$ signal decreases while the one of the $^{[4]}\text{B}$ increases. This is an indication that the trigonal boron present in the initial glass gets dissolved by alkaline activation and rearranged into a tetrahedral coordination in the geopolymer-like structure. After heat treatment, the boron in tetrahedral coordination remains in the final glass. The density of the $^{[4]}\text{B}$ signal increases and shows a negative shift, also indicating that there was some rearrangement of the boron-oxygen structural groups in the glass

after heat treatment. This is consistent with the conversion of BO_3 into BO_4 structural units in low B_2O_3 content borosilicate glasses.^{93, 94} All these differences suggest that the concentration of BO_3 units decrease with alkali activation of the glass, while the concentration of BO_4 units increases and this configuration remains stable in the heat-treated samples, suggesting the formation of borosilicate networks in the structure of the geopolymer-like gel, which, after heat treatment, become incorporated in the glass structure.

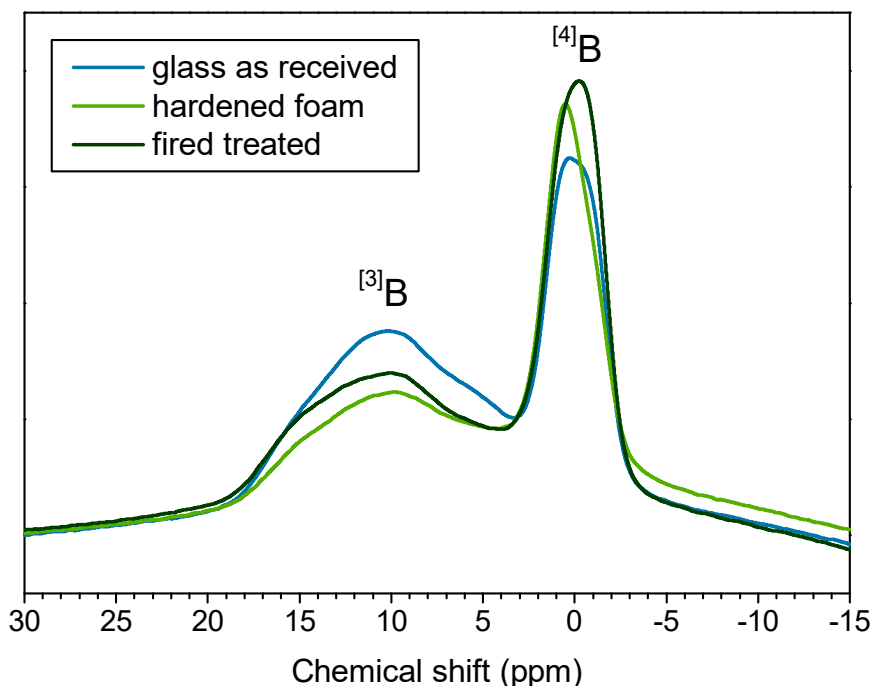


Figure 1. *11B MA BSG glass in the as-received state, after alkali activation (in ‘green’ foams, NaOH/KOH activation) and after firing (in final foams).*

It is possible to assume that alkali activation led to a complex amorphous hydrated gel, with a boro-alumino-silicate structure (embedding alkali, for charge compensation); the related spectroscopic signals were weak, due to the limited dissolution of the starting glass. The firing treatment, besides causing dehydration, determined an ‘absorption’ of the gel in the molecular structure of BSG: extra Na^+ and K^+ ions, from the activating solutions, were incorporated in the glass structure during the formation of extra BO_4 and AlO_4 units.

The different pore structure presented by the obtained foams, and produced through the activation with the different alkali solutions (foamed with Triton-X100) and heat treatment at $700\text{ }^\circ\text{C}$, is confirmed by the optical stereomicroscopy images shown in Figure 5.

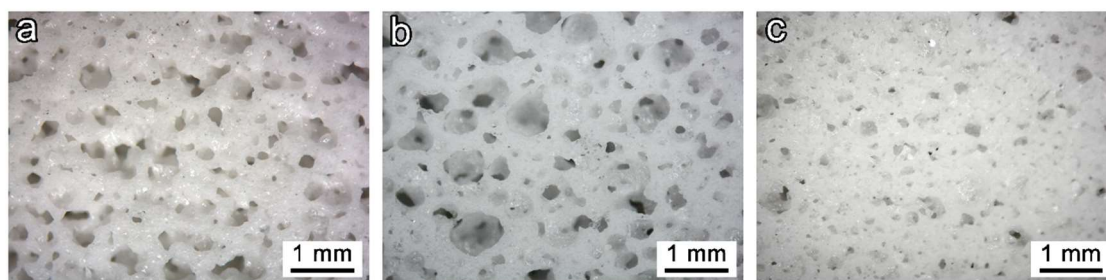


Figure 5. Microstructural details of the heat treated BSG foams obtained with different activation solutions: a) NaOH; b) NaOH/KOH; c) KOH

The sample prepared with NaOH as activating solution (Fig. 1a) presents the lowest microstructural uniformity. It is formed by irregular non-spherical shaped cells, with an average size around 300 μm , which are separated by thick walls with poor interconnections between them. Alternatively, the foams produced using a 2.5M KOH activating solution (Fig. 1c) feature a more homogenous cell structure but much smaller pores with an average size of $\sim 100 \mu\text{m}$. However, the foams produced with the alkaline activating solution of 2.5 M NaOH/KOH in a ratio 1:1 (Fig. 1b) presents the most homogeneous structure. A hierarchical pore structure can be detected, and the macro-pores formed by gel-casting present smaller pores in the cell struts. As the foams produced with NaOH/KOH in a ratio 1:1 present the best homogeneity, this activator was selected to carry out further experiments. The different pore structure developed with the different alkali activators could be related to the diverse viscosity of the formed gel after alkali activation.

The evolution of samples upon firing was further investigated by scanning electron microscopy, as shown in Figure 6, where the pore microstructure observed by optical microscopy was confirmed. The adopted firing temperature was evidently too low for a substantial softening of BSG; 700 $^{\circ}\text{C}$ is in fact the minimum temperature for the sintering of this specific glass (an optimum temperature for glass sintering can be estimated at 50 $^{\circ}\text{C}$ above the dilatometric softening temperature,⁹⁵ which is 650 $^{\circ}\text{C}$ for BSG.⁷⁸ In addition, the limited amount of hydrated phase prevented a secondary foaming and reshaping of pores (observed for soda-lime glass in Chapter II); the release of water vapour can only justify the small micro-sized pores (darker spots) visible on the surface of struts (Fig. 6d, e and f).

Due to the long setting times of the borosilicate geopolymeric gel developed in the glass particle surface, the tuning of porosity through changes in viscosity upon hardening (as in soda lime glass) was not sufficient. Therefore the foaming with different surfactants was chosen as a strategy to tune the porosity of the foams. Fig. 7 actually illustrates that the morphology could even be tuned by merely changing the chemistry of the adopted surfactant.

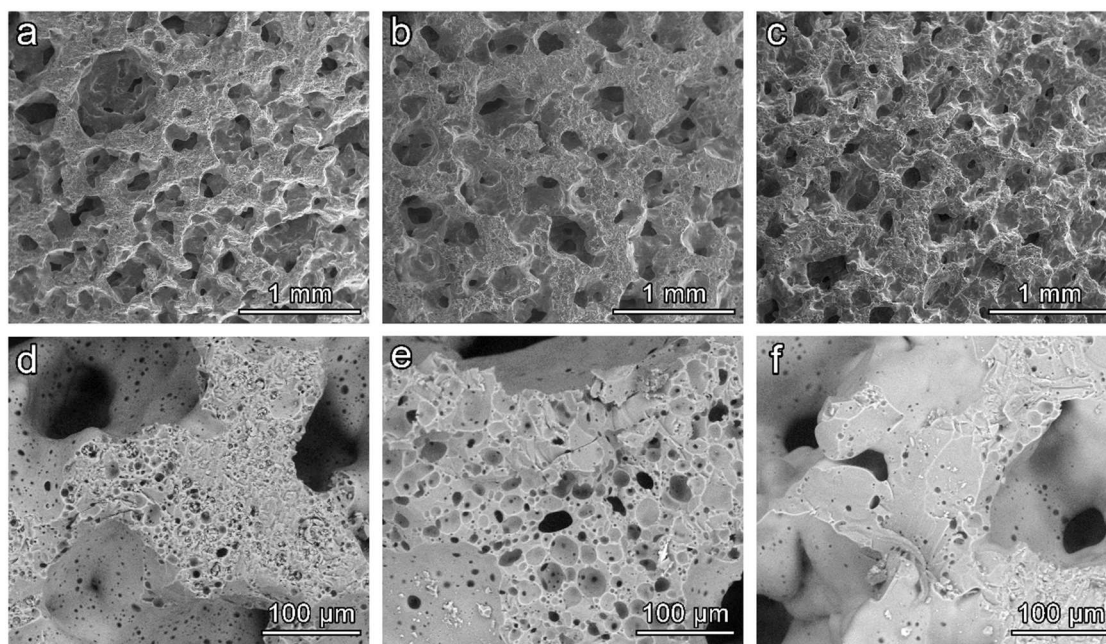


Figure 6. Morphology of BSG-derived glass foams (surfactant: Triton X-100): a) NaOH activation; b) NaOH/KOH activation c) KOH activation

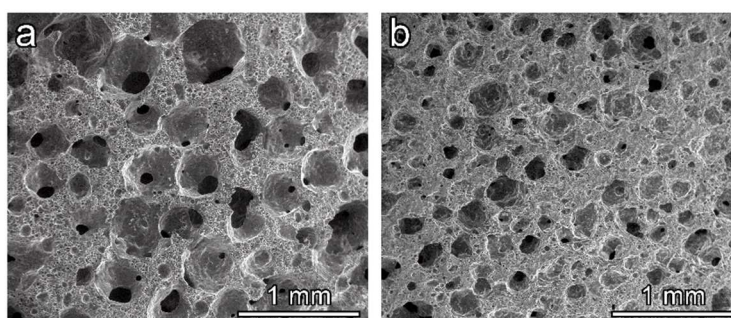


Figure 7. Examples of BSG-derived foams from different surfactants; a) Tween 80; b) SLS

The differences in cell size in the derived foams obtained with different surfactants are evident, showing a significant size difference in the macropores detected. As can also be noticed, the struts between adjacent cells contain several small pores.

The pore structure developed can be correlated with the porosity and mechanical properties of the produced foams. The density and porosity data of the heat treated foams at 700 °C produced with different alkali activating solutions and surfactants are reported in Table 2. Samples obtained with the activating solution of 2.5 M NaOH/KOH in a ratio 1:1 has the highest true density.

The highest total porosity, 68%, reflects the one of the samples activated with NaOH/KOH. The viscous flow is minimal when firing at this temperature, producing only a sintering effect between glass particles and leaving a predominantly open cell structure.

The foams obtained after alkali activation with NaOH or KOH solutions do not reach such high porosity values, retaining a 66 and 61% respectively. The best mechanical performance of 8.7 MPa is obtained by the sample prepared with the KOH activating solution, and this can be explained by the fact that it has the lowest porosity, which is mostly closed.

Surfactant	Activator solution	Density, ρ (g/cm ³)			Porosity (%)			Strength, σ_{comp} (MPa)
		geometric	apparent	true	total	open	closed	
	NaOH	0.75 ± 0.01	1.69 ± 0.03	2.25 ± 0.01	66 ± 1	55 ± 3	11 ± 2	4.3 ± 0.3
Triton X-100	NaOH/KOH	0.81 ± 0.02	1.69 ± 0.03	2.55 ± 0.01	68 ± 3	52 ± 4	16 ± 3	7.7 ± 0.4
	KOH	0.96 ± 0.02	1.67 ± 0.03	2.50 ± 0.02	61 ± 3	42 ± 4	19 ± 3	8.7 ± 0.2
Tween 80	NaOH/KOH	0.79 ± 0.01	1.76 ± 0.03	2.56 ± 0.02	69 ± 2	55 ± 3	13 ± 2	7.2 ± 0.3
SLS	NaOH/KOH	0.98 ± 0.01	1.93 ± 0.02	2.54 ± 0.01	61 ± 2	49 ± 2	12 ± 1	8.2 ± 0.5

Table 2. Physical and mechanical properties of BSG-derived foams treated at 700 °C under different conditions.

Samples produce with the activating solution of 2.5 M NaOH/ KOH present the most homogeneous pore structure, maintaining an excellent balance between the mechanical performance and keeping the open cell structure. According to the well-known Gibson-Ashby (GA) model,⁹⁶ the compressive strength of cellular solid, σ_c , depends on the relative density ($\rho_{\text{rel}}=1-P$, where P is the total porosity), as follows:

$$\sigma_c \approx \sigma_{\text{bend}} \cdot f(\Phi, \rho_{\text{rel}}) = \sigma_{\text{bend}} \cdot [C \cdot (\Phi \cdot \rho_{\text{rel}})^{3/2} + (1-\Phi) \cdot \rho_{\text{rel}}]$$

where σ_{bend} is the bending strength of the solid phase, C is a dimensionless calibration constant (~ 0.2), and f is a ‘structural function’. The quantity $(1-\Phi)$ expresses the mechanical contribution of solid positioned at cell faces, reasonably limited when open porosity is dominant. If we neglect this contribution ($\Phi \sim 1$),⁷⁸ the observed compressive strength could be correlated to a bending strength well exceeding 100 MPa, i.e. far above the measured values for pore-free sintered BSG. The open-celled morphology could be exploited for the infiltration of a secondary phase (e.g. elastomers, in composites for ballistic protection)⁹⁷ or the manufacturing of filters. These changes will be the reasonable focus of future investigations, especially at a semi-industrial scale.

IV.3.4 - Conclusions

We may conclude that:

- Alkali activation of glass slurries, followed by low-temperature sintering, was successfully applied to glass from discarded pharmaceutical vials.

- Owing to the specific glass chemistry, the hardening of slurries was not caused by the formation of a C-S-H gel, but rather by the formation of an amorphous hydrated boro-alumino-silicate gel, in limited quantities.
- Alkali activation and subsequent firing determined slight but measurable changes in the molecular structure of the adopted boro-alumino-silicate glass, with enhancement of BO_4 and AlO_4 units (by incorporation of ‘activating’ alkali ions).
- The cellular structure could be tuned depending on the chemistry of activating solution, but also on the chemistry of surfactants used in the foaming of activated glass slurries.
- The relatively low firing temperature and the limited quantity of hydrated phases favoured the retention of the open-celled morphology developed upon the foaming of activated slurries.
- The developed foams, in all processing conditions, demonstrated a favourable strength/density correlation.

References

- 1 Eurostat, 2016a, ‘Waste database municipal waste’ (http://appsso.eurostat.ec.europa.eu/nui/show.do?dataset=env_wasmun&lang=en), accessed 13 April 2018.
- 2 Best Available Techniques (BAT) Reference Document on Waste Incineration Industrial Emissions Directive 2010/75/EU (Integrated Pollution Prevention and Control) JOINT RESEARCH CENTRE Institute for Prospective Technological Studies Directorate B – Growth and Innovation Sustainable Production and Consumption Unit Circular Economy and Industrial Leadership Unit European IPPC Bureau DRAFT 1 (May 2017)
- 3 Brunner, P. H., & Rechberger, H. (2015). Waste to energy–key element for sustainable waste management. *Waste Management*, 37, 3-12.
- 4 Margallo M., Taddei M. B. M., Hernández-Pellón A., Aldaco R. & Irabien A. Environmental sustainability assessment of the management of municipal solid waste incineration residues: a review of the current situation. *Clean Technologies and Environmental Policy*, 2015, 17, 1333-53.
- 5 Toller S., Kärrman E., Gustafsson J. P. & Magnusson Y. Environmental assessment of incinerator residue utilisation. *Waste Management*, 2009, 29, 2071-7.
- 6 Hjelmar O., Holm J. & Crillesen K. Utilisation of MSWI bottom ash as sub-base in road construction: First results from a large-scale test site. *Journal of Hazardous Materials*, 2007, 139, 471-80.
- 7 Toraldo E., Saponaro S. A road pavement full-scale test track containing stabilized bottom ashes. *Environ. Technol.*, 2015, 36, 1114-22.

- 8 del Valle-Zermeño, R., Formosa, J., Chimenos, J. M., Martínez, M., & Fernández, A. I. (2013). Aggregate material formulated with MSWI bottom ash and APC fly ash for use as secondary building material. *Waste management*, 33(3), 621-627.
- 9 Li, X. G., Lv, Y., Ma, B. G., Chen, Q. B., Yin, X. B., & Jian, S. W. (2012). Utilization of municipal solid waste incineration bottom ash in blended cement. *Journal of Cleaner Production*, 32, 96-100.
- 10 Zhang, B., & Poon, C. S. (2015). Use of furnace bottom ash for producing lightweight aggregate concrete with thermal insulation properties. *Journal of cleaner production*, 99, 94-100.
- 11 Müller, U., & Rübner, K. (2006). The microstructure of concrete made with municipal waste incinerator bottom ash as an aggregate component. *Cement and Concrete Research*, 36(8), 1434-1443.
- 12 Li, X. G., Lv, Y., Ma, B. G., Chen, Q. B., Yin, X. B., & Jian, S. W. (2012). Utilization of municipal solid waste incineration bottom ash in blended cement. *Journal of Cleaner Production*, 32, 96-100.
- 13 Bingham, P. A., & Hand, R. J. (2006). Vitrification of toxic wastes: a brief review. *Advances in applied ceramics*, 105(1), 21-31.
- 14 Barberio, G., Buttol, P., Masoni, P., Scalbi, S., Andreola, F., Barbieri, L., & Lancellotti, I. (2010). Use of incinerator bottom ash for frit production. *Journal of Industrial Ecology*, 14(2), 200-216.
- 15 Monteiro, R. C. C., Alendouro, S. J. G., Figueiredo, F. M. L., Ferro, M. C., & Fernandes, M. H. V. (2006). Development and properties of a glass made from MSWI bottom ash. *Journal of Non-Crystalline Solids*, 352(2), 130-135.
- 16 Rincón, A., Marangoni, M., Cetin, S., & Bernardo, E. (2016). Recycling of inorganic waste in monolithic and cellular glass-based materials for structural and functional applications. *Journal of Chemical Technology & Biotechnology*, 91(7), 1946-1961.
- 17 Ferraris, M., Salvo, M., Ventrella, A., Buzzi, L., & Veglia, M. (2009). Use of vitrified MSWI bottom ashes for concrete production. *Waste Management*, 29(3), 1041-1047.
- 18 Saccani, A., Sandrolini, F., Andreola, F., Barbieri, L., Corradi, A., & Lancellotti, I. (2005). Influence of the pozzolanic fraction obtained from vitrified bottom-ashes from MSWI on the properties of cementitious composites. *Materials and structures*, 38(3), 367-371.
- 19 Yang, S. F., Chiu, W. T., Wang, T. M., Chen, C. T., & Tzeng, C. C. (2014). Porous materials produced from incineration ash using thermal plasma technology. *Waste management*, 34(6), 1079-1084.
- 20 Scarinci, G., Brusatin, G., Barbieri, L., Corradi, A., Lancellotti, I., Colombo, P., ... & Dall'igna, R. (2000). Vitrification of industrial and natural wastes with production of glass fibres. *Journal of the European Ceramic Society*, 20(14-15), 2485-2490.
- 21 Schabbach, L. M., Bolelli, G., Andreola, F., Lancellotti, I., & Barbieri, L. (2012). Valorization of MSWI bottom ash through ceramic glazing process: a new technology. *Journal of Cleaner Production*, 23(1), 147-157.
- 22 Appendino, P., Ferraris, M., Matekovits, I., & Salvo, M. (2004). Production of glass-ceramic bodies from the bottom ashes of municipal solid waste incinerators. *Journal of the European Ceramic Society*, 24(5), 803-810.

- 23 Ferraris, M., Salvo, M., Smeacetto, F., Augier, L., Barbieri, L., Corradi, A., & Lancellotti, I. (2001). Glass matrix composites from solid waste materials. *Journal of the European Ceramic Society*, 21(4), 453-460.
- 24 Giro-Paloma, J., Maldonado-Alameda, A., Formosa, J., Barbieri, L., Chimenos, J. M., & Lancellotti, I. (2017, October). Geopolymers based on the valorization of Municipal Solid Waste Incineration residues. In *IOP Conference Series: Materials Science and Engineering*(Vol. 251, No. 1, p. 012125). IOP Publishing.
- 25 Lancellotti, I., Cannio, M., Bollino, F., Catauro, M., Barbieri, L., & Leonelli, C. (2015). Geopolymers: An option for the valorization of incinerator bottom ash derived “end of waste”. *Ceramics International*, 41(2), 2116-2123.
- 26 Lancellotti, I., Ponzoni, C., Barbieri, L., & Leonelli, C. (2013). Alkali activation processes for incinerator residues management. *Waste management*, 33(8), 1740-1749.
- 27 Ruiz-Santaquiteria, C., Fernández-Jiménez, A., Skibsted, J., & Palomo, A. (2013). Clay reactivity: production of alkali activated cements. *Applied clay science*, 73, 11-16.
- 28 Silva, R. V., de Brito, J., Lynn, C. J., & Dhir, R. K. (2017). Use of municipal solid waste incineration bottom ashes in alkali-activated materials, ceramics and granular applications: A review. *Waste Management*, 68, 207-220.
- 29 Chen Z., Liu Y., Zhu W. & Yang E. Incinerator bottom ash (IBA) aerated geopolymer. *Construction and Building Materials*, 2016, 112, 1025-31.
- 30 Lancellotti, I., Ponzoni, C., Barbieri, L., & Leonelli, C. (2013). Alkali activation processes for incinerator residues management. *Waste management*, 33(8), 1740-1749.
- 31 Colombo, P. (2006). Conventional and novel processing methods for cellular ceramics. *Philosophical Transactions of the Royal Society of London A: Mathematical, Physical and Engineering Sciences*, 364(1838), 109-124.
- 32 Quian, S., Lin, J., & Tang, B. (2014). Preparation of glass foams from vitrified municipal solid waste incinerator ash. *Journal of the Chinese Ceramic Society*, 42(1), 108-112.
- 33 Lancellotti, I., Ponzoni, C., Barbieri, L., & Leonelli, C. (2013). Alkali activation processes for incinerator residues management. *Waste management*, 33(8), 1740-1749..
- 34 Ferraris, M., Salvo, M., Ventrella, A., Buzzi, L., & Veglia, M. (2009). Use of vitrified MSWI bottom ashes for concrete production. *Waste Management*, 29(3), 1041-1047.
- 35 Lancellotti, I., Catauro, M., Ponzoni, C., Bollino, F., & Leonelli, C. (2013). Inorganic polymers from alkali activation of metakaolin: Effect of setting and curing on structure. *Journal of Solid State Chemistry*, 200, 341-348.
- 36 Chen, Z., Liu, Y., Zhu, W., & Yang, E. H. (2016). Incinerator bottom ash (IBA) aerated geopolymer. *Construction and Building Materials*, 112, 1025-1031.
- 37 Rincón, A., Giacomello, G., Pasetto, M., & Bernardo, E. (2017). Novel ‘inorganic gel casting’ process for the manufacturing of glass foams. *Journal of the European Ceramic Society*, 37(5), 2227-2234.
- 38 Elsayed, H., Rincón Romero, A., Ferroni, L., Gardin, C., Zavan, B., & Bernardo, E. (2017). Bioactive glass-ceramic scaffolds from novel ‘inorganic gel casting’ and sinter-crystallization. *Materials*, 10(2), 171.
- 39 Rincón, A., Desideri, D., & Bernardo, E. (2018). Functional glass-ceramic foams from ‘inorganic gel casting’ and sintering of glass/slag mixtures. *Journal of Cleaner Production*, 187, 250-256.

- 40 Allali, F., Joussein, E., Kandri, N. I., & Rossignol, S. (2016). The influence of calcium content on the mixture of sodium silicate with different additives: Na₂CO₃, NaOH and AlO (OH). *Construction and Building Materials*, 121, 588-598.
- 41 Lancellotti, I., Ponzoni, C., Barbieri, L., & Leonelli, C. (2013). Alkali activation processes for incinerator residues management. *Waste management*, 33(8), 1740-1749.
- 42 Watanabe, T., Hashimoto, H., Hayashi, M., & Nagata, K. (2008). Effect of Alkali Oxides on Crystallization in CaO–SiO₂–CaF₂ Glasses. *ISIJ international*, 48(7), 925-933..
- 43 Avramov, I., Zanutto, E. D., & Prado, M. O. (2003). Glass-forming ability versus stability of silicate glasses. II. Theoretical demonstration. *Journal of non-crystalline solids*, 320(1-3), 9-20.
- 44 Gibson, L. J., & Ashby, M. F. (1999). *Cellular solids: structure and properties*. Cambridge university press.
- 45 Rincón, A., Marangoni, M., Cetin, S., & Bernardo, E. (2016). Recycling of inorganic waste in monolithic and cellular glass-based materials for structural and functional applications. *Journal of Chemical Technology & Biotechnology*, 91(7), 1946-1961.
- 46 Brezny, R., & Green, D. J. (1990). The effect of cell size on the mechanical behavior of cellular materials. *Acta metallurgica et materialia*, 38(12), 2517-2526.
- 47 Monich, P. R., Romero, A. R., Höllen, D., & Bernardo, E. (2018). Porous glass-ceramics from alkali activation and sinter-crystallization of mixtures of waste glass and residues from plasma processing of municipal solid waste. *Journal of Cleaner Production*, 188, 871-878.
- 48 Le Bourhis, E. (2014). *Glass: mechanics and technology*. John Wiley & Sons.
- 49 Axinte, E. (2011). Glasses as engineering materials: A review. *Materials & Design*, 32(4), 1717-1732.
- 50 Suzuki, M., Umesaki, N., Tanaka, T., Ohkubo, T., Kakihara, T., Hashimoto, T., & Kawashima, H. (2018). Structural behaviour of vanadium ions in alkali borosilicate glass for nuclear waste storage. *Physics and Chemistry of Glasses-European Journal of Glass Science and Technology Part B*, 59(4), 181-192.
- 51 Ponsot, I., Detsch, R., Boccaccini, A. R., & Bernardo, E. (2015). Waste derived glass ceramic composites prepared by low temperature sintering/sinter-crystallisation. *Advances in Applied Ceramics*, 114(sup1), S17-S25.
- 52 Chinnam, R. K., Boccaccini, A. R., Bernardo, E., & Epstein, H. (2015). Glass-Ceramic Composites from Borosilicate Glass and Alumina-Rich Residues. *International Journal of Applied Ceramic Technology*, 12, E19-E27.
- 53 Ponsot, I., Pontikes, Y., Baldi, G., Chinnam, R., Detsch, R., Boccaccini, A., & Bernardo, E. (2014). Magnetic glass ceramics by sintering of borosilicate glass and inorganic waste. *Materials*, 7(8), 5565-5580.
- 54 Bayer, G. (1980). Foaming of borosilicate glasses by chemical reactions in the temperature range 950–1150° C. *Journal of Non-Crystalline Solids*, 38, 855-860.
- 55 Lv, D. S., Li, X. H., Wang, L., Du, J. J., & Zhang, J. (2010). Effect of carbon as foaming agent on pore structure of foam glass. In *Advanced Materials Research* (Vol. 105, pp. 765-768). Trans Tech Publications.

- 56 Liu, S. J., Fu, G. Z., Shen, J. X., & Zhang, J. (2012). Impact of H₃BO₃ on Foaming Action of CaCO₃ in Borosilicate Foam Glasses. In *Advanced Materials Research* (Vol. 581, pp. 401-404). Trans Tech Publications.
- 57 Zhai, C., Li, Z., Zhu, Y., Zhang, J., Wang, X., Zhao, L., ... & Wang, P. (2014). Effects of Sb₂O₃ on the mechanical properties of the borosilicate foam glasses sintered at low temperature. *Advances in Materials Science and Engineering*, 2014.
- 58 Chinnam, R. K., Molinaro, S., Bernardo, E., & Boccaccini, A. R. (2014). Borosilicate Glass Foams from Glass Packaging Residues. *Ceramics for Environmental and Energy Applications II: Ceramic Transactions, Volume 246*, 203-210.
- 59 Chinnam, R. K., Bernardo, E., Will, J., & Boccaccini, A. R. (2015). Processing of porous glass ceramics from highly crystallisable industrial wastes. *Advances in Applied Ceramics*, 114(sup1), S11-S16.
- 60 Taurino, R., Lancellotti, I., Barbieri, L., & Leonelli, C. (2014). Glass–ceramic foams from borosilicate glass waste. *International Journal of Applied Glass Science*, 5(2), 136-145.
- 61 Boccaccini, A. R., Veronesi, P., & Leonelli, C. (2001). Microwave processing of glass matrix composites containing controlled isolated porosity. *Journal of the European Ceramic Society*, 21(8), 1073-1080.
- 62 Minay, E. J., Veronesi, P., Cannillo, V., Leonelli, C., & Boccaccini, A. R. (2004). Control of pore size by metallic fibres in glass matrix composite foams produced by microwave heating. *Journal of the European Ceramic Society*, 24(10-11), 3203-3208.
- 63 Wang, B., Matsumaru, K., Yang, J., Fu, Z., & Ishizaki, K. (2012). Mechanical behavior of cellular borosilicate glass with pressurized Ar-filled closed pores. *Acta Materialia*, 60(10), 4185-4193.
- 64 Van Deventer, J. S. J., Provis, J. L., Duxson, P., & Lukey, G. C. (2007). Reaction mechanisms in the geopolymeric conversion of inorganic waste to useful products. *Journal of Hazardous Materials*, 139(3), 506-513.
- 65 Bernal, S. A., Rodríguez, E. D., Kirchheim, A. P., & Provis, J. L. (2016). Management and valorisation of wastes through use in producing alkali-activated cement materials. *Journal of Chemical Technology & Biotechnology*, 91(9), 2365-2388.
- 66 Toniolo, N., & Boccaccini, A. R. (2017). Fly ash-based geopolymers containing added silicate waste. A review. *Ceramics International*.
- 67 Bagheri, A., Nazari, A., Hajimohammadi, A., Sanjayan, J. G., Rajeev, P., Nikzad, M., ... & Mendis, P. (2018). Microstructural study of environmentally friendly boroaluminosilicate geopolymers. *Journal of Cleaner Production*, 189, 805-812.
- 68 Nazari, A., Maghsoudpour, A., & Sanjayan, J. G. (2014). Characteristics of boroaluminosilicate geopolymers. *Construction and Building Materials*, 70, 262-268.
- 69 Bagheri, A., Nazari, A., Sanjayan, J. G., & Rajeev, P. (2017). Alkali activated materials vs geopolymers: role of boron as an eco-friendly replacement. *Construction and Building Materials*, 146, 297-302.
- 70 Al Saadi, T. H. A., Badanoiu, A. I., Nicoara, A. I., Stoleriu, S., & Voicu, G. (2017). Synthesis and properties of alkali activated borosilicate inorganic polymers based on waste glass. *Construction and Building Materials*, 136, 298-306.

- 71 Wijaya, S. W., Satria, J., Sugiarto, A., & Hardjito, D. (2016, May). The Use of Borax in Deterring Flash Setting of High Calcium Fly Ash Based Geopolymer. In *Materials Science Forum* (Vol. 857, No. 2016, pp. 416-420). Petra Christian University.
- 72 Liu, H., Sanjayan, J. G., & Bu, Y. (2017). The application of sodium hydroxide and anhydrous borax as composite activator of class F fly ash for extending setting time. *Fuel*, 206, 534-540.
- 73 Nazari, A., Maghsoudpour, A., & Sanjayan, J. G. (2015). Flexural strength of plain and fibre-reinforced boroaluminosilicate geopolymer. *Construction and Building Materials*, 76, 207-213.
- 74 Bagheri, A., Nazari, A., & Sanjayan, J. G. (2018). Fibre-reinforced boroaluminosilicate geopolymers: A comparative study. *Ceramics International*.
- 75 Khezrloo, A., Aghaie, E., & Tayebi, M. (2018). Split tensile strength of slag-based boroaluminosilicate geopolymer. *Journal of the Australian Ceramic Society*, 54(1), 65-70.
- 76 Taveri, G., Tousek, J., Bernardo, E., Toniolo, N., Boccaccini, A. R., & Dlouhy, I. (2017). Proving the role of boron in the structure of fly-ash/borosilicate glass based geopolymers. *Materials Letters*, 200, 105-108.
- 77 Monich, P. R., Romero, A. R., Höllen, D., & Bernardo, E. (2018). Porous glass-ceramics from alkali activation and sinter-crystallization of mixtures of waste glass and residues from plasma processing of municipal solid waste. *Journal of Cleaner Production*, 188, 871-878.
78. Bernardo, E., & Scarinci, G. (2004). Sintering behaviour and mechanical properties of Al₂O₃ platelet-reinforced glass matrix composites obtained by powder technology. *Ceramics international*, 30(5), 785-791.
79. Provis, J. L. (2014). Geopolymers and other alkali activated materials: why, how, and what?. *Materials and Structures*, 47(1-2), 11-25.
- 80 Jean, J. H., & Gupta, T. K. (1992). Crystallization kinetics of binary borosilicate glass composite. *Journal of materials research*, 7(11), 3103-3111.
- 81 Rincón, A., Giacomello, G., Pasetto, M., & Bernardo, E. (2017). Novel 'inorganic gel casting' process for the manufacturing of glass foams. *Journal of the European Ceramic Society*, 37(5), 2227-2234.
- 82 Elsayed, H., Rincón Romero, A., Ferroni, L., Gardin, C., Zavan, B., & Bernardo, E. (2017). Bioactive glass-ceramic scaffolds from novel 'inorganic gel casting' and sinter-crystallization. *Materials*, 10(2), 171.
- 83 Elbatal, H. A., Azooz, M. A., Saad, E. A., EzzELDin, F. M., & Amin, M. S. (2018). Corrosion Behavior Mechanism of Borosilicate Glasses Towards Different Leaching Solutions Evaluated by the Grain Method and FTIR Spectral Analysis Before and After Gamma Irradiation. *Silicon*, 10(3), 1139-1149.
- 84 El-Egili, K. (2003). Infrared studies of Na₂O–B₂O₃–SiO₂ and Al₂O₃–Na₂O–B₂O₃–SiO₂ glasses. *Physica B: Condensed Matter*, 325, 340-348.
- 85 Fernández-Jiménez, A., & Palomo, A. (2005). Mid-infrared spectroscopic studies of alkali-activated fly ash structure. *Microporous and Mesoporous Materials*, 86(1-3), 207-214.
- 86 Liu, M., Zhou, H., Zhu, H., Yue, Z., & Zhao, J. (2012). Microstructure and dielectric properties of glass/Al₂O₃ composites with various low softening point borosilicate glasses. *Journal of Materials Science: Materials in Electronics*, 23(12), 2130-2139.

- 87 Wan, J., Cheng, J., & Lu, P. (2008). The coordination state of B and Al of borosilicate glass by IR spectra. *Journal of Wuhan University of Technology-Mater. Sci. Ed.*, 23(3), 419-421.
- 88 Hou, Z. X., Wang, S. H., Xue, Z. L., Lu, H. R., Niu, C. L., Wang, H., ... & Su, C. (2010). Crystallization and microstructural characterization of B₂O₃-Al₂O₃-SiO₂ glass. *Journal of Non-Crystalline Solids*, 356(4-5), 201-207.
- 89 Malfait, W. J., Halter, W. E., & Verel, R. (2008). ²⁹Si NMR spectroscopy of silica glass: T1 relaxation and constraints on the Si-O-Si bond angle distribution. *Chemical Geology*, 256(3-4), 269-277.
- 90 Kinney, D. R., Chuang, I. S., & Maciel, G. E. (1993). Water and the silica surface as studied by variable-temperature high-resolution proton NMR. *Journal of the American Chemical Society*, 115(15), 6786-6794.
- 91 Duxson, P., Provis, J. L., Lukey, G. C., Separovic, F., & van Deventer, J. S. (2005). ²⁹Si NMR study of structural ordering in aluminosilicate geopolymer gels. *Langmuir*, 21(7), 3028-3036.
- 92 Risbud, S. H., Kirkpatrick, R. J., Tagliavere, A. P., & Montez, B. (1987). Solid-state NMR Evidence of 4-, 5, and 6-Fold Aluminum Sites in Roller-Quenched SiO₂-Al₂O₃ Glasses. *Journal of the American Ceramic Society*, 70(1), C-10.
- 93 Ramkumar, J., Sudarsan, V., Chandramouleeswaran, S., Shrikhande, V. K., Kothiyal, G. P., Ravindran, P. V., ... & Mukherjee, T. (2008). Structural studies on boroaluminosilicate glasses. *Journal of Non-Crystalline Solids*, 354(15-16), 1591-1597.
- 94 Chen, D., Miyoshi, H., Masui, H., Akai, T., & Yazawa, T. (2004). NMR study of structural changes of alkali borosilicate glasses with heat treatment. *Journal of non-crystalline solids*, 345, 104-107.
- 95 Ray, A., & Tiwari, A. N. (2001). Compaction and sintering behaviour of glass-alumina composites. *Materials chemistry and physics*, 67(1-3), 220-225.
- 96 Gibson, L. J., & Ashby, M. F. (1999). *Cellular solids: structure and properties*. Cambridge university press.
- 97 Colombo, P., Zordan, F., & Medvedovski, E. (2006). Ceramic-polymer composites for ballistic protection. *Advances in applied ceramics*, 105(2), 78-83.

CHAPTER V

Bioactive Glass-Ceramic Foam Scaffolds from ‘Inorganic Gel Casting’ and Sinter-Crystallization

V.1 - Aim of the study*

This chapter aims to investigate an extension to the gel casting foaming process, starting from alkali activation of glass powders, followed by sinter-crystallisation. The same procedure described in previous chapters was followed to create highly porous bioactive glass-ceramics scaffolds, thus proving the high versatility of the approach.

The higher dissolution rates of bioactive glasses were exploited applying weaker alkali activator concentrations, which allowed the formation of a gel. The pseudoplasticity developed by this reaction products after alkali activation led to the formation of a hardened foam. The nature of gels obtained from bioactive glasses was also investigated along with the final properties of the resulting foams.

In Section V.2 Wollastonite (CaSiO_3)-diopside ($\text{CaMgSi}_2\text{O}_6$) glass-ceramic foams have been successfully obtained using alkali activation. A Ca-Mg silicate glass (with a composition close to 50 mol % wollastonite - 50 mol % diopside, with minor amounts of

** This chapter was not the main focus of the PhD research, on valorisation of waste materials, but the foaming technique was applied to bioactive glasses as an extension and validation of the process.*

Na₂O and P₂O₅) was exploited, leading to well-dispersed concentrated suspensions subjected to progressive hardening by curing at low temperature (40 °C), thanks to the formation of a C-S-H (calcium silicate hydrate) gel. The direct foaming was achieved by vigorous mechanical stirring of partially gelified suspensions, also comprising a surfactant. The open-celled structure resulting from mechanical foaming could be ‘frozen’ with the subsequent sintering treatment at 900-1000 °C, causing a substantial crystallisation. A total porosity that exceeds 80%, including both well-interconnected macro-pores and micro-pores on cell walls, was accompanied by an excellent compressive strength, even above 5 MPa.

The same approach was exploited in Section V.3 to produce glass-ceramic foams from CEL2, a glass already known to yield a bioactive sintered glass-ceramic. The samples produced feature an abundant total porosity (from 60% to 80%) and well-interconnected macro- and micro-sized cells. The developed foams possessed a compressive strength from 2.5 to 5 MPa, which is in the range of human trabecular bone strength. Therefore, CEL2 glass-ceramics can be proposed for bone substitutions

V.2 - Wollastonite-diopside bioactive glass-ceramics foams*

V.2.1 - Introduction

Ca-silicates and Ca-Mg silicates are being increasingly investigated in the field of bioceramics for their bioactivity properties and their ability to stimulate body tissues to repair themselves, in particular for bone ingrowth. They can also be used in clinical applications.¹⁻⁷ Many experiments involved glass-ceramics from the controlled crystallisation of glasses belonging to the CaO-MgO-SiO₂ system with B₂O₃, Na₂O, CaF₂, and P₂O₅ additives, and they proved to retain their bioactive properties even after crystallisation.^{6, 8-10}

The use of bioactive glass-ceramics, instead of bioglasses, generally allows to maximise the mechanical properties of highly porous, open-celled foams. High porosities, and consequently low relative densities, determine a severe ‘downscaling’ of strength, given the exponential correlation. The further strengthening of the solid phase through crystallisation may provide a valid reward.¹¹

* *The following text, data and images are an adaptation of the results that were published in the article: “Elsayed, H., Rincón Romero, A., Ferroni, L., Gardin, C., Zavan, B., & Bernardo, E. (2017). Bioactive glass-ceramic scaffolds from novel ‘inorganic gel casting’ and sinter-crystallization. Materials, 10(2), 171”. It is partially reproduced in this section with slight modifications.*

The strength of the solid phase, however, is not simply tuned by the degree of crystallisation, but may depend on the ‘quality’ of the manufacturing process. More precisely, many glass and glass-ceramic foams are produced using the traditional replica method, i.e., by the coating of polyurethane sacrificial templates with glass slurries.¹¹⁻¹³ According to this method, glass undergoes viscous flow sintering with thermal treatment, along with burn-out of the substrate. The mechanical strength of the final cellular material can be negatively influenced by the formation of hollow struts through the sintering of glass around former polymeric struts, so that a careful control of the sintering conditions is needed; the viscous flow of glass under optimised conditions may lead to the removal of the internal porosity.¹⁴

A strategy to obtain highly porous foamed scaffolds with generally denser struts is gel-casting. This method produces a combinations of macro- and microporosity. Macropores (typically $>500\ \mu\text{m}$), like in replica-derived scaffolds, enable cell ingrowth and vascularisation, whereas micro-pores (and also nano-pores) in the cell struts facilitates cell attachment.^{13, 15} Starting from the early 2000s, gel casting has been widely applied to sol-gel formulations.^{13, 16} Air bubbles may be incorporated by mechanical stirring of solutions (‘direct foaming’) at the early stages of gelation (sol state), with the help of surfactants, and retained with progressive hardening (transition to the gel state). Intensive research, especially conducted by Jones and Hench,¹⁷⁻¹⁹ demonstrated that the pore architecture can be tuned, operating on the many variables of sol-gel processing, such as the chemistry of both glass and surfactants. In parallel, gel-casting has been applied even to suspensions of glass powders, subjected to gelation according to the addition of specific organic agents (monomers, cross-linkers, and catalysts).^{20, 21} Highly porous gelified suspensions are converted into glass scaffolds through a sintering treatment, also causing the burn-out of any organic fractions.

The formulation of W-D glass was the result of a series of experiments concerning another method for the production of highly porous glass-ceramics by direct foaming of precursor mixtures, based on preceramic polymers and reactive fillers previously developed at the University of Padova.^{22, 23} More precisely, wollastonite–diopside glass-ceramics were developed from silicone polymers filled with CaCO_3 and $\text{Mg}(\text{OH})_2$. The use of preceramic polymers enabled the fabrication of highly porous foams thanks to water release with the silicones, which were still in the polymeric state at low temperature (300-350 °C), following the introduction of small amounts of hydrated salts. Hydrated salts corresponded to sodium tetraborate decahydrate ($\text{Na}_2\text{O}\cdot 2\text{B}_2\text{O}_3\cdot 10\text{H}_2\text{O}$) and sodium phosphate dibasic heptahydrate ($\text{Na}_2\text{HPO}_4\cdot 7\text{H}_2\text{O}$); both salts formed a liquid phase at the final firing temperature (1100 °C), at which wollastonite and diopside developed according to the reaction between CaO and MgO (from fillers) and silica (from the oxidative decomposition of silicones). According to the MTT assay, polymer-derived wollastonite-diopside foams showed promising results in terms of cell viability, LDH activity, and compressive strength.^{22, 23}

V.2.2 - Experimental process

The reference material for the present investigation consisted of a glass type belonging to the CaO-MgO-SiO₂ system. The overall composition (SiO₂: 51.7 wt%; CaO: 32.1%; MgO: 11.5%; Na₂O: 2.2%; P₂O₅: 2.5%) presents a CaO:MgO:SiO₂ molar ratio equal to 2:1:3, theoretically leading to 50 mol % wollastonite (W, CaO·SiO₂) and 50% diopside (D, CaO·MgO·2SiO₂). The glass, hereinafter referred to as W-D glass, was produced from pure minerals and chemicals (silica, dolomite, calcium carbonate—all in powders <10 µm, Industrie Bitossi, Vinci, Italy and sodium phosphate-sodium pyrophosphate, Na₄P₂O₇, Sigma-Aldrich, Gillingham, UK), by melting in a platinum crucible at a temperature of 1400 °C (heating rate of 10 °C/min).

Despite the short holding time (15 min at 1400 °C), the mixture led to a homogeneous glass, which was suddenly cooled by direct pouring on a cold metal plate. The glass fragments were easily reduced into fine powders through ball milling and later manually sieved; only the particles with a diameter below 75 µm were retained.

W-D glass fine powders were added to an aqueous solution containing 1 M NaOH (reagent grade, Sigma-Aldrich), with a solid loading of 60 and 65 wt%. The glass powders were subjected to alkaline attack for 3 h, under low-speed mechanical stirring (500 rpm). After alkaline activation, the obtained suspensions of partially dissolved glass powders were cast and then added with 4 wt% Triton X-100. The mixtures were foamed through vigorous mechanical mixing (2000 rpm) for 5 min and later kept at 40 °C for 24 h in order to complete the gelation before demolding. It should be noted that the foamed samples were easily handled, after demolding, without any heat treatment applied. Finally, hardened foams were fired at 900-1000 °C for 1 h with a heating rate of 2 and 5 °C/min.

The characterisation of the obtained foams was performed using the standard methods and equipment described in Chapter I Section 1.6. Selected samples were studied through thermal analysis (TGA, STA409, Netzsch Gerätebau GmbH, Selb, Germany) operating at 10 °C/min, in static air, from room temperature up to 1200°C. Using Fourier-transform infrared spectroscopy (FTIR, FTIR model 2000, Perkin Elmer Waltham, MA, USA), the geometric, apparent and true densities of the samples were measured; and based on such data, the porosity of the samples was evaluated. Morphological and microstructural characterisations were performed using optical (AxioCam ERc 5s Microscope Camera, Carl Zeiss Microscopy, Thornwood, New York, US) and scanning electron microscopy (FEI Quanta 200 ESEM, Eindhoven, The Netherlands). The mineralogical analysis was conducted with x-ray diffraction analysis (Bruker D8 Advance, Karlsruhe), and the resulting foams were subjected to compression tests to evaluate their mechanical performance (Instron, Danvers, MA).

For cell culture studies,* samples were cut at 10 x 10 x 5 mm³ and sterilised by autoclaving at 121 °C for 20 min. Samples were then fixed to 48-well plates. Normal human adult dermal fibroblasts (ATCC®-PCS-201-012™; American Type Culture Collection, Manassas, VA, USA) were seeded at a density of 4 × 10⁵ cells/piece in cDMEM, which consisted of Dulbecco's Modified Eagle Medium (DMEM) (Lonza S.r.l., Milano, Italy), supplemented with 10 vol % Fetal Bovine Serum (FBS) (Bidachem-Spa, Milano, Italy) and 1 vol % Penicillin/Streptomycin (P/S) (EuroClone, Milano, Italy). The 3D cultures were incubated at 37 °C and 5% CO₂ for seven days, changing the media every two days. Control conditions were represented by cells cultured on tissue culture plates (TCP) in cDMEM for the same culturing time.

For SEM imaging, fibroblasts grown on samples for three and seven days were fixed in 2.5% glutaraldehyde in 0.1 M cacodylate buffer for 1 h, then progressively dehydrated in ethanol. All micrographs were obtained using a JSM JEOL 6490 SEM microscope (JEOL, Tokyo, Japan). The SEM analysis was performed at Centro di Analisi e Servizi Per la Certificazione (CEASC, University of Padova, Padova, Italy).

V.2.3 - Results and discussion

Figure 1 shows the FTIR spectra of W-D glass in the initial conditions, W-D glass foams after activation and drying (conditions of hardened foam), and the obtained foams after the heat treatment at 900 °C.

The hardening of the glass suspensions was attributed to the formation of C-S-H compounds; indicated by the appearance of a distinctive intense band in the FTIR spectra, in the 3000-3700 cm⁻¹ range, which can be linked to stretching vibration of O-H groups.²⁴ A weaker band also appears around 1650 cm⁻¹, assigned to deformation mode of O-H bond. In the initial glass, the broad band from 1290 to 900 cm⁻¹ could be ascribed to the Si-O-Si stretching mode and the bands at 800 and 450 cm⁻¹ with the rocking and bending of the Si-O-Si groups, respectively.²⁵⁻²⁷ In the alkali-activated state, the same bands appear wider and flattened, possibly due to the formation of a more irregular bonding in the gel.

Compared to glass powders in the as-quenched state, the alkali-activated material also showed a slight formation of carbonate compounds, highlighted by the sharp band at bands at 1420 cm⁻¹, which is associated to the vibration from the C-O bond; whereas, the bands centred at 2900 and 1400 cm⁻¹ are attributable to C-H vibrations of the organic surfactant. The plot of the heat-treated sample at 900 °C confirms the presence of these compounds, which decompose when subjected to thermal degradation. The heat-treated

* The cell tests were done by Letizia Ferroni and Chiara Gardin, under the supervision of Barbara Zavan at the Department of Biomedical Sciences, at the University of Padova. Padova, Italy.

spectrum presents a profile that is very similar to that of the starting glass, except for the appearance of new defined bands at low wavenumber (1070, 1020, 960, 900, and 860 cm^{-1}), attributed to the formation of crystalline silicates.

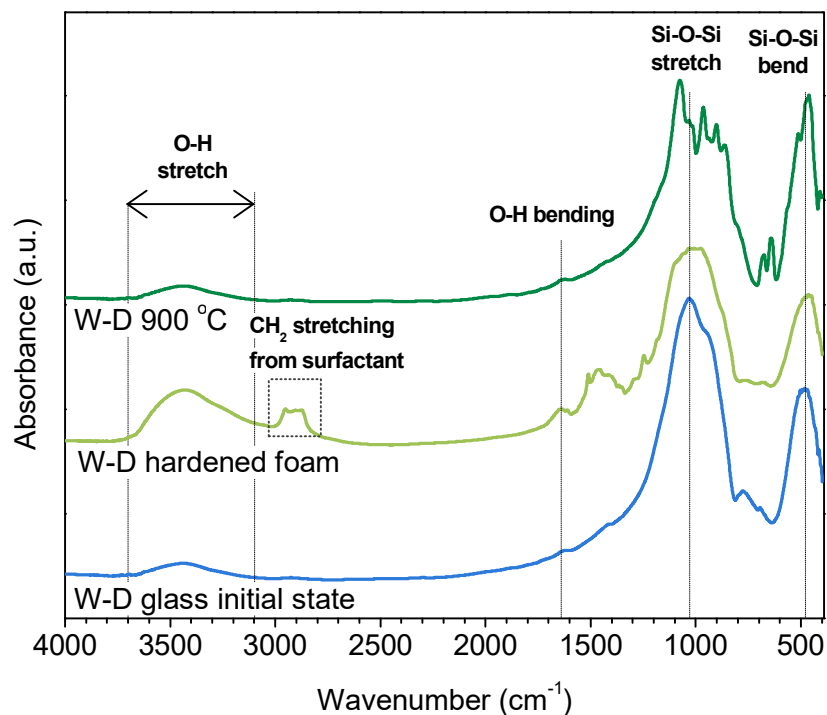


Figure 1. FTIR spectra of W-D glass, cured W-D glass foams, and W-D glass-ceramic foam after firing.

The thermal evolution of the alkali-activated material can be further explained through the thermo-gravimetric analysis reported in Figure 2a. The plot for the initial glass and the gelified foamed material is compared with that for pure Triton X-100; the latter plot is normalised according to the 4 wt% concentration of surfactant in the alkali-activated foams. It can be assumed that the weight loss at 300-500 °C of the alkali-activated material is not only dependant on the burn-out of surfactant, corresponding to ~12% but also on the heat treatment at 600 °C, well above the temperature at which the surfactant decomposes completely.

Consistently with the characterisation of soda-lime glass or VBA in previous chapters, the weight losses at low temperature (below 500 °C) can be ascribed to burn-out of surfactant and physically adsorbed water. The weight losses above 600 °C can be attributed to the decomposition of hydrated compounds, with the release of water from the removal of -OH groups. In fact, C-S-H compounds are actually known to release water at high temperatures.²⁸

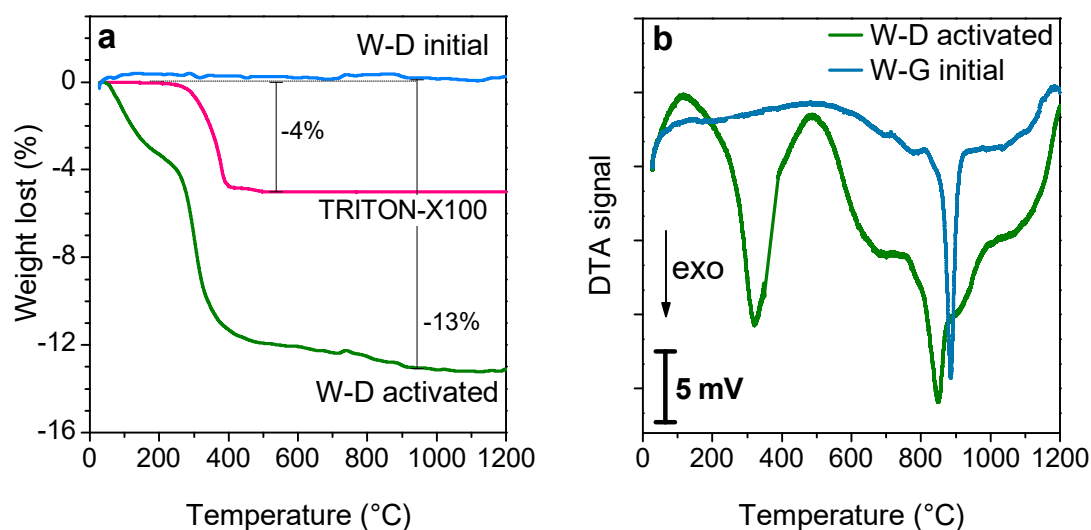


Figure 2. a) Thermo-gravimetric plot of initial W-D glass, alkali-activated W-D glass and surfactant. b) Differential thermal analysis plots of initial W-D glass, alkali-activated W-D

It is interesting that, on the one hand, W-D glass is sensitive to surface crystallisation, as demonstrated by the increased intensity of the crystallisation peaks with decreasing particle size, as an effect of surface nucleation (both silicates are known to crystallise via this mechanism),²⁹ and on the other hand to alkali activation. More precisely, the onset of crystallisation is almost constant in terms of particle size at about 830 °C for pure glass, whereas the starting of exothermic effect is downshifted at about 770 °C for W-D glass after alkali activation. Alkali-rich surface gels turned into an alkali-rich low viscosity liquid surrounding undissolved glass particles, which triggered ionic inter-diffusion and crystallisation (alkali-rich glasses feature lower activation energy for crystal growth).³⁰

The microstructure of the hardened foams obtained after low-temperature gelation and foaming with an initial solid content of 60 and 65 wt% is illustrated in Figure 3. The alkali concentration, quantity of surfactant and stirring speed were kept constant and, accordingly, the significant change on the foam microstructure can only be related to the change in the solid content. An increase of glass content from 60 wt% solid content (Figure 3a) to 65 wt% (Figure 3c) increased the viscosity of the suspensions. As a result, a decrease in the pore size is also evident due to the lower cell coalescence in the wet foams. The different pore size was confirmed and maintained after heat treatment. Figure 3b and 3d show the final microstructure obtained after firing at 1000 °C. It can be noted that, due to the high crystallisation tendency, the foam microstructure remained unaltered after heat treatment, showing a different overall porosity as reported in Table 1 (discussed later).

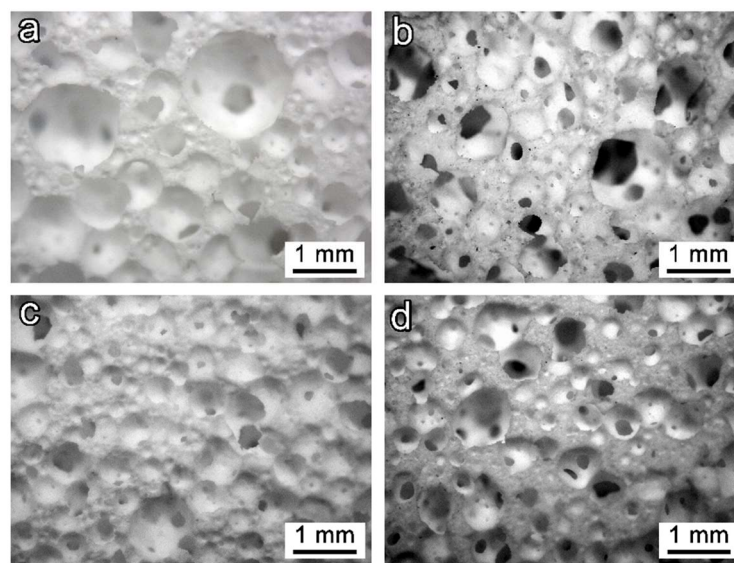


Figure 3. Microstructural and morphology details of W-D foams with different solid content of the starting suspensions, before and after firing at 1000 °C, respectively: a and b) foams with 60 wt%; c and d) foams with 65 wt%

The X-ray diffraction patterns in Figure 4 illustrate the progression of samples from the glass in its initial state, through hardened foams after alkali activation, and heat-treated samples at 900 and 1000 °C. The XRD pattern of the as-quenched glass does not include any crystalline phases, presenting a broad halo in the range of 22-35°. The cured W-D glass foams after demoulding remain amorphous, with a slight shift of the amorphous halo at higher 2θ angles, as a result of the incorporation of network modifiers of alkali-activated materials. Higher theta values indicate a decrease in the average spacing, providing an additional evidence of the formation of the gels.³¹ The patterns of the materials after firing at 900-1000 °C, on the other hand, clearly demonstrate the achievement of the desired phases, such as wollastonite (CaSiO_3 , PDF#27-0088) and diopside (actually a Mg-rich variant, $\text{Ca}_{0.89}\text{Mg}_{1.11}\text{Si}_2\text{O}_6$, PDF#87-698). As previously discussed, this combination of silicate phases is highly efficient thanks to the remarkable bioactivity of wollastonite and the mechanical strength of diopside.^{6, 32-35}

Table 1 reports the physical and mechanical properties of glass-ceramic foams after firing at 1000 °C. The higher solid content determined a decrease in the total porosity, implying an increase in the geometric density, as well as in the solid load. The heating rate may also be seen as a ‘tuning factor’. Given the remarkable crystallisation tendency, enhanced by the alkali activation, a low heating rate (2 °C/min) caused a limited viscous flow sintering, maximising both overall porosity and open porosity. In every case, the compressive strength is substantial, exceeding 5 MPa, and the resulting sample still shows a high open porosity. The combination of good mechanical properties and interconnected porosity undoubtedly make the developed materials ideal candidates for bone regeneration (overall porosities of about 80 vol % are typically associated to compressive

strength values not exceeding 2.5 MPa, in both sol-gel and melt-derived bioactive glass foams).^{20, 36}

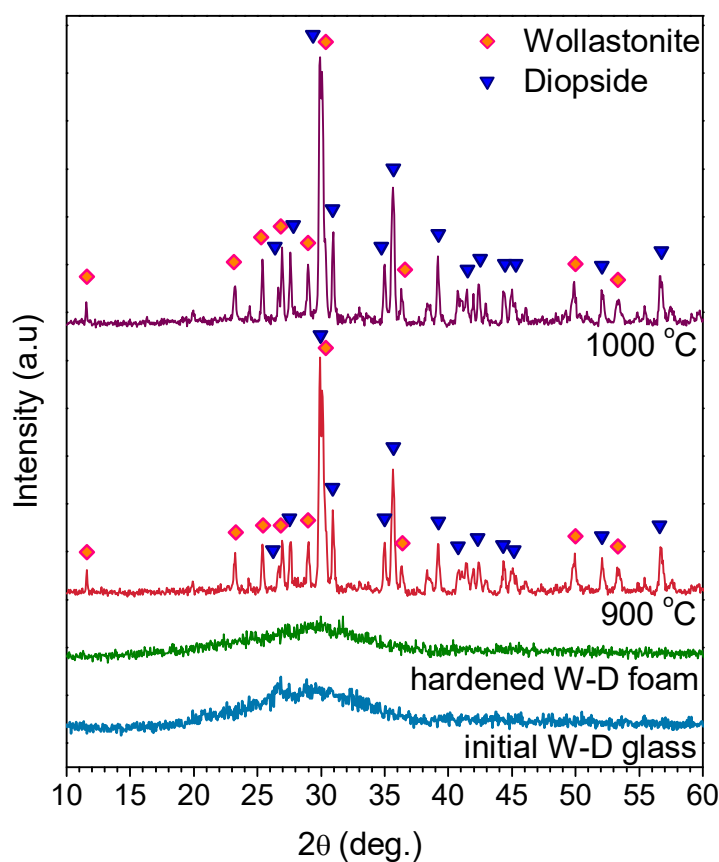


Figure 4. XRD patterns of W-D glass hardened W-D glass foam after demolding and W-D glass-ceramic foam after firing (heating rate: 5 °C/min).

Solid load (wt%)	Heating rate (°C/min) up to 1000°C	Density, ρ (g/cm ³)			Porosity (vol %)			Strength, σ_{comp} (MPa)
		geometric	apparent	true	total	open	closed	
60	2	0.29 ± 0.02	2.92 ± 0.01	2.94 ± 0.01	90 ± 2	90 ± 1	1 ± 2	3.5 ± 0.5
	5	0.42 ± 0.05	2.62 ± 0.01	2.95 ± 0.02	85 ± 3	83 ± 4	2 ± 2	2.2 ± 0.1
65	2	0.44 ± 0.03	2.82 ± 0.01	2.97 ± 0.01	86 ± 2	85 ± 4	1 ± 2	2.9 ± 0.5
	5	0.53 ± 0.04	2.85 ± 0.01	2.95 ± 0.01	81 ± 2	81 ± 2	0 ± 3	5.3 ± 0.7

Table 1. Physical and mechanical properties of W-D glass-ceramic foams produced by different solid contents.

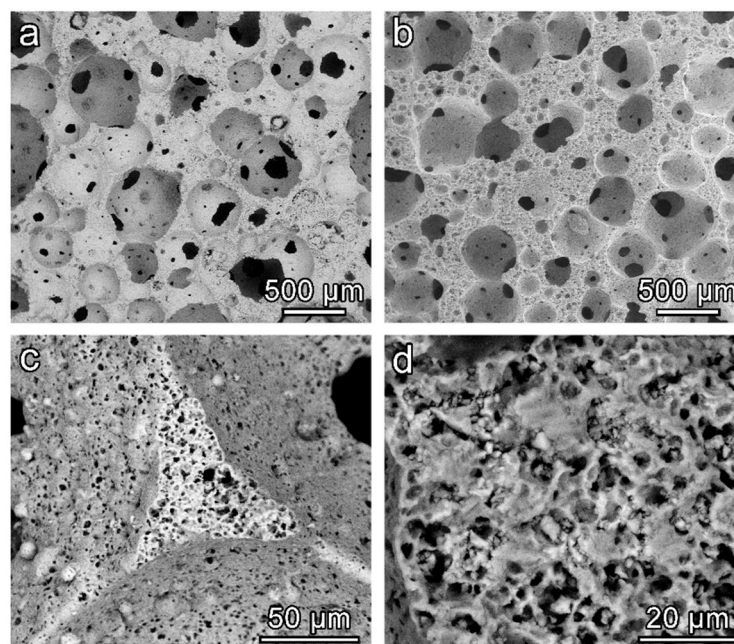


Figure 5. SEM images of W-D glass-ceramic foams with different solid content and after firing at 1000 °C; a) for foams with 60 wt% solid load; b) for foams with 65 wt%; c and d) high magnification details of cell struts.

Figure 5 collects microstructural details of porous W-D glass-ceramics from slurries with 60 and 65 wt% solids (heating rate: 2 °C/min), after firing at 1000 °C. The pore size was evaluated using the Image J software,³⁷ and expressed as the interquartile range. It is possible to detect the presence of open and interconnected cells, which again show a different morphology depending on the total solid content; slightly smaller pores at higher solid content can be noticed, ranging from 170-360 μm for the 60 wt% samples to 130–175 μm for the 65 wt% foams. This size pore reduction could be explained as an effect of increased viscosity with increasing solid content, in turn limiting cell coalescence. The SEM images of foams produced from 60 wt% slurry (see Figure 5a, b) show large openings between adjacent pores and thin struts. A higher solid load is accompanied by reduced interconnections (Figure 5b), which still exceed the threshold (100 μm)³⁸ for good cell ingrowth and vascularisation. The larger struts (Figure 5c) actually contain a multitude of micropores, leading to a ‘hierarchical porosity’ in the samples. The micropores are more visible in the high magnification details (Figure 5d); some dense areas could be ascribed to former glass granules surrounded by foamed material, which result from the thermal evolution of surface gels. The microporosity is undoubtedly favourable to cell attachment.

SEM images of the W-D glass-ceramic foams cultured with human fibroblasts are reported in Figure 6. After three days (Figure 6a, b) from seeding, fibroblasts were found to be spread and attached on the surface of the samples, showing their typical elongated morphology. After seven days (Figure 6c, d), cells had colonised the surface of the W-D

glass-ceramic foams, displaying a better adhesion and proliferation but still showing elongated shapes. Also, it is possible to note that at seven days from seeding, cells not only had populated the scaffold but also penetrated its pores (yellow arrows in Figure 6c). Cell proliferation rate was evaluated through activity and was measured using the lactate dehydrogenase activity assay (LDH), indicating the absence of cytotoxicity of the W-D glass-ceramic foams (a detailed study is described in the corresponding publication).³⁹ All these observations further validate the evidence of the biocompatibility of the material.

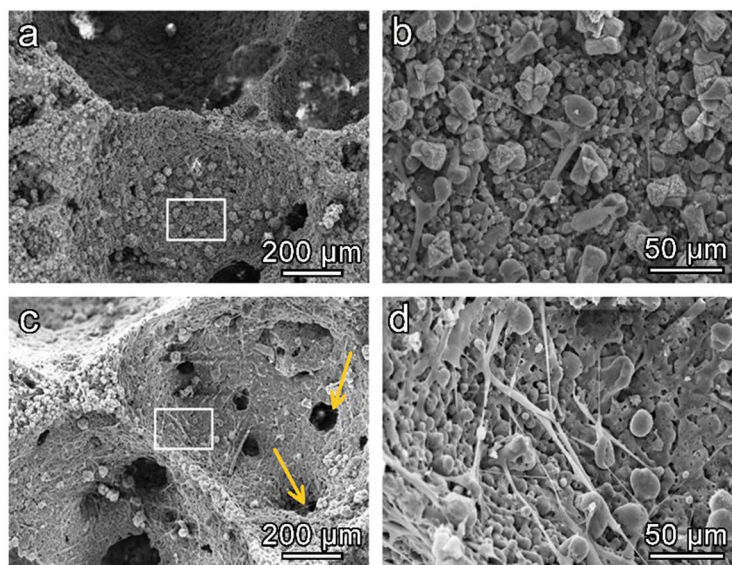


Figure 6. SEM images of fibroblasts cultured on W-D glass-ceramic foam for (a,b) three and (c,d) seven days. Note that cells can migrate into the pores (c, yellow arrows) of the scaffold after seven days from seeding. The white boxes in (a,c) represent the areas shown at higher magnification in (b,d).

V.2.4 - Conclusions

- Highly porous wollastonite-diopside glass-ceramics can be easily obtained through low temperature ‘inorganic gel-casting’, followed by sintering with concurrent crystallisation (sinter-crystallisation). Crystallisation limits the viscous flow so that the microstructure in the green state is substantially maintained during firing at up to 1000 °C.
- The foaming relies on the progressive hardening of aqueous glass suspensions, after alkali activation; the gelation, owing to FTIR analysis, is consistent with the development of calcium silicate hydrates (C-S-H), later subject to decomposition (as a result of the firing treatment).
- The overall process (mechanical stirring of alkali-activated suspensions with the help of a surfactant, drying, firing and sinter-crystallization) has a great

potential for the production of ‘hierarchically porous’ foams; the microstructure can be tuned through the adjustment of simple processing parameters, such as solid load in suspensions, and firing conditions (e.g., heating rate).

- The glass-ceramics developed with human fibroblasts can be considered as biocompatible. Forthcoming studies will focus on the detailed investigation of ionic releases and bioactivity.

V.2 – CEL2 bioactive glass-ceramics foams*

V.2.1 - Introduction

Owing to the worldwide increase of population and rise of life expectancy, there is an increasing demand for bone grafts or synthetic materials that can potentially replace, repair or regenerate bone defects.⁴⁰ Tissue engineering (TE) is one of the fundamental solutions, implemented to challenge this problem.⁴¹ Natural and synthetic materials, which are used to supply, replenish or enhance the living tissue functionality, are regarded as ‘biomaterials’.⁴² Within them, ‘bioceramics’, to be used for repairing and reconstructing of diseased or damaged parts of the musculoskeletal system, - also known as ‘bioceramics’, are classified as bioinert (alumina, zirconia), bioresorbable (tricalcium phosphate) or even bioactive (hydroxyapatite, bioactive glasses, and glass-ceramics).⁴³ A highly porous structure is often appreciated, e.g., for tissue ingrowth.⁴⁴

The bioactivity attributed to some glasses is due to the formation of a hydroxyl carbonated apatite layer (HCA) on their surface similar to bone mineral.⁴⁴ This HCA layer forms as a result of a rapid sequence of chemical reactions on the surface of the implant when in contact with body fluids. A well-recognised method to estimate the bone-bonding potential ability of a material, according to Kokubo et al.,⁴⁵ involves its immersion into simulated body fluid (SBF), followed by the evaluation of bone-like apatite formation on the surface. In other words, the behaviour in vivo may be predicted by using the SBF method in vitro, and observing the occurrence of several reactions, including the rapid release of soluble ionic species and the formation of a high surface area layer, consisting of hydrated silica and polycrystalline carbonated hydroxyapatite (HCA),^{46, 47} under rather strict conditions of pH. In fact, it is known that osteoblasts prefer a slightly alkaline

** The following text, data and images are an adaptation of the results that were published in the article: “Elsayed, H., Rincón Romero, A., Molino, G., Vitale Brovarone, C., & Bernardo, E. (2018). Bioactive Glass-Ceramic Foam Scaffolds from ‘Inorganic Gel Casting’ and Sinter-Crystallization. Materials, 11(3), 349”. It is partially reproduced in this section as a prove of the versatility of the foaming approach*

medium (pH = 7.8);⁴⁸ severe changes in pH, as a result of ion release, can inhibit osteoblast activity and can cause cell necrosis or apoptosis.^{49, 50}

CEL2 bioactive glass, belonging to the SiO₂-P₂O₅-CaO-MgO-K₂O-Na₂O system, was specifically tailored to control pH variations, due to ion leaching phenomena, when in contact with physiological fluids. Therefore, CEL2 glass features a lower overall alkali content (less than 20 mol %) and a slightly higher P₂O₅ content (3 mol %) compared to commercial bioactive glasses. CEL2 glass-ceramic was effectively found to be highly biocompatible and bioactive; in addition, unlike in many bioactive glasses, the positive effect on the mechanical properties imparted by the partial crystallisation is not negatively counterbalanced by any decrease of its bioactivity.^{51, 52}

As mentioned above, many bioceramics are in the form of highly porous, open-celled bodies, also known as 'scaffolds'. Glass and glass-ceramic scaffolds can be prepared by using different methods, such as free-form fabrication techniques,⁵³ sponge replication,^{54, 55} starch consolidation⁵⁶ and burn-out of sacrificial polymeric particles.⁵⁷ Concerning CEL2 glass-ceramic, macroporous scaffolds for possible use as bone substitutes were prepared both by sponge replication⁵² and burn-out method.⁵⁸ Both methods imply the quite delicate removal, by thermal degradation, of an organic phase, acting as a template for the cellular structure (e.g., operating with polyurethane sponge) or for the pores (e.g., operating with fugitive pore formers), followed by viscous flow sintering of glass powders, in turn accompanied by a partial crystallization. Especially in the case of sponge replication, the obtainment of high-quality components relies on a careful selection of all processing conditions. Before thermal processing, the impregnation of the starting sponge, with an aqueous slurry of glass powders added with a binder (polyvinyl alcohol, PVA), must be absolutely uniform. Upon firing, the viscous flow of the glass should be enough to fill the cavities left by the burn-out of former polymeric struts otherwise low mechanical strength can be expected.⁵⁹

The present paper illustrates the extension to CEL2 glass-ceramics of a gel casting process, recently established.^{60, 61} The method implies the obtainment of cellular structures by direct foaming of engineered glass slurries, followed by sintering. More precisely, CEL2 glass powders were exposed to an alkaline solution, with partial dissolution. The gelation of partially dissolved products ('inorganic gel casting') caused a marked hardening of glass suspensions, so that they could be significantly foamed by air incorporation, under intensive mechanical stirring, with the help of a surfactant. Highly porous cellular structures could be tuned simply by adjusting the formulation of slurries; the crystallisation of CEL2, upon firing, was significant in 'freezing' the microstructure, impeding any viscous collapse.

V.2.2 - Experimental process

The chosen bioactive glass used as a reference material for the present investigation consisted of a glass belonging to the $\text{SiO}_2\text{-P}_2\text{O}_5\text{-CaO-MgO-Na}_2\text{O-K}_2\text{O}$ system. This reference glass, named CEL2, had the following molar composition: 45% SiO_2 , 3% P_2O_5 , 26% CaO , 7% MgO , 15% Na_2O , 4% K_2O . The glass was prepared by melting reagent-grade reactants in a platinum crucible at 1400 °C for 1 h. The molten glass was poured into water to obtain a frit that was subsequently ball-milled to obtain powders, which were later manually sieved. CEL2 glass powder was analysed through differential thermal analysis (DTA, Netzsch STA 429, Selb, Germany), with heating rate of 10 °C/min up to 1000 °C in air, to evaluate its characteristic temperatures. For foaming experiments, only powders with a diameter below 75 μm were considered.

To fabricate CEL2 glass-ceramic scaffolds for bone substitutions, fine CEL2 glass powders were mixed with an aqueous solution containing 1 M NaOH (reagent grade, Sigma-Aldrich, Gillingham, UK), for a solid loading of 58 and 60 wt%. The glass slurries were kept under low-speed mechanical stirring (500 rpm) for 3h, for alkaline activation and partial gelation, and then cast in several polystyrene cylindrical moulds (60 mm diameter). After the addition of 4 wt% Triton X-100 (Sigma-Aldrich, Gillingham, UK), consisting of a non-ionic surfactant that does not interfere with ceramic dispersions,⁶² the slurries were foamed by vigorous mechanical mixing (2000 rpm), for 5 min.

The foamed slurries were later left at 40 °C for 24 h, in order to complete the gelation, before demolding. The obtained ‘green’ foams could be easily handled and placed in a muffle furnace, for the final sintering treatments, at 900-1000 °C for 1 h, followed by natural cooling. The thermal treatment comprised an intermediate step at 300 °C for 2 h to remove any absorbed water and organic residues, after a slow heating phase (2 °C/min); the subsequent heating up to the selected firing temperature was performed at 5 °C/min.

For understanding the thermal behaviour, CEL2 glass powders and foamed gels were subjected to thermogravimetric analysis (TGA, STA409, Netzsch Gerätebau GmbH, Selb, Germany), and Fourier transform IR spectroscopy (FTIR, FTIR model 2000, Perkin Elmer Waltham, MA, USA). X-ray diffraction on powdered samples (XRD; Bruker D8 Advance, Bruker AXS GmbH, Karlsruhe, Germany), supported by data from PDF-2 database (ICDD-International Centre for Diffraction Data, Newtown Square, PA, USA) and Match! program package (Crystal Impact GbR, Bonn, Germany).

Microstructural characterizations were performed by optical stereomicroscopy (AxioCam ERc 5 s Microscope Camera, Carl Zeiss Microscopy, Thornwood, NY, USA) and scanning electron microscopy (SEM, FEI Quanta 200 ESEM, FEI Company, Eindhoven, The Netherlands) and the resulting foams were subjected to compression tests to evaluate their mechanical performance (Instron, Danvers, MA). All the characterisation techniques followed were performed using the standard methods and equipment described in Chapter I Section 1.6.

V.2.3 - Results and discussion

Figure 1 shows the overall pore structure developed, by means of optical stereomicroscopy, it illustrates the great potential of the approach, despite its simplicity. The hardened foam produced with 60 wt% just after demoulding (Fig. 1a) clearly shows a homogeneous and highly porous open-celled structures. As previously observed, the partial gelation of glass slurries, upon alkaline activation, leads to a marked pseudoplastic behaviour. Air bubbles, incorporated by intensive mechanical stirring (aided by the surfactant), at high shear rates and low viscosity, remain trapped when stirring stops, at low shear rate and high viscosity.⁶³ In the present investigation, there was an increase of 100-150% in the volume of slurries, passing from the alkali-activated suspension to step to the hardened state.

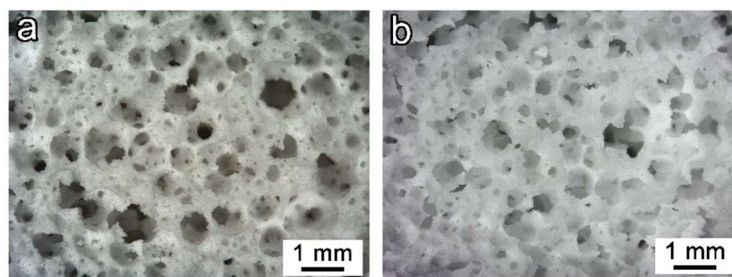


Figure 1. Microstructural and morphology details of CEL2 glass-ceramic foams, with 60 wt%, as solid load; (a) cured CEL2 green foam; (b) after firing at 900 °C.

The hardened foam presented pores with a diameter between 400-100 μm , also smaller pores in the cell struts are detected. The pore size was maintained after the heat treatment at 1000 °C as shown by Figure 1b where the final microstructure obtained after firing displays the same morphology as in the hardened state. As in previous experiences, this behaviour can be explained due to the high crystallisation tendency the foam microstructure remains unalterable preventing the remodelling of the cell structure after the heat treatment.

The hardened of CEL2 glass was determined by the same compounds previously found after alkali activation of other CaO-rich glasses (as is the case of SLG described in Chapter II or the WD glass described in the previous section). More precisely, CaO-rich glasses, upon alkali activation, have been proved to provide a gel that hardens thanks to the condensation products that could be identified as calcium silicate hydrate, or C-S-H.⁶⁴

The proof of C-S-H formation was given by FTIR analysis, as illustrated by Figure 2. In particular, the distinctive band associated to O-H stretching, in the 3200-3700 cm^{-1} range,⁶⁰ along with a band at approximately 1650 cm^{-1} , attributed to O-H bending, was clearly evident only in the FTIR spectrum of foams in the 'green' state, i.e., after gelation.

The bands from 1300 to 900 cm^{-1} and 800 to 450 cm^{-1} , related to stretching and bending mode of Si-O-Si bonds,^{65, 66} appeared wider and flattened, in the case of CEL2 green foam (compared to those of pure glass powders), as an effect of partial dissolution of the glass and formation of disordered hydrated gel.

Finally, further differences between green foams and starting glass concerned bands at 2950-2800 cm^{-1} , 1500-1400 cm^{-1} and approximately 1250 cm^{-1} . The first two bands were attributed to the IR absorption phenomena of the C-H bonds in the organic surfactant, whereas the third small band was attributed to the slight formation of carbonate compounds.

The FTIR spectrum of glass-ceramic foams was very similar to that of the starting glass, as an effect of the thermal instability of the hydrated compounds developed upon hardening. The only significant difference concerned the appearance of new bands at low wave number (at 1040, 925, 620, 530 and 450 cm^{-1}), attributed to the formation of silicate crystalline phases.

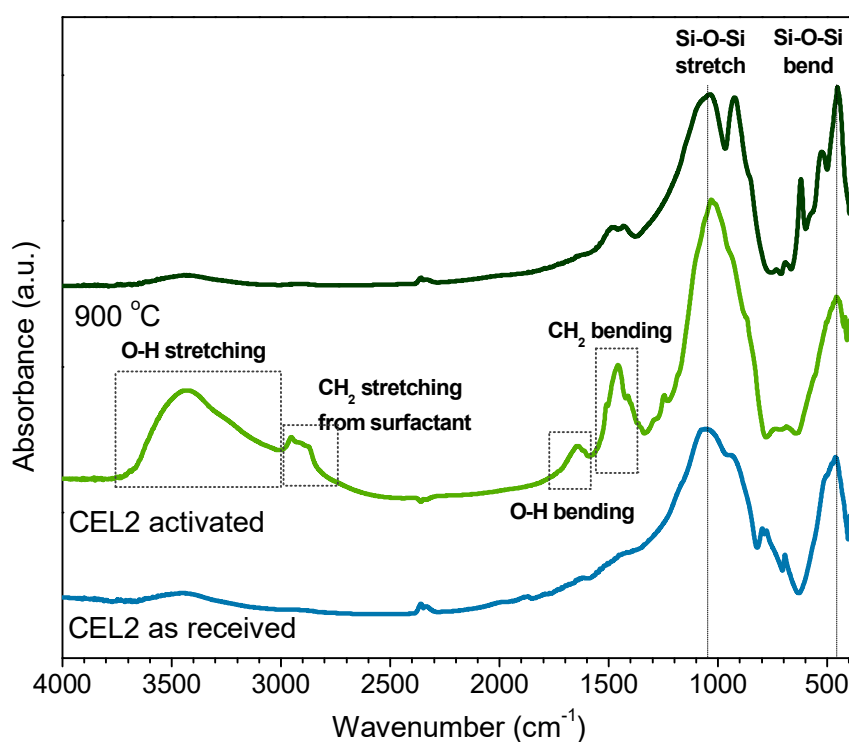


Figure 2. FTIR analysis of CEL2 glass, green CEL2 glass foams after alkaline activation and CEL2 glass-ceramic foam after firing.

The thermal instability of the compounds developed upon hardening was confirmed by the thermogravimetric analysis (TGA), shown in Figure 3a. Weight losses appeared at several stages, as a consequence of the overlapping of distinct phenomena, occurring below 500 °C (low T^a losses) and above 500 °C, up to about 900 °C (high T^a losses). The low-temperature losses comprise a contribution from the thermal decomposition of the

surfactant, illustrated by the same Figure 3a. The contribution was significant, but the low-temperature losses ($\sim 11.7\%$) were far above the overall content of the same additive (for comparison purposes, Figure 3a reports the weight losses of Triton X-100 normalised by the effective amount of additive employed, i.e. 4%). Like in previous cases,^{60, 61} we cannot exclude a remarkable contribution to the low-temperature losses of physically adsorbed water (below 200 °C) and decomposition of hydrated compounds.

The occurrence of high-temperature losses is consistent with the same nature of C-S-H gels. In fact, C-S-H compounds are actually known to release water even above 500 °C.⁶⁷

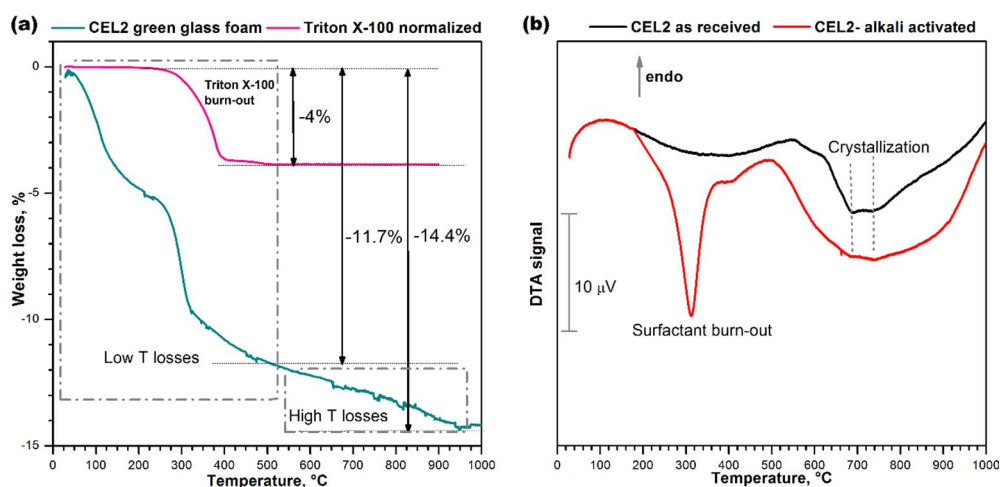


Figure 3. Thermal analysis of CEL2 glass before and after gel-casting; a) Thermo-gravimetric plot of alkali-activated CEL2 glass and surfactant “Triton X-100”; b) Differential thermal analysis of CEL2 glass powder and ‘green’ glass foam from alkali activation and direct foaming.

The differential thermal analysis (DTA) plots in Figure 3.b, for the starting glass and for a foam sample just after low-temperature hardening, are particularly interesting for the two exothermic peaks. The low-temperature strong peak, visible only in the plot for the green foam, undoubtedly corresponds to the burn-out of the surfactant, considering the exact match (at 300 °C) with the onset of the relative thermal loss (see upper plot in Figure 3a). The broader exothermic peaks at higher temperatures are significant for the differences between starting glass and green foam: in the as-received condition, CEL2 glass presented a broad ‘exothermic band’ that could be attributed to the overlapping of at least two crystallization peaks, at 700 and 750 °C; in the activated condition, the band became even wider and positioned at lower temperatures. This effect had not been detected with the alkali activation of previously investigated CaO-MgO-SiO₂ glass.⁶¹ In our opinion, this could be justified on the basis of the mixing of two distinct glass phases, consisting of material from the decomposition of the surface gels and undissolved glass.

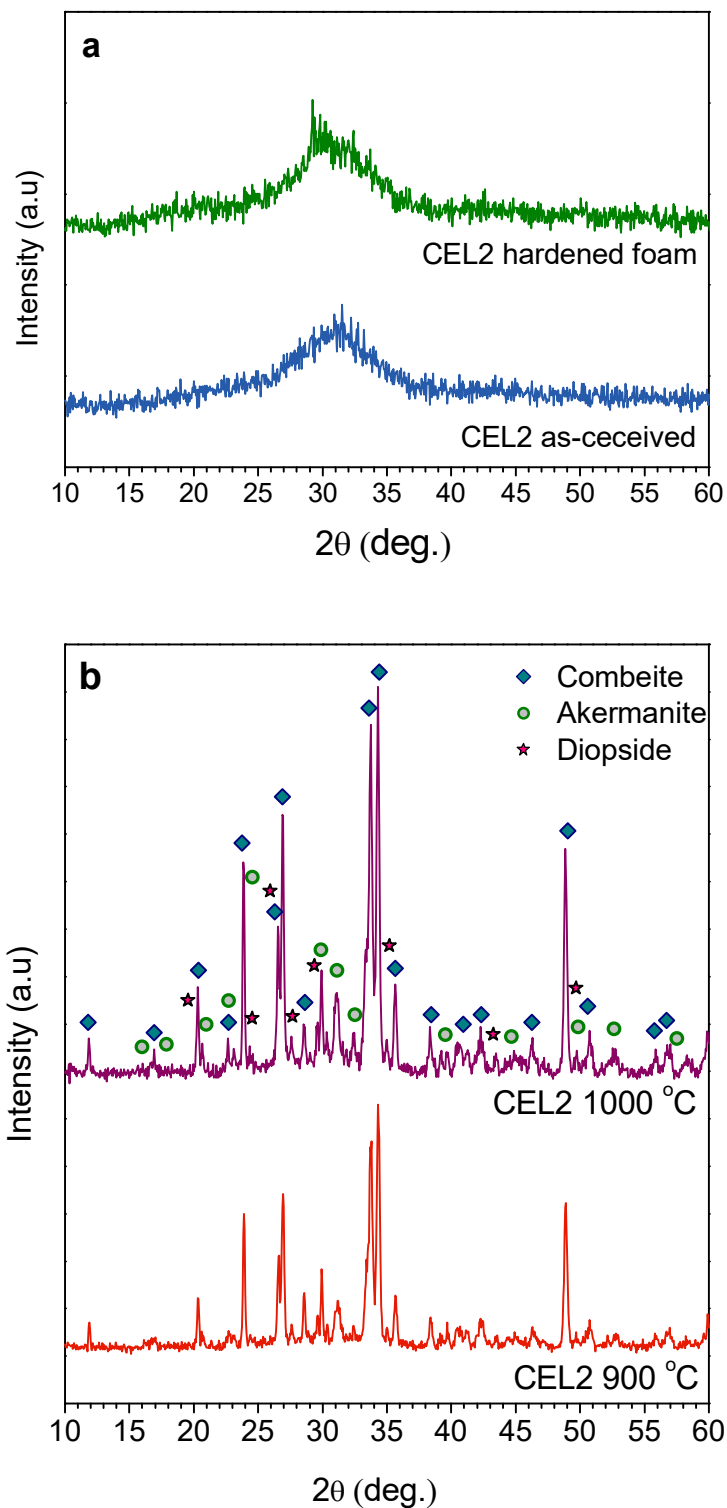


Figure 4. X-ray diffraction analysis of CEL2 glass-based materials: a) evolution from as received state to alkali-activated state; b) comparison between the sinter-crystallised samples at 900 and 1000 °C (foamed samples, from 60 % CEL2 solid loading).

In particular, the alkali enrichment of surface gels surrounding glass powders likely lowered the glass transition temperature (T_g), promoting the ionic inter-diffusion and the crystallisation of CEL2 glass (e.g. by reducing the activation energy for crystal growth).⁶⁸ The endothermic effect centred at about 500 °C was attributed to dehydration of the green foam. The promotion of the crystallisation had a remarkable impact on the microstructure after firing. As shown by Fig. 2b, the open-celled structure was confirmed after firing at 900 °C: the increase of apparent viscosity, operated by rigid crystal inclusion, evidently prevented any viscous collapse.

The X-ray diffraction patterns reported in Figure 4 provide an overview of the evolution of crystalline phases in the processing of CEL2 glass-ceramic foams. The XRD pattern of the alkaline-activated material provided further evidence of gel formation, after foaming and drying of the glass, due to the slight 2θ displacement the amorphous halo (Fig. 4a). The 2θ shift for the green glass foams, in fact, is consistent with the incorporation of network modifiers.⁶⁹

After firing at 900 °C (Fig. 4b), the typical crystalline phases of bioactive CEL2 glass-ceramic, such as combeite ($\text{Na}_4\text{Ca}_4\text{Si}_6\text{O}_{18}$, PDF#79-1089), akermanite ($\text{Ca}_2\text{MgSi}_2\text{O}_7$, PDF#83-1815),⁵² appeared. Interestingly, another Ca-Mg silicate (diopside, $\text{CaMgSi}_2\text{O}_6$, PDF#75-1092) formed as additional phase; to our opinion, this could be due to the decomposition of the hydrated silicate gels formed upon activation. The crystallisation degree (inferable from the intensity of diffraction lines) increased passing from 900 to 1000 °C (see Fig. 4b); in addition, there was a reduction of diopside, with increase of akermanite. In other words, the firing at 1000 °C made the phase assemblage of the present foams more similar to that previously reported.⁵³ The formation of Ca-Mg silicate crystal phases (akermanite or diopside) is very promising, due to the distinctive combination of remarkable mechanical strength with excellent bioactivity as well as controlled dissolution rate.^{70, 71}

Solid load (wt%)	T^a (°C)	Density, ρ (g/cm ³)			Porosity (vol %)			Strength, σ_{comp} (MPa)
		geometric	apparent	true	total	open	closed	
58	900	0.58 ± 0.03	2.38 ± 0.01	3.06 ± 0.01	81 ± 5	75 ± 5	6 ± 4	2.5 ± 0.4
	1000	0.92 ± 0.07	2.05 ± 0.09	3.13 ± 0.02	70 ± 8	55 ± 1	15 ± 5	3.9 ± 0.5
60	900	1.12 ± 0.02	2.49 ± 0.09	3.05 ± 0.01	63 ± 2	55 ± 5	9 ± 2	5.5 ± 0.2
	1000	1.16 ± 0.08	2.52 ± 0.04	3.16 ± 0.01	63 ± 7	52 ± 8	10 ± 3	15.5 ± 1.7

Table 1. Physico-mechanical properties of CEL2 glass-ceramic foams produced by different solid contents

Table 1 reports the physical and mechanical properties of CEL2 glass-ceramic foams after firing. It can be noticed that samples were produced according to several processing variants, aimed at exploring different viscosity conditions before firing and during firing. In fact, both steps could be interpreted according to the mechanics of suspensions, in which the apparent viscosity depends on the combination of the viscosity of the medium and the amount of suspended, rigid inclusions. An increase of the solid loading, from 58 to 60 wt%, was expected to cause an increase of the viscosity of slurries simply on the basis of the amount of inclusions, reducing the expansion upon intensive mechanical stirring. An increase of the firing temperature, from 900 to 1000 °C, on the one hand, was expected to reduce the viscosity of the residual glass phase, i.e. of the medium in which crystal inclusions were suspended, enhancing the densification by removal of smaller pores; on the other hand, the increased crystallization degree (Fig. 5b) could determine a substantial reinforcement of the solid phase.

The data reported in Table 1 confirm the expected ‘tuning’ of porosity operating on solid loading and/or on firing temperature. An increase of the solid loading, from 58 to 60 wt% produces a reduction in the overall porosity of the samples; the increase in the fire treatment temperature promotes the viscous flow sintering, leading to samples with more closed porosity. With a compressive strength ranging from 2.5 ± 0.4 to 15.5 ± 1.7 MPa, the developed foams compare well with the values for cancellous bone (2-12 MPa).^{72, 73}

It should be noted that the lightest foam, processed at low solid loading and low firing temperature and exhibiting the lowest strength, could not be considered as ‘weak’. The crushing strength of cellular solid, σ_c , according to the well-recognised Gibson-Ashby model,⁷⁴ actually depends on the relative density (ratio between bulk and true densities, ρ_{rel}), as follows:

$$\sigma_c \approx \sigma_{bend} \cdot f(\Phi, \rho_{rel}) = \sigma_{bend} \cdot [C \cdot (\Phi \cdot \rho_{rel})^{3/2} + (1 - \Phi) \cdot \rho_{rel}]$$

where σ_{bend} is the bending strength of the solid phase and f is a ‘structural function’, depending on the relative density (ρ_{rel} , the ratio between the bulk density of the foams and the true density, i.e. the density of the solid phase) and its distribution (open or closed porosity). The quantity $(1 - \Phi)$ expresses the fraction of solid positioned at the cell faces; C is a dimensionless calibration constant (~ 0.2). For the lightest foam, the amount of closed porosity was so limited that the linear contribution in the structural function could be neglected ($\Phi \sim 1$); the observed compressive strength could be correlated, given the low relative density, to a bending strength in the order of 150 MPa, typical for glass-ceramics.⁷⁵

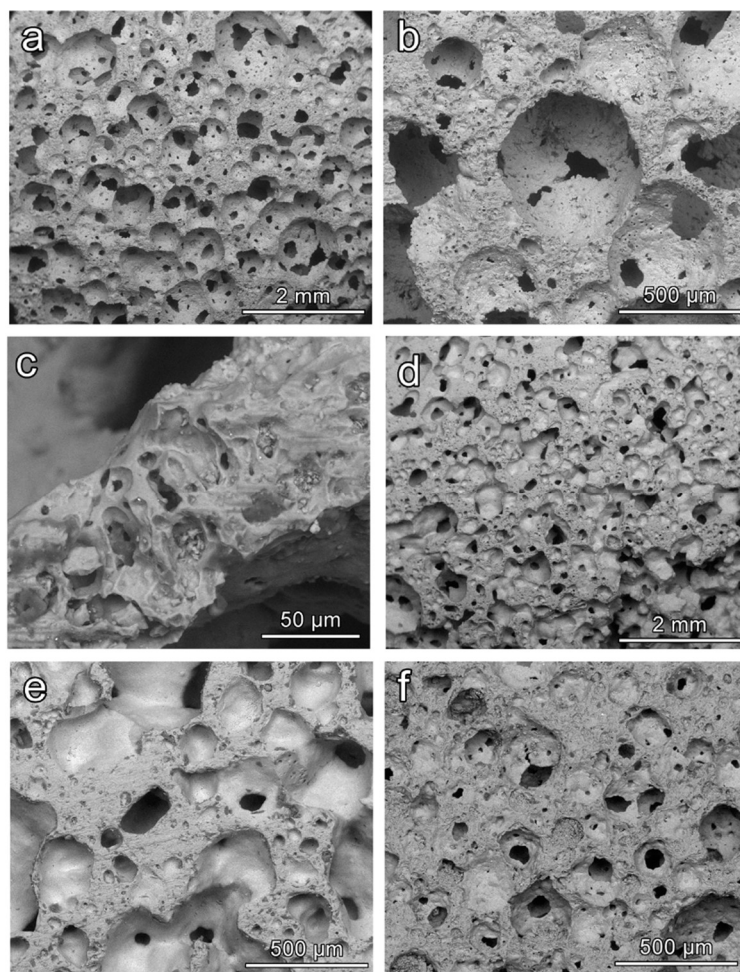


Figure 6. Examples of CEL2 glass-ceramic foams with different solid content after firing at 900-1000 °C for 1 h; a-c) foams with 58 wt% solid loading fired at 900 °C; d,e) for foams with 60 wt% solid loading fired at 900 °C; f) foams with 58 wt% solid loading fired at 1000 °C.

Figure 6 reports a selection of microstructural details of CEL2 glass-ceramics, collected using SEM, obtained from slurries with 58 and 60 wt% solid content and fired at different temperatures. In all cases, it is possible to observe the presence of quite homogeneously distributed interconnected cells. We can also roughly note a sort of ‘synergy’ between solid content and firing temperature. A low firing solid loading and a low firing temperature led to foams (Fig. 6a) with pronounced interconnectivity, i.e. with many openings between adjacent cells (Fig. 6b). The struts were by themselves highly porous (see Fig. 6c), promoting the cell attachment and the impregnation of fluids. An increase of solid loading (Figs. 6d, 6e) or firing temperature (Fig. 6f) determined the formation of some solid membranes between adjacent cells: the strength enhancement can be understood on the basis of an increased amount of solid positioned at the cell faces (linear term in the structural function ruling the impact of relative density on compressive strength).

The pore distribution and interconnectivity (not presented here) were further analysed using nano-CT,* specifically intended to verify the suitability of the developed foams in terms of morphological requirements for tissue engineering. In fact, an ideal porous scaffold should combine bioactive properties with a favourable structure, i.e. the interconnections between adjacent cells should have a diameter exceeding 100 μm , to allow effective tissue ingrowth and eventually vascularisation (required for complete bone regeneration).⁷⁶

The nominally strongest foam (60% solid loading, fired at 1000 °C), although still very porous, did not fulfil the requirements for bone tissue engineering, since most of the pores and interconnections were below 50 μm . The increase of firing temperature, as a consequence, cannot be considered as a valid ‘tuning’ parameter for the chosen application.

We can conclude that foams sintered at 900 °C may constitute a valid reference for future bone tissue engineering experiments. The excellent absolute strength (above 5 MPa, for 60% solid loading) and the strength-to-density ratio (for both 58 and 60% solid loading), combined with the optimum pore distribution, and a very good interconnectivity make them good candidates for bone tissue regenerations.

V.2.4 - Conclusions

We may conclude that:

- Highly porous CEL2 glass-ceramics can be easily manufactured by ‘inorganic gel-casting’, followed by sintering with sinter-crystallisation; the crystallisation limits the viscous flow so that the microstructure in the green state is substantially maintained upon firing up to 900-1000 °C.
- The overall foaming process (mechanical stirring of alkali-activated suspensions - with the help of a surfactant -, drying, firing with sinter-crystallization) has a great potential for the production of ‘hierarchically porous’ foams; the microstructure can be tuned operating on simple processing parameters such solid load, in suspensions, and firing conditions (e.g. heating rate).
- CEL2 glass-ceramic foams were fabricated, in selected conditions, with very uniform pore size (mean diameter of 170 μm) and good interconnectivity (well-defined openings are visible between adjacent cells).

* $\mu\text{-CT}$ measurements and its data interpretation, were done by Giulia Molino under the supervision and Chiara Vitale Brovarone.

References

- 1 De Aza, P. N., Guitian, F., & De Aza, S. (1994). Bioactivity of wollastonite ceramics: in vitro evaluation. *Scripta metallurgica et materialia*, 31(8), 1001-1005.
- 2 Lin, K., Zhai, W., Ni, S., Chang, J., Zeng, Y., & Qian, W. (2005). Study of the mechanical property and in vitro biocompatibility of CaSiO₃ ceramics. *Ceramics International*, 31(2), 323-326.
- 3 Wu, C., & Chang, J. (2007). Degradation, bioactivity, and cytocompatibility of diopside, akermanite, and bredigite ceramics. *Journal of Biomedical Materials Research Part B: Applied Biomaterials: An Official Journal of The Society for Biomaterials, The Japanese Society for Biomaterials, and The Australian Society for Biomaterials and the Korean Society for Biomaterials*, 83(1), 153-160.
- 4 Nonami, T., & Tsutsumi, S. (1999). Study of diopside ceramics for biomaterials. *Journal of Materials Science: Materials in Medicine*, 10(8), 475-479.
- 5 Wu, C., Ramaswamy, Y., & Zreiqat, H. (2010). Porous diopside (CaMgSi₂O₆) scaffold: a promising bioactive material for bone tissue engineering. *Acta biomaterialia*, 6(6), 2237-2245.
- 6 Sainz, M. A., Pena, P., Serena, S., & Caballero, A. (2010). Influence of design on bioactivity of novel CaSiO₃-CaMg (SiO₃)₂ bioceramics: In vitro simulated body fluid test and thermodynamic simulation. *Acta Biomaterialia*, 6(7), 2797-2807.
- 7 Ventura, J. M. G., Tulyaganov, D. U., Agathopoulos, S., & Ferreira, J. M. F. (2006). Sintering and crystallization of akermanite-based glass-ceramics. *Materials letters*, 60(12), 1488-1491.
- 8 Agathopoulos, S., Tulyaganov, D. U., Ventura, J. M. G., Kannan, S., Karakassides, M. A., & Ferreira, J. M. F. (2006). Formation of hydroxyapatite onto glasses of the CaO-MgO-SiO₂ system with B₂O₃, Na₂O, CaF₂ and P₂O₅ additives. *Biomaterials*, 27(9), 1832-1840.
- 9 Kansal, I., Tulyaganov, D. U., Goel, A., Pascual, M. J., & Ferreira, J. M. (2010). Structural analysis and thermal behavior of diopside-fluorapatite-wollastonite-based glasses and glass-ceramics. *Acta Biomaterialia*, 6(11), 4380-4388.
- 10 Tulyaganov, D. U., Agathopoulos, S., Valerio, P., Balamurugan, A., Saranti, A., Karakassides, M. A., & Ferreira, J. M. F. (2011). Synthesis, bioactivity and preliminary biocompatibility studies of glasses in the system CaO-MgO-SiO₂-Na₂O-P₂O₅-CaF₂. *Journal of Materials Science: Materials in Medicine*, 22(2), 217-227.
- 11 Vitale-Brovarone, C., Bairo, F., & Verné, E. (2009). High strength bioactive glass-ceramic scaffolds for bone regeneration. *Journal of Materials Science: Materials in Medicine*, 20(2), 643-653.
- 12 Gerhardt, L. C., & Boccaccini, A. R. (2010). Bioactive glass and glass-ceramic scaffolds for bone tissue engineering. *Materials*, 3(7), 3867-3910.
- 13 Bairo, F., & Vitale-Brovarone, C. (2014). Bioactive glass and glass-ceramic foam scaffolds for bone tissue restoration. In *Biomedical Foams for Tissue Engineering Applications* (pp. 213-248).
- 14 Bairo, F., Ferraris, M., Bretcanu, O., Verné, E., & Vitale-Brovarone, C. (2013). Optimization of composition, structure and mechanical strength of bioactive 3-D glass-

- ceramic scaffolds for bone substitution. *Journal of biomaterials applications*, 27(7), 872-890.
- 15 Hulbert, S. F., Morrison, S. J., & Klawitter, J. J. (1972). Tissue reaction to three ceramics of porous and non-porous structures. *Journal of biomedical materials research*, 6(5), 347-374.
 - 16 Sepulveda, P., Jones, J. R., & Hench, L. L. (2002). In vitro dissolution of melt-derived 45S5 and sol-gel derived 58S bioactive glasses. *Journal of Biomedical Materials Research: An Official Journal of The Society for Biomaterials, The Japanese Society for Biomaterials, and The Australian Society for Biomaterials and the Korean Society for Biomaterials*, 61(2), 301-311.
 - 17 Jones, J. R., & Hench, L. L. (2003). Effect of surfactant concentration and composition on the structure and properties of sol-gel-derived bioactive glass foam scaffolds for tissue engineering. *Journal of Materials Science*, 38(18), 3783-3790.
 - 18 Jones, J. R., & Hench, L. L. (2004). The effect of processing variables on the properties of bioactive glass foams. *J. Biomed. Mater. Res. B*, 68, 36-44.
 - 19 Poologasundarampillai, G., Lee, P. D., Lam, C., Kourkouta, A. M., & Jones, J. R. (2016). Compressive strength of bioactive sol-gel glass foam scaffolds. *International Journal of Applied Glass Science*, 7(2), 229-237.
 - 20 Wu, Z. Y., Hill, R. G., Yue, S., Nightingale, D., Lee, P. D., & Jones, J. R. (2011). Melt-derived bioactive glass scaffolds produced by a gel-cast foaming technique. *Acta Biomaterialia*, 7(4), 1807-1816.
 - 21 Novajra, G., Perdika, P., Pisano, R., Miola, M., Bari, A., Jones, J. R., ... & Vitale-Brovarone, C. (2015). Structure optimisation and biological evaluation of bone scaffolds prepared by co-sintering of silicate and phosphate glasses. *Advances in Applied Ceramics*, 114(sup1), S48-S55.
 - 22 Fiocco, L., Elsayed, H., Daguano, J. K. M. F., Soares, V. O., & Bernardo, E. (2015). Silicone resins mixed with active oxide fillers and Ca-Mg Silicate glass as alternative/integrative precursors for wollastonite-diopside glass-ceramic foams. *Journal of Non-Crystalline Solids*, 416, 44-49.
 - 23 Fiocco, L., Elsayed, H., Ferroni, L., Gardin, C., Zavan, B., & Bernardo, E. (2015). Bioactive wollastonite-diopside foams from preceramic polymers and reactive oxide fillers. *Materials*, 8(5), 2480-2494.
 - 24 Garcia-Lodeiro, I., Fernández-Jimenez, A., Pena, P., & Palomo, A. (2014). Alkaline activation of synthetic aluminosilicate glass. *Ceramics International*, 40(4), 5547-5558.
 - 25 Shah, A. T., Batool, M., Chaudhry, A. A., Iqbal, F., Javaid, A., Zahid, S., ... & ur Rehman, I. (2016). Effect of calcium hydroxide on mechanical strength and biological properties of bioactive glass. *Journal of the mechanical behavior of biomedical materials*, 61, 617-626.
 - 26 Chakradhar, R. S., Nagabhushana, B. M., Chandrappa, G. T., Ramesh, K. P., & Rao, J. L. (2006). Solution combustion derived nanocrystalline macroporous wollastonite ceramics. *Materials Chemistry and Physics*, 95(1), 169-175.
 - 27 Monsivais-Gámez, E., Ruiz, F., & Martínez, J. R. (2007). Four-membered rings family in the Si-O extended rocking IR band from quantum chemistry calculations. *Journal of sol-gel science and technology*, 43(1), 65-72.
 - 28 Zhang, Q., & Ye, G. (2012). Dehydration kinetics of Portland cement paste at high temperature. *Journal of thermal analysis and calorimetry*, 110(1), 153-158.

- 29 Karamanov, A., & Pelino, M. (2008). Induced crystallization porosity and properties of sintered diopside and wollastonite glass-ceramics. *Journal of the European Ceramic Society*, 28(3), 555-562.
- 30 Watanabe, Takashi, et al. "Effect of Alkali Oxides on Crystallization in CaO–SiO₂–CaF₂ Glasses." *ISIJ international* 48.7 (2008): 925-933.
- 31 Hemmings, R. T., & Berry, E. E. (1987). On the glass in coal fly ashes: recent advances. *MRS Online Proceedings Library Archive*, 113.
- 32 Ni, S., Chang, J., & Chou, L. (2006). A novel bioactive porous CaSiO₃ scaffold for bone tissue engineering. *Journal of Biomedical Materials Research Part A: An Official Journal of The Society for Biomaterials, The Japanese Society for Biomaterials, and The Australian Society for Biomaterials and the Korean Society for Biomaterials*, 76(1), 196-205.
- 33 Mohammadi, H., Sepantafar, M., & Ostadrahimi, A. (2015). The role of bioinorganics in improving the mechanical properties of silicate ceramics as bone regenerative materials. *J. Ceram. Sci. Technol*, 6(1).
- 34 Wu, C., & Chang, J. (2013). A review of bioactive silicate ceramics. *Biomedical materials*, 8(3), 032001.
- 35 Kansal, I., Goel, A., Tulyaganov, D. U., Pascual, M. J., Lee, H. Y., Kim, H. W., & Ferreira, J. M. (2011). Diopside (CaO· MgO· 2SiO₂)–fluorapatite (9CaO· 3P₂O₅· CaF₂) glass-ceramics: Potential materials for bone tissue engineering. *Journal of Materials Chemistry*, 21(40), 16247-16256.
- 36 Jones, J. R., Ehrenfried, L. M., & Hench, L. L. (2006). Optimising bioactive glass scaffolds for bone tissue engineering. *Biomaterials*, 27(7), 964-973.
- 37 ImageJ—Image Processing and Analysis in Java. Available online: <https://imagej.nih.gov/ij/>(accessed on 25 January 2016).
- 38 Rahaman, M. N., Day, D. E., Bal, B. S., Fu, Q., Jung, S. B., Bonewald, L. F., & Tomsia, A. P. (2011). Bioactive glass in tissue engineering. *Acta biomaterialia*, 7(6), 2355-2373.
- 39 Elsayed, H., Rincón Romero, A., Ferroni, L., Gardin, C., Zavan, B., & Bernardo, E. (2017). Bioactive glass-ceramic scaffolds from novel ‘inorganic gel casting’ and sinter-crystallization. *Materials*, 10(2), 171.
- 40 Tampieri, A., Celotti, G., & Landi, E. (2005). From biomimetic apatites to biologically inspired composites. *Analytical and bioanalytical chemistry*, 381(3), 568-576.
- 41 Hutmacher, D. W. (2006). Scaffolds in tissue engineering bone and cartilage. In *The Biomaterials: Silver Jubilee Compendium*(pp. 175-189).
- 42 Ramakrishna, S., Mayer, J., Wintermantel, E., & Leong, K. W. (2001). Biomedical applications of polymer-composite materials: a review. *Composites science and technology*, 61(9), 1189-1224.
- 43 Jones Julian, R. (2013). Review of bioactive glass: From Hench to hybrids. *Acta Biomater*, 9, 4457-4486.
- 44 Hench, L. L. (1991). Bioceramics: from concept to clinic. *Journal of the American Ceramic Society*, 74(7), 1487-1510. from ‘Inorganic Gel Casting’ and Sinter-Crystallization. *Materials*, 11(3), 349.
- 45 Kokubo, T., & Takadama, H. (2006). How useful is SBF in predicting in vivo bone bioactivity?. *Biomaterials*, 27(15), 2907-2915.

- 46 Rabiee, S. M., Nazparvar, N., Azizian, M., Vashae, D., & Tayebi, L. (2015). Effect of ion substitution on properties of bioactive glasses: a review. *Ceramics International*, 41(6), 7241-7251.
- 47 Wren, A. W. (2016). 45S5 Bioglass Based Scaffolds for Skeletal Repair. In *Biocompatible Glasses* (pp. 183-201). Springer, Cham.
- 48 Kaysinger, K. K., & Ramp, W. K. (1998). Extracellular pH modulates the activity of cultured human osteoblasts. *Journal of cellular biochemistry*, 68(1), 83-89.
- 49 El-Ghannam, A., Ducheyne, P., & Shapiro, I. M. (1997). Formation of surface reaction products on bioactive glass and their effects on the expression of the osteoblastic phenotype and the deposition of mineralized extracellular matrix. *Biomaterials*, 18(4), 295-303.
- 50 Brandao-Burch, A., Utting, J. C., Orriss, I. R., & Arnett, T. R. (2005). Acidosis inhibits bone formation by osteoblasts in vitro by preventing mineralization. *Calcified tissue international*, 77(3), 167-174.
- 51 Vitale-Brovarone, C., Verné, E., Robiglio, L., Martinasso, G., Canuto, R. A., & Muzio, G. (2008). Biocompatible glass-ceramic materials for bone substitution. *Journal of Materials Science: Materials in Medicine*, 19(1), 471-478.
- 52 Vitale-Brovarone, C., Baino, F., & Verné, E. (2009). High strength bioactive glass-ceramic scaffolds for bone regeneration. *Journal of Materials Science: Materials in Medicine*, 20(2), 643-653.
- 53 Stevens, B., Yang, Y., Mohandas, A., Stucker, B., & Nguyen, K. T. (2008). A review of materials, fabrication methods, and strategies used to enhance bone regeneration in engineered bone tissues. *Journal of Biomedical Materials Research Part B: Applied Biomaterials: An Official Journal of The Society for Biomaterials, The Japanese Society for Biomaterials, and The Australian Society for Biomaterials and the Korean Society for Biomaterials*, 85(2), 573-582.
- 54 Vitale-Brovarone, C., Verné, E., Robiglio, L., Appendino, P., Bassi, F., Martinasso, G., ... & Canuto, R. (2007). Development of glass-ceramic scaffolds for bone tissue engineering: characterisation, proliferation of human osteoblasts and nodule formation. *Acta Biomaterialia*, 3(2), 199-208.
- 55 Vitale-Brovarone, C., Miola, M., Balagna, C., & Verné, E. (2008). 3D-glass-ceramic scaffolds with antibacterial properties for bone grafting. *Chemical Engineering Journal*, 137(1), 129-136.
- 56 Lyckfeldt, O., & Ferreira, J. M. F. (1998). Processing of porous ceramics by 'starch consolidation'. *Journal of the European Ceramic Society*, 18(2), 131-140.
- 57 Vitale-Brovarone, C., Di Nunzio, S., Bretcanu, O., & Verné, E. (2004). Macroporous glass-ceramic materials with bioactive properties. *Journal of Materials Science: Materials in Medicine*, 15(3), 209-217.
- 58 Brovarone, C. V., Verné, E., & Appendino, P. (2006). Macroporous bioactive glass-ceramic scaffolds for tissue engineering. *Journal of Materials Science: Materials in Medicine*, 17(11), 1069-1078.
- 59 Baino, F., Ferraris, M., Bretcanu, O., Verné, E., & Vitale-Brovarone, C. (2013). Optimization of composition, structure and mechanical strength of bioactive 3-D glass-ceramic scaffolds for bone substitution. *Journal of biomaterials applications*, 27(7), 872-890.

- 60 Rincón, A., Giacomello, G., Pasetto, M., & Bernardo, E. (2017). Novel 'inorganic gel casting' process for the manufacturing of glass foams. *Journal of the European Ceramic Society*, 37(5), 2227-2234.
- 61 Rincon Romero, A.; Elsayed, H.; Bernardo, E. Highly porous mullite ceramics from engineered alkali activated suspensions, *J. Am. Ceram. Soc.* 2018, 101, 1036–1041.
- 62 Wang, X., Ruan, J. M., & Chen, Q. Y. (2009). Effects of surfactants on the microstructure of porous ceramic scaffolds fabricated by foaming for bone tissue engineering. *Materials Research Bulletin*, 44(6), 1275-1279.
- 63 Rincón Romero, A., Elsayed, H., & Bernardo, E. (2018). Highly porous mullite ceramics from engineered alkali activated suspensions. *Journal of the American Ceramic Society*, 101(3), 1036-1041.
- 64 Provis, J. L. (2014). Geopolymers and other alkali activated materials: why, how, and what?. *Materials and Structures*, 47(1-2), 11-25.
- 65 Shah, A. T., Batool, M., Chaudhry, A. A., Iqbal, F., Javaid, A., Zahid, S., ... & ur Rehman, I. (2016). Effect of calcium hydroxide on mechanical strength and biological properties of bioactive glass. *Journal of the mechanical behavior of biomedical materials*, 61, 617-626.
- 66 Chakradhar, R. S., Nagabhushana, B. M., Chandrappa, G. T., Ramesh, K. P., & Rao, J. L. (2006). Solution combustion derived nanocrystalline macroporous wollastonite ceramics. *Materials Chemistry and Physics*, 95(1), 169-175.
- 67 Zhang, Q., & Ye, G. (2012). Dehydration kinetics of Portland cement paste at high temperature. *Journal of thermal analysis and calorimetry*, 110(1), 153-158.
- 68 Watanabe, T., Hashimoto, H., Hayashi, M., & Nagata, K. (2008). Effect of Alkali Oxides on Crystallization in CaO–SiO₂–CaF₂ Glasses. *ISIJ international*, 48(7), 925-933.
- 69 Hemmings, R. T., & Berry, E. E. (1987). On the glass in coal fly ashes: recent advances. *MRS Online Proceedings Library Archive*, 113.
- 70 Wu, C., & Chang, J. (2013). A review of bioactive silicate ceramics. *Biomedical materials*, 8(3), 032001.
- 71 Mohammadi, H., Sepantafar, M., & Ostadrahimi, A. (2015). The role of bioinorganics in improving the mechanical properties of silicate ceramics as bone regenerative materials. *J. Ceram. Sci. Technol*, 6(1).
- 72 Thompson, I. D., & Hench, L. L. (1998). Mechanical properties of bioactive glasses, glass-ceramics and composites. *Proceedings of the Institution of Mechanical Engineers, Part H: Journal of Engineering in Medicine*, 212(2), 127-136.
- 73 Rahaman, M. N., Liu, X., & Huang, T. S. (2011). Bioactive Glass Scaffolds for the Repair of Load-Bearing Bones. *Advances in Bioceramics and Porous Ceramics IV: Ceramic Engineering and Science Proceedings*, 32, 65-78.
- 74 Gibson, L. J., & Ashby, M. F. (1999). *Cellular solids: structure and properties*. Cambridge university press.
- 75 Upadhyaya, G. S. (2004). Holland W., Beall G.: Glass-ceramic technology," *The American Ceramic Society*", Westerville, OH, USA, 2002, pp. 372. *Science of Sintering*, 36(3), 215-216.
- 76 Hulbert, S. F., Morrison, S. J., & Klawitter, J. J. (1972). Tissue reaction to three ceramics of porous and non-porous structures. *Journal of biomedical materials research*, 6(5), 347-374.

CHAPTER VI

Advance ceramics from engineered alkali activated suspensions

VI.1 - Aim of the study

The experience gained in the production of glass-ceramic foams through inorganic gel casting and sinter crystallisation was applied to two different emerging research topics in the field of geopolymers: the production of geopolymeric foams¹ by frothing, and the conversion of geopolymers into advanced ceramics through controlled heat treatment.²⁻⁴

The foaming of geopolymers by frothing relies on the significant increase of viscosity caused by the progressive curing of the geopolymeric oligomers, as in the case of the foaming method described in previous chapters. The marked pseudoplastic behaviour makes possible to incorporate air bubbles through intensive mechanical stirring.^{1, 5, 6}

The conversion of geopolymers into advanced ceramics generally involves the transformation of hydrated zeolite-like gels (i.e., alumino-silicate network structures, consisting of cross-linked AlO_4 and SiO_4 tetrahedra), incorporating alkali ions, such as Na^+ , K^+ , and Cs^+ (providing the charge balance), into anhydrous alkali alumino-silicates in the form of feldspathoids, at temperatures from 800 °C to 1400 °C.²⁻⁴ The chemical and thermal stability of the developed phases depend on the alkali ion: Cs-based geopolymers, for example, are known to lead to more refractory phases, such as pollucite ($\text{Cs}_2\text{O} \cdot \text{Al}_2\text{O}_3 \cdot 4\text{SiO}_2$),⁴ also featuring a low thermal expansion coefficient.⁷

The stoichiometric balance between alkali oxides, Al_2O_3 and SiO_2 , in the final ceramic obviously depends on the formulation of the geopolymer. Chemical treatments on the geopolymer could determine significant changes, especially for the removal of alkali. In fact, the charge balance of alumino-silicate networks with alkali ions can be modified replacing them with a range of other cations, not only for enhancing the functional properties of geopolymers (e.g., as antimicrobial agents or photocatalysts)^{8, 9} but also for modifying the thermal transformation products. In particular, alkali-free ceramics are fundamentally achievable through ion exchange of alkali ions with ammonium ions, before firing.^{8, 10, 11}

The progressive hardening associated with inorganic polymerisation configures an ‘inorganic gel casting’ and is used in this chapter to produce foams and scaffolds with advanced ceramics, such as mullite (Section VI.2) and cordierite (Section VI.3). Although the low $\text{Al}_2\text{O}_3/\text{SiO}_2$ ratio in geopolymers does not allow the formation of this relatively alumina-rich phases, these materials were obtained through the thermal treatment of engineered alkali activated suspensions consisting of a Na-geopolymer enriched with reactive $\gamma\text{-Al}_2\text{O}_3$ powders in the case of mullite, and reactive $\gamma\text{-Al}_2\text{O}_3$ and talc in the synthesis of cordierite.

Alkali activation and gelation treatments were studied in order to achieve a proper viscosity for trapping air during vigorous mechanical stirring or maintaining the shape of the scaffold struts derived from direct ink writing. After obtaining the hardened samples, sodium ions were extracted through ion exchange in ammonium nitrate solution, and the ion-exchanged foams were successfully converted into pure mullite or cordierite foams and scaffolds through the application of heat treatment.

VI.2 - Mullite ceramics produced from engineered alkali activated suspensions*

VI.2.1 - Introduction

Mullite ($3\text{Al}_2\text{O}_3 \cdot 2\text{SiO}_2$) is an essential material for advanced ceramic applications due to its physical properties, such as low thermal expansion coefficient ($\alpha = 5 \times 10^{-6} \text{ 1/K}$), low dielectric constant (6.5 at 1 MHz), and low thermal conductivity ($k=2.0 \text{ W} \cdot (\text{m} \cdot \text{K})^{-1}$). Therefore mullite has an excellent thermal shock resistance behaviour and is commonly

* *The following text, data and images are an adaptation of the results that were published in the article: “Rincón Romero, A., Elsayed, H., & Bernardo, E. (2018). Highly porous mullite ceramics from engineered alkali activated suspensions. Journal of the American Ceramic Society, 101(3), 1036-1041.” It is reproduced in this section with the incorporation of more results and slight modifications.*

used as refractory material. It also shows excellent mechanical properties at a high temperature, especially high creep resistance, which makes it suitable for structural applications at high-temperature, e.g. catalyst supports gas filters, heat exchangers for gas turbines, etc.

Mullite production has been widely investigated, and a significant number of synthesis techniques are proposed. The most studied method is the solid state reaction of pure silica and alumina,¹²⁻¹⁴ which typically occurs at temperatures above 1500 °C, reducing the particle size, and increasing the homogeneity¹⁵ of the starting materials.

The sintering temperature for mullite formation is decreased (between 1000 and 1350 °C), using a sol-gel process approach, which is applicable thanks to the high homogeneous distribution of the initial constituent components.¹⁶ Other techniques have been suggested for the production of mullite-based ceramics, including co-precipitation techniques, hydrothermal synthesis, or the use of preceramic polymers as a source for silica, in combination with Al₂O₃ or Al fillers.¹⁷⁻¹⁹ Although high purity mullite can be obtained with these methods, there are some drawbacks, such as the high cost of the starting materials and the complex processing parameters, which prevent its use in large-scale production or no high demanding technological applications.

Different types of natural clays, such as kyanite, sillimanite, andalusite or pyrophyllite,²⁰ have been proposed in the synthesis of mullite due to their reduced cost. Among them, kaolinite²¹ and kaolin^{22, 23} are the most studied, since mullite is the resulting primary phase after firing. However, the secondary phases, namely cristobalite and glassy silica, can deteriorate the properties of the final material.²⁴ Mullite can be produced increasing the Al content in the clay, and different sources were suggested such as alumina^{21, 25-27} aluminium hydroxide^{28, 29} or metallic aluminium.³⁰ Mullite production from these powder mixtures requires high-temperature treatments (1500–1600 °C) for several hours.

Porous mullite ceramics can be obtained with different methods and techniques, including polymeric gel casting processes using organic monomers and direct foaming.³¹ However one of the most common processing routes is the replica technique, which involves the impregnation of a polymeric sponge, functioning as a template with a ceramic suspension. After drying, the ceramic-coated sponge is pyrolysed; kaolin enriched with α -Al₂O₃ powders are also proposed as precursors in this route.^{32, 33}

In this investigation, the ceramic residue from the transformation of geopolymers after de-alkalinization is corrected in order to have nearly-pure mullite phase, through the introduction of a reactive alumina filler in the initial suspensions. A valuable inspiration came from previous experiments with geopolymers embedding a reactive carbon filler,^{11, 34} which enabled the carbothermal reduction and nitridation of ion-exchanged geopolymers, resulting in SiAlONs¹⁰ in the form of powders. A similar approach is known to lead to SiC nanoparticles.³⁵ In our case, the introduction of the filler, consisting of γ -

phase Al_2O_3 (which produces mullite through the interaction with silicone resins, pyrolysed in air, as silica precursors),³⁶ did not compromise the shaping into highly porous foams. The approach was later extended to the manufacturing of three-dimensional scaffolds, through direct ink writing of suspensions and their progressive gelation (similarly to what was previously done with conventional geopolymers).⁶

VI.2.2 - Experimental process

Metakaolin (Argical 1200s, AGS Mineraux) and commercial $\gamma\text{-Al}_2\text{O}_3$ (Puralox TH 100/150, with a mean particle size $<35\ \mu\text{m}$, SASOL, Hamburg, Germany) were dissolved in an aqueous solution of 2.5 M NaOH (reagent grade, Sigma–Aldrich, Gillingham, UK), in order to achieve an overall $\text{SiO}_2/\text{Al}_2\text{O}_3$ molar ratio of 0.67 ($\text{SiO}_2/\text{Al}_2\text{O}_3=2/3$, typical of mullite); the total solid content of the suspension was 28 wt%. The mixture was kept under mechanical stirring (500 rpm) at room temperature for 2h in order to achieve the dissolution of the metakaolin and the dispersion of the alumina filler in the slurry. The mixture was cast in closed polystyrene (PS) cylindrical moulds and underwent a pre-curing step of 2 h at 75 °C. Triton X-100 (Sigma-Aldrich, Gillingham, UK) surfactant, for a total amount of 4 wt%, was later added to the suspension, with subsequent mechanical stirring (2000 rpm, for 10 min) in polystyrene moulds. After curing at 40 °C for 48 h, foamed samples were demoulded and subjected to ion exchange, consisting of immersion for 24 h in a 0.1 M NH_4NO_3 solution (following the approach of Bortnovsky et al.),¹⁰ with a solid/liquid ratio of 1/100. Finally, ion-exchanged samples, once dried, were subjected to thermal treatment at 1300 °C for 1 hour (10 °C/min heating rate). A processing scheme for the production of the mullite foams is shown in Figure 1.

The partially gelified suspension, after the pre-curing step at 75°C for 2 h, could also be used for direct ink writing experiments. For this purpose, it was transferred into plastic syringes (having a volume of approx. 30 mm³), which served as a cartridge for extrusion, and loaded into a Delta printer (Delta Wasp 2040 Turbo, Wasproject, Massa Lombarda, Italy) equipped with a pressurised vessel. The syringe base system is provided with conical nozzles (Nordson Italia S.p.a., Segrate, IT) with a diameter of 400 μm , while the printer operated at a layer resolution of 50 μm . Printed pastes were finally subjected to curing, ion exchange and firing under the same conditions previously adopted for the foams.

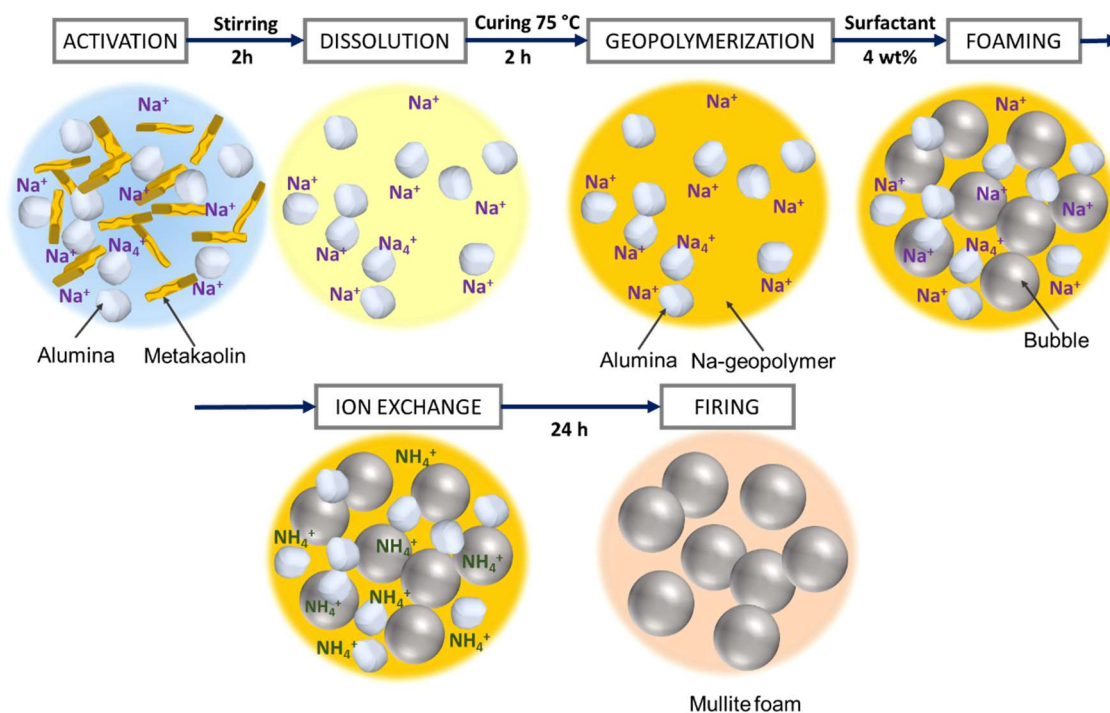


Figure 1. Processing scheme for the production of mullite foams.

Geopolymer composite samples were subjected to microstructural characterization before and after firing, by means of X-ray diffraction (Bruker D8 Advance, Karlsruhe, Germany - $\text{CuK}\alpha$ radiation, 0.15418 nm), as well as optical and electron microscopy (AxioCam ERc 5 s Microscope Camera, Carl Zeiss Microscopy, Thornwood, NY; FEI Quanta 200 ESEM, Eindhoven, The Netherlands). The phase identification from diffraction patterns relied on the Match!® program package (Crystal Impact GbR, Bonn, Germany), supported by data from the PDF-2 database (ICDD-International Centre for Diffraction Data, Newtown Square, PA). Selected samples were subjected to compression tests using an Instron 1121 UTS (Instron, Danvers, MA) machine, with a crosshead speed of 0.5 mm/min. The tests involved foam samples of about 10 mm \times 10 mm \times 10 mm, cut from larger specimens, as well as scaffold samples of about 10 mm \times 10 mm \times 6 mm. Each data point corresponded to 5-6 samples.

VI.2.3 - Results and discussion

The evolution of the porous foam microstructure through the preparation process is shown in Figure 2. From the hardened state sample, produced after the foaming and subsequent curing (Fig. 2a), it can be noticed a high microstructural uniformity with pore cells diameter below 100 μm . The small pores are obtained thanks to the high viscosity developed after the geopolymeric reaction that occurs during the pre-curing step. This is consistent with the experiments involving alkali activation of glass based compositions described before, where smaller pores were obtained for the slurries with the higher

viscosity. With a higher magnification (Fig. 2, lower images), the big pores appear surrounded by thick, micro-porous struts.

The structure does not undergo any substantial changes in the ‘de-alkalised’ condition, after ion exchange (Fig. 2b), or after heat treatment (Fig. 2c) where the same homogeneous foam microstructure is observed.

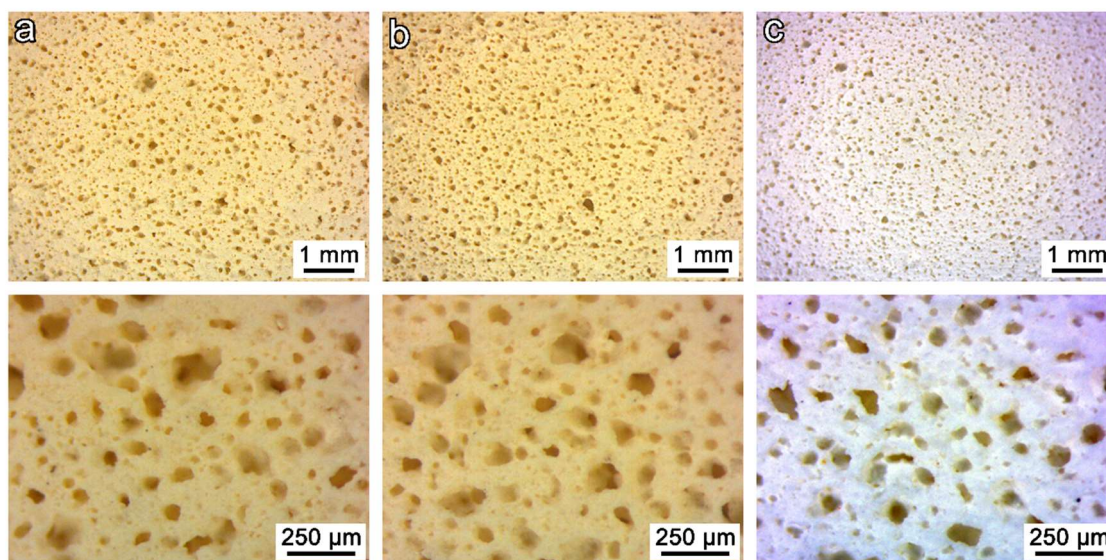


Figure 2. Microstructural details of the foams at various processing steps: a) after low-temperature curing; b) after ion exchange; c) after firing at 1300 °C. (upper part low magnification, lower images high magnification)

The X-ray diffraction analyses of the original materials and the geopolymer composite foam produced after alkali activation and curing are presented in Figure 3. Metakaolin is essentially amorphous, presenting a halo centred approximately at $2\theta = 22-24^\circ$, quartz (SiO_2 ; PDF#87-2096), with typical traces of muscovite ($\text{KAl}_2(\text{AlSi}_3\text{O}_{10})(\text{OH})_2$; PDF#07-00025) are present as impurities. The filler consists of $\gamma\text{-Al}_2\text{O}_3$ (PDF#49-0134). This phase remains clearly detectable in the geopolymer composite, after curing, along with minor traces of quartz (SiO_2 ; PDF#87-2096), previously present as an impurity in the metakaolin, as these phases are not affected by the alkaline activation process. Minor traces of paragonite ($\text{NaAl}_2(\text{Si}_3\text{Al})\text{O}_{10}(\text{OH})_2$, PDF#87-0091) are also detected. The later phase forms upon curing of Na-based synthetic alumino-silicate binders, and its presence indicates a structural rearrangement after the geopolymerization reaction.³⁷ The broad amorphous hump in the 2θ range of $18-40^\circ$, also indicates the reaction through the alkali activation and the formation of a gel, but its position and shape are not consistent with amorphous stoichiometric geopolymers, which typically shows a hump from 24 to 34° .⁴
³⁸ The developed gel did not match the zeolite-like structure found in true geopolymers, possibly due to the high amounts of water added in the foam preparation.³⁹

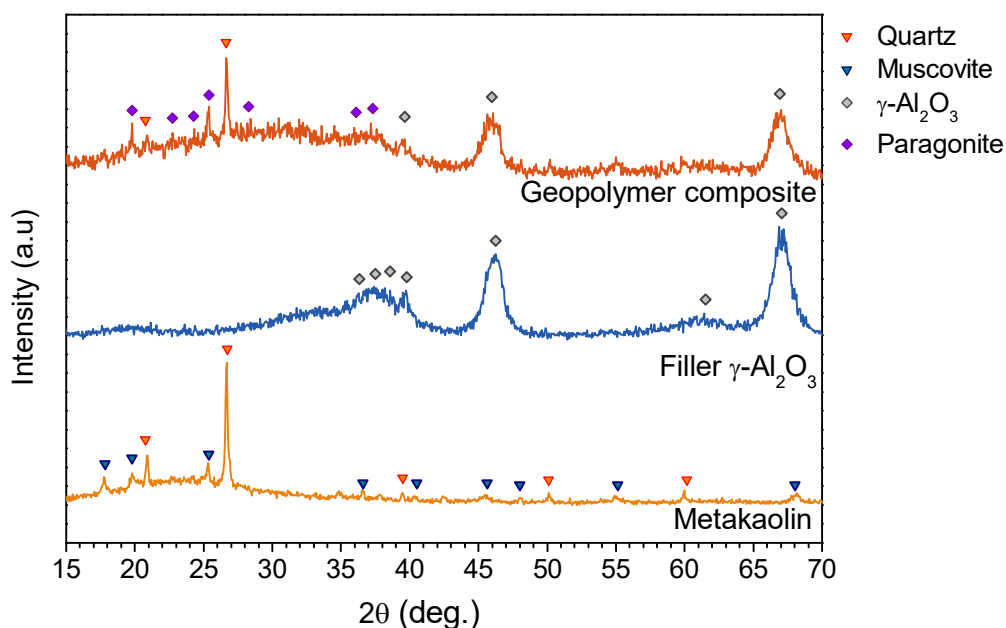


Figure 3. X-ray diffraction patterns of the initial materials and the hardened geopolymeric foam.

The thermal treatment was apparently sensitive to ion exchange. Fragments of geopolymer foam were not subjected to ion exchange, but to the same thermal treatment at 1300 °C applied to the ion-exchanged samples; their X-ray diffraction patterns are shown in Figure 4.

The non-exchanged foams led to a composite glass matrix, with intense peaks of $\alpha\text{-Al}_2\text{O}_3$ (PDF#75-1862) emerging from the typical ‘halo’ of the amorphous phase. A minor peak could be ascribed to nepheline (PDF#79-0992), as was the case in the firing of Na-based geopolymers previously discussed.³ In other words, with sodium still incorporated in the matrix, the matrix and filler substantially underwent an independent evolution. On the contrary, in the samples treated after ion exchange metakaolin $\gamma\text{-Al}_2\text{O}_3$ react leading to the formation of mullite (PDF#83-1881), which is clearly recognised as the dominant phase.

The flat background reveals the absence of a glass phase, while only minor peaks could not be ascribed to mullite. The best compliance with experimental data was provided by sillimanite (PDF#88-0889), i.e. a silica-rich alumino-silicate ($\text{Al}_2\text{O}_3 \cdot \text{SiO}_2$), and $\theta\text{-Al}_2\text{O}_3$ (PDF#86-1410), both attributable, in our opinion, to the incomplete reaction between the initial constituents. $\theta\text{-Al}_2\text{O}_3$ can be seen as the result of the thermal transformation of the γ -phase, with progressive dehydration (transition aluminas are known to transform into corundum under progressive heating, with the path: $\gamma \rightarrow \delta \rightarrow \theta \rightarrow \alpha$)^{40, 41} but its presence was quite surprising, being found after a treatment well above its stability range (1100 °C).⁴⁰ In our opinion, this could be due to a reaction between the hydroxyl groups of

alumina and a silicon-containing precursor (in this case represented by the geopolymer matrix), already known to stabilise the γ -phase.⁴² Longer treatments at 1300 °C would probably determine a complete reaction and will be the subject of further investigations.

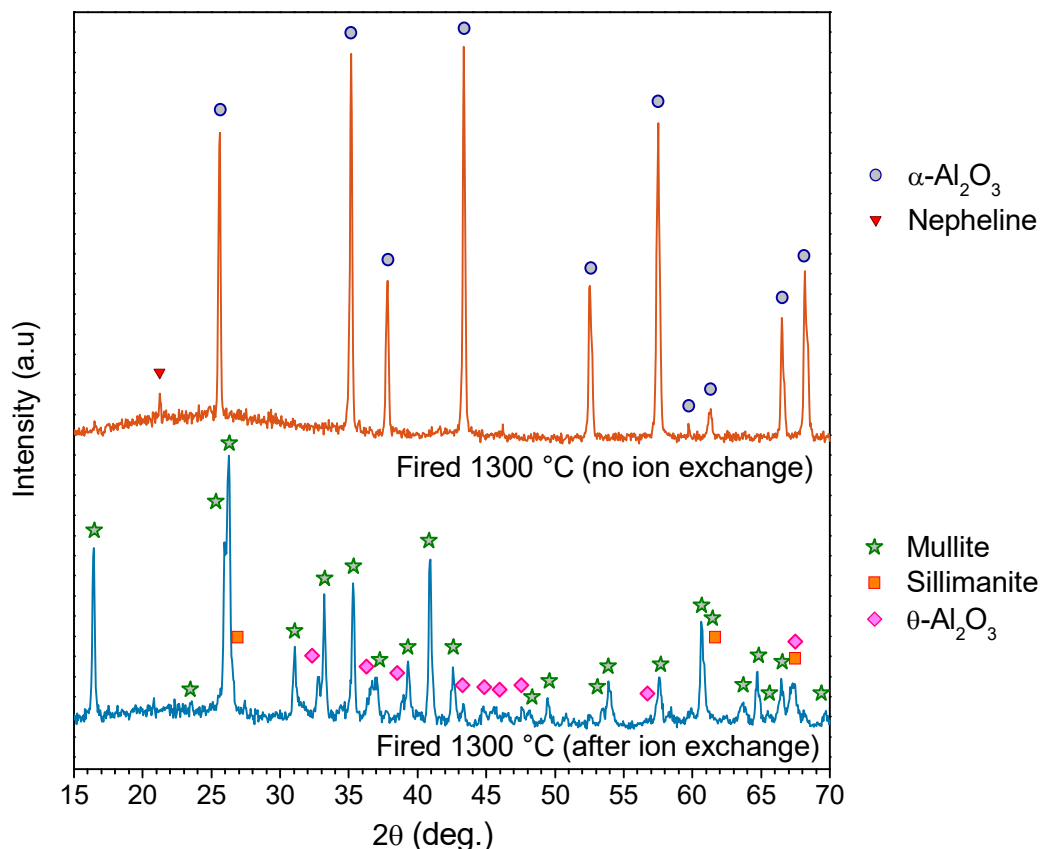


Figure 4. Mineralogical evolution of geopolymer composites after different various processing steps.

The high magnification SEM images of samples shown in Figure 5 represent the evolution of samples, from the hardened state after foaming and complete setting, through ion exchange and heat treatment. It can be noticed that, despite the significant filler loading, the inorganic gel casting approaches the homogeneous cellular structure obtained in the hardened state (Fig. 5a), which remains through all the transformations. The samples are not degraded by the ion-exchange process, as proved by the homogeneous appearance and the absence of cracks in the ‘de-alkalinized’ foam (Fig. 5b), which were confirmed after firing at 1300 °C (Fig. 5c).

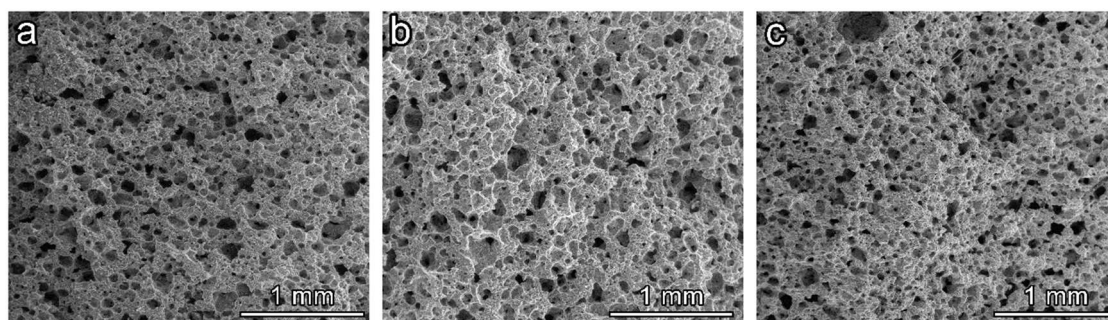


Figure 5. Morphology of geopolymer composites at various processing steps: a) after low-temperature curing; b) after ion exchange; c) after firing at 1300 °C.

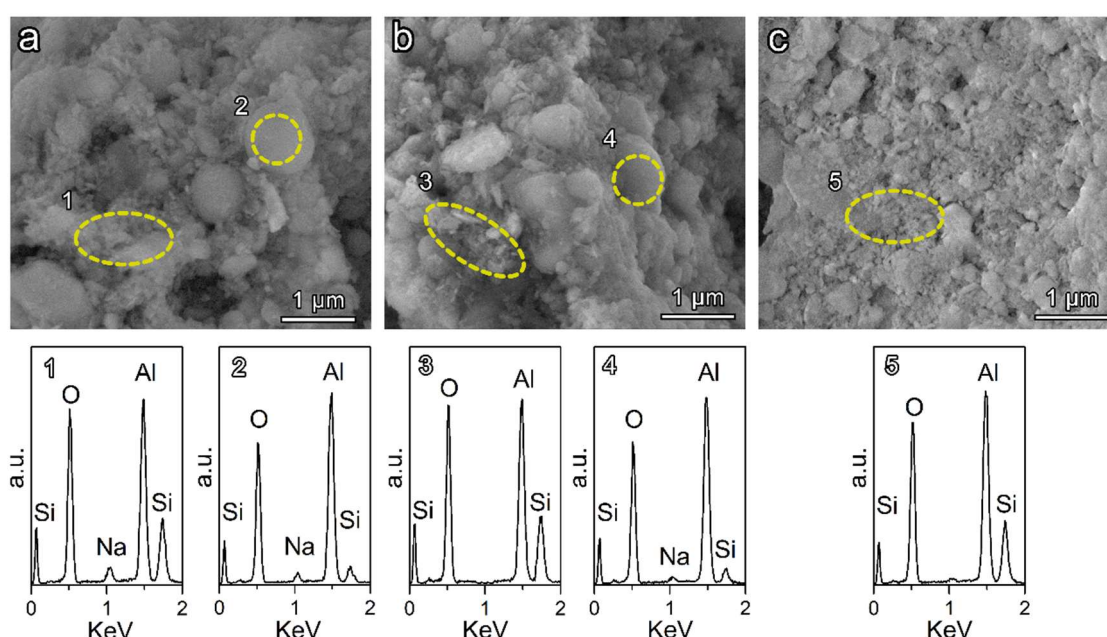


Figure 6. Microstructural strut details of geopolymer-derived mullite foams: a) after curing; b) after ion exchange c) after firing; (Bottom part, X-ray fluorescence signals of selected points).

The excellent permanence of the structure throughout the process could be explained by the high structural cohesion presented by the foams, as a consequence of the formation of the geopolymeric gel. This observation is further confirmed by the details of the struts microstructure under high magnification and EDX analysis on selected areas, as shown in Figure 6.

In the hardened foam (Fig. 5a) a heterogeneous amorphous phase with unreacted spherical particles embedded in the structure can be observed. Spectrum “1”, collected from the amorphous matrix, corresponds to a non-stoichiometric Na-geopolymeric gel, considering the Al/Si molar ratios near 2.5, which is closer to the one in mullite formulation rather than to the one in truly zeolite-like gel found in proper geopolymers.

Spectrum “2” corresponds to a γ - Al_2O_3 particle, with the EDX signals matching the characteristic elements present in it, even if some sodium and silicon are also detected.

This structure does not change significantly after ion exchange (Fig. 5b). The main differences arise in the EDX analysis where the Al/Si remain the same for the amorphous phase (Spectrum “3”) and for the γ - Al_2O_3 particle (Spectrum “4”), even though the absence of sodium signal is noticeable in both spectra, confirming the successful removal of Na^+ ions following ion exchange.

Finally, after heat treatment (Fig. 5c) a crystalline structure is identified where the spectrum “5” collected from it confirms the absence of Na^+ ions and the Al/Si molar ratios close to 3 matches the molar ratios of mullite.

The high filler loading also enabled a secondary shaping option. As shown in Figure 7a, direct ink writing of pastes available after the pre-curing step led to reticulated scaffolds with no evidence of viscous collapse. The overlapping filaments remained parallel after curing, keeping wide pores in the z-direction (Figure 7b).

The ion exchange and the firing did not determine any degradation. In Figure 7c we can observe that the transformations did not cause any microcracking, even for larger filament spacing (the absence of sagging, even for large voids, again indicated the marked pseudoplasticity of the pastes), as can be noticed in Figure 8, where an alternative scaffold geometry is presented.

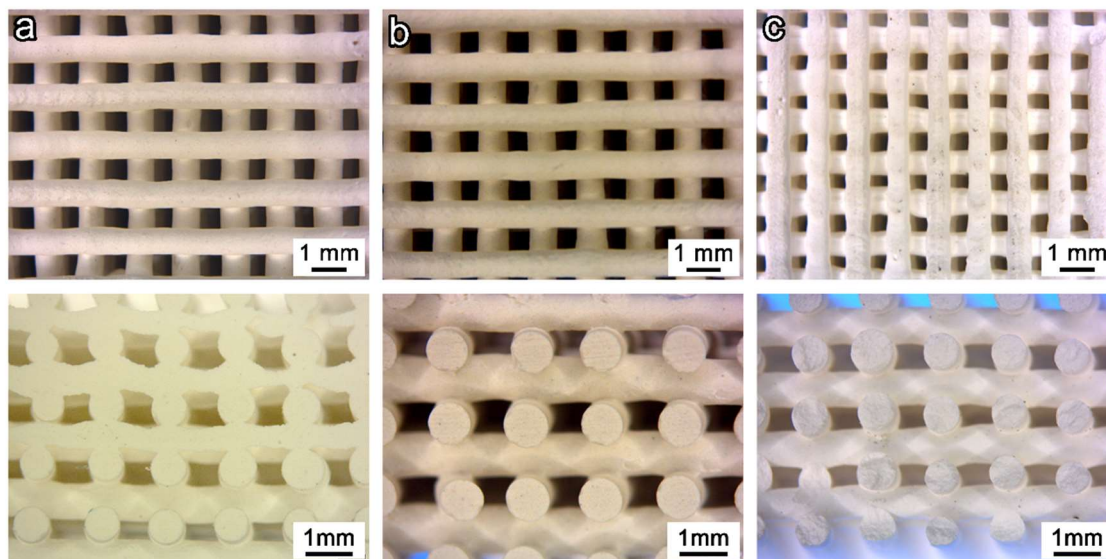


Figure 7. Morphology of geopolymer composites: a) typical scaffold geometry after curing; b) after ion exchange and c) after heat treatment (up, top view; down, cross section)

In Figure 9 the high magnification images of the obtained scaffold after hardening (Fig. 9a, top view; and c, cross section) and after heat treatment (Fig.9b, top view; and d, cross section) confirms the absence of degradation of the structure through the process and the obtainment of well-shaped dense rounded struts after the heat treatment.

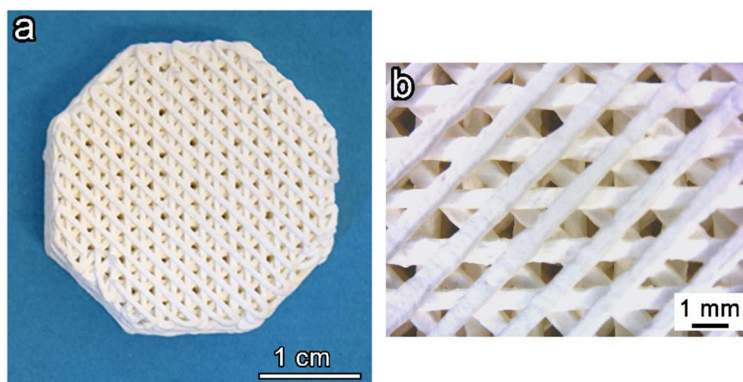


Figure 8. Alternative scaffold design

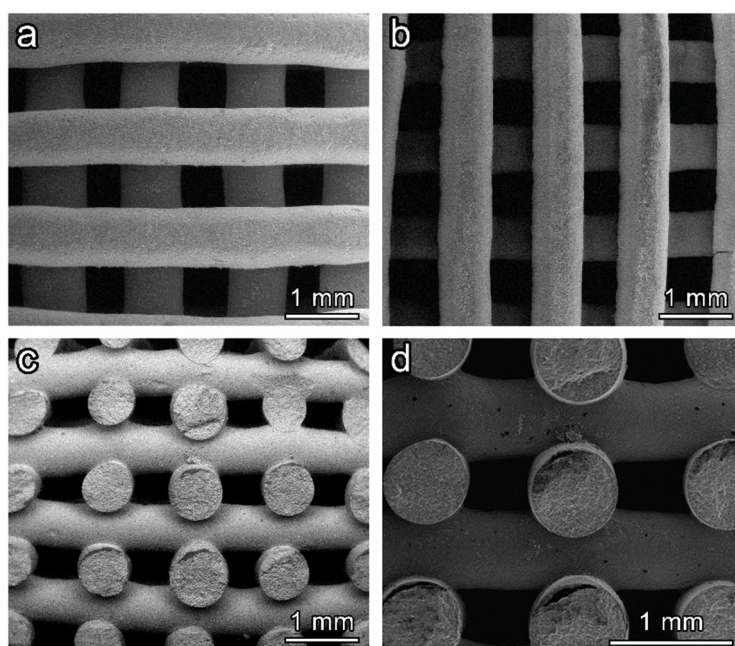


Figure 9. Microstructural details of geopolymer-derived mullite scaffolds: a) after curing; b) after firing and c) interpenetration of overlapping filaments

The practical absence of Na^+ was demonstrated throughout the filament (Figure 10), showing the elemental distribution through the diameter (obtained through the collection of X-ray fluorescence signals): the Na-related signal is flat and close to zero. The inherent microporosity and mesoporosity of geopolymers evidently enabled an in-depth ion exchange. The fluctuations in the Al and Si distributions along the diameter were

consistent with the X-ray analysis; some Al-rich granules (marked by arrows in Figure 10, right side) could be ascribed to θ -Al₂O₃.

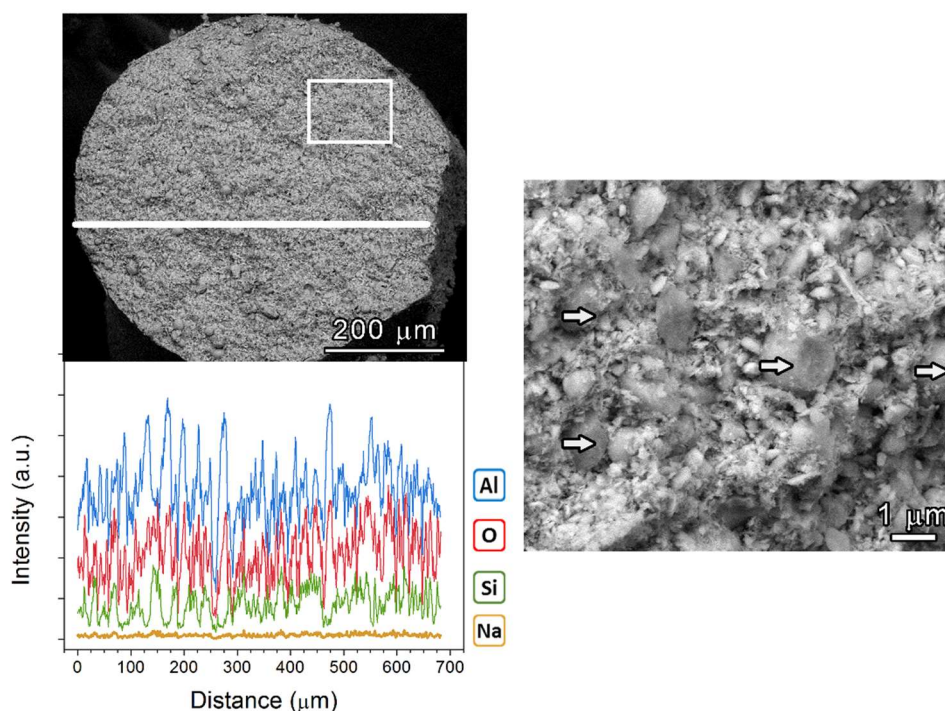


Figure 10. (Left) X-ray fluorescence signals through the filament diameter. (Right) high magnification of a strut (Al-rich granules marked by arrows)

Sample type	Density, ρ (g/cm ³)			Porosity (%)			Strength σ_{comp} (MPa)
	geometric	apparent	true	total	open	closed	
foam	0.81 ± 0.03	2.68 ± 0.03	3.03 ± 0.01	73 ± 3	65 ± 2	8 ± 6	11 ± 1
scaffold	0.84 ± 0.04	3.08 ± 0.02	3.14 ± 0.01	73 ± 5	72 ± 5	1 ± 2	5 ± 2

Table 1. Density, porosity and mechanical properties of the fired treated foams and scaffolds.

The absence of cracks in both foams and scaffolds indicates good strength-to-density ratios, as shown in Table 1. With an almost completely open porosity of $73\% \pm 3\%$ (pycnometry analysis revealed an open porosity of $65\% \pm 2\%$), the foams reached a compressive strength of 11 ± 1 MPa, in line with the values for commercial foams, typically used for thermal protection and metal filtration.^{43,44} Scaffolds (with a narrow spacing between filaments, like the ones in Figure 7c) achieved compressive strength of 5 ± 2 MPa, and a density of 0.84 ± 0.04 g/cm³ ($73\% \pm 5\%$ total porosity).

Given the application of time-consuming processes, such as ion exchange, the proposed approach might be quite impracticable compared to the processes already

applied for commercial mullite foams, though it may provide a better flexibility in the shaping process. As an example, the tuning of geopolymer foam processing through gel casting (leading to significant enhancement of both overall porosity and specific surface, owing to the overlapping of the effects surfactants and gas release, e.g., from the decomposition of H_2O_2)^{45, 46} could be reasonably applied to geopolymer composites. Additional potential benefits are connected with the control of free water segregation, e.g. by adding acrylate-functional silane coupling agents.⁴⁷ Direct ink writing, on the other hand, may be applied to obtain alternative shapes (an example is shown in Figure 8). Finally, the proposed technology has some potential even beyond applications involving mullite: treatments in alternative atmospheres (e.g., N_2) are currently under investigation for testing the formation of oxynitride phases (SiAlONs), consistently with what was done for ion-exchanged C-filled geopolymer powders.^{11, 34}

VI.3 - Cordierite ceramics produced from engineered alkali activated suspensions

VI.3.1 - Introduction

Cordierite ($2\text{MgO}\cdot 2\text{Al}_2\text{O}_3\cdot 5\text{SiO}_2$) presents low thermal expansion coefficient, excellent thermal shock resistance, low dielectric constant, and high chemical and mechanical durability that makes this phase very interesting to be applied in a wide range of applications such as in catalytic converter substrate, filters, membranes, and refractories.⁴⁸⁻⁵¹

Many authors have reported the preparation of cordierite by used various starting raw materials and different processing methods.⁵² Solid-state sintering at high temperature of individual oxides with the stoichiometric MgO , SiO_2 and Al_2O_3 ratio close to cordierite,^{53, 54} however, the final phases and properties of the final ceramic are influenced by the mechanical treatment by grinding of the initial materials.^{55, 56} The firing temperature can be reduced, and the whole cost-effectiveness of the process could be improved using natural mineral resources as starting materials, such as natural sands,⁵⁷ clays⁵⁸⁻⁶¹ or even waste materials such as fly ash coming from coal combustion^{62, 63} or rice husk.⁶⁴

Highly pure cordierite powders could be also synthesised using the sol-gel route⁶⁵⁻⁶⁷ but relatively high prices of the reagents and the solvents needed during sol-gel makes this route quite impracticable at an industrial scale.⁶⁸ Trials have been made to make sol-gel^{69, 70} more environment-friendly through the partial substitution of the expensive precursors with rice husk ash.⁷¹

Another interesting route rises from the production of cordierite trough the heat treatment of commercial silicone resins.⁷² The use of these preceramic polymers using different fillers such as talc and alumina⁷³ or nano-sized Al_2O_3 and MgO particles⁷⁴ to

modify the overall stoichiometric composition of the mixture to obtain highly pure cordierite ceramics after the heat treatment.

In this investigation as in the case of mullite ceramics described before, the geopolymeric gel produced after low alkali activation of metakaolin suspensions is modified by the introduction some reactive fillers (γ - Al_2O_3 and talc) in order to reach the stoichiometric balance of cordierite in the starting suspensions. The progressive gelation of the geopolymerisation products allows the production of foams and scaffolds, by foaming with a surfactant or by direct ink writing of the partially gelified suspension. After hardening sodium ions present in the geopolymer-like samples were extracted through ion exchange in ammonium nitrate solution, and finally, the ion-exchanged foams were successfully converted into highly pure cordierite foams and scaffolds with the application of an appropriate heat treatment.

VI.3.2 - Experimental process

Cordierite ceramics were achieved by polymerisation of engineered alkali activated suspensions. Metakaolin (Argical 1200s, AGS Mineraux), purified talc (Sigma-Aldrich Gillingham, UK) and commercial γ - Al_2O_3 (Puralox TH 100/150, of mean particle size $<35\ \mu\text{m}$, SASOL, Hamburg, Germany) were dissolved in an aqueous solution of 2.5 M NaOH (reagent grade, Sigma-Aldrich, Gillingham, UK), at a stoichiometric $\text{SiO}_2/\text{Al}_2\text{O}_3/\text{MgO}$ molar ratio prevised for cordierite. The total solid content of the suspension was 40 wt%, in order to achieve a homogeneous suspension just after the addition of the powders the slurry was sonicated for 5 min. The mixture was kept under mechanical stirring (500 rpm) at room temperature for 2h in order to achieve the activation of metakaolin and the dispersion of the fillers in the slurry. The mixture was cast in closed polystyrene (PS) cylindrical moulds and underwent a pre-curing step of 2 hours at 75 °C. After 2 hours of gelation the suspension was foamed with Triton X-100 (Sigma-Aldrich, Gillingham, UK) surfactant, for a total amount of 4 wt%, and subsequently subjected to intensive mechanical stirring (2000 rpm, for 10 min). The wet foams were cured at 40 °C for 48 h till complete setting. Hardened foams were subjected to ion exchange, consisting of the immersion in a 0.1 M NH_4NO_3 solution at a solid/liquid ratio of 1/100 for 24 hours. Finally, ion-exchanged samples were subjected to thermal treatment at 1200 °C with different holding times 1-3 hours at different heating rates (2-10°C/min heating rate). A processing scheme for the production of the mullite foams is shown in Figure 1.

The partially gelified suspension, after the pre-curing step of 2h at 75°C, could also be used for direct ink writing experiments. The suspension was transferred into plastic syringes (volume of approx. 30 mm³), which served as a cartridge for extrusion by means of a Delta printer (Delta Wasp 2040 Turbo, Wasproject, Massa Lombarda, Italy) equipped with a pressurised vessel. The syringe base system was fitted with conical nozzles

(Nordson Italia S.p.a., Segrate, IT) with a diameter of 400 μm ; the printer operated with a layer resolution of 50 μm . Printed pastes were subjected to curing, ion exchange and firing in the same conditions adopted for the foams.

Geopolymer composite samples were subjected to microstructural characterization before and after firing, by means of X-ray diffraction (Bruker D8 Advance, Karlsruhe, Germany – $\text{CuK}\alpha$ radiation, 0.15418 nm), optical and electron microscopy (AxioCam ERc 5 s Microscope Camera, Carl Zeiss Microscopy, Thornwood, NY; FEI Quanta 200 ESEM, Eindhoven, The Netherlands). The phase identification, from diffraction patterns, was performed using the Match!® program package (Crystal Impact GbR, Bonn, Germany), supported by data from the PDF-2 database (ICDD-International Centre for Diffraction Data, Newtown Square, PA). Selected samples were subjected to compression tests by using an Instron 1121 UTS (Instron, Danvers, MA) machine, with a crosshead speed of 0.5 mm/min. The tests involved foam samples of about 10 mm \times 10 mm \times 10 mm, cut from larger specimens, as well scaffold samples of about 10 mm \times 10 mm \times 6 mm. Each data point corresponded to 5-6 samples.

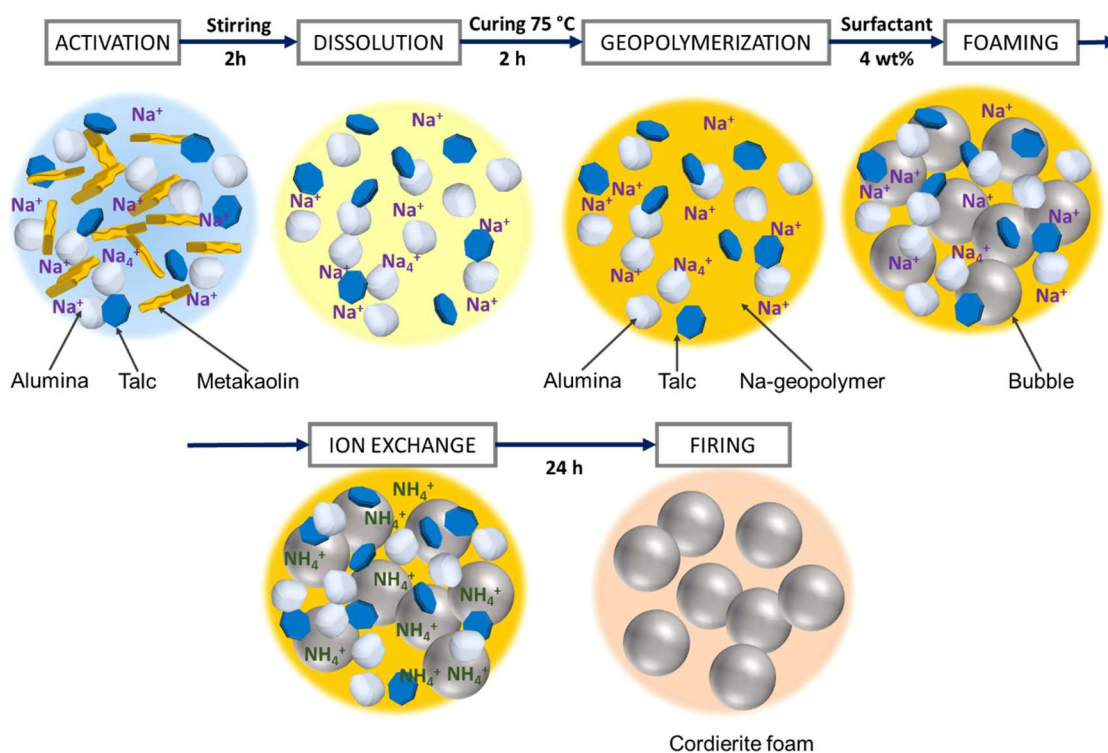


Figure 1. Processing scheme for the production of cordierite foams.

VI.3.3 - Results and discussion

The formation of cordierite from the engineered alkali activated suspensions, as in the case of mullite ceramics present before, is sensitive to the ion exchange. Fragments of the

hardened geopolymer foam were not subjected to the ion exchange process but were subjected to the same thermal treatment at 1200 °C as the ion-exchanged samples; their X-ray diffraction patterns are shown in Figure 2.

The samples not subjected to ion exchange led to a glass matrix composite, with intense peaks of spinel (MgAl_2O_4 ; PDF#75-1797) and olivine ($\text{Mg}_2(\text{SiO}_4)$; PDF#80-0943) emerging from the typical ‘halo’ of the amorphous phase, These phases are typical phases that appear after the heat treatment of magnesium-rich clays.⁷⁵ A minor peak could be ascribed to nepheline ($\text{Na}_{7.2}\text{Si}_{8.8}\text{O}_{32}$; PDF#79-0992), in analogy with the firing of Na-based geopolymers, its presence as previously mentioned, demonstrates the effective formation of an aluminosilicate tridimensional structure in the hardened foams, as this crystalline phase is usually present in the transformation of geopolymers at high temperature.⁷⁶⁻⁷⁸

This means that when sodium is still incorporated in the matrix, the geopolymeric gel formed during alkali activation has independent phase evolution with the undissolved metakaolin and fillers ($\gamma\text{-Al}_2\text{O}_3$ and talc). On the other hand, the formation of cordierite (MgAl_2O_4 ; PDF#84-1220) is clearly recognised in the samples treated after ion exchange process, indicating that the thermal treatment was apparently sensitive to ion exchange

In the samples treated at 1200 °C with 1 hour holding time at the maximum temperature, the presence of cordierite is very limited. The presence of the amorphous halo reveals the presence of a glassy phase, and the main phase detected corresponds to sapphirine ($(\text{Mg}_4\text{Al}_4)(\text{Al}_4\text{Si}_2)\text{O}_{20}$; PDF#19-0750), along with spinel (MgAl_2O_4 ; PDF#75-1797): when the heat treatment is conducted for longer times (3 hours) the formation of cordierite (MgAl_2O_4 ; PDF#84-1220), is clearly recognised as the dominant phase, with some traces of sapphirine ($(\text{Mg}_4\text{Al}_4)(\text{Al}_4\text{Si}_2)\text{O}_{20}$; PDF#19-0750), flat background in the diffractogram indicates the absence of glassy phase and therefore a higher degree of crystallisation.

The heat treated scaffolds at 1200 °C for 3 hours present a similar pattern to the foams with the formation of cordierite as the main crystalline phase with minor traces of sapphirine: The complete formation of cordierite would be probably possible with longer treatments and is the subject of further investigations that are still ongoing.

The evolution of the porous foam microstructure through all the different process steps is shown in Figure 3. In the hardened state sample, just obtained after the foaming and subsequent curing and hardening (Fig. 3a), it can be seen a high microstructural uniformity with pore cells diameter below 100 μm . The small pores are obtained thanks to the gel developed during the geopolymeric reaction and the high viscosity conferred to the suspension by the addition of the fillers. This small pore morphology is in agreement with the data acquired on the alkali activation of glass based compositions described before, where smaller pores were obtained for the slurries with higher viscosity

suspension. In a higher magnification (Fig. 3 a lower part) it can be noticed the good interconnectivity of the cells through the presence of windows in the struts.

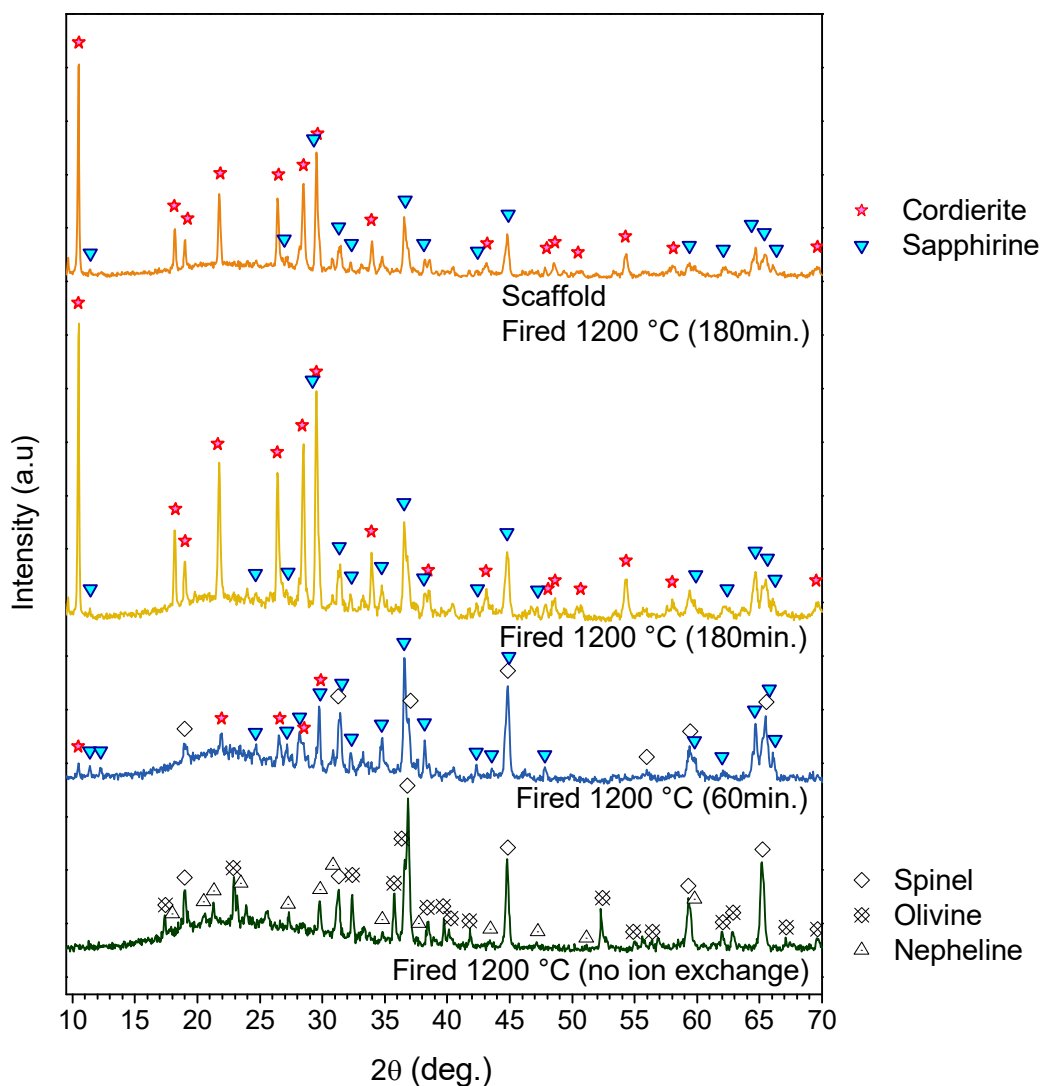


Figure 2. Mineralogical evolution of geopolymers after different various processing steps.

The structure does not suffer any substantial changes, after the ion exchange process (Figs. 3b) where the same homogeneous foam microstructure is perceptible, being noticeable the absence of cracks. In the heat treated samples at 1200 °C with a holding time of 3 hours (Figs. 3c) the same homogenous structure is achieved, however a significant reduction in the pore size is noticed due to the contraction of the samples during sintering, and despite this effect, no visible cracks or deformations were observed.

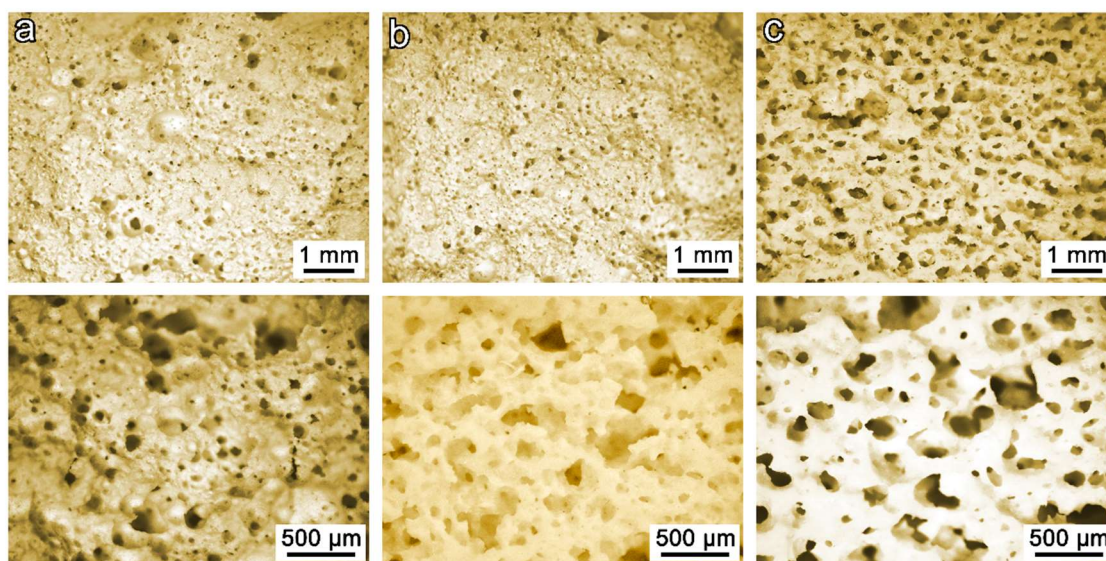


Figure 3. Microstructural details of the cordierite foams at various processing steps: a) after low-temperature curing; b) after ion exchange; c) after firing at 1300 °C. (Upper part low magnification, lower images high magnification)

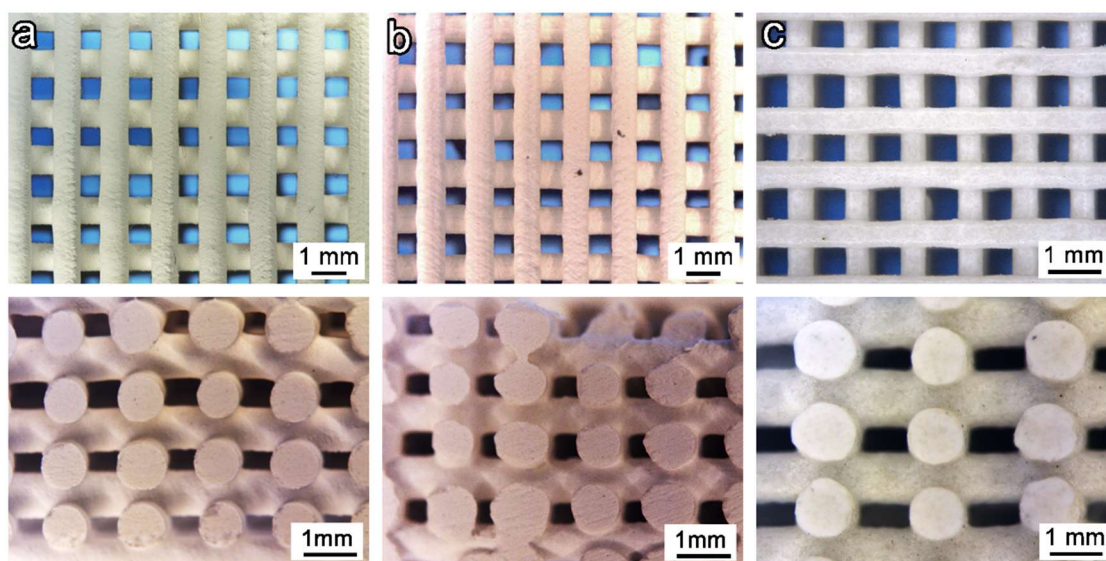


Figure 4. Morphology of geopolymer composites: a) typical scaffold geometry after curing; b) after ion exchange and c) cordierite scaffold after heat treatment (up, top view; down, cross section)

As in the case of mullite described before, the geopolymeric gel and the high filler loading also favoured a proper rheology to use the engineered alkali activated suspensions as inks in direct printing technique. As shown by Figure 4a (up and lower part) direct ink writing of pastes produced after the pre-curing step led to reticulated scaffolds with no evidence of viscous collapse, maintain the roundness of the struts and a homogeneous

interspacing of the filaments. The overlapping filaments that remained parallel after curing, keeping wide pores in the z-direction demonstrate the high ability of the activated suspension to be used as ink in direct ink printing

The ion exchange and the firing did not determine any degradation. From Figures 4b and c we can observe that the heat treatment did not cause any microcracking, as it can be noticed better in high magnification images presented in Figure 5 the obtained scaffold after hardening (Fig. 5a, top view; and c, cross section) and after heat treatment (Fig. 5b, top view; and d, cross section) confirms the absence of degradation of the structure through the process and the obtainment of well-shaped dense rounded struts after the heat treatment. (Figs. 5e and 5f)

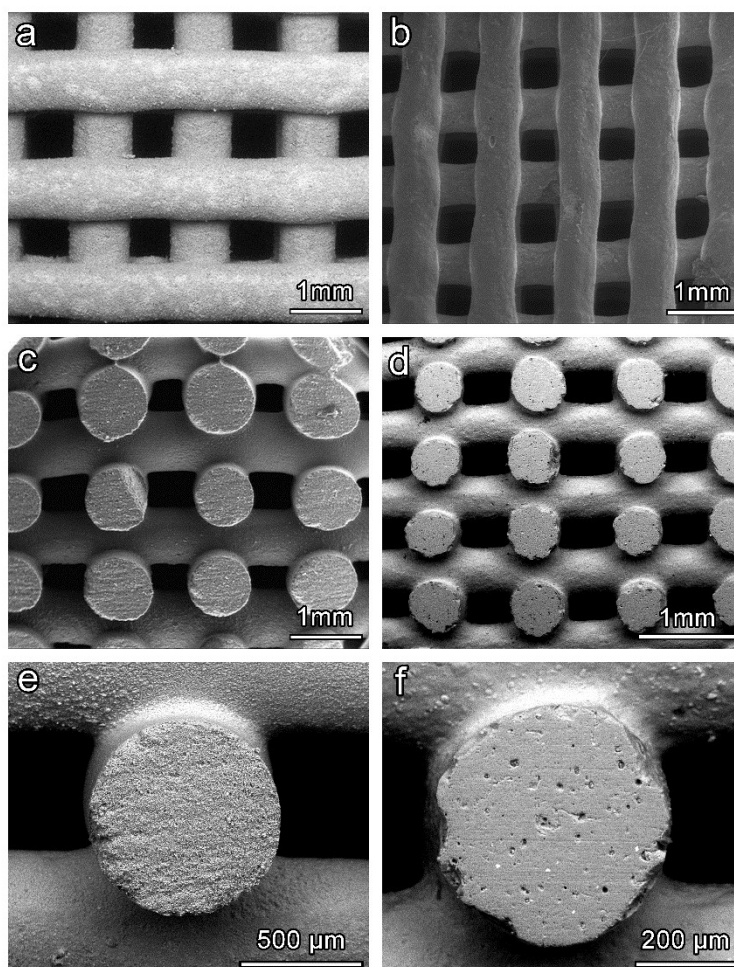


Figure 4. Microstructural details of geopolymer-derived cordierite scaffolds: a, c and e) after curing; b, d and f) after firing; a and b) top-view; c and d) cross-section; e and f) high magnification detail of the struts.

The absence of cracks in both foams and scaffolds is the reason for good strength-to-density ratios. With a porosity of $69\% \pm 7\%$, almost completely open (pycnometry analysis yielded an open porosity of $68\% \pm 9\%$) the foams reached a compressive strength of 4.7 ± 0.3 MPa, compliant with the values for commercial foams, typically used for thermal protection and metal filtration. Scaffolds (for a close filament spacing, like that in Figure 4.a) achieved a compressive strength 29 ± 2 MPa, with a density of 1.52 ± 0.05 g/cm³ ($43\% \pm 3\%$ total porosity).

Sample type	Density, ρ (g/cm ³)			Porosity (%)			Strength σ_{comp} (MPa)
	geometric	apparent	true	total	open	closed	
foam	0.82 ± 0.05	2.58 ± 0.06	2.67 ± 0.01	69 ± 7	68 ± 9	1 ± 3	4.7 ± 0.3
scaffold	1.52 ± 0.05	2.58 ± 0.06	2.65 ± 0.01	42 ± 3	40 ± 3	1 ± 2	29 ± 2

Table 1. Density, porosity and mechanical properties of the fired treated foams and scaffolds.

VI.4 - Conclusions

We may conclude that:

- Gel casting of engineered alkali-activated metakaolin suspensions can be exploited for the development of highly porous geopolymer composite foams and reticulated scaffolds, through frothing and direct ink writing, respectively.
- Both types of cellular geopolymer composites were successfully subjected to de-alkalinization, applying ion exchange in an aqueous solution of ammonium nitrate, with no degradation of the microstructure.
- Owing to the de-alkalinization, the geopolymer matrix could react easily with the secondary phases, leading to the development of nearly pure mullite or cordierite phases; again, the transformation did not cause any significant microstructural degradation.
- Geopolymers combined with engineered fillers and de-alkalinization treatments may have a significant potential for the production of advanced ceramics, with a distinctive coupling of synthesis and shaping.

References

- 1 Cilla, M. S., Colombo, P., & Morelli, M. R. (2014). Geopolymer foams by gelcasting. *Ceramics International*, 40(4), 5723-5730.

- 2 He, P., Jia, D., & Wang, S. (2013). Microstructure and integrity of leucite ceramic derived from potassium-based geopolymer precursor. *Journal of the European Ceramic Society*, 33(4), 689-698.
- 3 Kuenzel, C., Grover, L. M., Vandeperre, L., Boccaccini, A. R., & Cheeseman, C. R. (2013). Production of nepheline/quartz ceramics from geopolymer mortars. *Journal of the European Ceramic Society*, 33(2), 251-258.
- 4 Bell, J. L., Driemeyer, P. E., & Kriven, W. M. (2009). Formation of Ceramics from Metakaolin-Based Geopolymers: Part I—Cs-Based Geopolymer. *Journal of the American Ceramic Society*, 92(1), 1-8.
- 5 Kim, D., Lai, H. T., Chilingar, G. V., & Yen, T. F. (2006). Geopolymer formation and its unique properties. *Environmental geology*, 51(1), 103-111.
- 6 Franchin, G., Scanferla, P., Zeffiro, L., Elsayed, H., Baliello, A., Giacomello, G., ... & Colombo, P. (2017). Direct ink writing of geopolymeric inks. *Journal of the European Ceramic Society*, 37(6), 2481-2489.
- 7 Yanase I, Tamai S, Kobayashi H. (2003). Sintering of pollucite using amorphous powder and its low thermal expansion property. *Journal of the Japanese Ceram Society*. 111, 533-536.
- 8 O'Connor, S. J., MacKenzie, K. J., Smith, M. E., & Hanna, J. V. (2010). Ion exchange in the charge-balancing sites of aluminosilicate inorganic polymers. *Journal of Materials Chemistry*, 20(45), 10234-10240.
- 9 Gasca-Tirado, J. R., Manzano-Ramírez, A., Villaseñor-Mora, C., Muñoz-Villarreal, M. S., Zaldivar-Cadena, A. A., Rubio-Ávalos, J. C., ... & Mendoza, R. N. (2012). Incorporation of photoactive TiO₂ in an aluminosilicate inorganic polymer by ion exchange. *Microporous and Mesoporous Materials*, 153, 282-287.
- 10 Bortnovsky, O., Dědeček, J., Tvarůžková, Z., Sobalík, Z., & Šubrt, J. (2008). Metal ions as probes for characterization of geopolymer materials. *Journal of the American Ceramic Society*, 91(9), 3052-3057.
- 11 Bagci, C., Kutyla, G. P., & Kriven, W. M. (2014). In situ carbothermal reduction/nitridation of geopolymer composites containing carbon nanoparticles. In *Ceram Eng Sci Proc* (Vol. 35, pp. 15-28).
- 12 Saruhan, B., Albers, W., Schneider, H., & Kaysser, W. A. (1996). Reaction and sintering mechanisms of mullite in the systems cristobalite/ α -Al₂O₃ and amorphous SiO₂/ α -Al₂O₃. *Journal of the European Ceramic Society*, 16(10), 1075-1081.
- 13 Schmücker, M., Albers, W., & Schneider, H. (1994). Mullite formation by reaction sintering of quartz and α -Al₂O₃—a TEM study. *Journal of the European Ceramic Society*, 14(6), 511-515.
- 14 Yu, P. C., Tsai, Y. W., Yen, F. S., Yang, W. P., & Huang, C. L. (2015). Thermal characteristic difference between α -Al₂O₃ and cristobalite powders during mullite synthesis induced by size reduction. *Journal of the European Ceramic Society*, 35(2), 673-680.
- 15 Bartsch, M., Saruhan, B., Schmuecker, M., & Schneider, H. (1999). Novel low-temperature processing route of dense mullite ceramics by reaction sintering of amorphous SiO₂-coated γ -Al₂O₃ particle nanocomposites. *Journal of the American Ceramic Society*, 82(6), 1388-1392.

- 16 Cividanés, L. S., Campos, T. M., Rodrigues, L. A., Brunelli, D. D., & Thim, G. P. (2010). Review of mullite synthesis routes by sol-gel method. *Journal of Sol-Gel Science and Technology*, 55(1), 111-125.
- 17 Michalet, T., Parlier, M., Beclin, F., Duclos, R., & Crampon, J. (2002). Elaboration of low shrinkage mullite by active filler controlled pyrolysis of siloxanes. *Journal of the European Ceramic Society*, 22(2), 143-152.
- 18 Michalet, T., Parlier, M., Addad, A., Duclos, R., & Crampon, J. (2001). Formation at low temperature with low shrinkage of polymer/Al/Al₂O₃ derived mullite. *Ceramics international*, 27(3), 315-319.
- 19 Suttor, D., Kleebe, H. J., & Ziegler, G. (1997). Formation of mullite from filled siloxanes. *Journal of the American Ceramic Society*, 80(10), 2541-2548.
- 20 Sule, R., & Sigalas, I. (2018). Effect of temperature on mullite synthesis from attrition-milled pyrophyllite and α -alumina by spark plasma sintering. *Applied Clay Science*, 162, 288-296.
- 21 Liu, K. C., Thomas, G., Caballero, A., Moya, J. S., & De Aza, S. (1994). Mullite formation in kaolinite- α -alumina. *Acta metallurgica et materialia*, 42(2), 489-495.
- 22 Chen, C. Y., Lan, G. S., & Tuan, W. H. (2000). Microstructural evolution of mullite during the sintering of kaolin powder compacts. *Ceramics International*, 26(7), 715-720.
- 23 Sahnoune, F., Chegaar, M., Saheb, N., Goeuriot, P., & Valdivieso, F. (2008). Differential thermal analysis of mullite formation from Algerian kaolin. *Advances in Applied Ceramics*, 107(1), 9-13.
- 24 Duval, D. J., Risbud, S. H., & Shackelford, J. F. (2008). Mullite. In *Ceramic and glass materials* (pp. 27-39). Springer, Boston, MA.
- 25 Mohammadi, T., Pak, A., Nourian, Z., & Taherkhani, M. (2005). *Experimental design in mullite microfilter preparation*. *Desalination*, 184(1-3), 57-64.
- 26 Chen, C. Y., Lan, G. S., & Tuan, W. H. (2000). Preparation of mullite by the reaction sintering of kaolinite and alumina. *Journal of the European Ceramic Society*, 20(14-15), 2519-2525.
- 27 Sainz, M. A., Serrano, F. J., Amigo, J. M., Bastida, J., & Caballero, A. (2000). XRD microstructural analysis of mullites obtained from kaolinite-alumina mixtures. *Journal of the European Ceramic Society*, 20(4), 403-412.
- 28 Liu, Y. F., Liu, X. Q., Tao, S. W., Meng, G. Y., & Sorensen, O. T. (2002). Kinetics of the reactive sintering of kaolinite-aluminum hydroxide extrudate. *Ceramics international*, 28(5), 479-486.
- 29 Pascual, J., Zapatero, J., de Haro, M. C. J., del Valle, A. J. R., Pérez-Rodríguez, J. L., & Sánchez-Soto, P. J. (2000). Preparation of mullite ceramics from coprecipitated aluminum hydroxide and kaolinite using hexamethylenediamine. *Journal of the American Ceramic Society*, 83(11), 2677-2680.
- 30 Sahraoui, T., Belhouchet, H., Heraiz, M., Brihi, N., & Guermat, A. (2016). The effects of mechanical activation on the sintering of mullite produced from kaolin and aluminum powder. *Ceramics International*, 42(10), 12185-12193.

- 31 Yang, F. K., Li, C. W., Lin, Y. M., & Wang, C. G. (2012). Fabrication of porous mullite ceramics with high porosity using foam-gelcasting. *In Key Engineering Materials* (Vol. 512, pp. 580-585). Trans Tech Publications.
- 32 Akpınar, S., Kusoglu, I. M., Ertugrul, O., & Onel, K. (2012). In situ mullite foam fabrication using microwave energy. *Journal of the European Ceramic Society*, 32(4), 843-848.
- 33 Kalemtaş, A., Özey, N., & Aydin, M. T. A. (2018). Processing of layered porous mullite ceramics. *Journal of the Australian Ceramic Society*, 1-11.
- 34 O'Leary, B. G., & MacKenzie, K. J. (2015). Inorganic polymers (geopolymers) as precursors for carbothermal reduction and nitridation (CRN) synthesis of SiAlON ceramics. *Journal of the European Ceramic Society*, 35(10), 2755-2764.
- 35 Bağcı, C., Kutyla, G. P., Seymour, K. C., & Kriven, W. M. (2016). Synthesis and Characterization of Silicon Carbide Powders Converted from Metakaolin-Based Geopolymer. *Journal of the American Ceramic Society*, 99(7), 2521-2530.
- 36 Bernardo, E., Fiocco, L., Parciannello, G., Storti, E., & Colombo, P. (2014). Advanced ceramics from preceramic polymers modified at the nano-scale: A review. *Materials*, 7(3), 1927-1956.
- 37 Walkley, B., San Nicolas, R., Sani, M. A., Gehman, J. D., van Deventer, J. S., & Provis, J. L. (2016). Phase evolution of Na₂O–Al₂O₃–SiO₂–H₂O gels in synthetic aluminosilicate binders. *Dalton Transactions*, 45(13), 5521-5535.
- 38 Bell, J. L., Sarin, P., Driemeyer, P. E., Haggerty, R. P., Chupas, P. J., & Kriven, W. M. (2008). X-ray pair distribution function analysis of a metakaolin-based, KAlSi₂O₆·5.5 H₂O inorganic polymer (geopolymer). *Journal of Materials Chemistry*, 18(48), 5974-5981.
- 39 Davidovits, J. (Ed.). (2005). *Geopolymer, green chemistry and sustainable development solutions: proceedings of the world congress geopolymer 2005*. Geopolymer Institute.
- 40 Wen, H. L., & Yen, F. S. (2000). Growth characteristics of boehmite-derived ultrafine theta and alpha-alumina particles during phase transformation. *Journal of Crystal Growth*, 208(1-4), 696-708.
- 41 Łodziana, Z., & Parliński, K. (2003). Dynamical stability of the α and θ phases of alumina. *Physical Review B*, 67(17), 174106.
- 42 Beguin, B., Garbowski, E., & Primet, M. (1991). Stabilization of alumina toward thermal sintering by silicon addition. *Journal of catalysis*, 127(2), 595-604.
- 43 Cambridge Engineering Selector (CES), Granta Design, Cambridge, UK, 2016. <http://www.grantadesign.com/education/edupack/edupack2016.htm>
- 44 Gong, L., Wang, Y., Cheng, X., Zhang, R., & Zhang, H. (2014). Porous mullite ceramics with low thermal conductivity prepared by foaming and starch consolidation. *Journal of Porous Materials*, 21(1), 15-21.
- 45 Bell, J. L., & Kriven, W. M. (2009, April). Preparation of ceramic foams from metakaolin-based geopolymer gels. *In Ceram Eng Sci Proc* (Vol. 29, No. 10, pp. 97-112).

- 46 Cilla, M. S., Morelli, M. R., & Colombo, P. (2014). Open cell geopolymer foams by a novel saponification/peroxide/gelcasting combined route. *Journal of the European Ceramic Society*, 34(12), 3133-3137.
- 47 Glad, B. E., & Kriven, W. M. (2014). Geopolymer with hydrogel characteristics via silane coupling agent additives. *Journal of the American Ceramic Society*, 97(1), 295-302.
- 48 Al-Harbi, O. A., Özgür, C., & Khan, M. M. (2015). Fabrication and characterization of single phase cordierite honeycomb monolith with porous wall from natural raw materials as catalyst support. *Ceramics International*, 41(3), 3526-3532.
- 49 Grohol, D., Han, C., Pyzik, A. J., Goss, J. M., & Todd, C. S. (2010). Acicular Mullite–Cordierite Composites with Controllable CTE Values. *Journal of the American Ceramic Society*, 93(11), 3600-3603.
- 50 Kuscer, D., Bantan, I., Hrovat, M., & Malič, B. (2017). The microstructure, coefficient of thermal expansion and flexural strength of cordierite ceramics prepared from alumina with different particle sizes. *Journal of the European Ceramic Society*, 37(2), 739-746.
- 51 Bruno, G., Efremov, A. M., Clausen, B., Balagurov, A. M., Simkin, V. N., Wheaton, B. R., ... & Brown, D. W. (2010). On the stress-free lattice expansion of porous cordierite. *Acta Materialia*, 58(6), 1994-2003.
- 52 Studart, A. R., Gonzenbach, U. T., Tervoort, E., & Gauckler, L. J. (2006). Processing routes to macroporous ceramics: a review. *Journal of the American Ceramic Society*, 89(6), 1771-1789.
- 53 Mei, S., Yang, J., Monteiro, R., Martins, R., & Ferreira, J. M. (2002). Synthesis, Characterization, and Processing of Cordierite-Glass Particles Modified by Coating with an Alumina Precursor. *Journal of the American Ceramic Society*, 85(1), 155-160.
- 54 Yalamaç, E., & Akkurt, S. (2006). Additive and intensive grinding effects on the synthesis of cordierite. *Ceramics International*, 32(7), 825-832.
- 55 Tamborenea, S., Mazzoni, A. D., & Aglietti, E. F. (2004). Mechanochemical activation of minerals on the cordierite synthesis. *Thermochimica Acta*, 411(2), 219-224.
- 56 Shi, Z. M. (2005). Sintering additives to eliminate interphases in cordierite ceramics. *Journal of the American Ceramic Society*, 88(5), 1297-1301.
- 57 Wang, W., Shi, Z., Wang, X., & Fan, W. (2016). The phase transformation and thermal expansion properties of cordierite ceramics prepared using drift sands to replace pure quartz. *Ceramics International*, 42(3), 4477-4485.
- 58 Chandrasekhar, S., & Pramada, P. N. (2004). Kaolin-based zeolite Y, a precursor for cordierite ceramics. *Applied Clay Science*, 27(3-4), 187-198.
- 59 Bejjajoui, R., Benhammou, A., Nibou, L., Tanouti, B., Bonnet, J. P., Yaacoubi, A., & Ammar, A. (2010). Synthesis and characterization of cordierite ceramic from Moroccan stevensite and andalusite. *Applied Clay Science*, 49(3), 336-340.
- 60 Orosco, P., Ruiz, M. D. C., & González, J. (2014). Synthesis of cordierite by dolomite and kaolinitic clay chlorination. Study of the phase transformations and reaction mechanism. *Powder Technology*, 267, 111-118.
- 61 Neto, J. B. R., & Moreno, R. (2007). Rheological behaviour of kaolin/talc/alumina suspensions for manufacturing cordierite foams. *Applied Clay Science*, 37(1-2), 157-166.
- 62 Sampathkumar, N. N., Umarji, A. M., & Chandrasekhar, B. K. (1995). Synthesis of α -cordierite (indialite) from flyash. *Materials research bulletin*, 30(9), 1107-1114.

- 63 Goren, R., Ozgur, C., & Gocmez, H. (2006). The preparation of cordierite from talc, fly ash, fused silica and alumina mixtures. *Ceramics International*, 32(1), 53-56.
- 64 Guo, W., Lu, H. B., Feng, C. X., Sun, J., Sun, H. F., Zhou, J., & Shen, J. J. (2012). Low-Temperature Preparation of Porous Cordierite-Mullite Ceramics Using Rice Husk as Silica Source and Pore-Forming Agent. In *Applied Mechanics and Materials*(Vol. 217, pp. 86-90). Trans Tech Publications.
- 65 Tsuchiya, T., & Ando, K. (1990). Synthesis of MgO-Al₂O₃-SiO₂ glasses from sol-gel process and their thermal expansion. *Journal of Non-Crystalline Solids*, 121(1-3), 250-253.
- 66 Kumar, M. S., Perumal, A. E., Vijayaram, T. R., & Senguttuvan, G. (2015). Processing and characterization of pure cordierite and zirconia-doped cordierite ceramic composite by precipitation technique. *Bulletin of Materials Science*, 38(3), 679-688.
- 67 Bertran, C. A., da Silva, N. T., & Thim, G. P. (2000). Citric acid effect on aqueous sol-gel cordierite synthesis. *Journal of non-crystalline solids*, 273(1-3), 140-144.
- 68 Menchi, A. M., & Scian, A. N. (2005). Mechanism of cordierite formation obtained by the sol-gel technique. *Materials Letters*, 59(21), 2664-2667.
- 69 Kazakos, A. M., Komarneni, S., & Roy, R. (1990). Sol-gel processing of cordierite: Effect of seeding and optimization of heat treatment. *Journal of Materials Research*, 5(5), 1095-1103.
- 70 Yamuna, A., Johnson, R., Mahajan, Y. R., & Lalithambika, M. (2004). Kaolin-based cordierite for pollution control. *Journal of the European Ceramic Society*, 24(1), 65-73.
- 71 Petrović, R., Janačković, D., Zec, S., Drmanić, S., & Kostić-Gvozdenović, L. (2003). Crystallization behavior of alkoxy-derived cordierite gels. *Journal of sol-gel science and technology*, 28(1), 111-118.
- 72 Kumar, B. M., & Kim, Y. W. (2010). Processing of polysiloxane-derived porous ceramics: a review. *Science and technology of advanced materials*, 11(4), 044303.
- 73 Song, I. H., Kim, M. J., Kim, H. D., & Kim, Y. W. (2006). Processing of microcellular cordierite ceramics from a preceramic polymer. *Scripta Materialia*, 54(8), 1521-1525.
- 74 Fiocco, L., & Bernardo, E. (2015). Novel cordierite foams from preceramic polymers and reactive oxide fillers. *Materials Letters*, 159, 98-101.
- 75 Khalfaoui, A., Kacim, S., & Hajjaji, M. (2006). Sintering mechanism and ceramic phases of an illitic-chloritic raw clay. *Journal of the European Ceramic Society*, 26(1-2), 161-167.
- 76 Bakharev, T. (2006). Thermal behaviour of geopolymers prepared using class F fly ash and elevated temperature curing. *Cement and Concrete Research*, 36(6), 1134-1147.
- 77 Dombrowski, K., Buchwald, A., & Weil, M. (2007). The influence of calcium content on the structure and thermal performance of fly ash based geopolymers. *Journal of Materials Science*, 42(9), 3033-3043.
- 78 Kuenzel, C., Grover, L. M., Vandeperre, L., Boccaccini, A. R., & Cheeseman, C. R. (2013). Production of nepheline/quartz ceramics from geopolymer mortars. *Journal of the European Ceramic Society*, 33(2), 251-258.

CHAPTER VII

Alternative conformation techniques of porous materials through inorganic gel casting.

VII.1 - Aim of the study

A new generation of glass-based foamed granules is produced combining two different approaches: alkali activation and spheroidisation. The purpose of the study is to explore the gelation that occurs after alkali activation of glass and subsequent hardening, which configures an “inorganic gel casting” with alternative techniques using palletisation in a rotary drum.

Waste glass suspension goes through progressive hardening after alkali activation due to the formation of calcium silica hydrated compounds (C-S-H). Hardened suspensions, after alkali activation of waste glass, were crushed into fragments and cast in a rotating drum. Wet fragments were progressively rounded and dried through contact with fine glass powders, which were also added in the rotary drum. The subsequent firing at 800 °C still led to some foaming, owing to the decomposition of the C-S-H compound developed with alkali activation (and responsible for the hardening). The foamed granules are characterised by high strength and porosities in the order of 70%, with a minimum water absorption that makes them suitable for a number of added value applications (upcycling) such as aggregates in concrete.

VII.2 - Production of Lightweight aggregates from glass cullet by inorganic gel casting.

VII.2.1 - Introduction

The demand for lightweight aggregate (LWA) materials is increasing in the construction and building industry for the production of lightweight concrete, concrete blocks, and other precast products. They are mainly used to improve the thermal insulating properties and acoustic performance of concrete. Moreover, they are also used in other applications such as lightweight geotechnical fill, soil engineering, hydro-culture, drainage, roof gardens and filters.^{1,2}

Lightweight aggregates have a bulk density below 1.2 g/cm^3 and particle density values lower than 2.0 g/cm^3 according to the European Standard EN 13055-1.³ They are almost spherical, with a diameter of 4–14 mm, to ensure a high flowing ability of the fresh concrete pastes,⁴ and ideally present a rough surface, which enables the production of a robust aggregate-cement bond in concrete.⁵ The presence of a dense external layer is desired to prevent excessive water absorption during concrete preparation. Water absorption can cause heterogeneities in the wet paste, leading to different interfacial transition zones in the pastes and low concrete performance in the final product.^{6,7}

Certain low-density materials found in nature, like pumice, volcanic ashes or diatomite sand, were traditionally used in the production of lightweight concrete.^{8,9} However, the most frequently used LWA are expanded clay aggregates. They are artificially produced by thermal treatment of self-bloating clays as perlite, vermiculite or shale. These natural clays under high-temperature treatments, close to $1400 \text{ }^\circ\text{C}$,¹⁰ are transformed into a pyroclastic mass with an adequate viscosity, and they can expand due to the release of gases that remain entrapped inside them. The gases evolved from substances present in the clays, and they are derived from the interlayer water molecules and the decomposition of carbonates. In some cases, due to the specific formulation of the clays, they are also produced through the reduction of ferric oxides or the combustion of organic matter.¹¹

However, the intensive use of natural clays is associated with significant adverse environmental impacts, mainly related to quarrying, transport and high-temperature processing. In order to minimise this adverse environmental effects, natural clays were substituted with a wide variety of waste materials. Waste is not only more environmentally sustainable but also economically convenient as their use reduces the production and transportation costs (by choosing a waste material available close to the production plant) and avoids paying additional taxes on waste landfill.¹²

The production of lightweight aggregates coming from waste materials was studied with different sources, like incinerator bottom ash,¹² fly ash,¹³ sewage sludge ash,¹⁴⁻¹⁶ mining residues or waste glass,¹⁷ and they were used alone or mixed in different proportions in order to achieve a composition suitable for an effective bloating.¹⁸⁻²⁰

Their production is based on a pelletisation process, where the agglomeration of the fine waste powders is achieved with a controlled amount of water in a rotary drum, which enables the formation of the spherical particles. A foaming agent should also be added to the mixture to achieve the bloating of the material during subsequent fire treatment, and the addition of some clay or organic binder is used in many cases to enhance the cohesion and mechanical properties of the green pellet.²¹ Finally, the so obtained green pellets are treated in a rotatory tube furnace at temperatures from 1000 to 1300 °C, and the resulting gasses remain trapped in the glassy structure.

The high temperature needed in the treatment is the main disadvantage of the process since it increases energy cost and CO₂ emissions. Some attempts to reduce the sintering temperature were made by addition of fluxing agents like boric acid, or incorporation of waste glass for lowering the softening point temperature of the mixtures.²² However, the use of expensive foaming agents like MnO₂ or SiC also represents a major drawback in this production technique.²³ The introduction of SiC wastes from polishing ornamental stones and ceramic tiles was also studied to make the process economically viable.²⁴

In the production of granules at a lower temperature, the energy-consuming process of sintering is substituted with cold bonding pelletisation strategy, using cementitious binders like cement²⁵ or lime²⁶ in the granulation process. Using this approach, many waste materials such as blast furnace slag,²⁷ fly ash²⁸⁻³⁰ or bottom ash³¹ also proved to have the potential for being used as feedstock.

A low-temperature hardening strategy is followed to produce lightweight aggregates using alkali-activated materials also referred to as geopolymers. On them an alumina-silicate source is dissolved in a high alkaline solution, usually sodium-silicate, to produce three-dimensional structures with AlO₄ and SiO₄ units. The soluble alumina-silicate nature of a large proportion of industrial waste makes them optimum candidates to geopolymerization.³²

Several strategies were followed to obtain the geopolymeric LWA. The hardened geopolymers were produced and then crushed to obtain the desired shape granulation, and spheroidisation,³³ however, better results were obtained when the alkali-activated fly ash geopolymeric mass was mixed directly inside the palletisation device.³⁴ The pelletisation process was also applied using the alkali activator as a wetting agent in the spheroidisation process and dropped into the dried powders until the desired aggregate size was achieved.^{35, 36} Highly lightweight granules were also obtained exploring the decomposition of hydrogen peroxide in an alkaline medium by adding it to the geopolymeric mixture of basalt and clay wastes.³⁷

The main advantage of using geopolymeric lightweight aggregates is that they do not require heat treatment are hardened by curing at low temperature (room temperature or below 100 °C). This avoids the costs of sintering and using cement. Another advantage of geopolymeric aggregates is that they can immobilise the possible pollutants present in the initial waste, because they remain trapped in the geopolymeric structure.³⁸

This section is an extension of the previous studies exploring additional conformation techniques of alkali activation and gelation process for the production of proppants used in the gas and oil industry. The production and conformation of proppants were previously developed at the University of Padova, exploiting the ‘spheroidisation’ of glass powder beds, later subjected to sinter-crystallisation. In particular, glasses were obtained by melting inorganic waste, such as red mud from Bayer processes, municipal solid waste incinerator fly ash, or low-cost minerals.³⁹

Mixing the previous approaches, a new manufacturing process for lightweight granules was also developed. After alkali attack and subsequent gelation, the partially hardened mixtures were placed, in the form of small fragments, in a rotary drum with dry soda-lime glass powder. The rotational movement turned the fragments into core-shell green granules, which were then transformed into core-shell foamed granules by firing at 700-800 °C (causing the decomposition of the hydrated compounds).

VII.2.2 - Experimental process

Waste soda-lime glass, SLG, provided by SASIL S.r.l. (Brusnengo, Biella, Italy) in the form of fine powders with a mean particle size of 75 µm coming from crushed glass containers was used as raw material; the same fraction was also used in Chapter II.

The fine powders were placed in a 2.5M NaOH (technical grade) aqueous solution and subjected to alkaline attack for 3 hours, under low-speed mechanical stirring. After alkaline activation, the obtained suspension of partially dissolved glass powders was cast in a closed mould and cured at 75 °C for 2 hours to promote its gelation.

The hardened suspensions of soda-lime glass were reduced into fragments and cast on a specially designed rotary drum. The diameter of the pelletizing disc was 12 cm, set at an angle of 45°, whereas the revolution speed was set at 50 rpm. A schematic representation of the conformation process is shown in Figure 1a. Batches of 20 g of fragmented hardened suspensions were added to the rotary drum with the incorporation of 10 g of dry powder to prevent the aggregation of pellets and obtain the desired pellet diameters. The total pelletisation time was determined at 10 min. These parameters were established by observing the shape of pellet formations, keeping a balance in the movement of pellets inside the rotatory drum between the gravitational force and the centrifugal force. If one of these forces becomes dominant, then pellets lose their structure especially at high speed, where the centrifugal force is dominant, and the suspension gets stuck to the side walls.⁴⁰ The optimum pelletisation path followed by the granules is represented in Figure 1b.

These were dried overnight at 75 °C, and finally, the hardened green granules were sintered using a pilot scale continuous tunnel furnace (Nanetti ER-15S) at SASIL S. p. a. (Brusnengo, Biella, Italy). Heat treatments were conducted at different temperatures (700-800 °C) and different holding times. The optimum conditions were set at 800 °C

and 10 min holding time (the maximum speed permitted by the furnace) in order to induce homogeneous foaming, due to the decomposition of the C-S-H compounds developed after alkali activation and responsible for hardening.

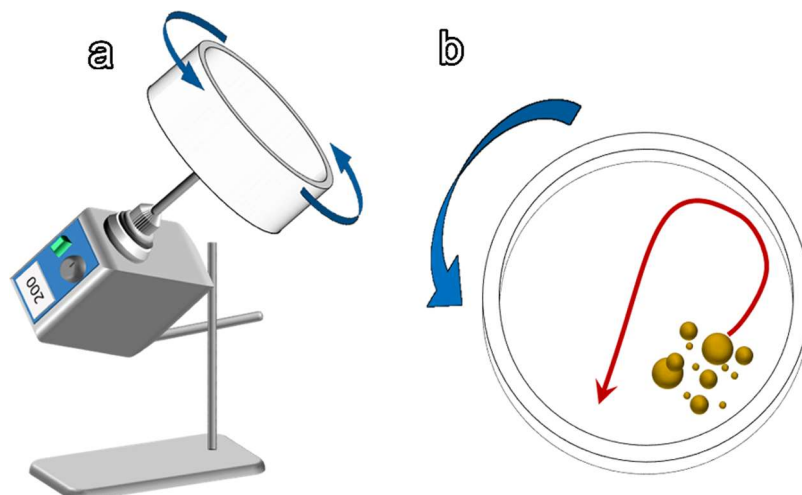


Figure 1. a) Scheme of the spheroidisation apparatus adapted for the manufacturing of 'green' glass granules; b) optimum pelletisation path followed by the granules.

The resulting aggregates were sieved into different fractions according to the requirements of the standard UNE-EN-13139. The morphological and microstructural characterisations were performed by optical stereomicroscopy (AxioCam ERc 5s Microscope Camera, Carl Zeiss Microscopy, Thornwood, New York, US). The geometric density (ρ_g) of the sintered aggregate was determined by carefully measuring the mass and the media of 3 diameters for each aggregate with a calliper on at least 10 granules for each fraction. The apparent (ρ_a) and true density (ρ_t) were measured using a helium pycnometer (Micromeritics AccuPyc 1330, Norcross, GA), operating on bulk or finely crushed samples, respectively. The three density values (ρ_g , ρ_a , and ρ_t) were used to compute the amounts of open and closed porosity for each fraction.

The water absorption of sintered aggregates was calculated as follows:⁴¹

$$\text{Water absorption} = (m_{\text{sat}} - m_{\text{dry}}/m_{\text{dry}}) \times 100 \quad (\text{Equation 1})$$

where m_{dry} is the dry mass of the granules, and m_{sat} is the mass of the pellets after immersion in water for 24 hours.

The compression tests were conducted on individual pellets using an Instron 1121 UTS (Instron, Danvers, MA). A key challenge of the single pellet compression test is the calculation of the critical stress that leads to the failure of the particle, taking into account the applied force divided by the projected area of the pellet. This procedure was selected due to its simplicity even if it is known that an underestimation of the mechanical properties occurs.

The mineralogical analysis was conducted by means of X-ray diffraction (XRD) (Bruker D8 Advance, Karlsruhe, Germany), using $\text{CuK}\alpha$ radiation, 40 kV, 40 mA, $2\theta = 10\text{--}70^\circ$, step size 0.05° , 2s counting time. The phase identification was completed using the Match![®] program package (Crystal Impact GbR, Bonn, Germany), supported by data from PDF-2 database (ICDD-International Centre for Diffraction Data, Newtown Square, PA).

VII.2.3 - Results and discussion

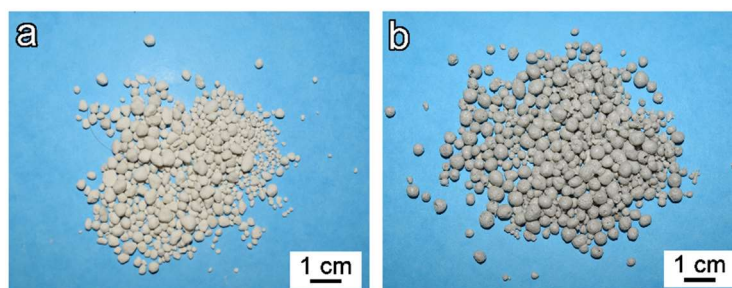


Figure 2. External morphology of LWA, a) before sintering, b) after heat treatment at 800°C .

Figure 2a shows the green pellets before the heat treatment; just after the conformation through spheroidisation and drying, they present a good spherical shape, and their mechanical properties are good enough for stacking during storage. It can be seen in Figure 2b that the spherical shape is perfectly maintained after the heat treatment process. The pellets enter the furnace feeding zone directly at 800°C , and they are subject to a rapid heating process that promotes a vitrified outer layer, as can be noticed by the shiny surface of the fired granules in Figure 2b

Figure 3 shows the morphology of single granules of different sizes. In Fig. 3a, 3b and 3c it is possible to observe a dense layer that recovers the pellets; in Fig. 3d, e and f the cross-section of the granules is shown. The firing of green granules was accompanied by significant foaming, due to the decomposition of C-S-H compounds developed during alkali activation. It can be noticed a highly porous core surrounded by a relatively dense thin shell. The granules contain a significant volume of isolated pores of an approximately spherical shape. These pores are mostly in the $10\text{--}50\ \mu\text{m}$ diameter range, although there is evidence of some larger pores.

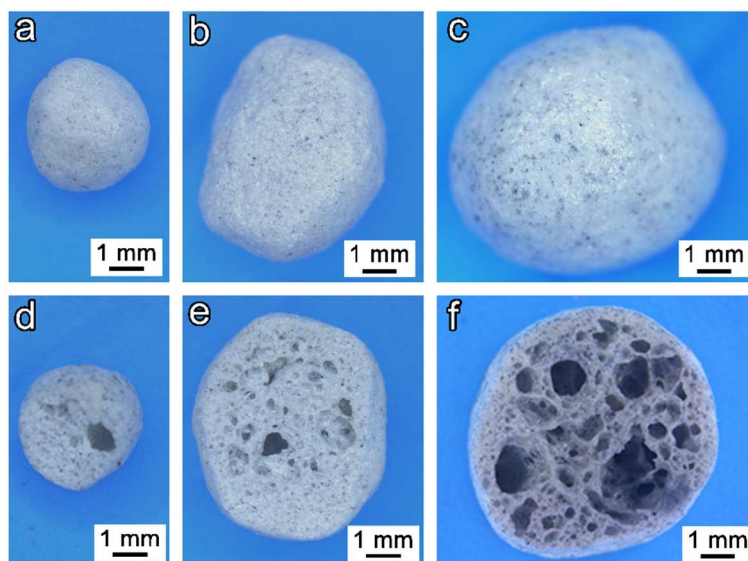


Figure 3. External aspect and cross section of waste glass derived granules

The presence of a denser outer layer was also clearly identified. This layer is formed by the dry glass added in the pelletisation process, since in the added glass there is no formation of C-S-H compounds, does not undergo foaming, and has no bubbles in the outer surface. The formation of this outer layers plays a crucial role in the final properties of the LWA as can be seen in Table 1, where the density, porosity and mechanical properties of heat-treated LWA are reported.

The produced granules present low densities and can be noticed a continuous decrease of the geometrical density with increasing granule size. This fact suggests more effective foaming in the bigger granules. However, all the sizes are below the reported data of other commercial lightweight aggregates such as Litag[®] and Optiroc[®].^{42,43}

The granules present very high porosities, all above 70%. It can be noticed an increase of the porosity with the bigger granules size. However, the most significant changes can be detected between the incidence of open and closed porosity. Bigger granules present higher open porosity, which indicates a higher degree of coalescence between the bubbles during the fire treatment.

All granule sizes present an excellent crushing strength, for the given, substantial porosity and the relatively low density. It should be noticed that due to the punctual application of the force under compression these values are underestimated, as the area considered in the application of the force was the projected area of the single granule. If we reduced the area in the calculations, the mechanical performance should be much higher. However, this value is not paramount, since the granules would find their final application in concrete. Some experiments on the addition of lightweight aggregates are currently ongoing and will be the scope of future investigations.

Fraction (mm)	Density, ρ (g/cm ³)			Porosity (%)			σ_{comp} (MPa)
	geometric	apparent	true	total	open	closed	
2 - 4	0.73 ± 0.05	0.98 ± 0.03	2.49 ± 0.02	70 ± 6	25 ± 5	45 ± 3	0.38 ± 0.05
4 - 6.3	0.74 ± 0.06	0.98 ± 0.01	2.45 ± 0.01	70 ± 1	25 ± 1	45 ± 2	0.48 ± 0.07
6.3 - 8	0.61 ± 0.04	0.98 ± 0.04	2.48 ± 0.01	75 ± 6	37 ± 9	37 ± 4	0.31 ± 0.03
8 - 10	0.56 ± 0.02	1.12 ± 0.04	2.49 ± 0.01	77 ± 6	49 ± 4	27 ± 2	0.25 ± 0.05
10 - 12.5	0.51 ± 0.02	0.98 ± 0.03	2.41 ± 0.01	76 ± 4	44 ± 7	35 ± 3	0.31 ± 0.04
12.5 - 14	0.51 ± 0.02	0.98 ± 0.04	2.48 ± 0.01	79 ± 3	49 ± 6	30 ± 3	0.07 ± 0.1

Table 1. Density, porosity and mechanical properties of heat-treated granules.

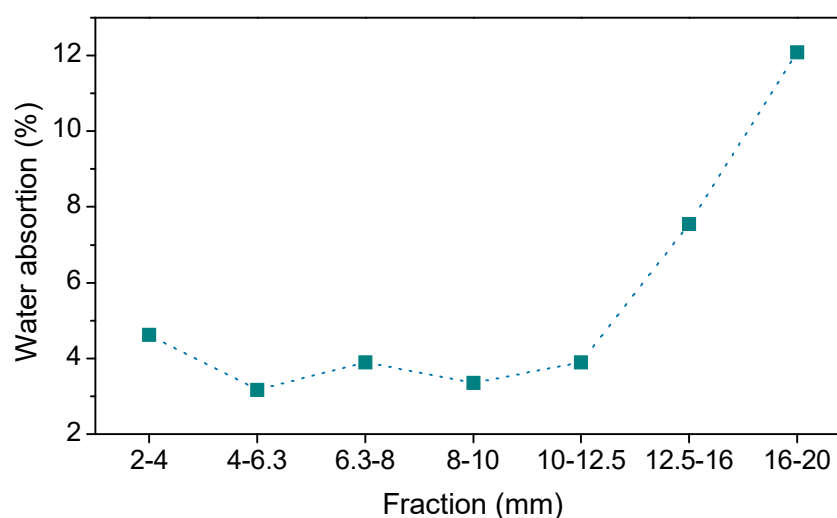


Figure 4. Water absorption of the fired aggregates.

Figure 4 shows that the water absorption of the aggregates, for the smaller aggregates, is very limited, remaining below 5%. However, a noticeable increase is detected for the granules above 12.5 mm. Water absorption is significantly influenced by the dense and hard shell on the surface, and this high variation in water absorption behaviour may depend on surface conditions.

In general, as the aggregate size decreases, the geometrical density increases. Water absorption, however, does not follow this trend and is stabilised in smaller granules. The granules during the sintering process inside the tunnel furnace were placed on a metallic plate, and it was observed that the bigger granules attached to it after treatment because of higher weight; when detached, the outer surface was damaged. The partial destruction of the outer layer could explain higher values in water absorption. The use of a rotatory kiln would allow to overcome this problem.

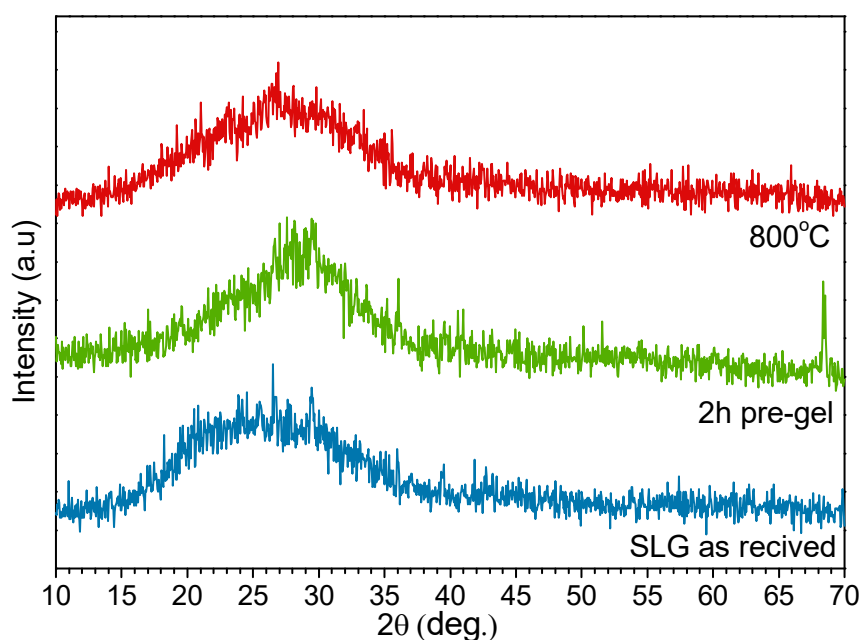


Figure 5. X-ray diffraction patterns of SLG as received, green granules after pelletisation and LWA after firing.

Figure 5 represents the diffraction patterns of the initial soda-lime glass and hardened granules after 2 hours of pre-gelation at 75 °C. In the samples, a broad halo attributed to the glassy phase does not allow the detection of any crystalline phase. However, it could be noticed the shifting of the hump, from approximately $2\theta = 24-26^\circ$, for glass powders, to $2\theta = 28-30^\circ$, in the activated samples. This shift, as in the case of foams produced with SLG explored in Chapter II, is connected with the incorporation of network modifiers in the glass

After the heat treatment at 800 °C, the structure remained amorphous, and the ‘halo’ shifted back to lower angles. In this perspective, this is consistent with the decomposition of the hydrated compounds and dissolution of oxides in new glass matrices.

Due to the amorphous nature of the glass aggregates produced, the possibility of alkali-silica reactivity, when they are added to the cement, has to be taken into account. This is especially the case for aggregates based on waste glass, as the incorporation of the alkali leads to glasses with poorer stability. The alkali-silica reaction is potentially deleterious and may cause expansion in cement. However, according to Ducman et al.,⁴⁴ even if the glass aggregate can be reactive, it does not cause expansion or cracks in the relevant mortar samples. This is attributed to the porous structure of the aggregate, which can accommodate the large amount of gel produced in the alkali-silica reaction. Nevertheless, before such aggregate can be considered safe for general use in concrete, longer-term concrete prism tests need to be carried out.

The economic viability associated with the cost of raw materials, transportation and LWA production is also an important aspect to be evaluated. The waste glass used in this study, thanks to the implementation of the separate waste collection, is widely available since it does not have any other application and is mainly landfilled. The processing involving pelletising could be as costly as the production of other commercially available lightweight aggregates that are typically manufactured. In addition, the lower sintering temperature could bring significant energy and cost savings, along with the reduction of CO₂ emissions, delivering sustainability benefits.

VII.3 - Conclusions

The following conclusions can be drawn:

- LWA were produced using a relatively simple process involving spheroidisation, alkali activation and gelification.
- The production of LWA occurs thanks to the decomposition of C-S-H compounds developed during alkali activation with low-temperature sintering,
- Lightweight aggregates can be produced at relatively low firing temperatures; resulting in substantial economic advantages.
- The dense outer layer developed by the addition of dry glass during pelletisation also plays a critical role as regards water absorption properties of the LWA produced.
- The LWA glass granules produced present an excellent crushing strength, for the given, substantial porosity.

References

- 1 Swamy, R. N., & Lixian, W. (1995). The ingredients for high performance in structural lightweight aggregate concrete. *In Proceedings of 1st international symposium on structural high strength lightweight aggregate concrete*, June (pp. 20-24).
- 2 Sarkar, S. L., Satish, C., & Leif, B. (1992). Interdependence of microstructure and strength of structural lightweight aggregate concrete. *Cement and concrete composites*, 14(4), 239-248.
- 3 BS EN 13055-1, Lightweight aggregates. Part 1: Lightweight aggregates for concrete, mortar and grout. ISBN: 0 580 39776 9, 2002.
- 4 Gesoglu, M., Güneyisi, E., Ozturan, T., Oz, H. O., & Asaad, D. S. (2015). Shear thickening intensity of self-compacting concretes containing rounded lightweight aggregates. *Construction and Building Materials*, 79, 40-47.

- 5 Cheeseman, C. R., & Viridi, G. S. (2005). Properties and microstructure of lightweight aggregate produced from sintered sewage sludge ash. *Resources, Conservation and Recycling*, 45(1), 18-30.
- 6 Dong, S. H.; Ge, Y.; Zhang, B. S.; Yuan, J., Effect of Lightweight Aggregate Moisture Content on Pore Structure of Concrete. *In Advances in Building Materials, Pts 1-3; Li, L. J., Ed.; Trans Tech Publications*
- 7 Newman, J. B. (1993). Properties of structural lightweight aggregate concrete. *Structural lightweight aggregate concrete*, 19-44.
- 8 Chandra, S., & Berntsson, L. (2002). *Lightweight aggregate concrete*. Elsevier.
- 9 Posi, P., Lertnimoolchai, S., Sata, V., Phoo-ngernkham, T., & Chindaprasirt, P. (2014). Investigation of properties of lightweight concrete with calcined diatomite aggregate. *KSCE Journal of Civil Engineering*, 18(5), 1429-1435.
- 10 Arioz, O., Kilinc, K., Karasu, B., Kaya, G., Arslan, G., Tuncan, M., ... & Kivrak, S. (2008). A preliminary research on the properties of lightweight expanded clay aggregate. *Journal of the Australian Ceramic Society*, 44(1), 23-30.
- 11 Ayati, B., Ferrándiz-Mas, V., Newport, D., & Cheeseman, C. (2018). Use of clay in the manufacture of lightweight aggregate. *Construction and Building Materials*, 162, 124-131.
- 12 Cheeseman, C. R., & Viridi, G. S. (2005). Properties and microstructure of lightweight aggregate produced from sintered sewage sludge ash. *Resources, Conservation and Recycling*, 45(1), 18-30.
- 13 Ramamurthy, K., & Harikrishnan, K. I. (2006). Influence of binders on properties of sintered fly ash aggregate. *Cement and Concrete Composites*, 28(1), 33-38.
- 14 Bhattu, J. I., & Reid, K. J. (1989). Moderate strength concrete from lightweight sludge ash aggregates. *International Journal of Cement Composites and Lightweight Concrete*, 11(3), 179-187.
- 15 Wang, K. S., Chiou, J., Chen, C. H., & Wang, D. (2005). Lightweight properties and pore structure of foamed material made from sewage sludge ash. *Construction and Building Materials*, 19(8), 627-633.
- 16 Cheeseman, C. R., & Viridi, G. S. (2005). Properties and microstructure of lightweight aggregate produced from sintered sewage sludge ash. *Resources, Conservation and Recycling*, 45(1), 18-30.
- 17 Limbachiya, M., Meddah, M. S., & Fotiadou, S. (2012). Performance of granulated foam glass concrete. *Construction and building materials*, 28(1), 759-768.
- 18 Huang, S. C., Chang, F. C., Lo, S. L., Lee, M. Y., Wang, C. F., & Lin, J. D. (2007). Production of lightweight aggregates from mining residues, heavy metal sludge, and incinerator fly ash. *Journal of hazardous materials*, 144(1-2), 52-58.
- 19 Tuan, B. L. A., Hwang, C. L., Lin, K. L., Chen, Y. Y., & Young, M. P. (2013). Development of lightweight aggregate from sewage sludge and waste glass powder for concrete. *Construction and building materials*, 47, 334-339.
- 20 Fan, C. S., Huang, C. Y., & Li, K. C. (2014). Bloating mechanism of the mixture of thin-film transistor liquid-crystal display waste glass and basic oxygen furnace slag. *Construction and Building Materials*, 66, 664-670.
- 21 Kockal, N. U., & Ozturan, T. (2011). Characteristics of lightweight fly ash aggregates produced with different binders and heat treatments. *Cement and Concrete Composites*, 33(1), 61-67.

- 22 Velis, C. A., Franco-Salinas, C., O'sullivan, C., Najorka, J., Boccaccini, A. R., & Cheeseman, C. R. (2014). Up-cycling waste glass to minimal water adsorption/absorption lightweight aggregate by rapid low temperature sintering: optimization by dual process-mixture response surface methodology. *Environmental science & technology*, 48(13), 7527-7535.
- 23 Ducman, V., & Mirtič, B. (2009). The applicability of different waste materials for the production of lightweight aggregates. *Waste Management*, 29(8), 2361-2368.
- 24 de'Gennaro, R., Graziano, S. F., Cappelletti, P., Colella, A., Dondi, M., Langella, A., & Gennaro, M. D. (2009). Structural concretes with waste-based lightweight aggregates: from landfill to engineered materials. *Environmental science & technology*, 43(18), 7123-7129.
- 25 Arslan, H., & Baykal, G. (2006). Utilization of fly ash as engineering pellet aggregates. *Environmental Geology*, 50(5), 761-770.
- 26 Colangelo, F., Messina, F., & Cioffi, R. (2015). Recycling of MSWI fly ash by means of cementitious double step cold bonding pelletization: Technological assessment for the production of lightweight artificial aggregates. *Journal of hazardous materials*, 299, 181-191.
- 27 Gesoğlu, M., Güneyisi, E., & Öz, H. Ö. (2012). Properties of lightweight aggregates produced with cold-bonding pelletization of fly ash and ground granulated blast furnace slag. *Materials and Structures*, 45(10), 1535-1546.
- 28 Ferone, C., Colangelo, F., Messina, F., Iucolano, F., Liguori, B., & Cioffi, R. (2013). Coal combustion wastes reuse in low energy artificial aggregates manufacturing. *Materials*, 6(11), 5000-5015.
- 29 Güneyisi, E., Gesoğlu, M., Altan, İ., & Öz, H. Ö. (2015). Utilization of cold bonded fly ash lightweight fine aggregates as a partial substitution of natural fine aggregate in self-compacting mortars. *Construction and Building Materials*, 74, 9-16.
- 30 Narattha, C., & Chaipanich, A. (2018). Phase characterizations, physical properties and strength of environment-friendly cold-bonded fly ash lightweight aggregates. *Journal of Cleaner Production*, 171, 1094-1100.
- 31 Cioffi, R., Colangelo, F., Montagnaro, F., & Santoro, L. (2011). *Manufacture of artificial aggregate using MSWI bottom ash*. *Waste Management*, 31(2), 281-288.
- 32 Duxson, P., Fernández-Jiménez, A., Provis, J. L., Lukey, G. C., Palomo, A., & van Deventer, J. S. (2007). Geopolymer technology: the current state of the art. *Journal of materials science*, 42(9), 2917-2933.
- 33 Jo, B. W., Park, S. K., & Park, J. B. (2007). Properties of concrete made with alkali-activated fly ash lightweight aggregate (AFLA). *Cement and Concrete composites*, 29(2), 128-135.
- 34 Yliniemi, J., Tiainen, M., & Illikainen, M. (2016). Microstructure and physical properties of lightweight aggregates produced by alkali activation-high shear granulation of FBC recovered fuel-biofuel fly ash. *Waste and Biomass Valorization*, 7(5), 1235-1244.
- 35 Bui, L. A. T., Hwang, C. L., Chen, C. T., Lin, K. L., & Hsieh, M. Y. (2012). Manufacture and performance of cold bonded lightweight aggregate using alkaline activators for high performance concrete. *Construction and Building Materials*, 35, 1056-1062.
- 36 Yliniemi, Paiva, Ferreira, Tiainen, & Illikainen. (2017). Development and incorporation of lightweight waste-based geopolymer aggregates in mortar and concrete. *Construction and Building Materials*, 131, 784-792.

- 37 Tataranni, P., Besemer, G. M., Bortolotti, V., & Sangiorgi, C. (2018). Preliminary Research on the Physical and Mechanical Properties of Alternative Lightweight Aggregates Produced by Alkali-Activation of Waste Powders. *Materials*, 11(7).
- 38 Yliniemi, J., Pesonen, J., Tiainen, M., & Illikainen, M. (2015). Alkali activation of recovered fuel–biofuel fly ash from fluidised-bed combustion: stabilisation/solidification of heavy metals. *Waste management*, 43, 273-282.
- 39 Toniolo, N., Romero, A. R., Marangoni, M., Binhussain, M., Boccaccini, A. R., & Bernardo, E. (2018). Glass-ceramic proppants from sinter-crystallisation of waste-derived glasses. *Advances in Applied Ceramics*, 117(2), 127-132.
- 40 Srb, J., & Ruzickova, Z. (1988). Pelletization of fines. *Elsevier Science Publishing Company*
- 41 Neville, A. M. (1995). Properties of concrete (Vol. 4). London: Longman.
- 42 <https://www.aggregate.com/our-businesses/lytag> (Last accessed August 2018)
- 43 <https://www.weber.com.pt/uploads/media/TechSpecsGeneralFill.pdf> (Last accessed August 2018)
- 44 Ducman, V., Mladenovič, A., & Šuput, J. S. (2002). Lightweight aggregate based on waste glass and its alkali–silica reactivity. *Cement and Concrete Research*, 32(2), 223-226.

CHAPTER VIII

Final Remarks

Sustainable development is recognised as a fundamental issue for the future growth of our society. A closed-loop approach to waste management is a critical way to promote and implement environmental protection strategies. However, the increasing production of hazardous and toxic waste, as well the lack of solutions for less problematic waste, such as unemployed glasses currently landfilled, are critical issues that should be carefully addressed. Alternative manufacturing techniques are needed to reduce production costs and increase economic and environmental sustainability.

Glass foams (or cellular glasses) present interesting properties for thermal and acoustic insulation, and they have been widely recognised as competitive products for building applications; in this work, a new technique for the production of glass foam is successfully developed as an alternative method to up-cycle different kind of waste materials. This new technique, which relies on the production of glass and glass-ceramic foams based on the alkali-activation of silica-rich waste materials, with subsequent inorganic gel casting foaming by means of a surfactant and final heat treatment, is based on a sinter-crystallisation process.

The most innovative aspect, in comparison with traditional methods, is that it relies on the net separation between foaming and sintering. This increases the versatility of waste materials that can be used as raw constituents, as demonstrated in a wide range of glass-based waste materials studied so far, such as waste soda lime glass cullet

alone(Chapter II) or incorporated with other industrial waste, like copper slag or fly ash (Chapter III) or vitrified bottom ash and borosilicate glass (Chapter IV).

The flexibility of the approach has also been demonstrated through the application of the technique to another type of glass not derived from waste sources, namely bioactive glasses, covered in Chapter V.

The cellular glass-based materials obtained with this innovative technique are the result of the simultaneous control of both formulations and manufacturing processes. Two main aspects were identified as critical in the final properties of the resulting materials. The formation of calcium-silicate-hydrate (C-S-H), sodium alumino-silicate hydrate (N-A-S-H) and calcium alumino-silicate hydrate (C-A-S-H) gels ('inorganic gel-casting'), responsible for low-temperature hardening of the suspensions and attributable to the alkaline attack, affects the hardened foam microstructure. The sinter-crystallisation process upon the treatments can be used for the advanced tuning of porous structure and the ratio between open and closed porosity.

The final microstructure (total amount of porosity, cell size) can be directly correlated with the degree of gelation. As a result, the tuning of the cellular structure is relatively easy to control by regulating the parameters that affect the gelation process after alkali activation. As evidenced by the experiments with soda-lime glass and the solid content, the duration of both activation and drying stages may affect the viscosity of glass slurries and accordingly modify the cellular structure in the 'green' state. These changes will be the reasonable focus of future investigations, especially at a semi-industrial scale. Actually, the morphology could also be adjusted by simply changing the chemistry of the adopted surfactant, as clearly demonstrated in the specific case of BSG.

The final sinter-crystallisation process allows a further tuning of the final microstructure, since it affects to the overall porosity and the final ratios between open and closed porosity. When the viscous flow is effective in joining adjacent glass particles, it also has some potential in reshaping the pores, leading to higher ratios of closed porosity. However, in case of glasses prone to crystallisation, the increase of viscosity of softened glass induced by crystal inclusions reduces the microstructural evolution, so that open-celled structures remain substantially unaltered.

As a result, a significant number of combinations of processing parameters can be modified (surfactants, activating solution, curing times or heat treatment conditions) allowing to tune and obtain the desired properties of the final glass-ceramic foams

The technique allows the incorporation of waste materials rich in specific oxides, particularly iron oxides, such as copper slag and fly ash (studied in Chapter III), which allow the easy incorporation of additional functionalities in the glass-ceramic foams (i.e. ferrimagnetism) and increase usability of the final products. The cases presented

here are only preliminary examples of the potential offered by the transformation of inorganic waste.

The assessment of the chemical stability of waste-derived materials are associated with an effective stabilisation of possible pollutants, especially the typical leaching of heavy metals, which was found to be particularly limited, and under the legal thresholds for marketing the relevant products

The proposed approach to cellular glasses is also interesting for its inherent flexibility in the chemical composition of the initial raw materials. The semi-industrial production of lightweight panels validates the foaming technique and demonstrates the viability of the process, which is undoubtedly favoured by the easy manufacturing. In addition, as in the case of the studied formulations, entirely based on waste sources, the technique would allow significant reductions of processing temperatures and energy consumption, and the use of inexpensive foaming agents in the foaming of waste-derived glasses into glass ceramics, proving the industrial sustainability of the process.

The progressive hardening associated with the inorganic polymerisation configuring an 'inorganic gel casting' has also successfully been exploited to produce advanced ceramics, such as mullite and cordierite foams, and scaffolds, by frothing and direct ink writing, respectively. The study (Chapter VI) confirms the versatility of the alkali activation process when applied to engineered suspension and fillers having a significant potential for the production of advanced ceramics, with a distinctive coupling of synthesis and shaping.

Finally, alkali activation and spheroidisation techniques were finally combined to create an innovative approach in the production of lightweight granules (Chapter VII), which would open up the way for new and innovative glass-ceramic materials for incorporation into thermal and acoustic insulation systems.